VOLUME 13 (1959) No. 4

NUCLEAR PHYSICS

JOURNAL DEVOTED TO THE EXPERIMENTAL AND THEORETICAL STUDY OF THE FUNDAMENTAL CONSTITUENTS OF MATTER AND THEIR INTERACTIONS

EDITOR: L. ROSENFELD - COPENHAGEN

R. K. GIRGIS, R. A. RICCI and R. VAN LIESHOUT, On the decay of ^{76}As 461

R. K. GIRGIS, R. A. RICCI, R. VAN LIESHOUT and J. KONIJN, The decay of ^{76}Br . 473

R. K. GIRGIS, R. A. RICCI and R. VAN LIESHOUT, Gamma radiation from ^{77}Br . 485

R. K. GIRGIS and R. VAN LIESHOUT, Investigations on the decay of ^{103}Ag, ^{104}Ag and ^{104}Rh 493

R. K. GIRGIS and R. VAN LIESHOUT, The level scheme of ^{104}Pd (Addendum) . 509

EDWARD J. BURGE, The total proton reaction cross section of carbon from 10–68 MeV by a new method 511

WIESLAW CZYŻ, TORLEIF ERICSON and SHELDON L. GLASHOW, A new model for multiple meson production at high energies. 516

J. R. BIRD, M. C. MOXON and F. W. K. FIRK, Gamma ray spectra and parameters of neutron resonances in mercury. 525

A. I. ALIKHANOV, G. P. ELISEYEV and V. A. LUIBIMOV, The energy dependence of the polarization of electrons and time parity 541

T. K. FOWLER and K. M. WATSON, The quasi-elastic scattering of fast particles by atomic nuclei 549

P. PAUL und U. STIERLIN, Gammaresonanzstreuung am 17.22 MeV-Zustand in C^{12}. 576

V. S. BARASHENKOV, V. M. MALTSEV and E. K. MIHUL, Central and peripheral collisions between fast nucleons (I) 583

ROGER BALIAN, Densité de niveaux d'un système de nucléons en interaction dans une couche 594

NORTH-HOLLAND PUBLISHING COMPANY - AMSTERDAM

November (2) 1959

EDITORIAL BOARD

AUSTRALIA & NEW ZEALAND:	H. Messel (Sydney), M. L. Oliphant (Canberra)
AUSTRIA:	B. Karlik, (Vienna), H. Thirring (Vienna)
BELGIUM:	M. de Hemptinne (Louvain), J. Verhaeghe (Ghent)
CANADA:	G. Volkoff (Vancouver)
DENMARK:	C. Møller (Copenhagen), S. Rozental (Copenhagen)
FINLAND:	L. Simons (Helsinki)
FRANCE:	A. Berthelot (Saclay), S. Gorodetzky (Strasbourg)
GERMANY (DEM. REP.):	G. Hertz (Leipzig)
GERMANY (FED. REP.):	W. Gentner (Freiburg i. B.), J. H. D. Jensen (Heidelberg)
GREAT BRITAIN:	S. Devons (Manchester), T. H. R. Skyrme (Harwell)
HUNGARY:	L. Janossy (Budapest)
INDIA:	H. Bhabha (Bombay), R. Ramanna (Trombay)
IRISH REPUBLIC:	J. McConnell (Maynooth)
ISRAEL:	G. Racah (Jerusalem)
ITALY:	E. Amaldi (Rome)
JAPAN:	S. Kikuchi (Tokyo), S. Tomonaga (Tokyo)
MEXICO:	M. Moshinsky (Mexico)
NETHERLANDS:	H. Brinkman (Groningen), S. R. de Groot (Leiden)
NORWAY:	E. Hylleraas (Oslo), A. Lundby (Oslo), H. Wergeland (Trondheim)
POLAND:	L. Infeld (Warsaw)
PORTUGAL:	J. M. Araújo (Porto), J. R. de Almeida Santos (Coimbra)
SOUTH AMERICA:	G. Beck (Saõ Paulo), J. Leite Lopes (Rio de Janeiro)
SPAIN:	J. M. Otero (Madrid), C. Sanchez del Rio (Madrid)
SWEDEN:	O. Klein (Stockholm), K. Siegbahn (Uppsala), I. Waller (Uppsala)
SWITZERLAND:	P. Huber (Basel), P. Scherrer (Zürich)
U.A.R. & ARAB COUNTRIES:	F. El Bedewi (Alexandria), M. G. Nooh (Cairo)
U.S.A.	H. H. Barschall (Madison, Wisconsin), V. Weisskopf (Cambridge, Mass.)
U.S.S.R.:	M. A. Markov (Moscow), I. S. Shapiro (Moscow), D. V. Skobeltzyn (Moscow)
YUGOSLAVIA:	I. Supek (Zagreb)

CONTRIBUTIONS may be sent to the Editor, Professor L. Rosenfeld, NORDITA, Blegdamsvej 17, Copenhagen Ø, either directly, or preferably through the intermediary of one of the members of the Editorial Board of the country or region in which the author is working. They may be written in English, French or German.

NUCLEAR PHYSICS is published in fortnightly issues. The subscription price per volume of 700 pages is fl 57.00; 114s; $ 15.00. Post-free.

SUBSCRIPTIONS should be sent to the publishers, NORTH-HOLLAND PUBLISHING COMPANY, P.O.Box 103, Amsterdam or to any subscription-agent.

BOOKS FOR REVIEW should be sent to Professor Rosenfeld.

No part of this issue may be reproduced in any form, by print, photoprint, microfilm or any other means without written permission from the publisher. Reprints, photoprints or microfilms are obtainable at cost from the publisher.

Printed in the Netherlands

1.E.1:
3.A:4.E

Nuclear Physics **13** (1959) 461—472; © *North-Holland Publishing Co., Amsterdam*
Not to be reproduced by photoprint or microfilm without written permission from the publisher

ON THE DECAY OF ^{76}As

R. K. GIRGIS †, R. A. RICCI †† and R. VAN LIESHOUT
Instituut voor kernphysisch Onderzoek, Amsterdam

Received 3 August 1959

Abstract: The gamma rays emitted in the decay of ^{76}As were investigated with the help of scintillation spectrometers. Gamma-gamma coincidences were performed using the summing technique with a cylindrical well-type crystal and also with a fast-slow coincidence set-up. New gamma rays of 760, 860, 1530, 1630, 1860 and 2110 keV were found. The existence of the recently reported gamma rays of 2410 and 2640 keV and that of the disputed 1770 keV gamma ray is confirmed. It is shown that both the 560 and 1210 keV gamma peaks correspond to more than one gamma transition. Results of the detailed analysis of the spectrum are given (table 1): a decay scheme is proposed (fig. 7).

1. Introduction

The level scheme of ^{76}Se, adopted as a result of several investigations on the decay of ^{76}As performed by many groups [1–21]), consists mainly of four levels of energies 0, 560, 1210 and 2610 keV, having spins and parities 0^+, 2^+, 2^+ and 3 successively. These levels are reported to be populated by negaton groups of energies 2970, 2410, 1760 and 360 keV. Two other reported beta ray groups of energies $\approx$ 1200 and 880 keV have not been incorporated into the decay scheme; the same applies to a gamma ray of 1760 keV whose existence was still in doubt. Recently [21]), weak gamma rays of 2650 and 2420 keV were found. The reported values for the relative intensities of most of the gamma rays are strongly in disagreement, in particular for the 640 and 1210 keV transitions.

There is a growing interest [23, 24]) in the intensity ratio between the crossover and stopover transitions from the second 2^+ level in even-even nucleides. Among these ^{76}Se forms an interesting case, since this ratio, according to the published data, seems to be rather high when compared with the general trend for this family of nucleides. There is, however, some indication that the 1.21 MeV gamma ray, assumed to originate at the second excited 2^+ level of the same energy, corresponds to more than one gamma ray transition. For instance, the reported intensity [25]) for the 560 keV gamma ray (44.6 %) and that of the 2970 keV beta group (52$\pm$1 %) would leave only $3\frac{1}{2}$ % for any other gamma transition to the ground state, whereas the intensity of the 1210 keV transition alone has been reported [14, 15]) to be already responsible for 8 to 10 %.

† On leave of absence from the Faculty of Science, University of Cairo, Giza, Egypt, U.A.R.
†† On leave of absence from the Istituto di Fisica Sperimentale del Politecnico, Torino, Italia. Present address: Istituto Nazionale di Fisica Nucleare, Sottosezione di Napoli, Italia.

With the aim of establishing a more consistent decay scheme of ^{76}As its gamma spectrum was examined and a detailed analysis was performed; gamma-gamma coincidences were also carried out.

2. Production and Chemical Procedure

A target of magnesium pyroarsenate was irradiated with $\approx 15\mu$Ah of 21-MeV deüterons from the synchro-cyclotron of this Institute. The target was dissolved in 6*N* HCl. To separate the selenium activity from the solution, 50 mg of sodium selenite was added as carrier; the selenium was precipitated with hydroxylamine hydrochloride and filtered off. This separation was performed twice. In the filtrate the arsenic was precipitated as ammonium magnesium arsenate, filtered off and dried.

Sources of ^{76}As were examined within a few hours after production in order to minimize the contribution of ^{74}As which is produced by a (d, dn) reaction. Its contribution at the start of the measurements was always less than 2 % of the total activity.

3. Measurements and Results

3.1. GAMMA RAY SPECTRUM

The gamma spectrum was examined using a NaI(Tl) cylindrical crystal of 25×25 mm mounted on a 6292 DuMont photomultiplier and also with another cylindrical crystal of the same material and of 62×62 mm optically coupled to a 6363 Du Mont photomultiplier. This last crystal is of the well-type, it has a hole of 9 mm diameter and 31 mm depth. The sources were placed far enough from the detector to ensure suppression of summing effects in the crystals, especially for the bigger one where this effect is more pronounced. The spectra were displayed on a 100 channel kicksorter (Radiation Instrument Development Laboratory, Chicago).

Fig. 1 and fig. 2 show the characteristic spectrum of ^{76}As in two energy regions measured with the smaller crystal. The analysis of the spectrum was carried out in the way applied and described in several other publications from this Institute. This procedure consists in peeling off peaks interpolated from standard peaks chosen especially for the nucleide under investigation. Characteristic peaks of ThC'', ^{38}K, ^{42}K, ^{22}Na, ^{54}Mn, ^{137}Cs and ^{207}Bi were used in this case. Special attention was paid to the determination of the energies of the various peaks. The energy value of 2640 ± 15 keV for the highest energy gamma ray in the spectrum was determined from several comparisons with the 2620 keV ThC'' gamma ray. Table 1 gives the energies and relative intensities of the gamma rays found in this work, together with the value reported by other groups.

The existence of the 1770 keV gamma ray is beyond doubt as shown by its

height above the Compton shoulder of the 2100 keV gamma ray. The presence of the weak gamma rays of 2400 and 2640 reported recently [21]) is confirmed. New weak transitions of 1860±20, 1630±20, 1530±20, 860±20 and 760±20 have been resolved. The peak at 2100 keV appears to be double since it is rather wide for a single one. It was therefore compared with the single peak in ^{38}K of nearly the same energy (2160 keV). The peak could be resolved into two

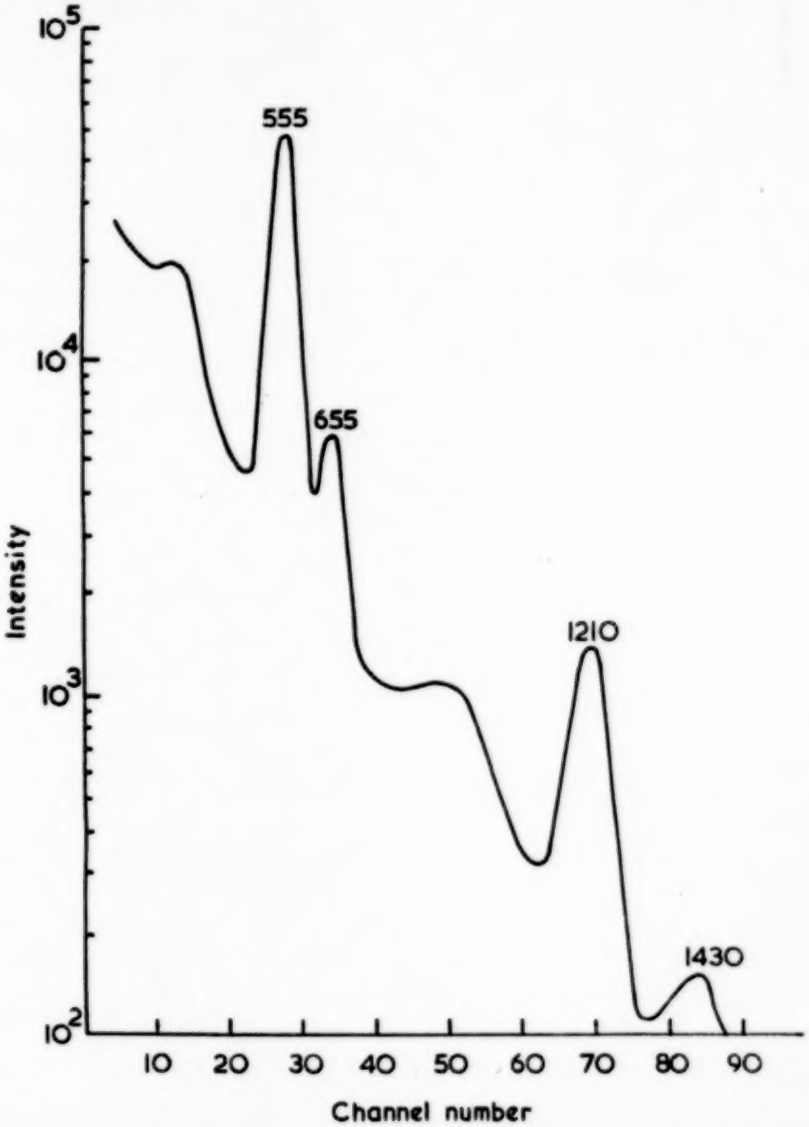

Fig. 1. Gamma ray spectrum of ^{76}As in the region from 300 to 1500 keV as measured with a 1″ NaI(Tl) crystal.

components of 2110 and 2080 keV. The error in estimating the relative intensity of each peak is relatively large, since it is difficult to attain high precision in such a procedure when the energy values of the two components are close.

The existence of the 1770 keV gamma ray together with the reported negaton group of about 1200 keV [14, 20]) indicates the presence of a level in ^{76}Se at 1770

keV, which may be the origin of transitions to the well known levels at 560 and 1210 keV. These transitions would have values of 1210 keV and 560 keV which coincide exactly with the values of the transitions from the first and second levels in ^{76}Se. This renders the detection of these gamma rays from the direct spectrum impossible. In order to clear up this situation, coincidence measurements were undertaken.

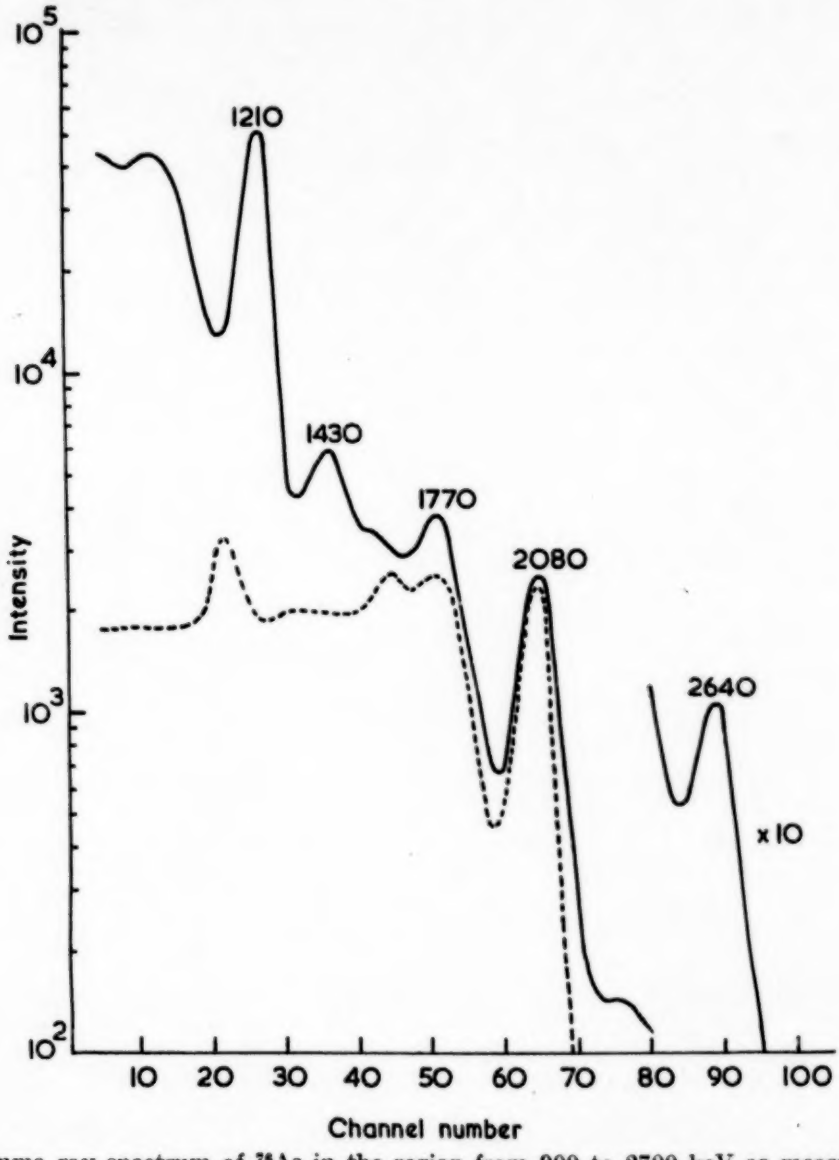

Fig. 2. Gamma ray spectrum of ^{76}As in the region from 900 to 2700 keV as measured with a 1″ NaI(Tl) crystal. The dashed line represents the pulse height distribution due to a single gamma ray peak of 2080 keV.

3.2. COINCIDENCE MEASUREMENTS

In order to obtain a preliminary idea about the possible coincidences, a source was examined when inserted inside the hole of the well-type crystal. The source was placed in a tube of copper thick enough to absorb all negatons.

TABLE 1

Energies and relative intensities of the gamma rays from ^{76}As as reported by different groups. The 1210 keV transition has been normalized to 100

Siegbahn [3]) sl pe		Hubert [14]) sl pe		Kurbatov [15]) scin, sl pe		Grigorév [21]) s		Present investigation † scin	
Energy	Int.	Energy	Int.	Energy	Int.	Energy	Int.	Energy	Rel. int.
548	310	555±2	400	549± 4	475			555± 5	770 ±50
		648±2	40	643± 6	95			655± 5	115 ±10
								760±20	7 ± 2
								860±20	7 ± 3
1200	100	1210±5	100	1200± 6	100	1210	100	1210±10	100
		1410±6	6.4	1402±15	9.5	1430	10	1430±10	8.1± 1.0
								1530±20	2.3± 0.5
								1630±20	2 ± 1
1700	13					1760	7	1770±15	5 ± 2
								1860±20	2 ± 1
		2060	24	2053	4.8	2100	14	2080±20	10 ± 2
								2110±30	5 ± 2 } 15±2
						2420	0.6	2410±20	1.0± 0.3
						2650	0.6	2640±15	0.9± 0.3

† No 2280 keV gamma ray (<0.3);
No 1070 keV gamma ray (<2);
Gamma-gamma coincidences:
(555γ)(560, 655, 1210, 2100γ)
(1210γ)(555, 655, 1210, 1430γ)

Fig. 3 shows the spectrum obtained in the energy region from 800 to 3000 keV. The increase in height of the 2640 peak is very evident and checks with the reported coincidence between the 2100 and 560 keV gamma ray, the 2100 keV peak indeed becoming lower. Also, the 1770 keV peak seems to gain in height; this would mean that it comes from a level from which additional cascading gamma transitions originate.

Coincidences were then performed with a conventional fast-slow coincidence set-up with a resolving time: $2\tau = 17\pm3$ ns, a single channel analyzer selecting the gating peak and the coincident spectrum being displayed on the kicksorter. The correct functioning of the apparatus was established using sources of ^{60}Co and ^{22}Na.

The spectrum in coincidence with the 560 keV peak was examined over the whole energy region, that coincident with the 1210 keV peak was studied only below 1.5 MeV. The results obtained are listed in table 1. Figs. 4, 5 and 6 show these coincident spectra. Fig. 4 represents the energy region between 300 and 1400 keV in coincidence with the 560 keV peak. The well known coincidence between the 560 and 650 keV peaks is confirmed. It is certain that a gamma ray of 560±10 keV is in coincidence with the 560 keV transition. Part of the 1210 keV transition is also in coincidence with the 560 keV peak.

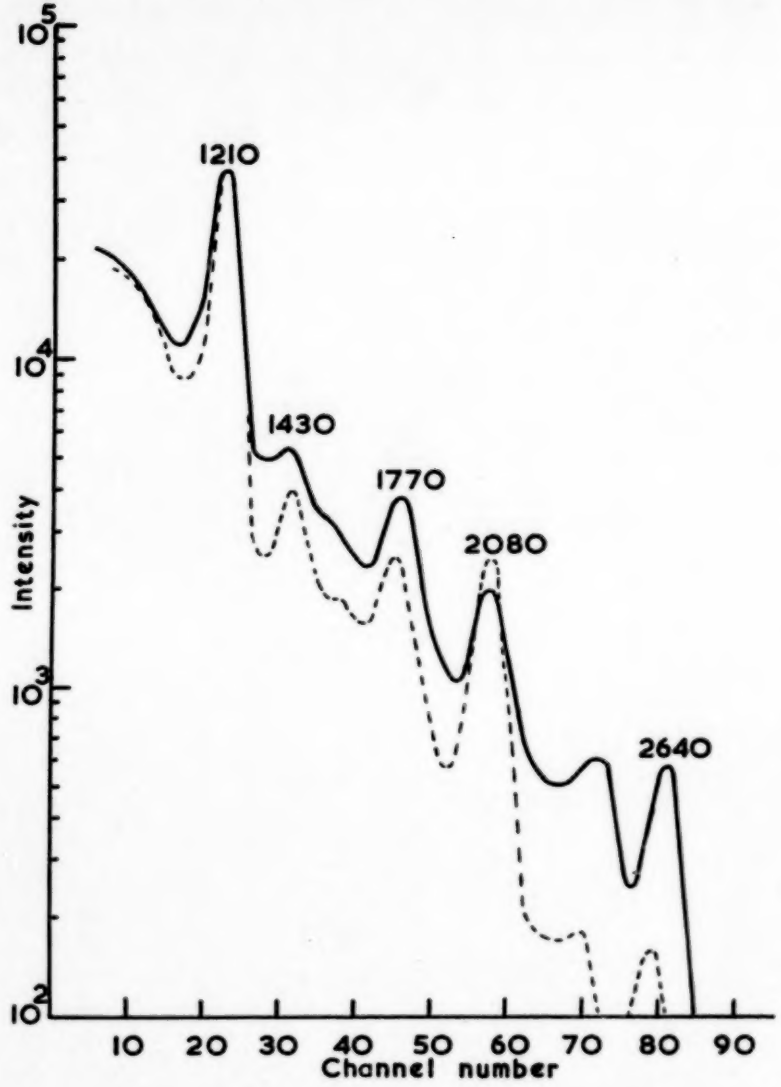

Fig. 3. Gamma ray spectrum of ^{76}As in the region from 800 to 3000 keV (full drawn line) as measured in the well of a $2\frac{1}{2}'' \times 2\frac{1}{2}''$ NaI(Tl) crystal. The spectrum, measured with the same crystal and the source outside the well, is drawn in for comparison (dashed line); the two spectra are arbitrarily normalized at the 1210 keV peak.

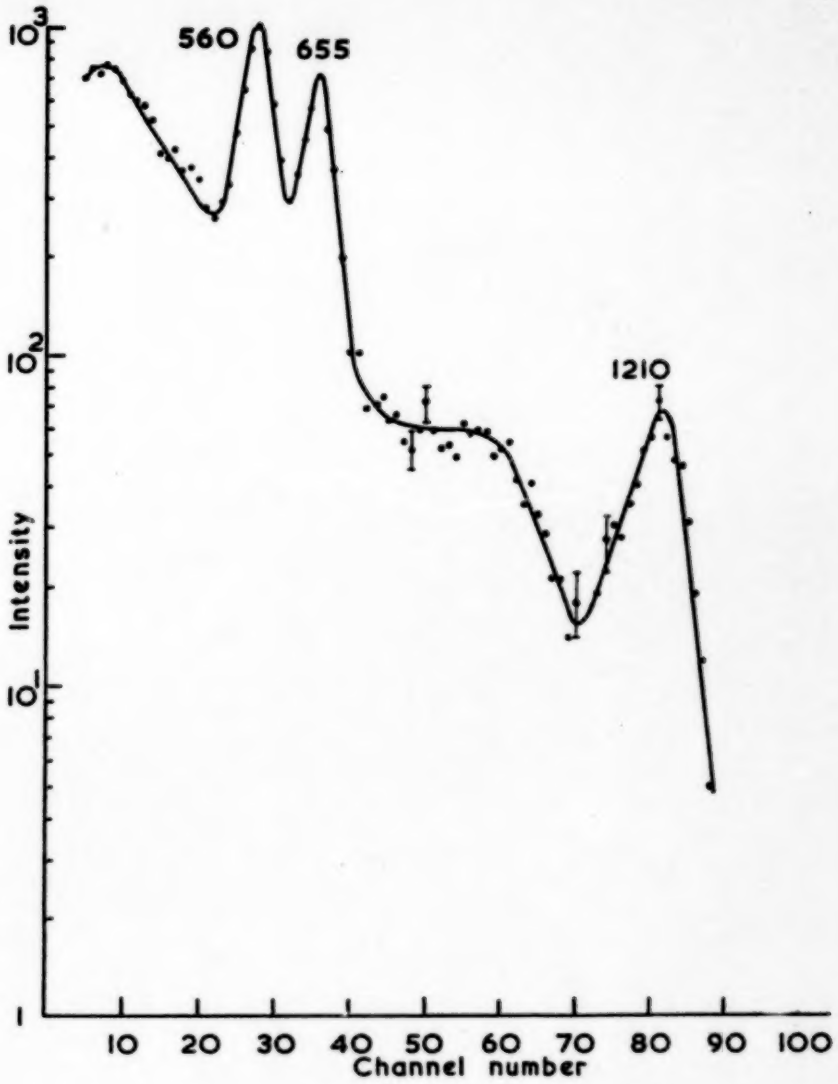

Fig. 4. Spectrum in coincidence with the 555 keV peak; lower region only.

1210 keV peak.

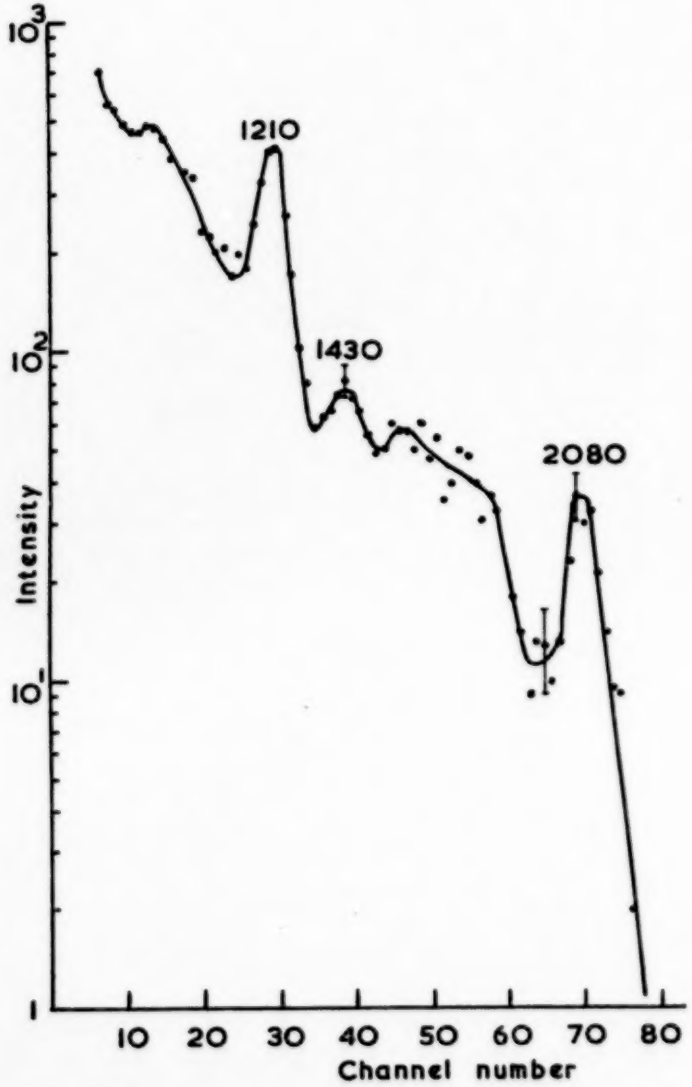

Fig. 5. Spectrum in coincidence with the 555 keV peak; higher region only.

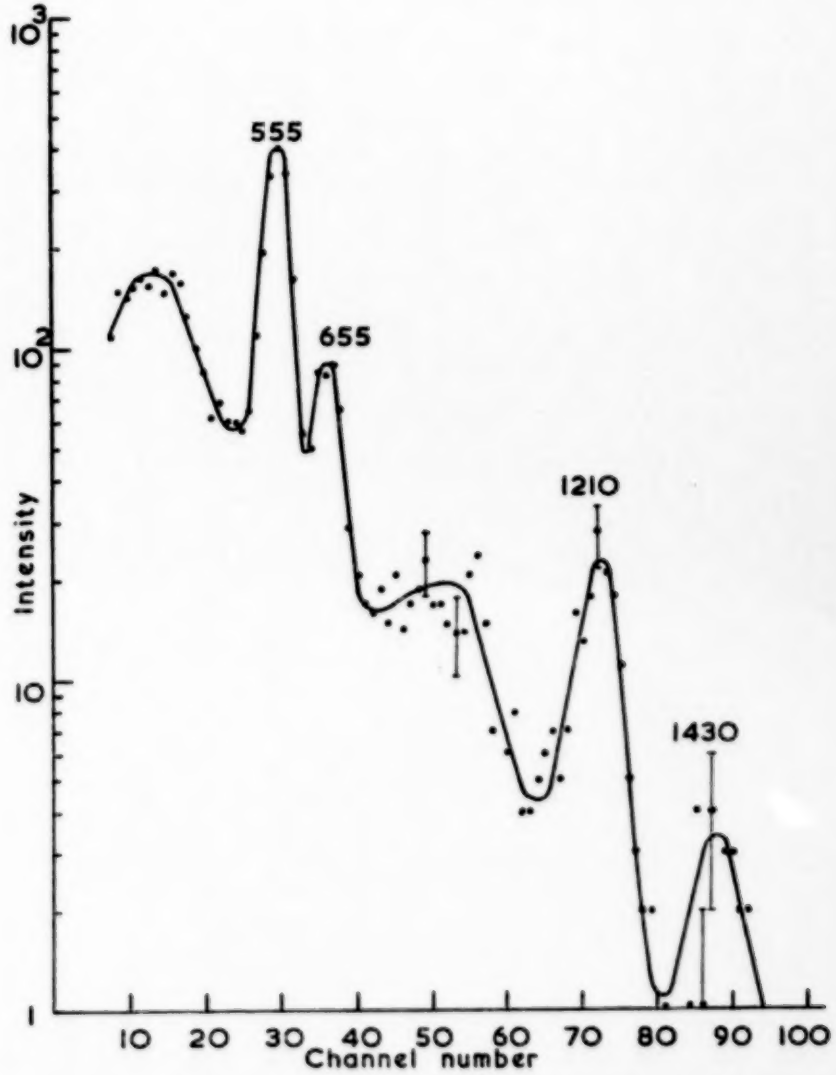

Fig. 6. Spectrum in coincidence with the 1210 keV peak; lower region only.

Selecting the same peak of 560 keV and displaying the higher energy spectrum (fig. 5), the coincidence with the 1210 peak is again established. The reported [15,22]) coincidence with the 2100 keV gamma ray is confirmed, but due to low statistics it is impossible to decide which of the two transitions in this peak is involved in the coincidence. Also it is clear that the 1430 keV gamma ray peak is coincident with the 560 keV peak. Although statistics are low in the region of the 1770 keV gamma ray, it can be seen that this part of the coincidence spectrum is less intense compared with the corresponding part in the direct spectrum, which means that the 1770 keV gamma is a ground state transition originating from a level of the same energy. Fig. 6 shows the low energy region of the spectrum in coincidence with the 1210 keV gamma ray as selected in the single channel. The 560 keV—1210 keV coincidence is again evident. The 650 keV gamma ray is in coincidence with the 1210 keV gamma peak. Also the latter is certainly in coincidence with itself. It must be mentioned that the chance coincidences in all cases were negligible relative to the true coincidences obtained.

4. Discussion

A possible level scheme, accommodating all gamma rays found in this work, is presented in fig. 7. The new levels are proposed from energy matching and coincidence relations. Further information on the level scheme can be derived

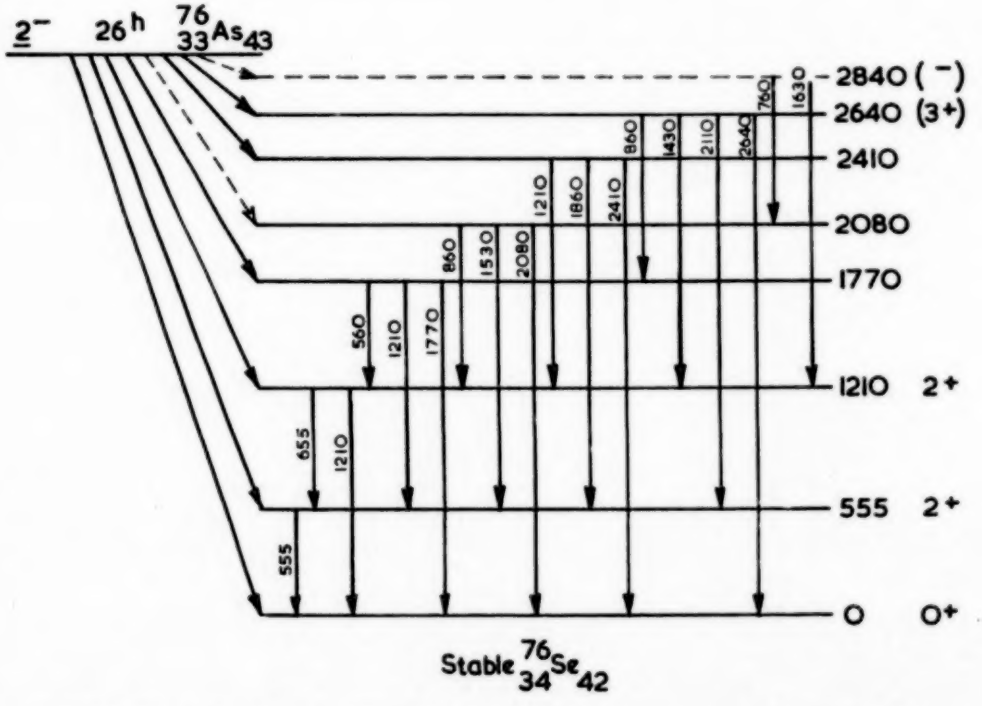

Fig. 7. Tentative level scheme for ^{76}Se as derived from the decay of ^{76}As.

TABLE 2

Energies and relative intensities of the beta ray spectra as reported by various groups

Marty [7]) s		Tomlinson [9]) sd		Hubert [14]) sl		Kurbatov [15]) sl		Kokoszka [20]) s		Grigorév [21]) s	
Energy	Int. %	Energy	Int. %	Energy	Int. %	Energy	Int. %	Energy	Int. %	Energy	Int. %
400	7	480	3	350	3	360	3	360		350	4
										880	3
1500	19			1200	6			≈1200			
		1760	12	1750	6	1760	16	1760		1760	7
2570	21	2400	33	2400	32	2410	31	2410		2410	28
3150	53	2980±10 †	52	2960±10 †	53	2965±10 †	50	2970		2960	58

† $\Delta J = 2$, yes shape.

from table 2, which gives the results of measurements performed by various groups of the beta ray spectrum.

The ground state spin of ^{76}As has been measured [26, 27]) to be 2; the parity is odd as shown by the unique first forbidden beta transition to the ground state of ^{76}Se. The first and second excited states in ^{76}Se both have spin 2^+; this follows from the angular correlation of the cascading gamma rays from the second excited state [12, 22, 23, 28]). This argument is not invalidated by the fact that the 560 keV peak consists of two transitions, since the additional component is too weak to influence the correlation pattern. The existence of the level at 1770 keV seems to be beyond doubt, as shown by the coincidence measurements; it is probably populated by the reported beta group [14, 20]) of 1200 keV and deexcites to all three levels below it. The level at 2100 keV also populates all three known members of the 0^+, 2^+, 2^+ vibrational band. The reported beta group [21]) of 880 keV would fit here, but its existence is not completely certain. The fact that the 1210 keV peak is in coincidence with itself and with the 650 keV gamma ray, together with the existence of a gamma transition of 2410 keV points to a level at 2410 keV. The weak 1860 keV gamma ray can also originate at the 2410 keV level, although a level at 1860 keV is equally possible.

A weak ground state transition is observed from the well known level at 2640 keV; part of the 860 keV gamma ray also possibly originates at this level in addition to the known 2110 and 1430 keV transitions. Beta-gamma [20]) and gamma-gamma coincidences [15]) and angular correlations [22, 23]) involving this level have been performed. However, in those cases where the 1.20 MeV gamma transition was used as the gating peak by selection of the integral gamma ray spectrum above 1.2 MeV, most of the coincidences must have involved the 1.20—1.20 MeV cascade plus the 1.20—1.40 MeV cascade. Therefore, the conclusions drawn from some of the angular correlation measurements [22, 23]) may have to be revised.

Finally, the level at 2840 keV can certainly be populated, the log *ft*-value being of the order of $5\pm\frac{1}{2}$ for a branch of 130 ± 20 keV and ≈ 0.6 % intensity. The parity would then be odd which might explain the occurrence of gamma transitions (1630 and 760 keV) to some of the higher levels and the absence of the ground state gamma transition. The existence of this level is, however, far less certain than that of the others, since it is based entirely on the energy match of the 760, 860 and 1630 keV gamma rays.

An important conclusion from the work reported above is, that both the 555 and the 1210 keV gamma ray peaks consist of more than one gamma transition. Numerical treatment of the single spectrum and coincidence results yields the fraction of each component in the two peaks; the results are reported in table 3. From this result it follows that the branching ratio of the cross-over to the stop-over gamma transition from the second excited 2^+ level fits very well with the systematic trend for this ratio. Moreover, there is no longer any

difficulty about the total intensity of the beta and gamma transitions to the ground state, since part of the 555 and 1210 keV gamma rays have been placed in other positions.

TABLE 3

Composition of the 555 and 1210 keV gamma peaks

Gamma ray peak			
555 keV		1210 keV	
Origin	Intensity †	Origin	Intensity †
1770→1210	90±30	2400→1210	15±10
555→ 0	680±60	1770→ 555	25±10
		1210→ 0	60±10

† Relative to an intensity of 100 for the composite 1210 keV peak (see table 2). Corrected for the contribution of coincidences with Compton distributions of gamma rays of higher energies.

In order to study the levels of ^{76}Se further, a study was made of the decay of ^{76}Br. The results are reported in the following article [29]), together with a more thorough discussion of the level scheme of ^{76}Se.

After this work was finished an additional study of the decay of ^{76}As was brought to our attention [30]) *. Most of the weak gamma rays reported above were also found by the authors quoted; the agreement in energy and relative intensity is very satisfactory.

The authors would like to thank Prof. Dr. P. C. Gugelot and Prof. Dr. A. H. Wapstra for their interest in this work. They are also indebted to Miss J. C. Kapteijn for performing the chemical separations and to the personnel of the synchro-cyclotron for the irradiations.

This work was performed as part of the research program of the "Stichting voor Fundamenteel Onderzoek der Materie (F.O.M.)", which is financially supported by the "Nederlandse Organisatie voor Zuiver-Wetenschappelijk Onderzoek (Z.W.O.)". One of the authors (R. K. G.) is indebted to the Egyptian Atomic Energy Commission for a grant.

* The authors wish to thank Dr. C. L. McGinnis of the Nuclear Data Project, Washington D.C., for bringing these results to their attention.

References

1) K. Way, R. W. King, C. L. McGinnis and R. van Lieshout, Nuclear Level Schemes A = = 40−A = 92, AEC Report TID−5300, Washington D.C. (1955)

2) L. C. Miller and L. F. Curtiss, Phys. Rev. **70** (1946) 983

3) K. Siegbahn, Arkiv Mat. Astron. Fysik **34A** No. 7 (1947)
4) C. S. Wu, W. W. Havens Jr. and L. J. Rainwater, Phys. Rev. **74** (1948) 1248A, Z2
5) M. Walter, O. Huber and W. Zünti, Helv. Phys. Acta **23** (1950) 697
6) W. Mims and H. Halban, Proc. Phys. Soc. A **64** (1951)311
7) N. Marty, J. Labeyrigue and H. Langevin, Compt. Rend. **228** (1949) 1722; Ann. Phys. **6** (1951) 662
8) J. K. Bair and F. C. Maienschein, Phys. Rev. **81** (1951) 463
9) E. P. Tomlinson and S. L. Ridgway, Phys. Rev. **88** (1952) 170A, 14
10) H. Rose, Phil. Mag. **44** (1953) 739
11) F. R. Metzger and W. B. Todd, J. Franklin Inst. **256** (1953) 277
12) J. J. Kraushaar and M. Goldhaber, Phys. Rev. **89** (1953) 1081
13) D. R. Hamilton, A. Lemonick and F. M. Pipkin, Phys. Rev. **92** (1953) 1191
14) P. Hubert, J. Phys. Radium **12** (1951) 823; Physica **18** (1952) 1129; Ann. Phys. **8** (1953) 662
15) J. D. Kurbatov, B. B. Murray and M. Sakai, Phys. Rev. **98** (1955) 67
16) N. Ryde and B. Andersson, Proc. Phys. Soc. B **68** (1955) 1117
17) C. F. Coleman, Phil. Mag. **46** (1955) 1135
18) A. V. Pohm, R. C. Waddell and E. N. Jensen, Phys. Rev. **101** (1956) 1315
19) G. Bäckstrom, Arkiv Fysik, **11** (1957) 357
20) F. T. Kokoszka, D. R. Cartwright and J. D. Kurbatov, Bull. Am. Phys. Soc. **3** (1958) 207, RA8
21) E. P. Grigorév, L. V. Gustova, A. V. Zolotavin, B. Kratsik, T. V. Poleschuk and O. V. Chubinskii, Vestnik Leningrad Univ., Ser. Fiz. Khim, No. **10** (1957) 37; Physics Abstracts **61** No. 739 (1958)
22) E. G. Funk, Jr. and M. L. Wiedenbeck, Phys. Rev. **109** (1958) 922
23) C. F. Coleman, Nuclear Physics **7** (1958) 488
24) M. Jean and J. Touchard, J. Phys. Radium **19** (1958) 56
25) R. L. Macklin, N. H. Lazar and W. S. Lyon, Phys. Rev. **107** (1957) 504
26) F. M. Pipkin and J. W. Culvahouse, Phys. Rev. **106** (1957) 1102; **109** (1958) 1423
27) R. L. Christensen, H. G. Bennewitz, D. R. Hamilton, J. B. Reynolds and H. H. Stroke, Phys. Rev. **107** (1957) 633
28) T. Lindqvist and I. Marklund, Nuclear Physics **4** (1957) 189
29) R. K. Girgis, R. A. Ricci and R. van Lieshout, Nuclear Physics **13** (1959) 473
30) B. S. Dzhelepov, V. P. Prikhodtseva, A. I. Feoktistov and Iu. V. Khol'nov, Izvest. Akad. Nauk. SSSR; Ser. Fiz. **20** (1956) 1361 (Columbia Technical Transl. p. 1245)

1.E.1:
3.A:4.E

Nuclear Physics **13** (1959) 473—484; © *North-Holland Publishing Co., Amsterdam*
Not to be reproduced by photoprint or microfilm without written permission from the publisher

THE DECAY OF ^{76}Br

R. K. GIRGIS †, R. A. RICCI ††, R. VAN LIESHOUT
Instituut voor kernphysisch Onderzoek, Amsterdam

and

J. KONIJN
Laboratorium voor technische Physica der technische Hogeschool, Delft

Received 3 August 1959

Abstract: The radiations of 16.1 ± 0.2 hour ^{76}Br have been studied with single-crystal and coincidence scintillation spectrometers; beta-gamma coincidences were also studied with a proportional counter-scintillation crystal coincidence spectrometer. Three positon groups of maximum energies (and relative intensities) of 3.68 ± 0.10 (45^{+}), 3.15 ± 0.10(100^{+}) and 1.9 ± 0.2 MeV($< 40^{+}$) were resolved; the ratio of electron capture to positon emission was determined as 0.6 ± 0.2. The 3.68 MeV positon group is a ground state transition, since it is not in coincidence with the 0.56 MeV gamma ray. A total number of 15 gamma rays with energies ranging from 0.56 to 4.42 MeV were resolved (see table 1). For a few selected gamma rays coincidence measurements performed with the proportional counter yielded the relative amount of positons feeding these gamma transitions.

In view of the complexity of the gamma ray spectrum no unambiguous decay scheme for ^{76}Br can be proposed. Some features of the level scheme of ^{76}Se are discussed especially in relation to the results obtained from a separate study of the decay of ^{76}As.

1. Introduction

The nucleide ^{76}Br has been produced by various groups [1, 2]), who applied a variety of production methods. The good agreement between the reported values of the half-life ($\approx$ 16 hours) for this activity, together with the different nuclear reactions employed in the production and the establishment of the genetic relationship [3]) with mass-separated ^{76}Kr, make the assignment of the period to ^{76}Br quite certain. Hollander [4]) reported a value of 3.5 MeV for the maximum energy of the positon spectrum, Fultz and Pool [5]) reported a value of 3.57 MeV. These latter authors also resolved four lower energy groups (1.7, 1.1, 0.8 and 0.6 MeV) and determined their relative intensities. Moreover, they showed that the 3.57 MeV branch is a direct ground state transition. The gamma ray spectrum has been studied by Fultz and Pool [5]) and by Thulin [3]). The two sets of results are in disagreement and neither can be made to match with the positon branches nor with the level scheme of ^{76}Se as deduced [1, 2, 6])

† On leave of absence from the Faculty of Science, University of Cairo, Giza, Egypt, U.A.R.
†† On leave of absence from the Istituto di Fisica Sperimentale del Politecnico, Torino, Italia. Present address: Istituto Nazionale di Fisica Nucleare, Sottosezione di Napoli, Italia.

from the decay of ^{76}As. The relative intensities of the gamma rays are not known.

Recently the spin of the 16 hour ^{76}Br has been measured [7]) to be 1.

In view of the above mentioned disagreements and in order to examine the level scheme of ^{76}Se, a study of the radiations from ^{76}Br was undertaken and a detailed analysis of the gamma ray spectrum was performed.

2. Production and Chemical Procedures

The bromine activity was produced by irradiating arsenic in the form of magnesium pyroarsenate with 50-MeV alpha particles ($\approx 10\mu$Ah) from the synchro-cyclotron. For the beta ray work a carrier free chemical separation was performed. The irradiated target was dissolved in boiling 1*N* nitric acid. Gallium and copper holdback carriers were added as well as 10μg of NaBr. The solution was oxidized with permanganate and the bromine extracted into an equal volume of carbon tetrachloride. This extraction was repeated a number of times and the successive water layers were retained for the non-carrier free procedure.

The bromine in the last CCl_4 fraction was then extracted with a small amount of a 0.1*N* ammonium hydrosulfite solution, again extracted back into CCl_4 and finally evaporated to dryness after addition of a few drops of ammonia.

The various water fractions from the above extraction process were collected and used to obtain a non-carrier free bromine source for the gamma ray work. After addition of 25 mg of NaBr a new extraction into CCl_4 was performed, followed by extraction into a 0.1*N* ammonium hydrosulfite solution. Silver nitrate solution was added, and the precipitate of silver chloride collected on a fine filter and dried with alcohol and ether.

The sources were studied approximately 12 hours after the end of the irradiation in order to reduce the amount of ^{74}Br and ^{75}Br, but soon enough to avoid a large quantity of the 57 hour ^{77}Br in the source.

3. Measurements and Results

3.1. GAMMA RAY SPECTRUM

The gamma rays following the decay of ^{76}Br were studied with a NaI(Tl) crystal of 25 mm diameter by 25 mm height, optically coupled to a 6292 DuMont photomultiplier. The spectrum was displayed on a 100 channel RIDL pulse height analyzer. Figs. 1, 2 and 3 show this spectrum for energy regions between 150 and 1350 keV, between 800 and 3500 keV and between 1800 and 5000 keV respectively. No gamma rays below 150 keV were found to belong to the decay of ^{76}Br, except the X-ray. The decay of this peak was followed for $\approx$ 14 days. Two periods were found, one of 58.0$\pm$0.5 hours,

assigned to the ^{77}Br activity, and a period of 16.1 ± 0.2 hours, assigned to the ^{76}Br activity.

Since the total decay energy of ^{77}Br is known to be 1350 keV, all gamma rays above this energy limit should belong to ^{76}Br. In agreement with this it was

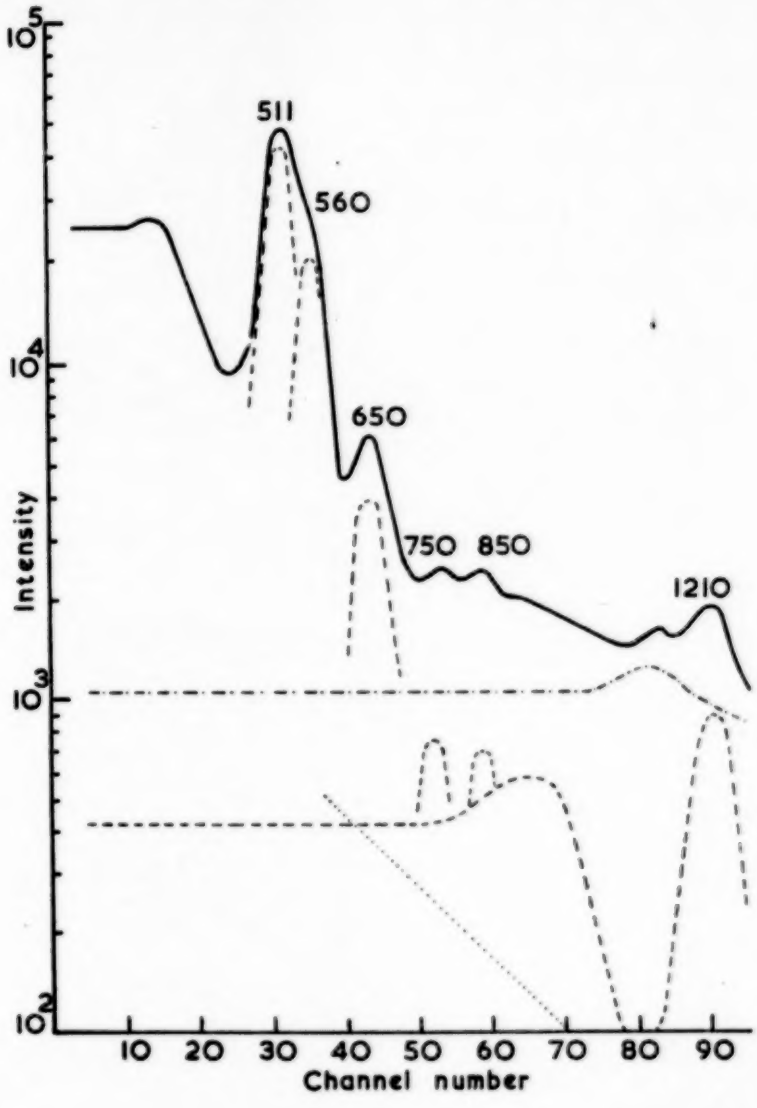

Fig. 1. Gamma ray spectrum of ^{76}Br, as measured with the 1″ NaI(Tl) crystal, in the region from 150 to 1350 keV. The contribution due to annihilation in flight is indicated by the dotted line; the dot-dashed line represents the Compton distribution of the higher energy gamma rays.

found that all gamma ray peaks in the region between 1200 and 4400 keV decayed with the correct ^{76}Br period. In the region below 1200 keV the decay showed both the 58 and 16 hours period. The pulse height distribution due to ^{77}Br was obtained several days after the start of the measurements on ^{76}Br; it was then subtracted from the initial composite spectrum after application of a decay correction.

A detailed analysis of the pulse height distribution of ^{76}Br was undertaken. The contributions due to the background and to annihilation in flight of positons were subtracted from the measured pulse height distribution. The distribution due to pair peaks of high energy gamma rays was taken into account.

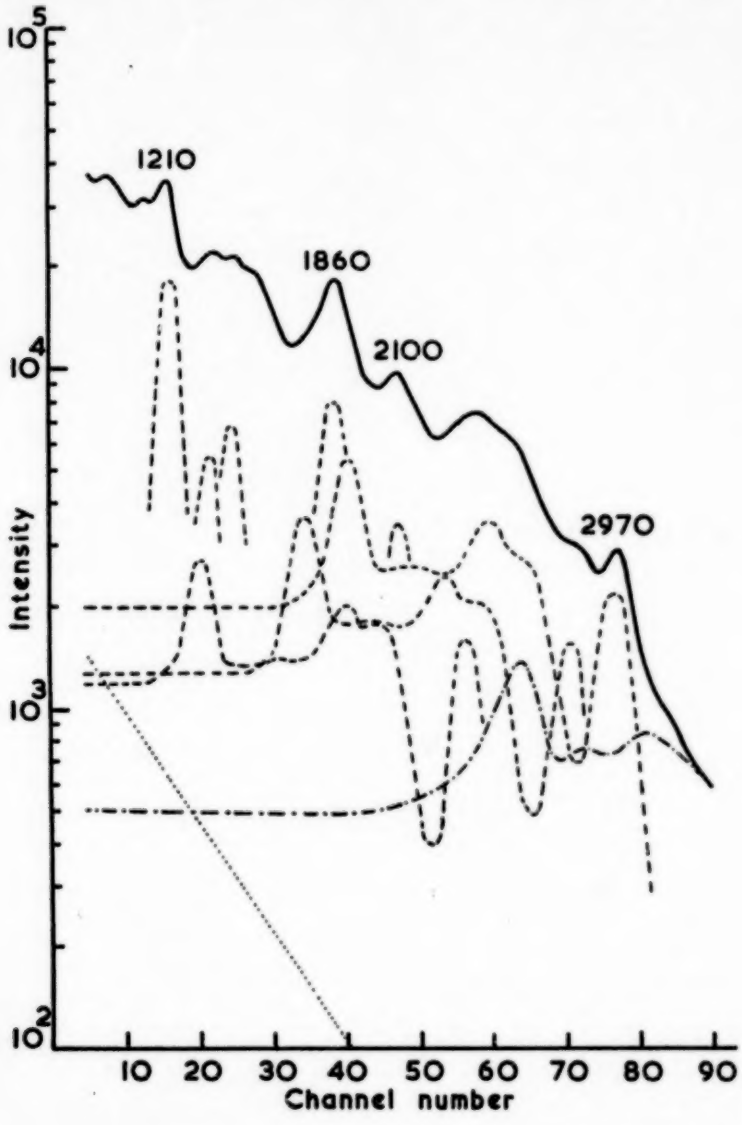

Fig. 2. Gamma ray spectrum of ^{76}Br in the energy region from 800 to 3500 keV. The dotted line represents the annihilation in flight contribution, the dot-dashed line that due to the higher energy gamma rays. The pulse height distribution of some of the resolved gamma transitions has been indicated by the dashed lines.

Where necessary the shapes of the standard peaks were measured using the same aluminium absorbers which were employed to ensure complete annihilation of the positons; appropriate corrections were applied to the relative intensities in this case. Table 1 gives the energies and relative intensities of the gamma rays resolved.

3.2. POSITON SPECTRUM

The positon spectrum was examined with a 4 cm by 1 cm cylindrical stilbene crystal mounted on a 6292 DuMont photomultiplier. The window of the housing of the crystal consisted of an $\approx$ 2.5 mg/cm^2 aluminium foil. The combination was

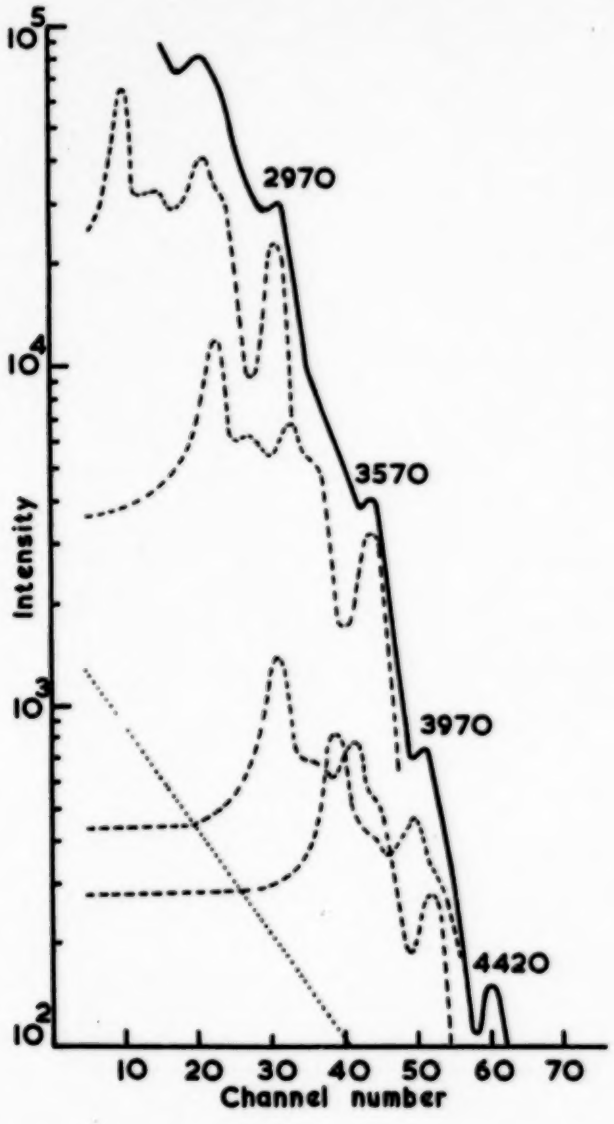

Fig. 3. High energy gamma ray spectrum of ^{76}Br. For explanation see caption of fig. 2.

calibrated for energy using ^{66}Ga (4.15 MeV), ^{76}As (2.97 MeV), ^{32}P (1.71 MeV) and the 0.976 MeV conversion peak in ^{207}Bi. Carrier free sources were prepared for this investigation; they were mounted on thin cellotape backing. Fig. 4 shows the Fermi-Kurie plot. Corrections for resolution effects [8]) were applied. Three positon branches of 3.68$\pm$0.10, 3.15$\pm$0.10 and 1.9$\pm$0.2 MeV could be resolved. Table 2 lists the results of the analysis of the positon spectrum. No branches lower than the 1.9 MeV group were resolved, since the scattering effects below

TABLE 1

Gamma radiation from the decay of ^{76}Br

^{76}Br produced by ^{75}As(50-MeV α, 3n) chem $T_{\frac{1}{2}} = 16.1 \pm 0.2$ hour			
Energy (keV)	Relative intensity	Energy (keV)	Relative intensity
$\gamma^{\pm}$	2 ×100	1860±10	17 ±2
560±10	95 ± 8	2100±20	10 ±1
650± 5	28 ± 2	2390±20	6 ±1
750±20	9 ± 1	2780±20	8.0 ±1.5
850±20	10 ± 1	2970±20	12 ±2
1210±10	19 ± 2	3570±30	3.0 ±0.7
1370±20	7.0 ± 1.5	3970±30	0.2 ±0.1
1470±20	10 ± 2	4420±40	0.07±0.04
Doubtful peaks			
1140±30	4±4		
2600±50	3±3		
No 1530 keV γ	(<3)		
No 1630 keV γ	(<3)		
No 1760 keV γ	(<2)		

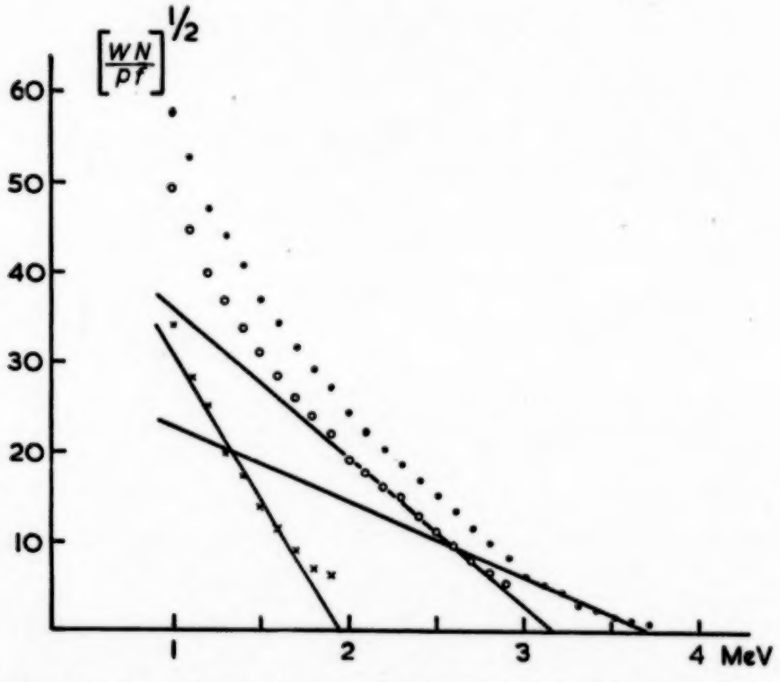

Fig. 4. Fermi-Kurie diagram of the positon spectrum of ^{76}Br.

this energy are expected to distort the spectral shape. The presence of ^{77}Br cannot distort this spectrum since it only has a weak (0.6 %) positon branch of 0.34 MeV maximum energy. The half-life was again confirmed from the decay

of the positons, yielding the same value reported above for the gamma rays.

TABLE 2

Positon groups in the decay of ^{76}Br; beta-gamma coincidence results

Energy (MeV)	Relative intensity
3.68 ± 0.10	45 ± 10
3.15 ± 0.10	100
1.9 ± 0.2	<40
$\varepsilon/\beta^+ = 0.6 \pm 0.2$	
$(0.56\gamma)(3.2\beta^+)$	
No $(0.56\gamma)(3.7\beta^+)$	
$\beta^+(0.65,\ 0.85,\ 1.86\gamma)$	

3.3. BETA-GAMMA COINCIDENCES

In view of the discrepancy between the results of the positon spectrum of this investigation and those of Fultz and Pool [5]) concerning the existence of the

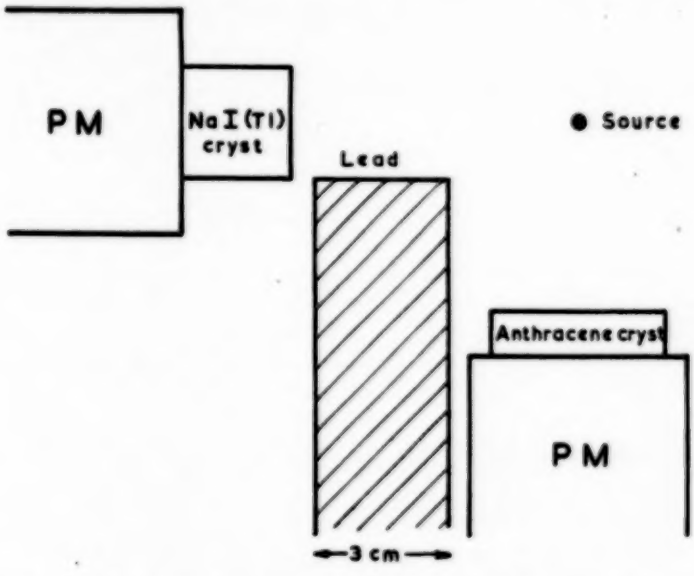

Fig. 5. Geometry and shielding employed to avoid coincidences between positons and annihilation radiation.

second branch of 3.15 MeV, beta-gamma coincidences were examined to make certain that the highest energy positon branch is a ground state transition. A conventional fast-slow coincidence set-up was used for this purpose. The resolving time of this circuit is $2\tau = 17 \pm 3$ nsec. It was used in combination with a single channel pulse height selector.

The 560 keV peak in the gamma ray spectrum of ^{76}Br was selected in the single channel, and the positon spectrum was displayed on the 100 channel pulse height analyzer. Since this 560 keV gamma ray in the spectrum partially

overlaps with the annihilation peak, the correct transition was selected by using an ^{76}As source which has the same strong gamma ray of 560 keV. To avoid coincidence between the 511 keV annihilation peak and the positon spectrum, the geometry shown in fig. 5 was adopted.

The Fermi-Kurie plot of the coincident positon spectrum yields a maximum energy of 3.20±0.15 MeV, thus confirming the results obtained by Fultz and Pool [5]), that the highest branch present in the total positon spectrum is a ground state transition.

Further coincidence experiments were performed in which the gamma ray was detected with a 2″ by 2″ NaI(Tl) crystal and the positons (and X rays) were measured with a proportional counter † filled with krypton with a 10 % ethane admixture under a pressure of 500—600 mm Hg. By selecting a gamma ray peak in the scintillator and measuring its intensity (N_γ) in the direct spectrum and also in coincidence with the total positon spectrum registered in the proportional counter ($N_{\beta\gamma}$), the fraction (p^+) of positons in coincidence with the selected gamma ray can be obtained:

$$p^+ = N_{\beta\gamma}/N_\gamma \Omega^+$$

where Ω^+ is the solid angle in which the positons are detected by the proportional counter. In this manner it was found that the 650 keV gamma ray was in coincidence with positons for (39±3)% due to feeding of the level by positons directly or through gamma rays which are also in coincidence with positons, the rest of the feeding (61±3)%, thus being due to electron capture. For the 850 keV peak this fraction was (55±16)% and (38±5)% for the 1860 keV transition.

3.4. ELECTRON CAPTURE TO POSITON RATIO

In the proportional counter the K X-ray is easily discernible above the continuous positon distribution. The capture to positon ratio can be calculated from the relative intensity of the two components and was found to be:

$$\varepsilon/\beta^+ = 0.6 \pm 0.2$$

a value which disagrees with that of Fultz and Pool [5]). Corrections for fluorescent yield and for capture from higher shells were applied [10]). The contribution of ^{77}Br to the K X-ray peak was determined and subtracted.

4. Discussion

None of the gamma rays with energy above 1300 keV observed in this work have been reported before, with the exception of the 1.86 MeV peak. This latter peak was observed by Thulin [3]), who reported a half-life of ≈ 30 hours for it. An accurate check of its period in this work showed that it decays with exactly

† This experimental arrangement has been developed [9]) at the Technical University, Delft.

the same half-life as the rest of the spectrum above 1300 keV. Some of the gamma rays between 0.5 and 1.3 MeV were also reported by Thulin [3]) and by Fultz and Pool [5]), but according to the results reported in table 1 there are no gamma rays below 0.5 MeV in the decay of ^{76}Br. The energy of the ground state positon branch agrees well with the value reported by Fultz and Pool [5]), although the branch to the first excited state of ^{76}Se listed in table 2 has not been observed by others.

A number of levels in ^{76}Se has been established with certainty from the decay of ^{76}As (for a review, see the preceding article [6])).

The two strongest gamma rays of 560 and 650 keV can therefore be placed unambiguously between the ground state, first and second excited states respectively. The 1210 keV peak originates mainly at the second excited 2^+ state ($\approx \frac{4}{5}$) as derived from the known branching ratio from ^{76}As. The rest might originate from levels at 1770 and 2410 keV. The first possibility must be excluded since there is no accompanying 1770 keV gamma ray in the decay of ^{76}Br. Therefore part of the 1210 keV peak ($\approx \frac{1}{5}$) has been placed between the 2410 and 1210 keV levels. The strong 1860 keV transition can only for a very small part occur between the 2410 keV level and the first excited state, as can be concluded from the known branching ratio of the 2410, 1850 and 1210 keV transitions from this level in the decay of ^{76}As. (This also proves that the major part of the 2410 keV transition does not originate at the 2410 keV level.) The major part of the 1860 keV gamma ray must come from another level, which cannot lie above 2.8 MeV, since otherwise the positon branch feeding it would become too weak relative to the capture branch to explain the coincidence results reported in section 3.3. Barring the possibility that the 2410 keV level consists of a close doublet, this leaves only a level at 1860 keV as origin of a gamma ray transition of this same energy. The 1.9 ± 0.2 MeV positon branch then probably goes to this level.

The 850 keV gamma ray is for a large part fed by positons (55 ± 16 %, see 3.3); this indicates that the 850 keV gamma transition cannot originate at a level above 2.7 MeV. It has therefore been assumed to originate at the 2.10 MeV level (although it cannot be excluded that this gamma ray originates at an even lower level in ^{76}Se).

The level at 2640 keV in ^{76}Se does not seem to be fed from ^{76}Br, because there is no gamma ray of 2640 keV, nor of 1430 keV in the decay of ^{76}Br. A spin 3 has been proposed for this level and this would explain the absence of a positon branch; on the other hand the spin assignment for the 2460 keV level has become somewhat doubtful in view of the results on ^{76}As reported in the preceding paper [6]). The level at 2840 keV, proposed from the ^{76}As results, also seems to be populated from the side of ^{76}Br. The absence of a 1630 keV gamma transition, in the ^{76}Br decay, which has been assumed to originate at the 2840 keV level as deduced from the ^{76}As decay, is no argument to the contrary, since

its intensity should be so low that it is completely hidden by the strong neighbouring gamma rays. A level at 3570 keV is proposed, since it would explain

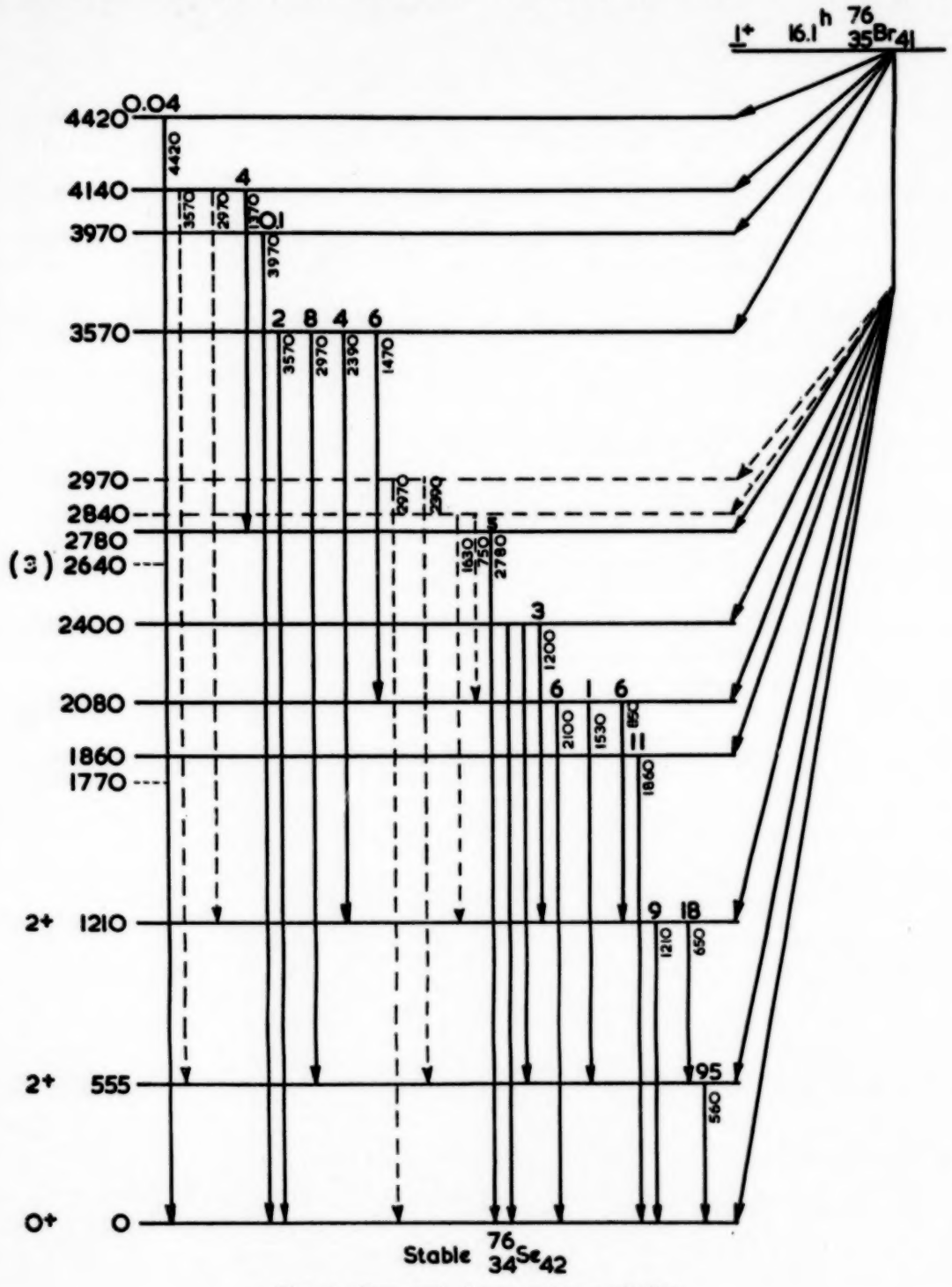

Fig. 6. Proposed decay scheme of ^{76}Br.

the gamma rays of 3570, 2970, 2390 and 1470 keV. The other levels in ^{76}Se are proposed to accommodate the rest of the gamma rays.

It should be emphasized that the proposed decay scheme (fig. 6) is very tentative. The complexity of the gamma ray spectrum of ^{76}Br makes an unambiguous interpretation difficult. Some of the features discussed above seem, however, rather well established.

The intensity of the various beta branches can be calculated on the basis of the decay scheme and the gamma ray intensities. Energy values, intensities and log *ft*-values for each of the branches are collected in table 3. The large error on

TABLE 3

Energy and intensity values of the positon and electron capture branches, calculated from the adopted decay scheme

Level (MeV)	E_ε (MeV)	Population (% per disint) †		log *ft*
		ε	β^+	
4.42	0.28	0.044±0.025	–	7.0±0.4
4.14	0.56	4.4 ±1.0	–	5.7±0.1
3.97	0.73	0.13 ±0.06	–	7.2±0.4
3.57	1.13	20 ±2	–	5.5±0.1
2.84	1.86	4.8 ±0.7	2.2±0.3	6.4±0.1
2.78	1.92	–	–	–
2.40	2.30	≈1	≈2	≈7
2.08	2.62	≈0.5	≈1.5	≈8
1.860	2.84	1.5 ±0.3	8.5±1.0	7.3±0.2
1.210	3.49	1.1 ±0.7	11.5±4.0	7.9±0.2
0.555	4.15	–	33 ±6	7.8±0.1
g.s.	4.70	–	8 ±8	≧8.3

† Total intensity ($\varepsilon+\beta^+$) calculated from gamma-ray balance; ε/β^+ calculated from theory for allowed transitions.

the intensity of the ground state positon branch is due to the accumulation of the errors on the intensity of all other positon branches.

The spin of ^{76}Br can be explained on the basis of shell model assignments of $p_{\frac{3}{2}}$ for the 35th proton and $p_{\frac{1}{2}}$ for the 41st neutron. The parity of the ground state of ^{76}Br is then even. From this it follows that the allowed positon transition between the ground states is appreciably slowed down.

The authors would like to thank Prof. Dr. P. C. Gugelot, Prof. Dr. A. H. W. Aten Jr. and Prof. Dr. A. H. Wapstra for their interest in this work. They are indebted to the cyclotron personnel for performing the various irradiations and to Mrs. A. Funke-Klopper for the chemical separations.

This work was performed as part of the research program of the "Stichting voor Fundamenteel Onderzoek der Materie (F.O.M.)", which is financially supported by the "Nederlandse Organisatie voor Zuiver-Wetenschappelijk Onderzoek (Z.W.O.)". One of the authors (R. K. G.) is indebted to the Egyptian Atomic Energy Commission for a grant.

References

1) K. Way, R. W. King, C. L. McGinnis and R. van Lieshout, Nuclear Level Schemes $A = 40-A = 92$; AEC Report TID-5300 (Washington D.C. 1955)
2) D. Strominger, J. M. Hollander and G. T. Seaborg, Table of Isotopes, Revs. Mod. Phys. **30** (1958) 585
3) S. Thulin, Arkiv Fysik **9** (1955) 137
4) J. M. Hollander, UCRL-1396 (1951)
5) S. C. Fultz and M. L. Pool, Phys. Rev. **86** (1952) 347
6) R. K. Girgis, R. A. Ricci and R. van Lieshout, Nuclear Physics **13** (1959) 461
7) T. M. Green, H. L. Garvin and E. Lipworth, Bull. Am. Phys. Soc. **3** (1958) 318, E6
8) M. S. Freedman, T. B. Novey, F. T. Porter and F. Wagner Jr., Revs. Sci. Instr. **27** (1956) 716
9) H. L. Hagedoorn, Thesis Technical University, Delft (1958);
H. L. Hagedoorn and J. Konijn, Physica **23** (1957) 1069
10) A. H. Wapstra, G. J. Nijgh and R. van Lieshout, Nuclear Spectroscopy Tables (North Holland Publishing Company, Amsterdam, 1959)

1.E.1:
3.A:4.E

Nuclear Physics **13** (1959) 485—492; © *North-Holland Publishing Co., Amsterdam*
Not to be reproduced by photoprint or microfilm without written permission from the publisher

GAMMA RADIATION FROM ^{77}Br

R. K. GIRGIS †, R. A. RICCI †† and R. VAN LIESHOUT
Instituut voor kernphysisch Onderzoek, Amsterdam

Received 3 August 1959

Abstract: The gamma ray spectrum emitted in the decay of ^{77}Br was studied with a scintillation spectrometer. Energy values and relative intensities of the various gamma rays were determined (see table 2). In addition to gamma transitions known from other studies on the decay of ^{77}Br, three new weak gamma rays were found. These have energies of 200 ± 10, 380 ± 10 and 450 ± 10 keV and involve a level at 455 keV in ^{77}Se known from Coulomb excitation experiments. A decay scheme is proposed (fig. 3) and log *ft*-values for the various capture branches are calculated (table 3).

1. Introduction

The gamma rays following the decay of ^{77}Br have been studied by Canada and Mitchell [1]), by Fultz and Pool [2]) and by Bunker, Prestwood and Starner [3]). There is good agreement among these three groups with respect to the energy values of a number of the gamma rays [4]). Only Canada *et al.* [1]) roughly estimated relative intensities for the various gamma rays.

Some of the levels in ^{77}Se, known from the ^{77}Br decay, are also populated from the side of ^{77}As; further information on the deexcitation of levels in ^{77}Se has been derived from Coulomb excitation results [5, 6]).

A level scheme for ^{77}Se, consistent with most of the experimental data, has been proposed [4]). However, a few discrepancies still remain. For instance, the level at 245 keV is supposed to decay either directly to the ground state or by an 86 keV transition to the 17.5 sec isomeric state of ^{77}Se at 160 keV. The relative intensities of the 245 and 86 keV transitions, as obtained from the three independent modes of excitation of the 245 keV level, are, however, reported to be different (see table 1). This would strengthen the conjecture by Temmer and Heydenburg [5]) that the 86 keV transition does not lead to the 160 keV level, although these authors did not detect any other gamma ray going to the isomeric state. The level at 457 keV, known from Coulomb excitation experiments [5, 6]), has not been reported in the decay of ^{77}Br or ^{77}As, although the proposed spin of $\frac{5}{2}^-$ for the 457 keV level makes direct population by beta branches possible.

† On leave of absence from the Faculty of Science, University of Cairo, Giza, Egypt, U.A.R.
†† On leave of absence from the Istituto di Fisica Sperimentale del Politecnico, Torino, Italia. Present address: Istituto Nazionale di Fisica Nucleare, Sottosezione di Napoli, Italia.

TABLE 1

Energy values and relative intensities of some of the gamma transitions in ^{77}Se as reported by different groups †

^{77}As												^{77}Se		^{77}Br	
Saraf [8] scin		Bunker [3] scin		Reynolds [9] scin		Rasetti [10] scin		Langevin [11] scin		Bisi [12] scin		Temmer [5] scin		Canada [1] sl pe, ce	
32		23, 28	0.93	33	?										
87	15.1	86	13.3			88	12.2	86	5.2± 2.8	86	11	86	≈2		
160	4.9	160	6.7			155	≈8.7	160	10.4± 2.9	161	5	160	≈1	160	3
247	100	246	100	250	100	245	100	245	100	243	100	244	100	237	100
270	1.8	283	<0.7							284	<0.4			284	1
														298	1.3
520	30.1	523	33.3	530	35.7	528	30.4	525	32±10	525	31			520	500

† For each author the first column gives the energy of the gamma ray in keV, the second column the photon-intensity, normalized to 100 for the 245 keV transition.

The ^{77}Br activity was always produced in the sources prepared by 50-MeV alpha bombardment of ^{75}As, which sources were used mainly for the study [7]) of ^{76}Br. It was thought interesting to report the main features of the ^{77}Br spectrum as obtained from these sources.

2. Measurements and Results

The gamma ray spectrum was studied with the same apparatus and experimental technique described in the preceding article [7]). Figs. 1 and 2 show the

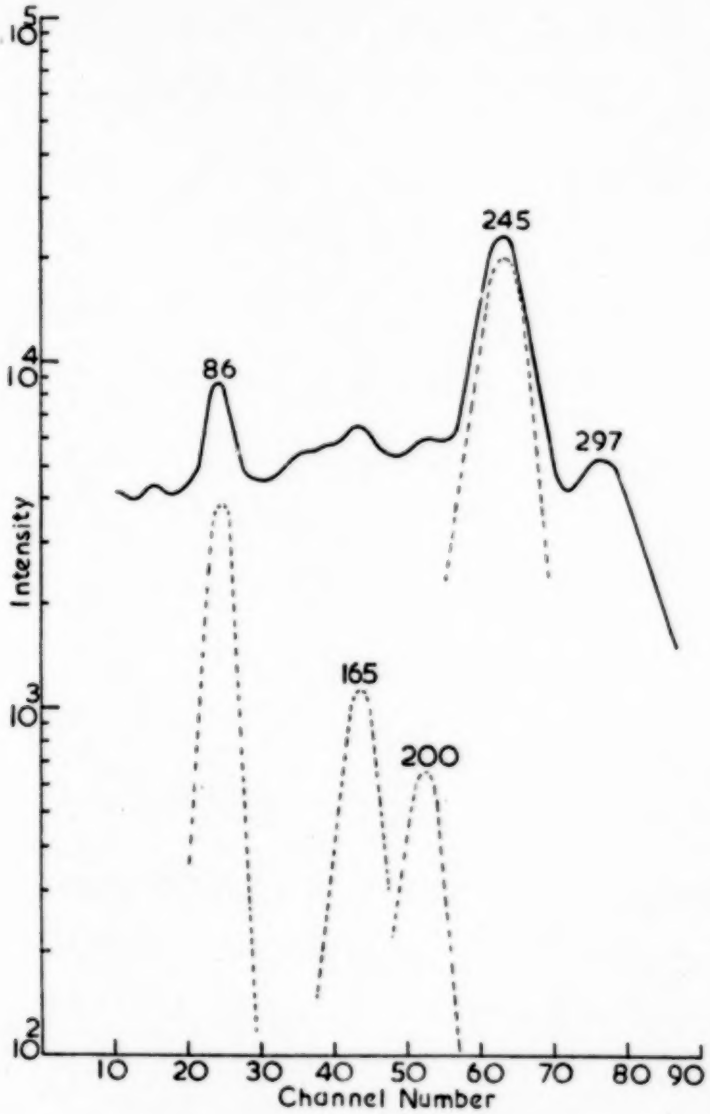

Fig. 1. Gamma ray spectrum from ^{77}Br; lower energy region.

pulse height distributions obtained in two energy regions. Table 2 presents the energy values and the relative intensities for the various gamma ray peaks, normalized to 100 for the 245 keV peak. New gamma rays of 200 ± 10, 380 ± 10

and 450±10 keV were found. The presence of the 86 keV line in the decay of ^{77}Br was confirmed (see fig. 1). The doubtful 23 keV gamma ray, reported in both the decays of ^{77}As and ^{77}Br, was not found. As a check, the low energy part of the spectrum was also measured with a thin (2 mm) NaI(Tl) crystal covered with a beryllium window; the K X-rays of Se were easily seen, but the 23 keV peak was not discernible above background. The whole spectrum decays with a half-life of 58.0±0.5 hours.

A well-type NaI(Tl) crystal mounted on a DuMont 6363 photomultiplier

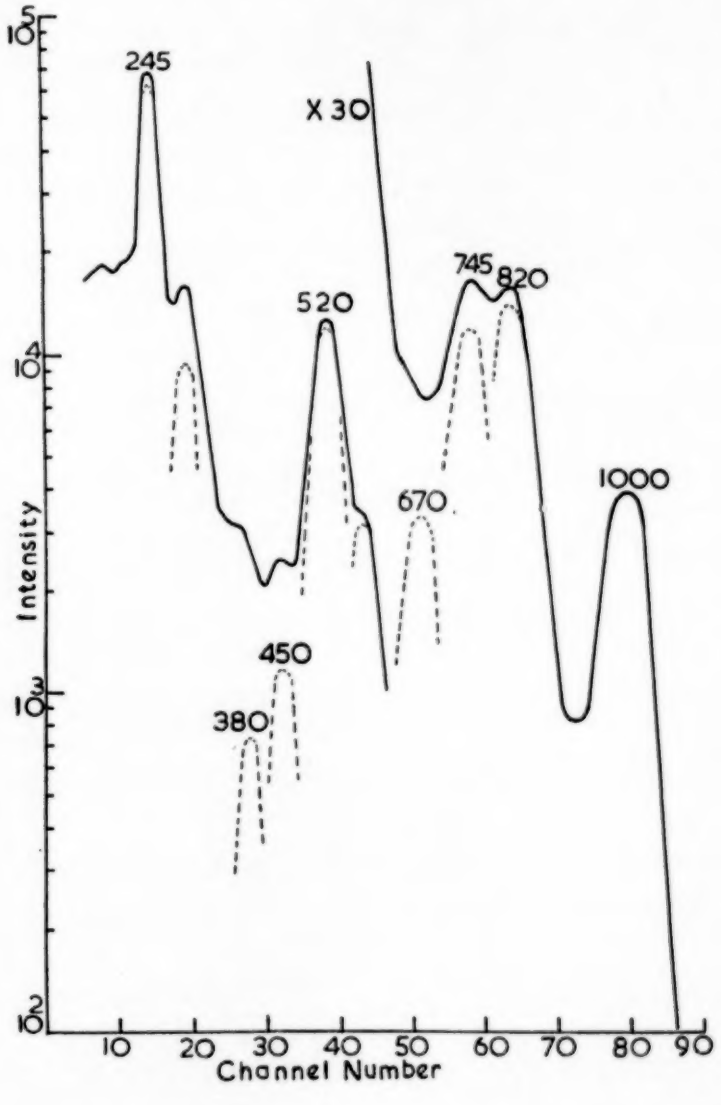

Fig. 2. Gamma ray spectrum from ^{77}Br; higher energy region.

was used to search for strong gamma-gamma coincidences by means of the summing technique. The crystal has 62×62 mm size, the well is 31 mm deep and 9 mm wide. The peaks at 820 and 1000 keV increased strongly relative to

TABLE 2

Energy values and relative intensities of the gamma rays in the decay of ^{77}Br

Energy (keV)				Assumed multipol.	Relative intensities	
Canada [1]	Fultz [2]	Bunker [3]	This work		photons (this work)	total
		86	86± 3	M2	4.5±2.0	12 ±5
160±1	160±3	160	165± 5	E3	3.0±1.5	6.5±3.5
			200±10	M1, E2	2.2±1.0	2.2±1.0
237±2	234±3	246	245± 5	M1, E2	100	103
298±3	299±3	300	297± 5		22 ±3	22 ±3
			380±10		2.1±1.0	2.1±1.0
			450±10		5.6±2.0	5.6±2.0
520±2	521±4	524	520± 5		74 ±6	74 ±6
		580	575±10		24 ±3	24 ±3
641±3		No 641	670±20		1.1±0.5	1.1±0.5
		760	750±10		5.4±1.0	5.4±1.0
813±5		820	820±10		7.5±1.0	7.5±1.0
		1000	1000±20		3.0±1.0	3.0±1.0
284±3		23?	(23)		<0.5	absent

the others when the source was placed inside the well, thus confirming the existence of levels with these energies, deexciting by cascading gamma transitions.

3. Discussion

The gamma ray energies determined in this work agree very well with those reported earlier [1, 2, 3]. All gamma rays reported by Bunker *et al.* [3] are confirmed, whereas the absence of the doubtful gamma ray at 23 keV seems well established. The additional gamma rays listed in table 2 can be incorporated quite easily into the level scheme for ^{77}Se shown in fig. 3. The 450 and 200 keV gamma rays undoubtedly originate at the level at 457±5 keV, first found in Coulomb excitation experiments [5, 6]. The equality of the relative intensities of these two gamma rays, both in the decay of ^{77}Br and from Coulomb excitation is a strong argument for the correctness of this interpretation. The 380 keV gamma ray can populate this same level of 457 keV; it can also be placed between the 520 and 160 keV levels, but even the fastest transition possible between these two latter states (E1 or M2) would probably be undetectably weak. The weak 670 keV gamma ray has tentatively been placed between the 820 and 160 keV levels, making this an E1 or M2 transition; the branching ratio from the 820 keV level is not in disagreement with empirical data on M2 transition probabilities [13]. A 284 keV line could not be resolved from the strong 297 and 245 keV

lines; therefore nothing can be said about the possible existence of the 284 keV transition.

The dilemma about the deexcitation of the 245 keV level still cannot be

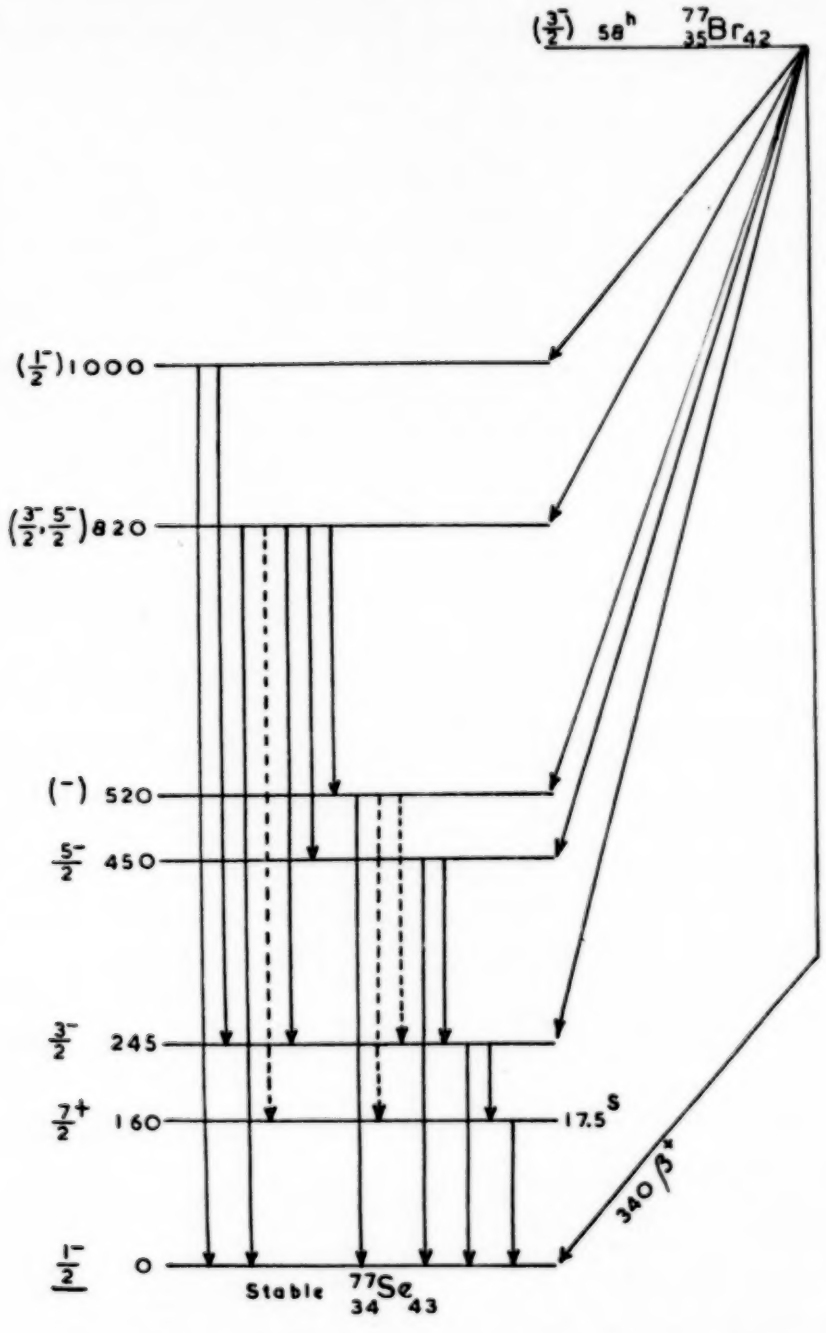

Fig. 3. Proposed level scheme of ^{77}Se; for intensities of the gamma rays and capture branches, see table 2 and 3.

resolved from this work. First of all it must be remarked that the total intensities of the 86 keV and 245 keV transitions (i.e. after applying a correction for

internal conversion assuming an M2 (86 keV) and E3 (160 keV) transition) are the same within the rather wide error limits (see table 2). Moreover, there is no other gamma transition having the correct intensity to be responsible for population of the 160 keV level. This strongly suggests that the 86 and 160 keV transitions, are directly in cascade. However, as Temmer *et al.*[5]) pointed out, the branching ratio of the 86 keV gamma ray relative to the 245 keV transition is far too high to be compatible with the multipolarities following from the adopted spin values for the lower levels. A change of these spin assignments would lead to other difficulties [5]). It is therefore still not excluded that the 86 keV line does not originate at the 245 keV level. The non-constancy of the 86 keV to 245 keV intensity ratio would also point in this direction. However, the present authors do not consider this point well established. In fact the 86 keV and 160 keV lines are very weak ones in the decay of ^{77}As and ^{77}Br. In this energy region the continuous gamma spectrum due to background and "noise" effects begins to make an important contribution to the total gamma intensity. This has been shown, for instance, in the work of Langevin [11]) on ^{77}As. It will therefore be rather difficult to obtain reliable estimates of the relative intensities of the lower energy gamma rays.

A further study of the level scheme of ^{77}Se, especially with coincidence and angular correlation techniques seems certainly interesting.

Canada *et al.* [1]) report a positon branch in the decay of ^{77}Br to the ground state of ^{77}Se with an energy of 336 keV; according to Sehr [14]) the K-capture branch to the ground state comprises 38 % of the total amount of K-capture. Adopting these values, the energies of the various capture branches to the different levels in ^{77}Se can be calculated; their intensities follow from those of the gamma transitions between the levels. These data, together with the log *ft*-values are listed in table 3. In these calculations it has been assumed that the 520 keV peak originates entirely at the 520 keV level and not from a transition between the 1000 and 520 keV levels.

TABLE 3

Intensities and log *ft*-values for the various capture branches of ^{77}Br

Level (MeV)	E_ε (MeV)	Intensity (% per dis.)	log *ft*
1.00	0.36	2.6±0.5	5.7
0.82	0.54	18 ±2	5.2
0.52	0.84	16 ±2	5.6
0.45	0.91	1.7±0.8	6.6±0.2
0.25	1.11	23 ±4	5.8
0.16	1.20	—	—
g.s.	1.36	(39)	5.5

The authors would like to thank Prof. Dr. P. C. Gugelot and Prof. Dr. A. H. Wapstra for their interest in this work, Mrs. A Funke-Klopper for the chemical separations and the personnel of the synchro-cyclotron for the irradiations. This work was performed as part of the research program of the "Stichting voor Fundamenteel Onderzoek der Materie (F.O.M.)", which is financially supported by the "Nederlandse Organisatie voor Zuiver-Wetenschappelijk Onderzoek (Z.W.O.)". One of the authors (R. K. G.) is indebted to the Egyptian Atomic Energy Commission for a grant.

References

1) R. Canada and A. C. G. Mitchell, Phys. Rev. **83** (1951) 955
2) S. C. Fultz and M. L. Pool, Phys. Rev. **86** (1952) 347
3) M. E. Bunker, R. J. Prestwood and J. W. Starner, Phys. Rev. **91** (1953) 1021
4) K. Way, R. W. King, C. L. McGinnis and R. van Lieshout, Nuclear Level Schemes $A = 40$ to $A = 92$,U.S. Atomic Energy Commission Report TID-5300 (U.S. Government Printing Office, Washington D.C., 1955)
5) G. M. Temmer and N. P. Heydenburg, Phys. Rev. **104** (1956) 967
6) D. G. Alkhazov, D. S. Andreyev, A. P. Greenberg and I. Kh. Lemberg, Nuclear Physics **2** (1956) 65
7) R. K. Girgis, A. A. Ricci, R. van Lieshout and J. Konijn, Nuclear Physics **13** (1959) 473
8) B. L. Saraf, J. Varma and C. E. Mandeville, Phys. Rev. **91** (1953) 1216
9) S. A. Reynolds, G. W. Leddicotte and H. A. Mahlman, Phys. Rev. **19** (1953) 333
10) F. Rasetti and E. C. Booth, Phys. Rev. **91** (1953) 1192
11) H. Langevin, Journal phys. radium **16** (1955) 238
12) A. Bisi, E. Germagnoli, L. Zappa and E. Zimmer, Nuovo Cimento **2** (1955) 290
13) A. W. Schardt, Phys. Rev. **108** (1957) 398
14) R. Sehr, Z. Phys. **137** (1954) 523

1.E.1:3.A:
4.E

Nuclear Physics **13** (1959) 493—508; © *North-Holland Publishing Co., Amsterdam*
Not to be reproduced by photoprint or microfilm without written permission from the publisher

INVESTIGATIONS ON THE DECAY OF ^{103}Ag, ^{104}Ag AND ^{104}Rh

R. K. GIRGIS † and R. VAN LIESHOUT
Instituut voor kernphysisch Onderzoek, Amsterdam

Received 11 August 1959

Abstract: The ^{103}Ag and ^{104}Ag isotopes were produced by irradiating ^{103}Rh with alpha particles. Bombarding energies of 50, 40, 30 and 20 MeV were used, whereby these isotopes were produced in different proportions, thus facilitating the assignment of the various radiation characteristics. The 60 minute ^{103}Ag was found to decay mainly by an $\approx$ 1.2 MeV positon transition to the ground state of ^{103}Pd; a weak gamma ray of 120 keV may also be present in the decay of this isotope. Gamma rays of 555, 745, 780, 860, 935, 1260, 1340, 1540, 1640 and 1810 keV were assigned with certainty to the decay of the 70 minute ^{104}Ag. Most of these gamma rays also occur in the decay of 4.4 minute ^{104}Rh, which was examined under the same experimental conditions. No positons with energy > 1.2 MeV are present in the 70 minute ^{104}Ag activity. The decay of the 27 minute ^{104}Ag shows gamma rays of 555 and 780 keV and two positon groups of 2.6 and 1.9 MeV. A level scheme is proposed for ^{104}Pd.

1. Introduction

Several investigations [1–5]) have been undertaken on the neutron deficient Ag-isotopes, one of the results being the assignment of a 1.1 hour period to either ^{103}Ag or ^{104}Ag. Table 1 summarizes the various investigations in connection with this subject. Fig. 1 is a part of the chart of nucleides including the isotopes involved in the various reactions quoted below.

Cd 103 ?	Cd 104 59m	Cd 105 55m	Cd 106 1.22 %	Cd 107 6.7 h	Cd 108 0.88 %
Ag 102 16m ?	Ag 103 60m	Ag 104 70m | 27m	Ag 105 40d	Ag 106 8.3d | 24m	Ag 107 51.4 %
	Pd 102 1.0 %	Pd 103 17d	Pd 104 11 %	Pd 105 22.2 %	Pd 106 27.5 %
			Rh 103 100 %	Rh 104 44m | 42s	

Fig. 1. Part of the chart of nucleides including the various isotopes involved in the production procedures of ^{103}Ag and ^{104}Ag.

† On leave of absence from the Faculty of Science, University of Cairo, Giza, Egypt, U.A.R.

TABLE 1

Survey of the various investigations made on neutron deficient Ag activities

Authors	Bombarding particles	Energy of irradiation (MeV)	Target	Periods found in the separated Ag-activity	Characteristics of various periods	Assignment
Enns [1])	p	50	Pd	2.3 m 25 m 8 d 16.3 m 73 m 45 d	 K capt. K capt. K capt.	^{108}Ag ^{106}Ag ^{106}Ag^{m} ^{104}Ag ^{102}Ag ^{105}Ag
Bendel [2])	d	12	Pd	66 m	γ's 554 keV ce 764 keV ce	^{102}Ag or ^{104}Ag
Haldar [3])	p	80, 100, 170	Ag	8 d 40 d 1.1 h 25 m	 β^+ 1.3 MeV a γ's 0.6 MeV ce parent 17 d ^{103}Pd 	 ^{103}Ag ^{104}Ag or ^{106}Ag
Johnson [4]) †	p	50	^{107}Ag	59 m	γ's 556 keV ce 550 scin 740 930 1300 β^+ 1.69 MeV sl 0.8 γ 556 keV ce β^+ 2.7 MeV sl daughter ^{104}Cd	^{104}Cd ^{104}Ag
Haldar [5])	p	40, 60 60	^{106}Cd Cd	18 m 27 m 1.1 h 5.2 h		^{102}Ag ^{104}Ag, ^{106}Ag ^{103}Ag ?
Reynolds [6])	p	18.8	Pd	27 m 24 m 1.2 h	spin 2 spin 1 spin 2	^{104}Ag ^{106}Ag ^{104}Ag or (^{102}Ag)
Ewbank [7])	α	48	Rh	59 m	spin 7/2	^{103}Ag

† see text.

Johnson [4]) performed an extensive study of the ^{104}Cd—^{104}Ag activities produced by irradiating enriched ^{107}Ag with 50 MeV protons. Both ^{105}Cd and ^{107}Cd were found to be present along with ^{104}Cd, whereas the presence of the unknown ^{103}Cd could not be excluded because of the high proton energy used. The Cd fraction showed a growth of a 27 minute activity along with the decay

of the 59 minute ^{104}Cd. On this basis the 27 minute period was assigned to ^{104}Ag. Several conversion lines were found with the beta spectrum. A line corresponding to a gamma ray of 556 keV, converted in Pd, was found to grow with a period of 27 minutes and to decay with a half life of 59 minutes. In a scintillation spectrometer, besides low energy gamma rays known to belong to Cd activities, peaks of 511 (annihilation radiation), 550, 740, 930 and 1300 keV were found. Only the 550 keV gamma ray was assigned to ^{104}Ag, while all those with higher energy were assigned to Cd activities. The positon spectrum could be resolved into branches of 2.70, 1.69 and $\approx$ 0.8 MeV. The first was assigned to ^{104}Ag and the lower energy branches to ^{105}Cd. Milked Ag activity decayed with periods of 6.7 hours, 59 minutes and 27 minutes. The presence of the weak 6.7 hour component, which was assigned to ^{107}Cd, led Johnson [4]) to conclude that the chemical separation was incomplete and to assign the 59 minute component to a mixture of ^{105}Cd and ^{103}Ag. The 27 minute component was assigned to ^{104}Ag.

Recent [6, 7]) spin measurements show, with certainty, the presence of a 1.1 hour period in both ^{103}Ag and in an even mass Ag isotope, most probably ^{104}Ag. It follows that the previously assigned characteristics of the 1.1 hour activity to either ^{103}Ag or ^{104}Ag could have been subject to error due to the presence of both activities in most of the sources.

The aim of the present work was to produce both ^{103}Ag and ^{104}Ag in different proportions and to try to differentiate between their characteristic radiations. An examination of the gamma radiation following the decay of ^{104}Rh under the same experimental conditions, would be of help in identifying with certainty those following the decay of ^{104}Ag since both these decays excite levels in ^{104}Pd.

2. Source Preparation and Chemical Procedure

Sources of ^{103}Ag and ^{104}Ag were prepared by irradiating Rh with the alpha particle beam of the synchrocyclotron of this Institute. Alpha beams with energies of 50, 40, 30 and 20 MeV were used to produce sources with different proportions of the various activities of interest; the target thickness corresponded to $\approx$ 10 MeV. Since the threshold for the (α, 4n)reaction on ^{103}Rh is $\approx$ 33 MeV and that of the (α, 3n) reaction is $\approx$ 25 MeV, it is expected that the 50 MeV alpha bombardment will result in high enrichment of ^{103}Ag while both ^{103}Ag and ^{104}Ag will be present in approximately equal abundance from the 40 MeV alpha bombardment. No ^{103}Ag is expected to be present in the Ag fractions produced by an alpha beam of 30 MeV since this energy lies below the threshold of the (α, 4n) reaction. Samples produced with an alpha beam of 20 MeV are expected to consist mainly of ^{105}Ag and ^{106}Ag.

The thickness of the targets and the duration of the irradiation (20 minutes) were the same for all irradiations performed. The chemical procedure to sepa-

rate the Ag fraction, described below, was the same in all cases and in every case the measurements were started 25 minutes after the end of the irradiations.

Targets of rhodium powder were dissolved in sulphuric acid and calcium bisulphate. Silver carrier and 0.1 N HCl were added. The silver activity was separated as silver chloride. Several ^{104}Rh sources were produced by the (d, p) reaction on ^{103}Rh. The rhodium metal was irradiated with deuterons of $\approx$ 10 MeV for $\approx$ 2 minutes; no chemistry was performed. The sources were examined within a few minutes after the end of the bombardment.

3. Measurements and Results

3.1. DIRECT GAMMA RAY SPECTRUM

Gamma ray spectra were studied using a 25×25 mm cylindrical NaI(Tl) crystal optically coupled to a 6292 DuMont photomultiplier. The spectra were displayed on a 100 channel RIDL analyzer. The crystal was calibrated for relative efficiency over an energy region from $\approx$ 20 to 3000 keV. Sources were placed far enough ($\approx$ 8 cm) from the crystal to suppress summing effects.

The Ag sources were sandwiched between 5 mm thick discs of aluminium to ensure annihilation of all positons at the source position. The decay of the source was followed for several days to subtract the contribution of long lived activities due to ^{105}Ag and ^{106}Ag, whenever necessary.

The gamma ray spectra of the various sources were examined over an energy region extending from 10 keV to $\approx$ 3 MeV. Sources produced by irradiations with 50, 40 and 30 MeV alpha particles showed the same characteristics except for a slight difference in intensity of the annihilation radiation peak and for a weak bump at $\approx$ 120 keV, which seemed to grow stronger with higher energy of the alpha beam. The long lived background was in general not important in the beginning of these runs.

Figs. 2 and 3 show the relevant part of the spectrum for a source produced by irradiating Rh with 40 MeV alpha particles. At the high energy side of the 511 keV annihilation peak lies a 555 keV gamma ray. Peaks of 780 and 930 keV, a double peak at $\approx$ 1.3 MeV and one of 1.5 and 1.8 MeV are clearly present.

All peaks with energies above 600 keV decay with a half-life of 70±3 minutes. The gross decay of the weak 1.81 MeV peak, for which the contribution due to the annihilation in flight is important, yielded a shorter half-life ($\approx$ 60 minutes), but after subtraction of the annihilation in flight contribution, the half-life proved also to be 70 minutes. The decay of both the 555 keV peak and of the annihilation peak showed the two periods of 27 and 70 minutes, the relative intensities of the two peaks being dependent upon the choice of the bombarding energy. By following the decay of each peak, their composition could be calculated at each moment. As an example the relative intensities of the four components have been calculated for $t = 0$, i.e. the end of the bombardment, in the

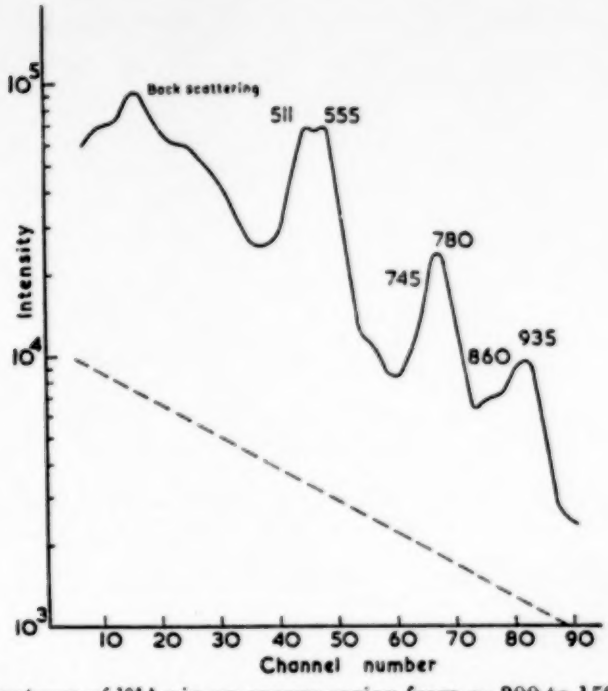

Fig. 2. Gamma ray spectrum of ^{104}Ag in an energy region from ≈ 300 to 1500 keV, the dashed line represents the annihilation in flight continuum.

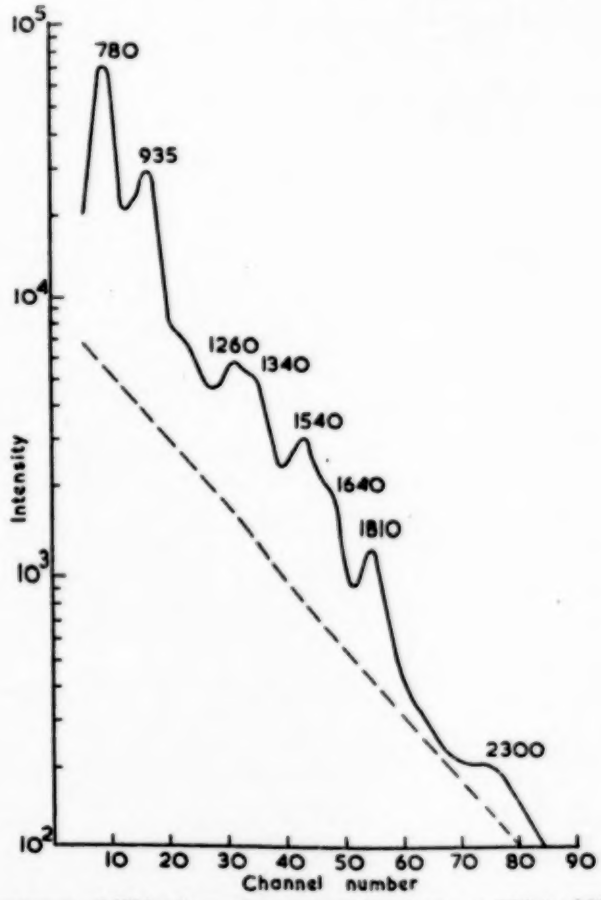

Fig. 3. Gamma ray spectrum of ^{104}Ag in an energy region from ≈ 800 to 2500 keV, the dashed line represents the annihilation in flight continuum. The bump at 2300 keV is due to residual summing.

case where 50 MeV alpha particles were used (see table 2). No ^{106}Ag is present in these sources, but the 70 min contribution in the 511 keV peak is certainly partly due to ^{103}Ag. As discussed in section 5, the ratio of the positons to the 555 keV gamma transition in the 27 min activity ($\approx$ 1) is in agreement with the decay scheme proposed on the basis of other arguments. The absence of a strong annihilation radiation in the 70 minute ^{104}Ag is in agreement with the positon measurements.

TABLE 2

Composition of various radiations from a source produced with 50 MeV alpha particles, determined at the end of bombardment

Energy (MeV)	70 min activity	27 min activity
$\gamma^{\pm}$	90 ± 30 †	200 ± 30+
0.555γ	200 ± 40	90 ± 40
$2.6\beta^{+}$	$\leqq 10$	100+

† Partly due to ^{103}Ag. +Normalized to 100 positons of the 27 min activity.

The spectrum was analyzed into its various components in the usual manner mentioned in previous publications [8]). Standard peaks of ^{88}Y, ^{42}K, ^{22}Na, ^{54}Mn,

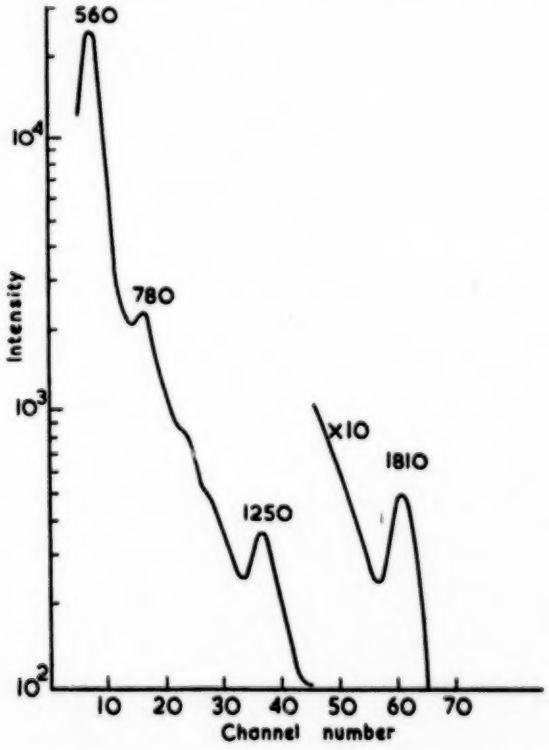

Fig. 4. Gamma ray spectrum of ^{104}Rh in an energy region from $\approx$ 400 to 2000 keV.

^{137}Cs and ^{85}Sr were used for this analysis. The contribution due to the annihilation in flight of positons was interpolated between those obtained with pure

positon emitters measured under the same conditions as reported in a previous publication [9]). This contribution was subtracted from the total spectrum before the analysis was performed. Corrections for the absorption in the annihilators were applied. Table 3 gives the energy values of the peaks resolved in the spectrum, together with their relative intensities. A large error is placed on the intensities of both the 740 and 780 keV peaks since it is difficult to resolve them with higher accuracy. The broad bump at $\approx$ 2.3 MeV was found to be entirely due to residual summing effects (cascade of 930+1340, 930+780+550 and perhaps 1810+511 keV).

Sources produced with a 20 MeV alpha beam showed a completely different gamma ray spectrum. The gamma rays were mainly those characteristic of ^{105}Ag and ^{106}Ag. The strongest peak in the spectrum was the 511 keV peak decaying with a half-life of 24$\pm$1 minute and showing a weak tail having a long half-life. No 70 minute component was found, in agreement with the assignment to mass 106.

The gamma ray spectrum of ^{104}Rh was measured with the same scintillation spectrometer used for the measurements of the silver activities, in order to

TABLE 3

Energies and relative intensities of the gamma rays following the decay of ^{104}Rh and ^{104}Ag.

Gamma rays from the decay of ^{104}Rh				Gamma rays from ^{104}Ag	
Bunker [10]), scin		Present work, scin		Present work, scin	
Energy (keV)	Int. [a])	Energy (keV)	Int. [b])	Energy (keV)	Int.
556	100	560		555$\pm$ 5	100 [c])
745	4.7	(745) †		745$\pm$10	20 $\pm$6
780	5.7	780		780$\pm$10	57 $\pm$8
				860$\pm$10	15 $\pm$2
930	1.4	930		935$\pm$ 5	35 $\pm$5
		1250	1	1260$\pm$10	4.0$\pm$1.0
1340	0.6	(1340) †		1340$\pm$10	10.0$\pm$1.5
1530	1.9	(1530) †		1540$\pm$10	8.3$\pm$1.0
				1640$\pm$15	9.0$\pm$1.5
		1810	$\approx$1	1810$\pm$15	8 $\pm$1
Also reported 1240 keV γ from 42 sec ^{104}Rh, but no 1810 keV γ ($<$5% of 1240 keV γ)		† gamma rays not resolved but probably present		Beta radiations from ^{104}Ag	
				70 min period	27 min period
				1.2 MeV? no β^+ with E_β<1.4 MeV	2.6$\pm$0.1 MeV

[a]) Equilibrium mixture of the 42 sec and 4.4 min activities.

[b]) Non-equilibrium mixture.

[c]) Composition at the time of measurement: 80$\pm$10 due to the 70 min, 20$\pm$10 due to the 27 min activity.

compare the structure of these two spectra. The pulse height distribution due to a non-equilibrium mixture of the 42 sec ^{104}Rh and the 4.4 min ^{104}Rh^{m} is shown in fig. 4. Gamma rays of 555, 780, 930, 1250 and 1810 keV were observed. These energy values are in excellent agreement with those reported by Bunker, Mize and Starner [10]). However, Bunker *et al.* report the absence of the 1.81 MeV gamma ray, which we observe. In fact, these authors place an upper limit on its intensity of 1/20 of that of the 1250 keV peak. Since the existence of the 1.81 MeV peak plays a role in the interpretation of the level scheme of ^{104}Pd, its reality was established by performing various irradiations. It was checked that it cannot be due to summing. Although no chemical separations were performed, the assignment to ^{104}Rh seems reasonably certain, since the half-life of the 1.81 MeV peak was certainly of the order of a few minutes. The only reasonable acceptable contamination would be 2.3 min ^{28}Al, but the presence of aluminium and magnesium with the target assembly has been avoided. Therefore, we assign the 1.81 MeV transition to ^{104}Rh; the discrepancy with the results reported in ref. [10]) is not understood.

Table 3 lists the energies of the gamma rays from ^{104}Rh as reported by Bunker *et al.* [10]), as well as their relative intensities in an equilibrium mixture of the two isomers. The energies from the work reported here, as well as some other data, are also listed.

3.2. POSITON SPECTRUM OF THE SILVER ACTIVITIES

Positon spectra of the several sources produced by the various irradiations mentioned above, were studied with an anthracene crystal of 4 cm diameter and 1 cm thickness. This crystal was optically coupled to a 6292 DuMont photomultiplier. An energy calibration was made using sources of ^{90}Sr+^{90}Y (2.25 MeV), ^{32}P (1.71 MeV), ^{207}Bi (976 keV conversion line) and ^{137}Cs (624 keV conversion peak).

The Ag sources were of considerably high specific activity; they were smeared out on plastic tape and they were all examined under the same conditions. The contribution of gamma rays detected by the anthracene crystal was subtracted using the available devices of the RIDL kicksorter. The decay of the sources was followed for several hours. The general features of the positon spectrum were the same for all sources produced with 50, 40 or 30 MeV alpha particles. The part of the positon spectrum with an energy > 1.4 MeV decayed with a half-life of 27 ± 1 minutes; no 70 min contribution could be detected (< 10 % of the 27 min activity at the end of the bombardment). The decay of the part with energy < 1.4 MeV showed an additional period of 70 ± 3 min.

Fig. 5 shows the Fermi-Kurie diagram for the positon spectrum of a source produced with 40 MeV alpha particles. It could be resolved into three branches having end point energies of 2.6 ± 0.1, 1.9 ± 0.1 and ≈ 1.2 MeV. The energy of the last branch could not be determined more accurately, since it lies in the

region where scattering from the 2.6 MeV branch becomes important. The existence of the $\approx$ 1.2 MeV branch is certain, since it is still present after the decay of the higher energy positon branches of shorter half-life. It is impossible to say, whether, in addition to the 70 min $\approx$ 1.2 MeV branch, there is also an independent 27 min $\approx$ 1.2 MeV branch.

The only difference between the beta ray spectra of the sources produced at 50, 40 or 30 MeV bombarding energy, occurred in the relative abundances of the three branches in these composite spectra. Relative to that of the 2.6 MeV branch, the $\approx$ 1.2 MeV partial spectrum increases in intensity with higher bombarding energy of the alpha particle beam, while the 1.9 MeV branch diminishes in intensity.

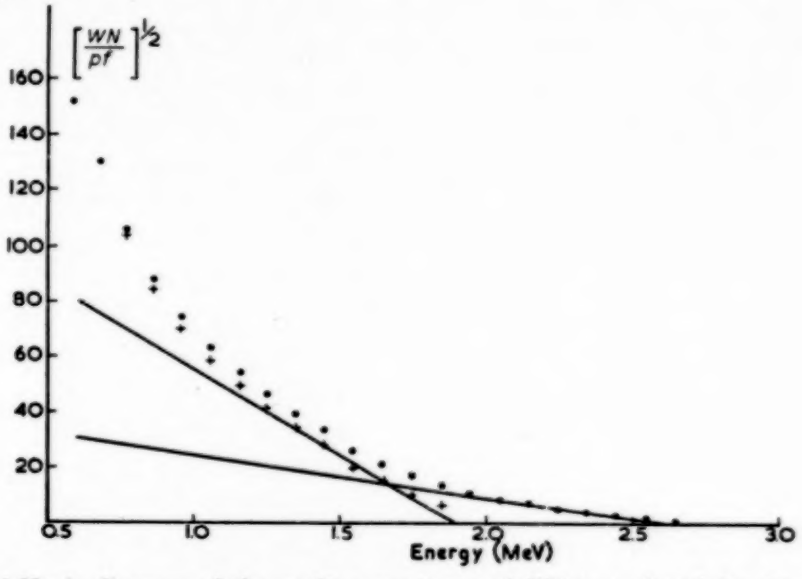

Fig. 5. Fermi-Kurie diagram of the positon spectrum of ^{104}Ag produced by irradiating ^{103}Rh with 40 MeV alpha particles.

The Ag sources produced with the 20 MeV alpha particle beam showed a different structure of the positon spectrum. The end point lies at 2.0 ± 0.1 MeV and the whole part of the spectrum above 0.8 MeV decays with a half-life of 24 ± 1 min (followed over 8 periods). In addition a very weak indication for a branch of $\approx$ 1 MeV was found. These characteristics suggest that the observed spectrum was mainly due to ^{106}Ag, whereas a ^{104}Ag activity, if present, could only have been very weak.

4. Conclusions

The gamma ray spectrum and the positon spectrum of sources produced by irradiating ^{103}Rh with 20 MeV alpha particles, show that those sources consisted mainly of ^{106}Ag and ^{105}Ag as expected. Sources prepared with higher energies of the alpha particle beam contained only a few percent of these activities.

A weak gamma ray peak of 120 keV was found in sources produced with 50 and 40 MeV alpha particles; it disappeared in sources produced with a lower energy of the alpha particle beam. It is therefore reasonable to assign this peak to the decay of ^{103}Ag. It may be identical with a gamma ray of 118 keV, found by Johnson [4]) to be converted in Pd. The presence of weak gamma rays which are hidden by stronger ones cannot be excluded, in partiular in the region of the backscattering peak at $\approx$ 180 keV.

All other gamma rays (except for the annihilation peak) found in the spectra of sources produced with 50 and 40 MeV alpha particles, fit exactly, both in energy and in relative intensity, with those of sources produced with an alpha beam of 30 MeV energy. In particular, the intensity of the 555 keV peak relative to that of the various higher energy peaks, taken, for instance, at the end of the bombardment, is the same for all three bombarding energies. Since the 555 keV peak is composite, this means that the relative abundance of the 27 min and the 70 min activities which contribute to this peak, is not strongly dependent upon the bombarding energy. This may be interpreted as a further argument that both periods in the 555 keV peak are assignable to the same mass number.

The energy values of the various gamma rays are in excellent agreement with those following the decay of ^{104}Rh as found in this work and as reported by Bunker *et al.* [10]). The intensity ratio of two couples of gamma rays (780, 1340 keV and 740, 1530 keV), which supposedly originate from levels at 1340 and 2080 keV respectively in the decay of ^{104}Rh, is the same in both the decay of the 70 min Ag activity and of ^{104}Rh, confirming their common origin.

It follows from the above arguments that all gamma rays reported in table 3 and found in the analysis of the gamma ray spectrum of a source produced by irradiating ^{103}Rh with 40 MeV alpha particles can be assigned with certainty to the decay of ^{104}Ag.

The general features of the gamma ray spectrum found in this work and assigned to ^{104}Ag are in close agreement with those found by Johnson [4]) and assigned to Cd activities. No Cd isotopes can be present in the sources used in the present study, as is obvious from the method of production, whereas ^{104}Ag was certainly present in the sources examined by Johnson. The numerous isotopes present in the sources studied by the last author, together with the similarity of their periods, probably led to confusion in the assignment of the various gamma rays found in the spectrum. It is also possible that the assignment of certain radiation characteristics to ^{103}Ag made by Haldar *et al.* [3, 5]) is not correct, since it must be expected that the 70 min ^{104}Ag was present in the sources investigated by this last group.

The positon branch of 2.6 MeV in the sources produced by 50, 40 and 30 MeV alpha particles belongs to the decay of ^{104}Ag since this part of the spectrum decayed with a half life of 27 minutes; it cannot belong to the decay of the

24 minute ^{106}Ag since the total decay energy of the last isotope is not large enough to allow such a transition. The 1.9 MeV branch may belong to both the 27 minute ^{104}Ag and the 24 minute ^{106}Ag. The variation of its intensity in the manner mentioned above suggests that it is mainly due to the ground state transition from ^{106}Ag to ^{106}Pd. This conclusion finds confirmation from the gamma ray intensities (see following section).

The gain in intensity of the branch of $\approx$ 1.2 MeV with an increase of the bombarding energy of the alpha beam may indicate the presence of ^{103}Ag in these sources with high abundance. This cannot be considered as a definite proof of the presence of the ^{103}Ag activity in these sources, since a change in the bombarding energy of the alpha beam may result in different abundances of the two ^{104}Ag isomers (although one would not expect this effect to be very pronounced, since the same angular momentum transfer is involved). However, the fact that Ewbank *et al.* [7]) produced ^{103}Ag by the same reaction and with about the same bombarding energy used in the present investigation, makes it certain that ^{103}Ag was present in the sources. In addition, the characteristic radiation of the daughter nucleide ^{103}Pd was observed decaying with the correct half-life.

The highest energy branch of 2.6 MeV found in this work and assigned to ^{104}Ag is in good agreement with that found by Johnson [4]) and assigned to the same isotope. The two other branches of 1.9 and $\approx$ 0.8 MeV found by the last author and assigned to ^{105}Cd may also be partly due to ^{104}Ag activities.

5. Proposed Decay Schemes of the ^{104}Ag Isomers

Fig. 6 shows the proposed decay schemes for the two ^{104}Ag activities. The results of the present investigation substantiate the level scheme of ^{104}Pd adopted by the Nuclear Data Group [11]) and constructed mainly on the basis of the results of the study made by Bunker *et al.* [10]) of the decay of the ^{104}Rh isomers. Most of the gamma rays from 70 min ^{104}Ag can be fitted into this level scheme. There can therefore hardly be any doubt that the mass assignment of the 70 min activity is correct.

The 1.81 MeV gamma ray has been assumed to originate at the level of the same energy. This interpretation is supported by the fact that the relative abundance of the 1.81 and 1.25 MeV gamma transitions is about the same from ^{104}Rh and ^{104}Ag, although these relative abundances could not be determined very accurately from the ^{104}Rh decay (see table 3). (The discrepancy between our results and those of Bunker *et al.* [10]) with regard to the relative intensity of the 1.81 MeV gamma ray has been discussed in section 4.) The 1.81 MeV level must have a spin 1 or 2 and even parity, since it is populated by an allowed transition from the 42 sec ground state of ^{104}Rh, to which ground state a spin 1^+ has been assigned, because it decays by allowed beta transitions to both the 0^+ ground state and the 2^+ first excited state [12, 13, 14]) of ^{104}Pd. The observation of

the new 1.81 MeV gamma ray in the decay of ^{104}Rh supports these considerations.

Two additional gamma rays of 1.64 and 0.860 MeV are observed in the decay of 70 min ^{104}Ag. A new level at 2.20 MeV would explain the presence of these transitions; the first one is then a transition to the first 2^+ level, the second one populating the second excited state, which probably also has a spin 2^+. This interpretation is based on the energy match; it is impossible to confirm it from intensity considerations since the gamma rays turned out to be too weak in the

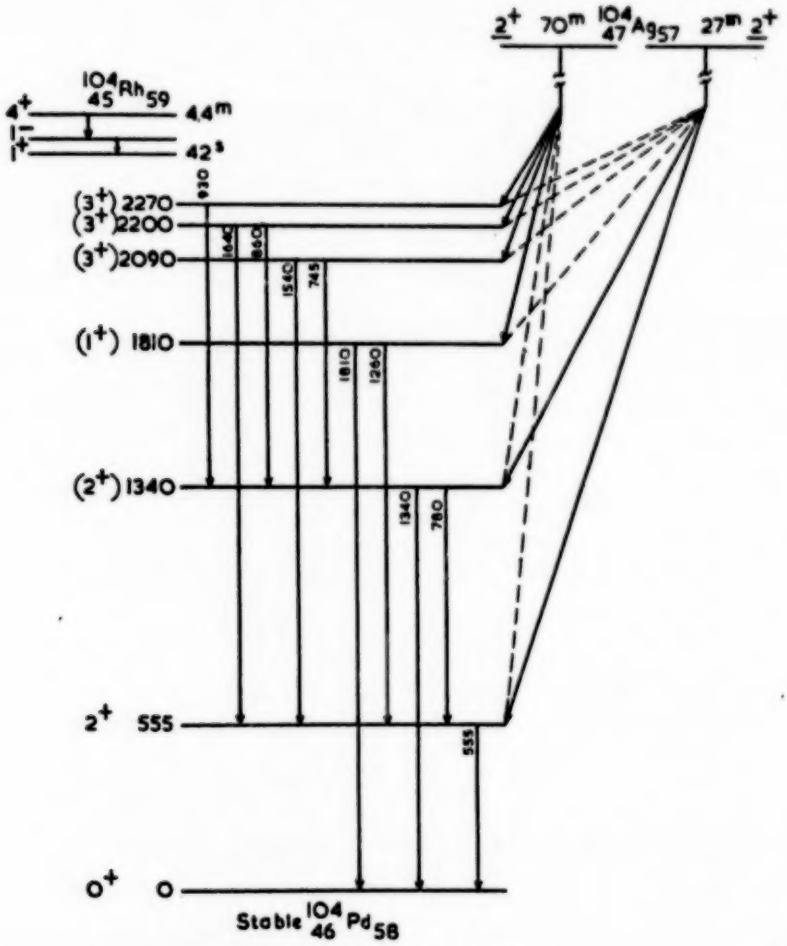

Fig. 6. Level scheme of ^{104}Pd as deduced from the decay of the two ^{104}Ag isomers.

decay of ^{104}Rh to be resolved from the spectrum. The spin of the 2.20 MeV level is probably 3 or 4, since the ground state gamma transition is absent.

The same arguments mentioned in connection with the spin of the 2.20 MeV level apply to that of the levels at 2.09 and 2.27 MeV. As shown below (table 4) all three levels are populated by allowed transitions from the 70 min ^{104}Ag isomer, for which a spin 2 has been reported [6]), a spin 3 is therefore assigned to these levels. Two of these levels are also populated from the 4.4 min ^{104}Rh by allowed beta-transitions. Therefore, the spin assignments for the levels in

^{104}Rh shown in fig. 6 are preferred over those listed in the Nuclear Data Sheets [11]). (The reported absence of a possible 128 keV M3 transition could still be compatible with these spin assignments.)

The level at 1.34 MeV in ^{104}Pd is very probably the second 2^+ level, since both its position relative to the first excited state and its decay properties are in agreement with the general characteristics of the second 2^+ level in even nucleides in this mass region [12, 13]). Fig. 7 gives the energy values of the first and second 2^+ levels in Ru, Pd and Cd nucleides plotted against their neutron numbers. It can be seen that a value of 1.34 MeV for a possible second 2^+ level in ^{104}Pd agrees with the general trend of the neighbouring nucleides.

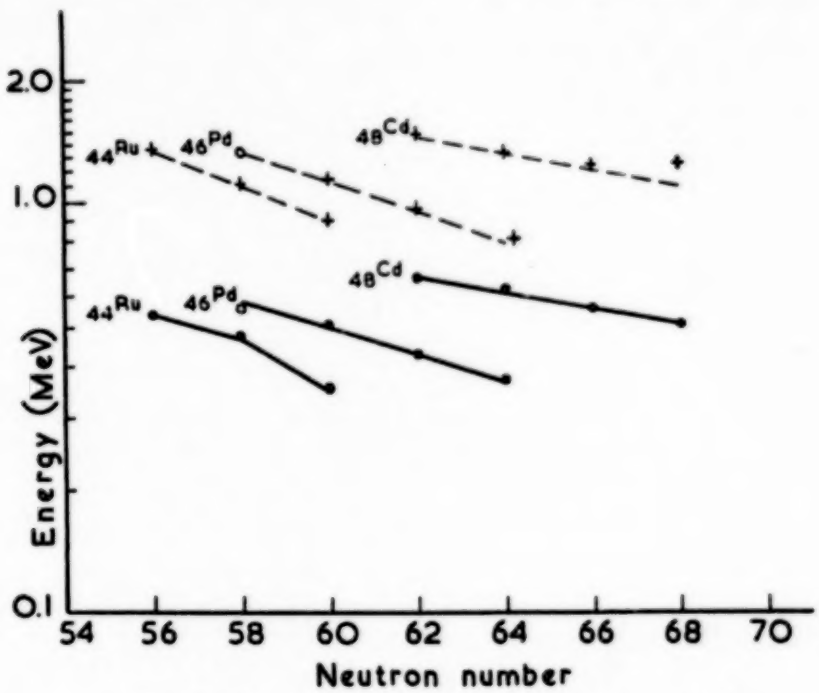

Fig. 7. Energy of the first and second excited 2^+ states in Ru, Pd and Cd isotopes plotted as a function of their neutron numbers. The dashed line represents the second 2^+ state. The energy of the second excited state in ^{104}Pd (1.34 MeV) is plotted as a circle, since its spin assignment is uncertain.

The total available decay energy of both ^{104}Ag isomers is estimated as $\approx$ 4.2 MeV from beta decay energy systematics [15]). There is no appreciable 70 min component in the part of the positon spectrum above 1.5 MeV and the intensities of the various gamma transitions show that only the levels above 1.7 MeV are populated by positon and capture transitions from 70 min ^{104}Ag. Since the spin of 70 min ^{104}Ag has been measured [7]) to be 2 and since all these beta transitions are allowed, all parities involved must be positive. The absence of the expected allowed positon branches to the first ($\log ft \geqq 6.4$) and second 2^+ state ($\log ft \geqq 6.1$) remains unexplained.

The decay of the 27 min ^{104}Ag takes place almost exclusively to the first

excited state of ^{104}Pd. The mass assignment seems to be well established from the spin value, decay energy considerations and from the various production methods and the genetic relationship [4]) with the 60 min ^{104}Cd. The allowed character of the 2.6 MeV positon branch to the 2^+ level at 0.56 MeV fixes the spin of the 27 min ^{104}Ag as 2^+. The 1.9 MeV positon branch decaying with a 27 min period belongs mainly to the decay of 24 min ^{106}Ag. The intensity of a possible positon transition to the 2^+ level at 1.34 MeV, can only be calculated rather inaccurately from the amount of 27 minute activity in the 0.78 MeV gamma ray. The log *ft* value (see table 4) is compatible with that for an allowed transition. Table 4 gives the log *ft* values for the various beta branches from both ^{104}Ag isomers, calculated mainly from the gamma ray intensity. For both a total decay energy of 4.2 ± 0.2 MeV has been accepted; intensities have been calculated from the balance between the gamma rays populating and deexciting the various levels.

TABLE 4

Intensities and log *ft* values for the various beta branches from ^{104}Ag

Level (MeV)	Calculated positon energy (MeV)		% population ε	% population β^+	log *ft*
2.270	0.88	70 m	30	5	5.0
2.200	0.95	70 m	20	4	5.1
2.090	1.06	70 m	22	6	5.2
1.810	1.34	70 m	8	4	5.7
1.340	1.81	70 m	$\leqq 6$	$\leqq 9$	$\geqq 6.1$
		27 m	$\leqq 15$	$\leqq 25$	$\geqq 5.4$
0.555	2.60	70 m	$\leqq 3$	$\leqq 12$	$\geqq 6.4$
		27 m	$\geqq 12$	$\geqq 48$	5.3

There remains the question of the relative positions of the two ^{104}Ag activities. It is obvious that there can be no isomeric transition of appreciable intensity between them since there is neither a detectable amount of high energy positons in the 70 min period, nor an important 27 min component in the higher energy part (> 0.6 MeV) of the gamma ray spectrum at a time when both activities are known to be present in the source in comparable abundances. Some special slowing down mechanism must therefore exist which suppresses the isomeric transition.

6. The Decay of ^{103}Ag

The present work does not give enough information to construct a definite decay scheme of ^{103}Ag. However, an examination of the neighbouring palladium isotopes, may give some insight into the general features of the ^{103}Pd level scheme, to which ^{103}Ag decays.

Table 5 gives the ground state spins of these isotopes and it also lists some of the known levels with their spin value as deduced from beta and gamma ray studies. From this table it can be concluded that a spin $\frac{7}{2}^+$ or $\frac{5}{2}^+$ is likely for the ground state of ^{103}Pd, while the presence of an $\frac{11}{2}^-$ level as the first excited state is almost certain. The spin of ^{103}Ag was found [7]) to be $\frac{7}{2}$, and even parity is therefore to be expected. This means that the decay of ^{103}Ag will populate the ground state of ^{103}Pd by an allowed transition. The log *ft*-value for such a transition, assuming an energy of 1.2 MeV and 100 % abundance for this branch, is $\approx$ 4.7, which agrees with the above conclusions. A level of $\frac{11}{2}^-$, if present, could also be populated in the decay of ^{103}Ag by a first forbidden unique transition. Such a branch should be very weak. This may indicate that the 120 keV transition which was found in this work and assigned to the decay of ^{103}Ag can be the ground state transition from the first excited state in ^{103}Pd.

TABLE 5

Ground state spins and levels in some odd mass Pd nucleides. Values of ground state spins in parentheses are deduced from beta decay investigations. The underlined value is directly measured, for references see Nuclear Data Sheets.

Nucleide	ground state spin	1st excited state		2nd excited state	
		Energy (keV)	spin	Energy (keV)	spin
^{99}Pd	$(\frac{5}{2}^+)$				
^{101}Pd	$(\frac{5}{2}^+)$				
^{103}Pd	$(\frac{5}{2}^+)$				
^{105}Pd	$\underline{\frac{5}{2}^+}$	220	$\frac{11}{2}^-$	268	$\frac{3}{2}^+$
^{107}Pd	$(\frac{5}{2}^+)$	216	$\frac{11}{2}^-$	305	
^{109}Pd	$(\frac{5}{2}^+)$	170	$\frac{11}{2}^-$		
^{111}Pd	$(\frac{5}{2}^+)$	170	$\frac{11}{2}^-$		

The authors would like to thank Prof. Dr. P. C. Gugelot, Prof. Dr. A. H. W. Aten, Jr. and Prof. Dr. A. H. Wapstra for their interest in this work, Mrs. A. Funke-Klopper for performing the chemical separations and the personnel of the synchro-cyclotron for performing the irradiations.

Thanks are also due to Dr. R. A. Ricci for interesting discussions.

This work was performed as part of the research program of the „Stichting voor Fundamenteel Onderzoek der Materie (F.O.M.)", which is financially supported by the "Nederlandse Organisatie voor Zuiver-Wetenschappelijk Onderzoek (Z.W.O.)". One of the authors (R. K. G.) is indebted to the Egyptian Atomic Energy Commission for a grant.

References

1) T. Enns, Phys. Rev. **56** (1939) 872

2) W. L. Bendel, F. J. Shore, H. N. Brown and R. A. Becker, Phys. Rev. **90** (1953) 888

3) B. C. Haldar and E. O. Wiig, Phys. Rev. **94** (1954) 1713
4) F. A. Johnson, Can. J. Phys. **33** (1955) 841
5) B. C. Haldar and E. O. Wiig, J. Indian Chem. Soc. **35** (1958) 79
6) J. B. Reynolds, R. L. Christensen, D. R. Hamilton, W. M. Hooke and H. H. Stroke, Phys. Rev. **109** (1958) 465
7) W. B. Ewbank, L. L. Marino, W. A. Nierenberg, H. A. Shugart and H. B. Silsbee, Bull. Am. Phys. Soc. **3**, no 7 M2 (1958) 370
8) R. K. Girgis and R. van Lieshout, Physica **25** (1959) 133
9) R. A. Ricci, R. K. Girgis and R. van Lieshout, Nuovo Cimento **11** (1959) 156
10) M. E. Bunker, J. P. Mize and J. W. Starner, Phys. Rev. **99** (1955) 659 A
11) Nuclear Data Sheets, National Research Council, Washington, D. C. Sheet N.R.C. 58-9-71
12) G. Scharff-Goldhaber and J. Weneser, Phys. Rev. **98** (1955) 212
13) K. Way, D. N. Kundu, C. L. McGinnis and R. van Lieshout, Annual Review of Nuclear Science **6** (1956) 129
14) G. M. Temmer and N. P. Heydenburg, Phys. Rev. **104** (1956) 467;
P. H. Stelson and F. K. McGowan, Phys. Rev. **110** (1958) 489
15) K. Way and M. Wood, Phys. Rev. **94** (1954) 119

1.E.1:
3.A:4.E

Nuclear Physics **13** (1959) 509—510; © *North-Holland Publishing Co., Amsterdam*
Not to be reproduced by photoprint or microfilm without written permission from the publisher

THE LEVEL SCHEME OF ^{104}Pd

(ADDENDUM)

R. K. GIRGIS† and R. VAN LIESHOUT

Instituut voor kernphysisch Onderzoek, Amsterdam

Received 29 September 1959

Abstract: The results obtained in the study of the decay of ^{104}Rh and ^{104}Ag are reviewed in the light of the new spin value reported for 70 minute ^{104}Ag.

After the results of the study reported in the preceding article [1]) had been submitted for publication, new data on the spins of the two ^{104}Ag activities have become available. Ewbank, Marino, Nierenberg, Shugart and Silsbee [2]) have now measured the spin of the 27 minute activity to be 2, in agreement with the earlier measurement by Reynolds, Christensen, Hamilton, Hooke and Stroke [3]), but that of the 70 minute ^{104}Ag activity turned out to be 5, instead of 2 as reported earlier in ref.[3]) as a possible spin assignment for this isomer. This higher spin value for the 70 minute activity resolves the question raised about the apparent absence of a genetic relationship between the two isomers (see the last paragraph of section 5 of the preceding article [1])). Moreover, with the new spin value it has become understandable why the decay of the two isomers involves quite different levels in ^{104}Pd. Therefore, we can conclude that the results on the decay of 70 minute ^{104}Ag are in good agreement with a spin 5, but not with a spin 2 for this isomer.

Accepting then spins of 5 and 2 for the 70 and 27 minute periods respectively and applying the same argumentation in the interpretation of the data reported in the preceding article, new and more certain spin values can be derived for the levels in ^{104}Pd. It also follows that the spins and parities for the levels in ^{104}Rh, involved in the decay of the 42 sec and 4.4 min activities, are in complete accord with those originally assigned by the Nuclear Data Group [4]).

In view of these changes a new decay scheme is proposed for the mass 104 nucleides, which differs from the one originally suggested (see ref.[1]), fig. 6) in the spin and parity assignments (fig. 1).

If a 4^+ level existed in ^{104}Pd at $\approx$1.3 MeV, it would probably have been populated to an appreciable extent by positons in the decay of the 70 minute activity; no indication for such a branch was found, however. It would seem therefore, that the lowest 4^+ level appears at 2.09 MeV.

† On leave of absence from the Faculty of Science, University of Cairo, Giza, Egypt, U.A.R.

A spin of 1^+ has been assigned to the 1.81 MeV level in the preceding article [1]). If the 1.81 MeV gamma ray corresponds to a ground state transition, the spin of the 1.81 MeV level cannot be higher than 2. It is then impossible that this

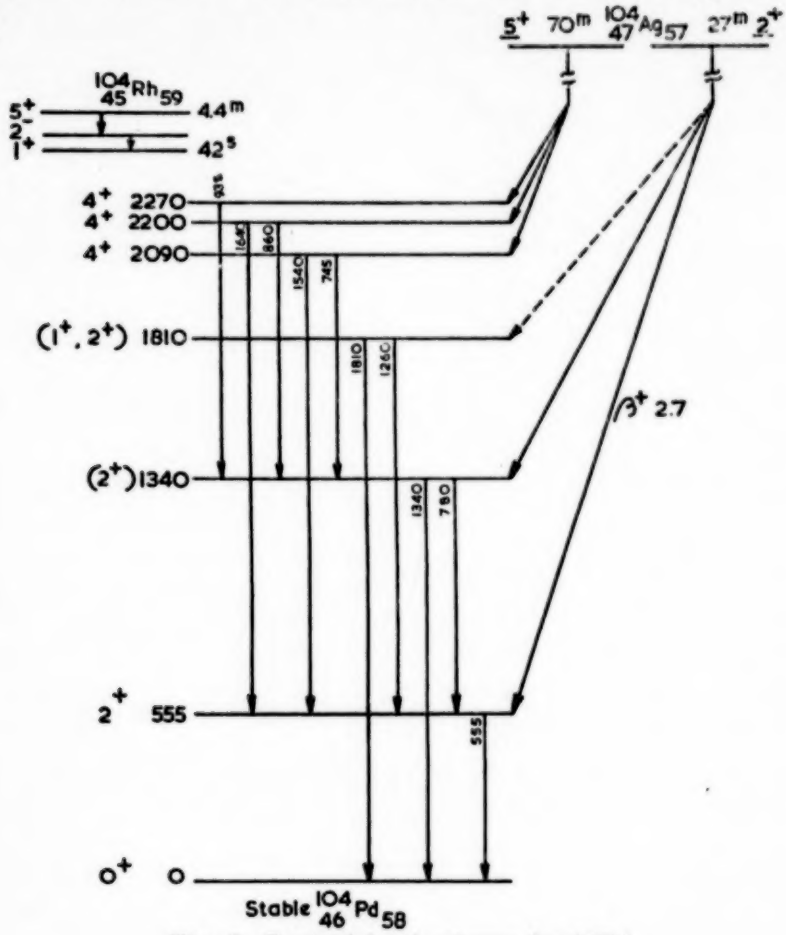

Fig. 1. Revised level scheme for ^{104}Pd.

state is fed directly by a beta transition from the 70 minute ^{104}Ag. It is, however, not excluded that part of the 1.81 MeV gamma ray should be placed elsewhere in the decay scheme.

This work was performed as part of the research program of the "Stichting voor Fundamenteel Onderzoek der Materie (F.O.M.)", which is financially supported by the "Nederlandse Organisatie voor Zuiver-Wetenschappelijk Onderzoek (Z.W.O.)". One of the authors (R.K.G.) is indebted to the Egyptian Atomic Energy Commission for a grant.

References

1) R. K. Girgis and R. van Lieshout, Nuclear Physics **13** (1959) 493
2) W. B. Ewbank, L. L. Marino, W. A. Nierenberg, H. A. Shugart and H. B. Silsbee, Phys. Rev. Letters **3**, no. 3 (1959) 153, Abstract
3) J. B. Reynolds, R. L. Christensen, D. R. Hamilton, W. M. Hooke and H. H. Stroke, Phys. Rev. **109** (1959) 465
4) Nuclear Data Sheets, National Research Council, Washington, D.C., Sheet NRC 58-9-61

2.A.1:
6.A

Nuclear Physics **13** (1959) 511—515; © *North-Holland Publishing Co., Amsterdam*
Not to be reproduced by photoprint or microfilm without written permission from the publisher

THE TOTAL PROTON REACTION CROSS SECTION OF CARBON FROM 10—68 MeV BY A NEW METHOD

EDWARD J. BURGE

Wheatstone Laboratory, King's College, London

Received 4 August 1959

Abstract: Inelastic interactions in scintillators produce a low energy tail in the pulse height spectrum. The fractions of pulses in the tails for protons of various energies are used directly to determine the total reaction cross-section as a function of energy. The method applies only to nuclei in scintillators. Results for carbon are presented for 10—68 MeV.

1. Introduction

Part of the interest in measurements of total reaction cross sections lies in comparisons with the values predicted by the optical model using parameters suggested by elastic differential cross-sections. Sometimes two or more sets of parameters are found which provide almost equally good fits to the elastic scattering data but predict significantly different total reaction cross sections. At energies below 135 MeV the only measurements completed are those of Gooding [1]) for C, Al, Fe, Sn and Pb at 34 ± 2.5 MeV and Eisberg [2]) for the same nuclei at 62 MeV. The method used was essentially to measure the total number of protons incident on a target using a dE/dx counter, and the number elastically scattered into a known solid angle using an E-counter. The number of inelastic events in the E-counter was several times the number in the target and this necessitated a subtraction method. It is shown here that the inelastic events in the E-counter can be used to estimate the total reaction cross section for the nuclei of the scintillator.

2. Method

The method depends on a measurement of the low energy tail of the pulse height spectrum for a scintillator bombarded with mono-energetic protons. The scintillator must consist of a single nuclear species, or a single species associated with hydrogen. Pulses smaller than those in the main peak are produced by protons that have lost energy as the result of a nuclear interaction, e.g. an inelastic collision or a reaction with a negative Q-value. Elastic collisions with a nucleus of mass M produce protons with energies down to $[1-4Mm/(M+m)^2]$ of the incident energy, where m is the mass of the proton. The number

with energies significantly smaller than the incident energy is not large and can be accurately estimated from the elastic differential cross section. The recoil nucleus from an elastic collision produces a small scintillation which will slightly increase the height of the pulse from the associated proton, but the effect is completely negligible at most energies.

A collision between an incident proton and a hydrogen nucleus of the scintillator material will produce two protons with a total energy equal to that of the incident particle at the time of the collision. Provided that the pulse height is proportional to the energy, the scintillation will clearly be equal in magnitude to that produced by an incident proton brought to rest by the usual electromagnetic interactions. Hydrogen in the scintillator will therefore not contribute to the low energy tail, and will simply reduce the fraction of pulses in the tail by a known amount.

The energies of the protons producing inelastic collisions and reactions range from the incident energy (E_1) to the threshold energy of the interaction with the smallest negative Q-value. If protons of slightly higher incident energy (E_2) are used the increase in the tail will be caused by inelastic collisions and reactions of protons with energies between E_1 and E_2. The thickness of scintillator producing these events is simply that required to reduce the energy from E_2 to E_1. Therefore a measure of the fractions in the tail for E_1 and E_2, and a knowledge of the range-energy relation, will give a value for the average total reaction cross-section between E_1 and E_2. If the magnitudes are expressed as the fractions per g/cm^2 the total reaction cross-sections are given directly by dividing these values by the number of nuclei (excluding hydrogen nuclei) per g of the scintillator.

3. Analysis of Measurements

Johnston, Service and Swenson [3]) and Service [4]) have measured the pulse height spectrum for a plastic scintillator, NaI(Tl), KI and CsI at three energies. An analysis has been made of the results of Service for Scintilon plastic. At 10, 40 and 68 MeV he found the fractions in the tail to be 0.0015 ± 0.00025, 0.025 ± 0.0025 and 0.064 ± 0.005 respectively. The composition of Scintilon was assumed to be $(CH)_n$. When the average cross section for each of the intervals is calculated, the values are found to be 376 ± 40 mb for $E = 25\pm15$ MeV and 355 ± 50 mb for $E = 54\pm14$ MeV. These results are shown in the figure, together with the value measured by Gooding at 34 MeV and the values predicted at 40 MeV by Glassgold and Kellogg [5]), at 17 MeV and 31.5 MeV by Melkanoff, Nodvik and Saxon [6]), and at 17 MeV by Glassgold and Kellogg [7]), from the optical model analysis of elastic differential cross-sections. The value measured at 134 MeV by Cassels and Lawson [8]) was 220 ± 24 mb.

A detailed discussion of the results will not be attempted because the data

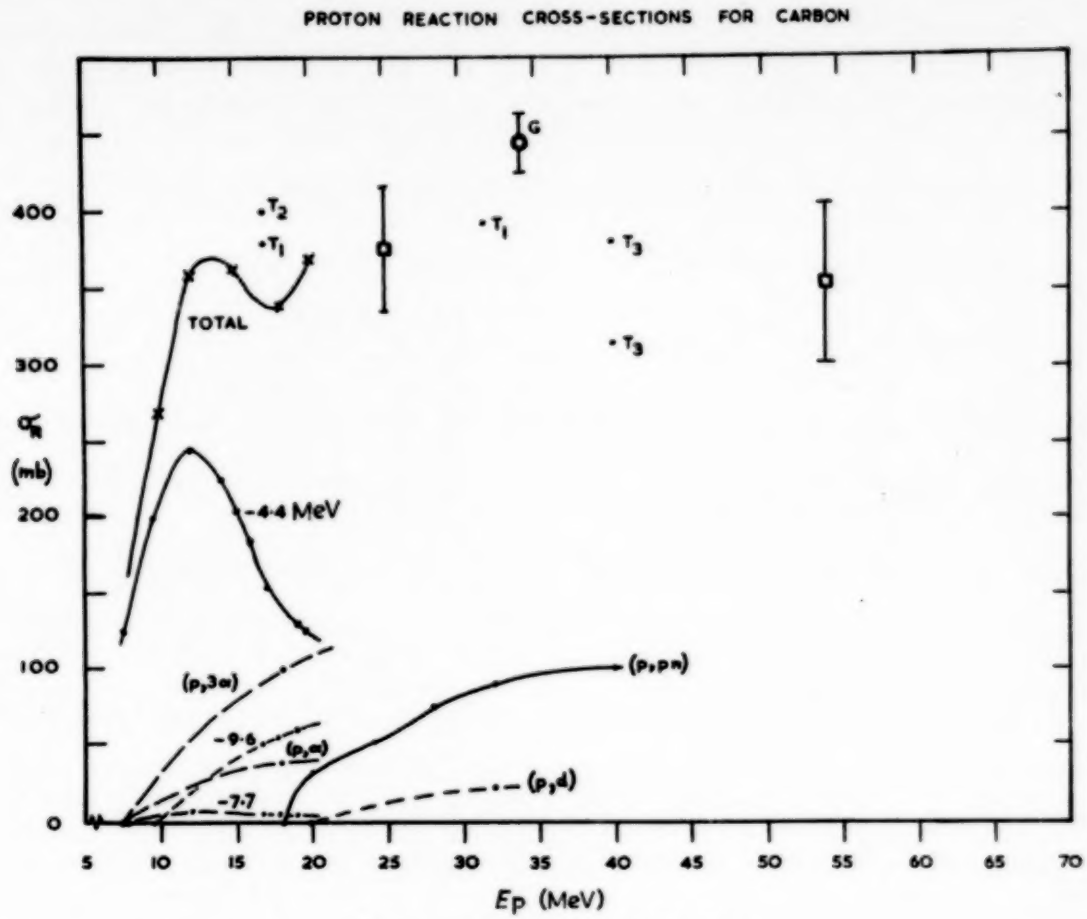

References for experimental points

(p, p′)

9.5 MeV : W. E. Burcham, W. M. Gibson, A. Hossain and J. Rotblat, Phys. Rev. **92** (1953) 1266
10 : G. E. Fischer, Phys. Rev. **96** (1954) 704
12 : H. E. Conzett, Phys. Rev. **105** (1957) 1324
14—19.4 : R. W. Peelle, Phys. Rev. **105** (1957) 1311
30—340 : D. Cohen, B. J. Moyer, H. Shaw and C. Waddell, Phys. Rev. **96** (1954) 714

(p, ?n) for all neutron producing reactions

18—32 : Y. K. Tai, G. P. Millburn, S. N. Kaplan and B. J. Moyer, Phys. Rev. **109** (1958) 2086

(p, pn), (p, d)

18—300 : R. L. Aamodt, V. Peterson and R. Phillips, Phys. Rev. **88** (1952) 739
(18—)461 : A. H. Rosenfeld, R. A. Swanson and S. D. Warshaw, Phys. Rev. **103** (1956) 413
31.5 : R. Britten, Phys. Rev. **88** (1952) 283
20—100 : N. M. Hintz and N. F. Ramsey, Phys. Rev. **88** (1952) 19

(p, α), (p, 3α)

19 : J. B. Reynolds, Phys. Rev. **98** (1955) 1289
29 : J. L. Need, Phys. Rev. **99** (1955) 1356

Fig. 1. Individual and total reaction cross-sections for carbon. The curve marked 'Total' gives the sum of the cross-sections for the individual reactions. The point 'G' is the experimental value found by Gooding. The points 'T' are theoretical values from optical model calculations: T_1-Melkanoff, Nodvik, Saxon and Woods [6]); T_2, T_3-Glassgold and Kellogg [7, 8]).

The points ⊥□⊥ are the results from the present work.

used are provisional and only three energies have been measured. The estimation of the tail for low energies is rather difficult and the method will almost certainly be more reliable at higher energies. Some indication of the errors introduced by spurious low energy particles can be estimated by considering the interval between 10 MeV and 4.4 MeV, the minimum energy for inelastic scattering to take place. The value for the tail at 10 MeV, given by Service, suggests an average cross-section of 360 ± 60 mb. It is of interest therefore to analyse the available information for individual reactions at the lower energies to try to estimate the total reaction cross-section. Some of the data are shown in the figure. It is clear that the total reaction cross-section between 4.4 and 10 MeV is much less than 360 mb. The method of calculation weights the cross-section towards the values for higher energies, since the range-energy relation is not linear, but the value is still too high. The difference is probably caused by background particles, despite the care taken to avoid slit scattering and other effects. However, the method is essentially concerned with differences and it can be expected that the background contributions will tend to cancel out.

An upper limit to the average total reaction cross section between 10 and 40 MeV can be set by assuming that the tail at 10 MeV is zero. The value is found to be 400 ± 40 mb, for $E = 25\pm15$ MeV. This is still rather lower than Gooding's value of 445 ± 20 mb at 34 ± 2.5 MeV, but may be partly attributed to a significant increase of the cross-section between 10 and 40 MeV, although the weighting of higher energies explained above acts in the opposite direction.

An estimate of the expected uncertainties in the application of the method can be made on the basis of Service's data. If γ_1 is the fraction of the total T_1 in the tail for energy E_1, and γ_2 and T_2 are the values for E_2, the percentage statistical uncertainty in the difference $\gamma_2-\gamma_1$ is approximately given by

$$u \approx \frac{100(\gamma_1/T_1+\gamma_2/T_2)^{\frac{1}{2}}}{\gamma_2-\gamma_1},$$

i.e. for $T_1 = T_2 = T$,

$$T = \frac{(\gamma_1+\gamma_2)10^4}{u^2(\gamma_2-\gamma_1)^2}.$$

From the results of Service for $(CH)_n$ plastic scintillator with a value of $\gamma_2 = 0.015$ and $\gamma_1 = 0.007$ for $E_2 = 30$ MeV and $E_1 = 20$ MeV, it follows that T should be 4×10^5 counts for a 3 % statistical uncertainty in the reaction cross-section. However, difficulties arising from the assignment of pulses to the tail especially at these energies may introduce comparable errors. At higher energies (65 MeV, say, for CH) the value of T would be almost the same.

4. Further Applications of the Method

A limitation on the method is imposed by considerations of decay time, energy resolution, and the cross-sections for the smaller Q-values, and in the

case of hydrogenous targets by the requirement of an approximately linear relation between pulse-height and energy. Several possible scintillators are available apart from hydrocarbons. Liquid and solid argon, krypton and xenon have been shown to scintillate [9]), and they have some promising characteristics. It is suggested [10]) that one half or more of the light observed is emitted in less than 15 ns, and the total light output is comparable with that for NaI(Tl). There is some evidence for a linear relation between pulse height and energy at low energies, but a satisfactory energy resolution may not be easy to achieve without very carefully designed optics. Liquid neon and helium have not yet been studied. Experiments are in progress to test liquid oxygen and nitrogen, H_2O (ice) and NH_3. When the total cross-section for carbon is better known it may be convenient to try other compounds such as CCl_4, and use a difference method.

An important feature of this method for reaction cross-sections is that the detector is also the 'target'. This is, of course, the situation in bubble chambers and nuclear emulsions, although the latter present ambiguities in the identification of the nuclear species involved.

References

1) T. J. Gooding, Minnesota Progress Report 1957-58 and private communications
2) R. M. Eisberg, Florida Optical Model Conference Report and private communication (1959)
3) L. H. Johnston, D. H. Service and D. A. Swenson, Minnesota Progress Report 1957-58
4) D. H. Service, Minnesota Progress Report (Nov. 1958)
5) A. E. Glassgold and P. J. Kellogg, Phys. Rev. **109** (1958) 1291
6) M. A. Melkanoff, J. S. Nodvik, D. S. Saxon and R. D. Woods, Phys. Rev. **106** (1957) 793
7) A. E. Glassgold and P. J. Kellogg, Phys. Rev. **107** (1957) 1372
8) J. M. Cassels and J. D. Lawson, Proc. Phys. Soc. A **67** (1954) 125
9) J. A. Northrop, J. M. Gursky and A. E. Johnsrud, Sixth Scintillation Counter Symposium (Washington, 1958);
J. A. Northrop and R. Nobles, Nucleonics **14**, No. 5 (1956) 36
10) J. A. Northrop, private communication

8.C

Nuclear Physics **13** (1959) 516—524; © *North-Holland Publishing Co., Amsterdam*

Not to be reproduced by photoprint or microfilm without written permission from the publisher

A NEW MODEL FOR MULTIPLE MESON PRODUCTION AT HIGH ENERGIES

WIESLAW CZYŻ †, TORLEIF ERICSON †† and SHELDON L. GLASHOW †††

Institute for Theoretical Physics and NORDITA (*Nordisk Institut for Teoretisk Atomfysik*), *Copenhagen* ††††

Received 17 August 1959

Abstract: A new approach to the multiple meson production process is proposed, which is based upon the peripheral nature and energy-independent behaviour of high-energy nucleon-nucleon collisions. A specific model suggested by the analogy with Čerenkov radiation is described.

1. Introduction

Recent experiments indicate several startling characteristics of ultra-high-energy nucleon-nucleon collisions that are not easily understood with current theoretical models. The observed low inelasticities [1, 2, 3]) and apparently large cross-sections of the multiple production events strongly suggest that they result from peripheral nucleon-nucleon collisions, in which the identity of the participating nucleons is retained. Thus, the statistical models of multiple meson production, requiring an immediate sharing of energy between incident and target nucleons, appear untenable if the nucleon is regarded as a core in which most of the mass is concentrated, surrounded by a large and more diffuse meson cloud. Moreover, a model in which the meson production is assumed to result from the decay of two highly excited nucleon isobars is certainly inconsistent with the observed low inelasticities, since the final nucleons (in the centre-of-mass system) must travel much more rapidly than the centres of mass of their meson emitting "fireballs" [4]).

Multiple production events, at energies of at least 5×10^{11} eV per nucleon, display a surprising degree of energy independence [1, 2]). Neither the mean multiplicity nor the distribution of transverse momenta of the shower particles seems to vary significantly over several orders of magnitude of primary energy; more striking still, the transverse momenta are not even correlated with the angle of emission of the shower particles, and generally fall quite close to 0.4 GeV/c [5]). Further, the inelasticity of these events is at most a weakly

† Present address: Instytut Badan Jądrowych, Kraków, Bronowice, Poland.

†† On leave from the Institute for Theoretical Physics, Lund, Sweden. Present address: MIT, Cambridge, Massachusetts.

††† National Science Foundation Postdoctoral Fellow.

†††† A preliminary report of this work was communicated by Prof. B. Peters to the 1959 Conference on Cosmic Rays in Moscow.

varying function of energy, perhaps assuming a small constant value at the higher energies.

The experiments clearly indicate [6, 7, 9]) that the emitted particles are mostly concentrated in two cones whose angles vary with the energy of the primary nucleon.

We should like to suggest a new model of the multiple production process which is at once founded upon the peripheral nature and the energy-independent behaviour of these high-energy collisions. During the peripheral interaction of two nucleons there is not sufficient time for the two energy-bearing cores to exchange signals: hence we shall assume that both the incident and the target nucleon, upon passing through the meson cloud of the other, act independently as emitters of shower particles. A two-cone structure of the event emerges naturally from the existence of two distinct meson sources.

With our hypothesis, it is convenient to describe the total angular distribution as a sum of the mesons produced by each nucleon core. Let $F_0(\theta, \gamma)$ be the most likely number of shower particles produced, at angles less than θ, by a nucleon of Lorentz factor $\gamma = (1-\beta^2)^{-\frac{1}{2}}$ (β denotes the nucleon velocity) passing through the periphery of another nucleon at rest. Those mesons produced by the passage of the target core through the incident cloud will have a similar angular distribution in the system of coordinates in which the incident nucleon is at rest. Transformed to the laboratory system, the integral angular distribution of mesons emitted by the target core is

$$F_0(\pi, \gamma)-F_0(\theta', \gamma),$$

where θ' is the angle in the system where the incident nucleon is at rest, corresponding to θ in the laboratory system:

$$\tan\theta = \frac{1}{\gamma}\,\frac{\sin\theta'}{\beta/u-\cos\theta'} \approx \frac{1}{\gamma}\cot\tfrac{1}{2}\theta'.$$

That both the meson's velocity u and the incident nucleon's velocity β are usually close to that of light, justifies the approximate expression. For most angles and energies occurring in practice, $\theta' \approx 2/\gamma\theta$ will be a sufficiently close approximation. Thus, the total angular distribution takes the form

$$F(\theta, \gamma) = F_0(\theta, \gamma)+F_0(\pi, \gamma)-F_0(2/\gamma\theta, \gamma). \tag{1.1}$$

Let us suppose that $F_0(\theta, \gamma)$ varies, as a function of θ, only in a region about θ_1, or equivalently, that a core passing through a cloud produces a cone of emitted particles. In general, θ_1 would depend upon energy. A critical energy $\gamma_1 = \cos\theta_1/(1-\cos\theta_1)$ may be defined at which $\theta_1 = \theta'(\theta_1)$. For events of about this energy, the cones produced by each nucleon core coincide; the resulting angular distribution will show a single cone structure. For $\gamma < \gamma_1$, the mesons emitted by the incident core will constitute the narrow cone, while those produced by the target core constitute the wide cone. For $\gamma > \gamma_1$ the

reverse is true and the target-nucleon core is the source of the high-energy mesons of the narrow cone. The prediction of a distinct two-cone structure for nucleon-nucleon events at energies either large or small compared to γ_1, and of a transition region of energies near γ_1 in which the two cones merge, is unique to this model and provides a crucial test of its validity.

2. Energy Independence

To incorporate into our model the energy-independent behaviour of multiple-production events, we shall assume that meson emission accompanying the passage of a nucleon core through a stationary cloud is independent of the energy of the incident nucleon. This is a realistic hypothesis only at sufficiently high energies. It implies that the function $F_0(\theta)$ is independent of γ. Thus, the entire energy dependence of the process arises from the purely kinematic dependence of θ' upon θ. In particular, the multiplicity and the distribution of transverse momenta will be energy-independent. The integral angular distribution of shower particles becomes

$$F(\theta) = F_0(\theta)+F_0(\pi)-F_0(2/\gamma\theta). \tag{2.1}$$

At energies large compared with the critical energy, $F(\theta)$ exhibits a cone $F(\theta) \approx F_0(\theta)$, near $\theta = \theta_1$, which is now a fixed angle, and a narrower cone, $F(\theta) \approx F_0(\pi)-F_0(2/\gamma\theta)$, near $\theta = 2/\gamma\theta_1$. For $\gamma \ll \gamma_1$, contrariwise, the narrow cone occurs at $\theta = \theta_1$ and the wider one at $\theta = 2/\gamma\theta_1$.

To compare our predictions with experiment, it is convenient to introduce a parameter Δ which is a measure of the separation in angle between the two cones. Most of the experimental data are given as plots of $\log [F/(1-F)]$ vs. $\log \tan \theta$ [6, 7, 9]; the angular distributions are normalized in such a way that $F(\pi)=1$ and $F_0(\pi)=\frac{1}{2}$. These curves exhibit two wings of steep increase (corresponding to the two cones) separated by a more or less extended plateau. The parameter Δ may then be determined by linearly extrapolating the two wings to their intersection with the $F = \frac{1}{2}$ axis. The difference in abscissa between these points is conveniently defined to be Δ. For an infinitely sharp cone, $F'_0(\theta) \propto \delta(\theta-\theta_1)$, Δ is identically $|\log(\gamma/\gamma_1)|$, while in general it may be expected to behave like $|\log(\gamma/\gamma_1)|$ far from the critical energy and to have a minimum at $\gamma = \gamma_1$. On fig. 1 are shown the existing experimental data in this connexion as well as the function $|\log(\gamma/\gamma_1)|$. The critical energy is estimated to be 1.5×10^{13} eV corresponding to a cone angle of $\theta_1 = 10^{-2}$ radians.

It is also illuminating to display the evolution in energy of the angular distribution for a reasonable choice of $F_0(\theta)$. Although we have not determined the function for which eq. (2.1) gives the best fit to experiment, we have considered the trial functions $F_0^{(n)} = \frac{1}{2}[1+(\theta_1/\theta)^n]^{-1}$. The $\log (F/(1-F))$ vs. $\log \tan \theta$ curves most resemble the experimental data for $n \approx 3$ (see fig. 2). At energies greater than γ_1 the point $\theta = \theta_1$ is approximately that of greatest

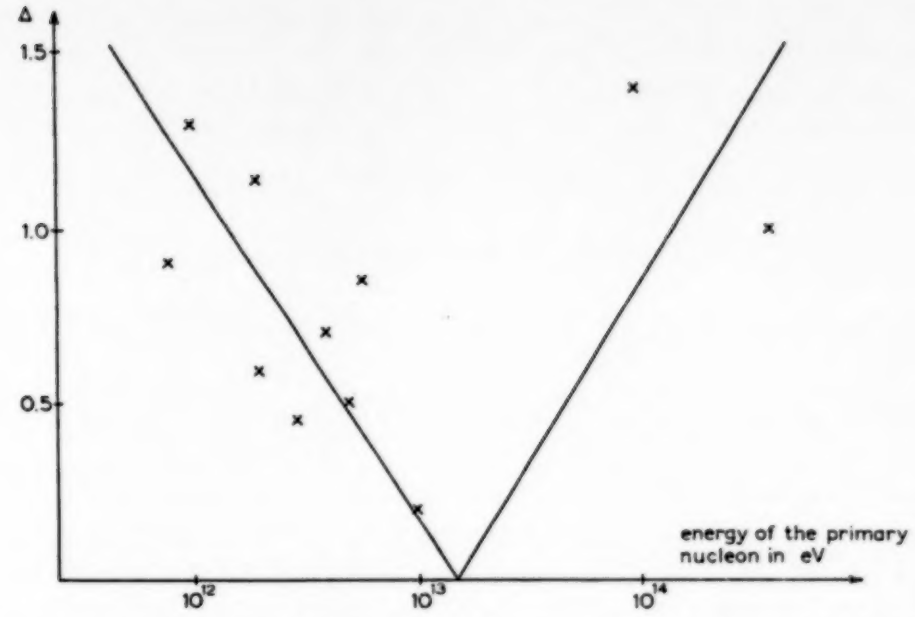

Fig. 1. The parameter Δ versus energy of the primary nucleon. × correspond to values of Δ obtained graphically from the curves collected by G. Cocconi, ref. [6]), fig. 2. Events identified Warsaw 4, Bristol 3, 4, 5, 7, are excluded because they do not clearly display the S shape. The solid curve shows $|\log(\gamma/\gamma_1)|$.

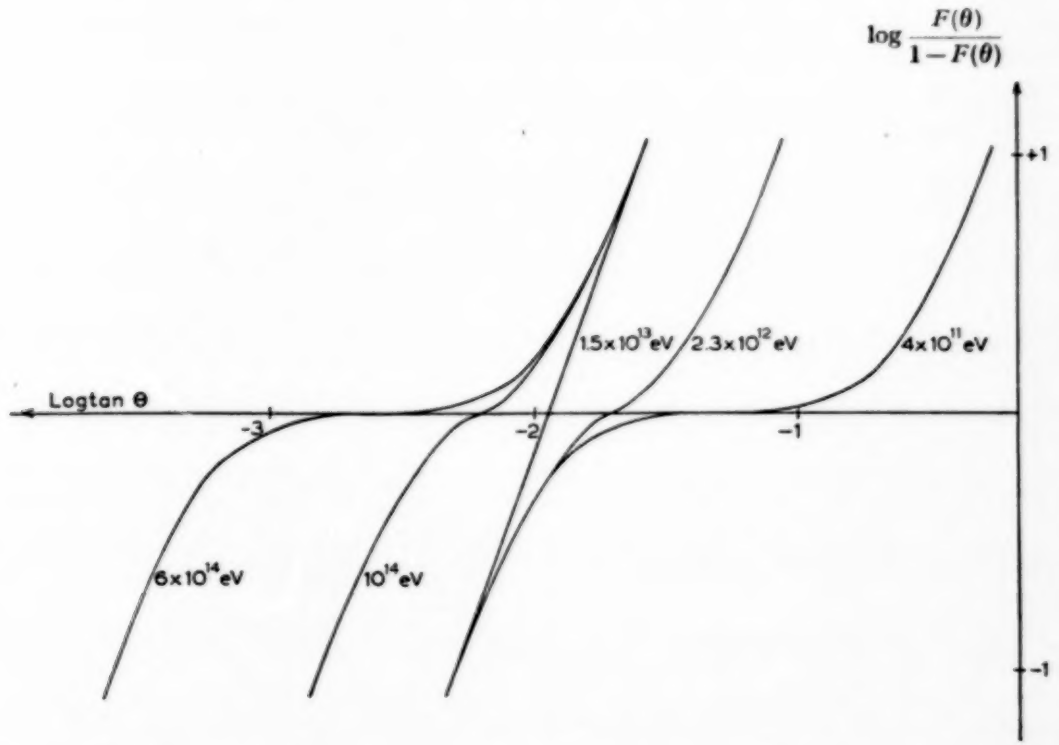

Fig. 2. Plot of $\log[F/(1-F)]$ versus $\log\tan\theta$ at several representative energies. $F(\theta)$ is given by eq. (1.1) with $F_0(\theta) = \frac{1}{2}[1+(\theta_1/\theta)^2]^{-1}$. θ_1 is determined from fig. 1.

curvature of the right-hand wing of the curve, while at low energies it is near the point of greatest curvature of the left-hand wing. That this is in agreement with the behaviour of the experimental curves [6, 7]) is evidence that one of the cones is indeed energy-independent.

From this picture we can estimate the contribution K' to the inelasticity coefficient † K arising from the formation of the two-cone structure. Assuming constancy of transverse momenta and approximating

$$2\int F_0'(\theta)\theta \mathrm{d}\theta \quad \text{by} \quad \theta_1,$$

$$2\int F_0'(\theta)\theta^{-1}\mathrm{d}\theta \quad \text{by} \quad 1/\theta_1,$$

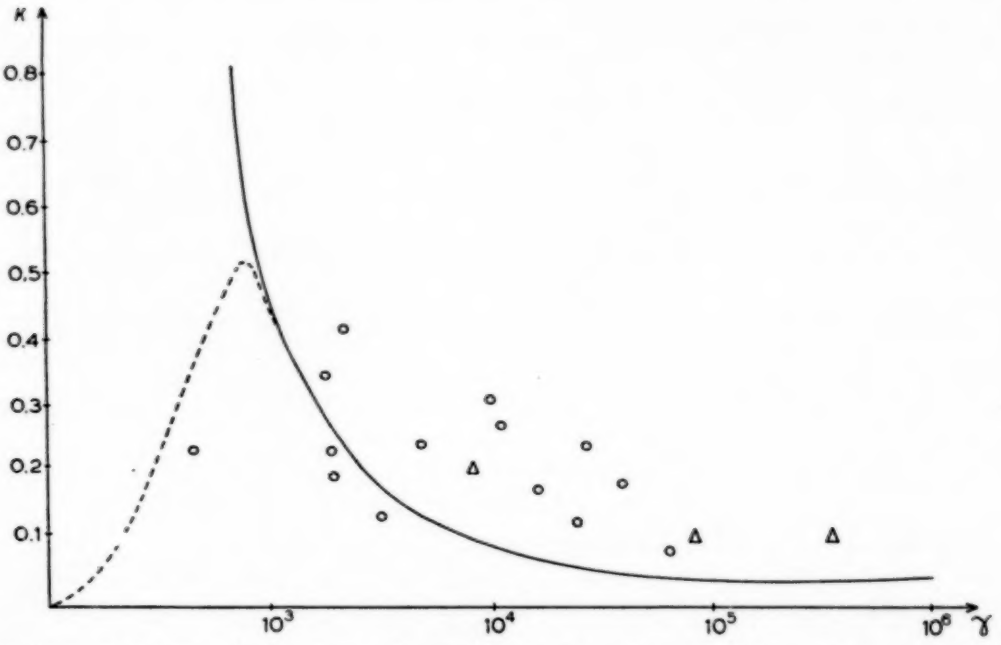

Fig. 3. Inelasticity K versus energy of primary nucleon (measured in nucleon mass units): o estimates for primary jets given by B. Edwards *et al.* [2]), △ estimates communicated privately by M. Mięsowicz. The solid curve shows the contribution of the two-cone structure to the inelasticity coefficient following from the energy-independence hypothesis (see eq. (2.2)). The dotted curve exhibits the corrections introduced if the analogy with Čerenkov radiation is pursued and recoil effects are included.

we obtain for the energy content of the energy-independent cone $\frac{3}{2}(\frac{1}{2}N)(k_T/\theta_1)$ and for that of the energy-dependent cone $\frac{3}{2}(\frac{1}{2}N)(\frac{1}{2}k_T\theta_1\gamma)$. Here N is the observed multiplicity of the shower particles, k_T is their mean transverse momentum, and the factor $\frac{3}{2}$ accounts for neutral pions. We obtain

$$K' = \tfrac{3}{2}(\tfrac{1}{4}N)k_T\theta_1\left(1+\frac{2}{\gamma\theta_1{}^2}\right);$$

† The coefficient K is defined as the ratio of all the energy of the created secondary particles to the kinetic energy of the incident nucleon in the laboratory system.

thus, for $N = 20$, $k_T = 0.46\, M/c$, (M = nucleon mass), $\theta_1 = 10^{-2}$,

$$K' = 0.03(1+2\times 10^4\gamma^{-1}). \tag{2.2}$$

In fig. 3 are shown several observed total inelasticities which are seen to tend to lie above the calculated value of K'.

3. Beginnings of a Theory

The production of mesons by a nucleon core passing through the periphery of another nucleon may be analogous to the appearance of Čerenkov photons along the trajectory of a charged particle moving sufficiently rapidly through a dielectric medium. If the self-field accompanying the incident nucleon cannot keep pace with the core, i.e. if the phase velocity of the mesons constituting the self-field is less than the velocity of the core, it is stripped from the core to emerge from the medium as one of the cones of shower particles. The composition of the shower is expected to be similar to that of the nucleon self-field, and a relatively large admixture of K-mesons is anticipated.

If we define a refractive index for the nucleon cloud by the formula

$$k' = kn(k^2) \tag{3.1}$$

(in which k' denotes the momentum in the medium of a meson which emerges with momentum k), the condition for coherent radiation of mesons (at angle θ with respect to the direction of motion of the moving core) becomes

$$\cos\theta = \frac{1}{\beta}\frac{k_0}{k}\frac{1}{n(k^2)}, \tag{3.2}$$

where k_0 denotes the energy of the meson: $k_0 = \sqrt{(k^2+\mu^2)}$, μ being the meson mass. Because the medium is not infinite, the nucleon core is not a point, and $n(k^2)$ is not constant throughout the nucleon periphery, there will occur upper and lower limits to the energies of the emitted mesons, as well as a finite spread in angle of emission of mesons with given momenta.

Assuming that the medium becomes transparent to sufficiently energetic mesons, we may write

$$n(k^2) \approx 1 + \frac{\lambda^2}{k^2} \quad \text{for} \quad k^2 \gg \lambda^2 \tag{3.3}$$

(λ^2 is positive if $n(k^2)$ arises from an attractive pion-pion interaction). From (3.2) and (3.3) follows the lack of dependence of the transverse momenta of the shower particles upon either incident energy or angle of emission—one of the few well-documented facts about the multiple production events:

$$k_T = k\sin\theta \approx \sqrt{2\lambda^2-\mu^2}. \tag{3.4}$$

Using the experimental values $k_T = 0.46\, M/c$ and $\theta_1 = 10^{-2}$ radians, we find

$\lambda^2 \approx 5\mu^2$, and a refractive index of roughly 1.000 05 for the typical shower particle.

The Čerenkov analogy provides the energy-independence assumed in the previous section so long as the incident nucleon is sufficiently fast: $(n-1)/(1-\beta) \gg 1$, or $\gamma \gg 10^{11}$ eV. But at lower energies the Čerenkov process must break down. Thus, we should not expect the constancy of transverse momenta to continue to energies less than several hundred GeV. The energy at which this mechanism fails is two orders of magnitude less than the "critical energy" at which the two cones merge, and there is a large region in which the results of the earlier sections are applicable.

We must, however, take into account the velocity-dependence of the Čerenkov mechanism in the formula for inelasticity. Assuming that the amount of energy coherently radiated [10]) behaves as $1-(n\beta)^{-2}$, and taking into account the recoil corrections discussed in the appendix, we find that the contribution to the inelasticity (due to the formation of the two-cone structure) is modified by the multiplicative factor

$$c(\gamma) = \begin{cases} (\gamma\varepsilon)^{-1}(\gamma-\theta_1^{-1})^2 & \text{for } \theta_1^{-1} \leqq \gamma \leqq \varepsilon+\theta_1^{-1}, \\ 1-(\gamma^2-\gamma\varepsilon)^{-1}\theta_1^{-2} & \text{for } \varepsilon+\theta_1^{-1} < \gamma, \end{cases}$$

where ε is the energy of the target cone $\frac{3}{4}Nk_T/\theta_1 \approx 600$ GeV. This is again consistent with the data, since the modified expression for K' never exceeds unity.

The existence of a refractive index governing the propagation of mesons through the periphery of a nucleon necessarily gives rise to some pion-nucleon scattering. Eq. (3.3) has been assumed for meson energies of order $k_0 \approx k_T/\sin\theta_1 \approx 40$ GeV. If its validity may be extrapolated to ≈ 2 GeV (at which $k^2 \approx 40\lambda^2$), a connexion is established to the experimentally observed pion-nucleon cross-sections. In order for the nucleon cloud to display the refractive index of eq. (3.3), a pion must satisfy the Klein-Gordon equation ($\hbar = c = 1$)

$$\left(-\nabla^2 - E^2 + \mu^2 - 2\lambda^2 H(x)\right)\phi(x) = 0, \tag{3.5}$$

where $H(x)$ defines the extent of the nucleon cloud:

$$H(x) = \begin{cases} 1 \text{ for } |x| \leqq a \\ 0 \text{ for } |x| > a. \end{cases}$$

For the purpose of an estimate, we put the size of the nucleon's periphery equal to one pion Compton wavelength, $a = \mu^{-1}$. Then the total cross section, in Born approximation for $ka \gg 1$, is [8]) †

$$\sigma = 2\pi\mu^{-2}(\lambda/\mu)^4(\mu/E)^2. \tag{3.6}$$

At 2 GeV this becomes 14 mb whereas the observed pion-nucleon cross-section at this energy is 30 mb [9]).

† Eq. (26.30) of ref. [8]) is relevant with the substitutions $E \to E^2/2\mu$ and $V_0 \to \lambda^2/\mu$ for $E^2 \gg \mu^2$.

4. Conclusion

In the sections 1 and 2 we have outlined a new and simple model of the ultra-high-energy nucleon-nucleon collisions which accounts for at least the grosser features of the process. Certainly, however, not all the meson production can occur in this fashion†, nor must every event fall into the predicted pattern: for example, we have not considered a direct core-core interaction which must certainly be responsible for some of the meson production. In section 3 we have suggested one plausible direction in which a proper theory may lie, although there is now no adequate theoretical justification for the appearance of such a refractive index as we require, or indeed, for the very existence of a mesonic Čerenkov effect.

We are much indebted to Professors A. Bohr and B. Peters and to Doctors J. Goldstone and K. Gottfried for stimulating and fruitful discussion and criticism, as well as to Professor M. Mięsowicz and his group for making available unpublished experimental material. We wish to thank Professor Niels Bohr for the hospitality extended to us at his Institute, and for a fellowship awarded to one of us (W. C.).

Appendix

We want to discuss the effect upon our results of the recoil of the participating nucleons. At high energies this is a small effect, vanishing with the inelasticity. It may be estimated in the idealized limit of perfectly rigid nucleons. Assuming symmetry in the centre-of-mass system and azimuthal symmetry of the meson production, we find for the recoil of the target nucleon in the laboratory system

$$\gamma_R = 1 + \frac{K^2}{2(1-K)},$$

where K is the actual inelasticity. Similarly, $\gamma' = (1-K)\gamma$ is the final energy of the incident nucleon. Because the systems of reference in which one nucleon is at rest change during the course of the collision, an averaging must be performed which will smear the target cone between θ_1 and $(1-K)\theta_1$, and the incident cone between $2/\gamma\theta_1$ and $(1+K)2/\gamma\theta_1$. The effect upon angular distributions is small provided that the inelasticity is small, but it may serve to increase the apparent transition energy to $(1+K)\gamma_1$. As the energy at which the Čerenkov mechanism becomes inoperative is approached, the effects of recoil become more pronounced. This is included in the corrections to the inelasticity mentioned

† The energy content of the two-cone structure yields a contribution to the inelasticity that becomes 4 % at the highest observed energies. The experimentally determined inelasticities in this region are generally at least 10 %.

in § 3 and in the modified expression for K' plotted in fig. 3. We should also anticipate a reduction of the value of the transverse momentum observed in the lower energy jets, perhaps amounting to a factor of one-half at 500 GeV.

References

1) Z. Koba and S. Takagi, Fortschritte der Physik **7** (1959) 1
2) B. Edwards *et al.*, Phil. Mag. **3** (1958) 237
3) N. A. Dobrotin *et al.*, preprint
4) K. Niu, Nuovo Cimento **10** (1958) 994
5) O. Minakawa *et al.*, Nuovo Cimento Supplemento **11** (1959) 125
6) G. Cocconi, Phys. Rev. **111** (1958) 1701
7) P. Ciok *et al.*, Nuovo Cimento **10** (1958) 741
8) L. Schiff, Quantum Mechanics (1949) p. 167
9) Proc. Sixth Rochester Conference (1956) IV-8
10) See, e.g., J. V. Jelley, Čerenkov Radiation and its Applications (1958) p. 19

2.C

Nuclear Physics **13** (1959) 525—540; © *North-Holland Publishing Co., Amsterdam*

Not to be reproduced by photoprint or microfilm without written permission from the publisher

GAMMA RAY SPECTRA AND PARAMETERS OF NEUTRON RESONANCES IN MERCURY

J. R. BIRD, M. C. MOXON and F. W. K. FIRK

A.E.R.E., *Harwell, Didcot, Berks.*

Received 5 August 1959

Abstract: The gamma ray spectra from resonant neutron capture in mercury suggest that resonances in Hg^{199} at 33.5, 175, 263 and 315 eV have $J = 1$, while the 128 eV resonance has $J = 0$. These results are in agreement with the results of transmission measurements. Resonance parameters are determined for seven resonances up to 209 eV. The gamma ray spectra for resonances in other isotopes show end points which are in agreement with binding energies calculated from mass measurements. The shape of the various spectra show the presence of fluctuations of at least 5 : 1 in the intensity of individual gamma rays, from resonance to resonance. The presence of gamma ray peaks at either 368 or 439 keV assists in the allocation of resonances to either Hg^{199} or Hg^{201}.

1. Introduction

Detailed measurements have been made of the gamma ray spectra from thermal neutron capture in many elements (e.g. Kinsey [1]), Groshev *et al.* [2]). However, similar measurements for resonant neutron capture have been limited by the lack of suitable gamma ray detectors for use with the relatively weak sources of resonance energy neutrons.

The Yale Group [3]) have observed individual low energy gamma rays (below 1 MeV) which are prominent in the spectra from capture in a variety of heavy nuclei. These gamma rays usually correspond to transitions between rotational energy levels in deformed nuclei and have intensities which in many cases are proportional to the capture area for each resonance. Kennett and Bollinger [4]) have observed coincidences between low and high energy gamma rays for manganese and mercury. They observed significant fluctuations from resonance to resonance in the intensity of individual high energy gamma rays.

Landon and Rae [5]) and Rae and Firk [6]) have observed a difference in the high energy part of the gamma ray spectra from thermal capture in Hg^{199} and from capture at the 33.5 eV resonance. This nucleus has spin $\frac{1}{2}$ so that the capturing state in Hg^{200} will have spin 0 or 1. In the former case radiation to the spin 0 ground state is forbidden. Thus the presence or absence of the ground state transition at a particular resonance establishes the spin of the capturing state involved. Effects of this kind have been observed by Fox *et al.* [7]) and Vinh-Dinh Huynh *et al.* [8]) for capture by W^{183} and Pt^{195} using a single channel to select gamma rays close to the binding energy in each case.

Preliminary results of the measurement of high energy gamma rays following neutron capture in tungsten and mercury have been reported previously by Bird [9]), indicating that measurements of this kind can provide a considerable amount of information concerning the final nuclei involved. The present paper gives the gamma ray spectra for all the major resonances in mercury up to 300 eV, together with the results of transmission measurements. Since spin $\frac{1}{2}$

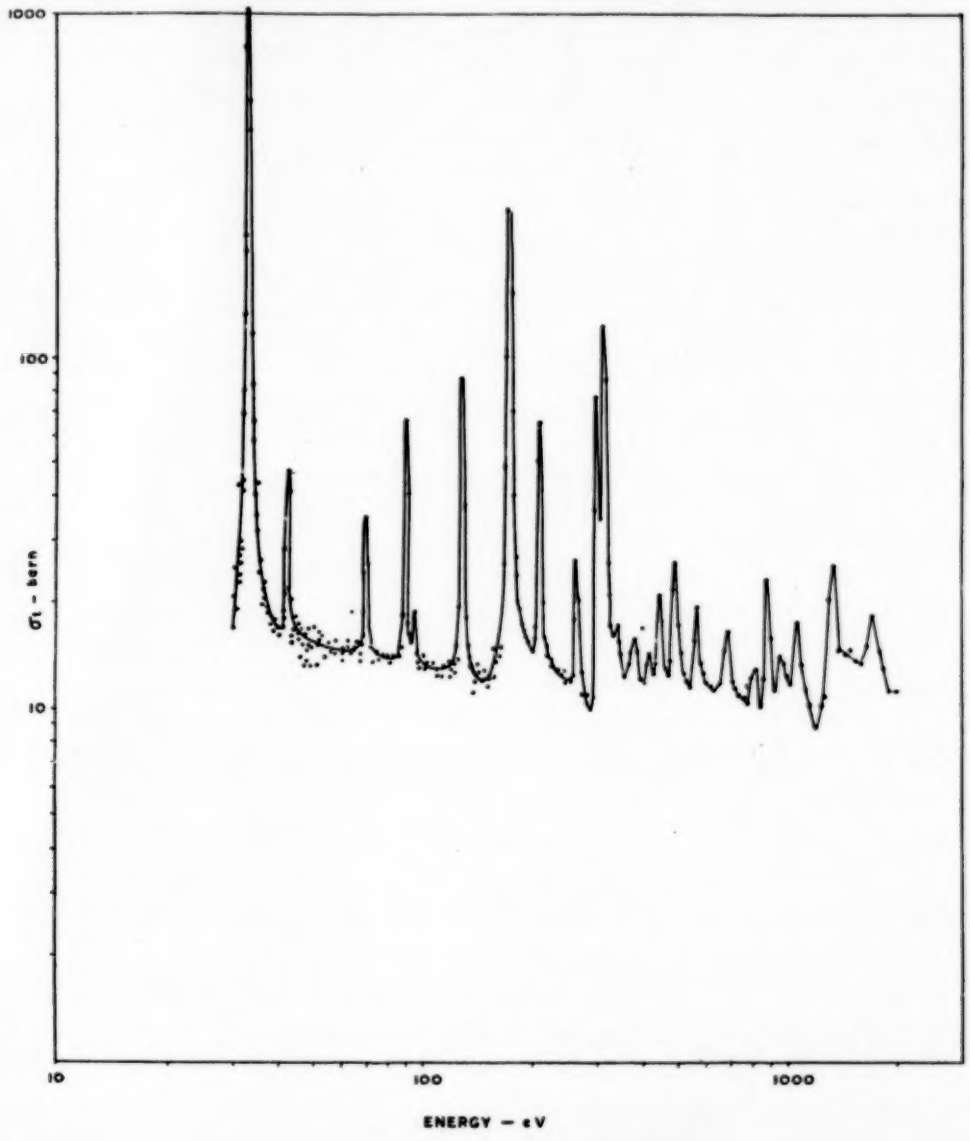

Fig. 1. Total neutron cross section of mercury.

nuclei are particularly suitable for the determination of resonance spins by cross section measurements it is of interest to compare these results with those deduced from the gamma ray spectra. In this way it is also possible to obtain the parameters for most of the resonances. The low energy parts of the gamma

ray spectra are also given since these allow information to be obtained on the isotopic allocation of the various resonances.

2. Isotope Assignment

The total cross section of mercury obtained from transmission measurements for neutrons in the energy range 30 to 2000 eV is shown in fig. 1. An additional resonance at 23 eV is not shown. These results were obtained with a time of flight resolution of 0.03 microseconds per metre. The resonance energies and their isotopic allocation given by Palmer and Bollinger [10]) are shown in table 1.

TABLE 1

Isotope assignment of mercury resonances

Resonance energy (eV)	Low energy gamma rays		Isotope transmission	
	Energy (keV)	Isotope	Palmer and Bollinger [10])	Carpenter and Bollinger [11])
23	—	Even	198	198
33.5	368	199	199	199
43	439	201	201	201
71	439	201	199?	
90	—	Even	198?	198
94				
128	368	199		199
175	368	199	199	199
209	439	201		201
263	368	199		199
270				202?
302				198
312	368	199	198	201
315				199

Mercury has two odd mass stable isotopes which will contribute many of the low energy neutron resonances. Capture in these isotopes leads to the formation of Hg^{200} and Hg^{202} which have first excited states at 368 and 439 keV respectively. Ground state transitions from these states are found to be prominent in the capture gamma ray spectra. Since such transitions will be fed by a multitude of different cascades from the high energy capturing state, their intensity should not vary greatly from resonance to resonance. Thus the identification of such transitions should help to determine the isotope responsible for each resonance.

Gamma rays in the energy range 0.2 to 0.6 MeV have been observed for most of the resonances up to 300 eV using a 2″ by 2″ sodium iodide crystal. The results are shown in fig. 2. The spectra for the 23 and 90 eV resonances show no structure other than annihilation radiation at 510 keV. This is consistent with their allocation by Palmer and Bollinger to capture by Hg^{198} since Hg^{199} has too many low lying excited states for these to be distinguished by this method.

All the other resonances show a definite peak due to a gamma ray at either 368 or 439 keV. Each can therefore be attributed to capture by either Hg^{199} or Hg^{201} and these results are included in table 1. The group of resonances between 300 and 315 eV were not resolved in this work but the small 368 keV gamma ray peak in the combined spectrum is assumed to indicate that one of the resonances at least is due to Hg^{199}.

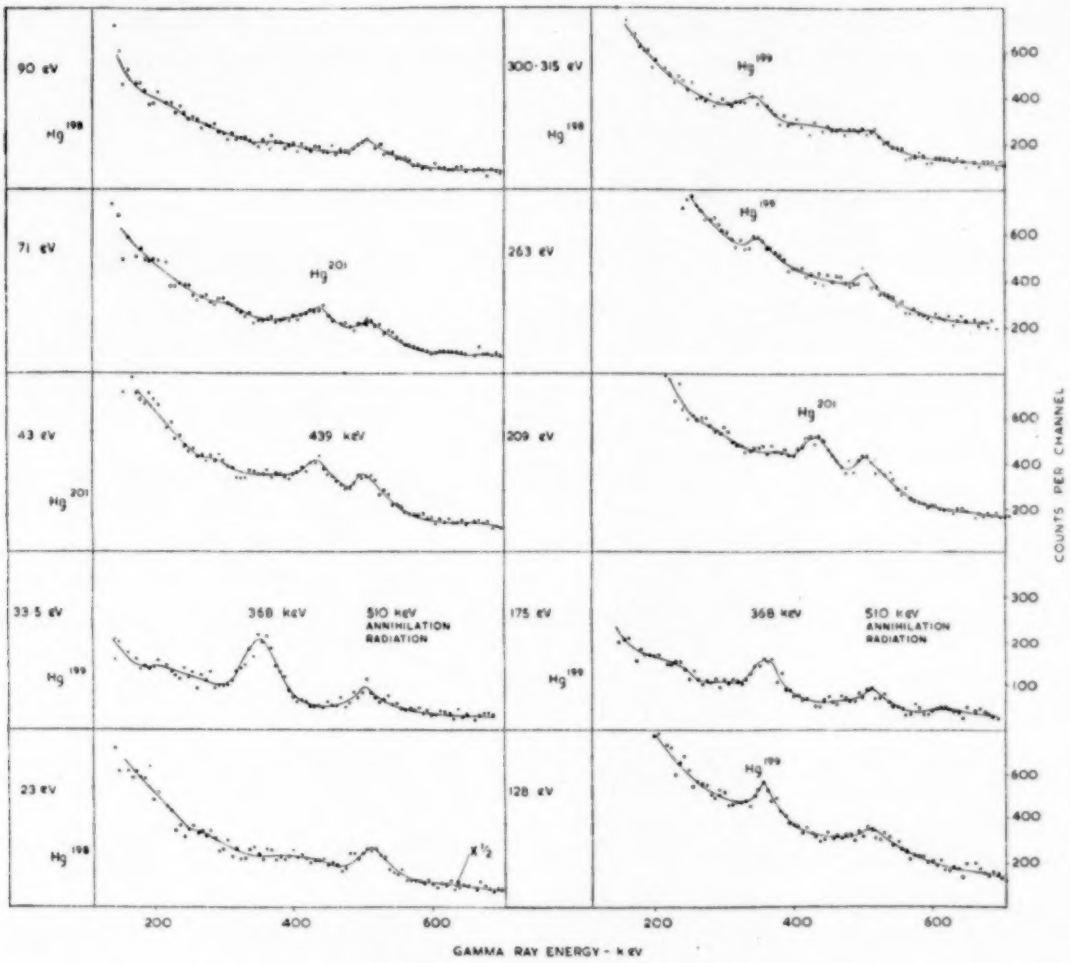

Fig. 2. Low energy gamma rays from mercury resonances.

Transmission measurements on separated mercury isotopes have recently been reported by Carpenter and Bollinger [11]) and their results are also given in table 1. The results of the different experiments are in agreement in most cases but several small resonances remain unassigned. Such resonances are too small to make major contributions to the gamma ray spectra but their presence may limit the reliability of intensity measurements in some cases.

The relative intensities of the low energy gamma rays observed for each resonance are compared in table 2. The area in each peak was obtained by subtracting the background which was assumed to follow a smooth curve. The areas were then normalised to the same number of captured neutrons for each

resonance. The errors are the statistical errors in the determination of gamma ray intensities and capture areas. Two sets of results are given for the Hg^{199} resonances and the relative γ-yields are seen to be constant provided that Hg^{199} is responsible for only one third of the capture in the resonances from 300 to 315 eV. The γ-yields for the Hg^{201} resonances are also constant. Thus the intensity of the transition from the first excited state to the ground state is proportional to the total capture area to within about 10 %.

TABLE 2

Intensities of low energy gamma rays

Resonance energy (eV)	Relative areas of gamma ray peaks		
	368 keV (Hg^{199})		439 keV (Hg^{201})
33.5	194 ± 5	188 ± 10	
43			104 ± 17
73			107 ± 20
128	195 ± 27	180 ± 25	
175	206 ± 32	178 ± 25	
209			107 ± 17
263	155 ± 50	240 ± 70	
300–315	67 ± 13	58 ± 10	

3. Gamma Ray Spectra

3.1. METHOD

Measurements of gamma rays in the energy range 4 to 9 MeV have been made using the arrangement shown in fig. 3. A target of 400 grams of mercury

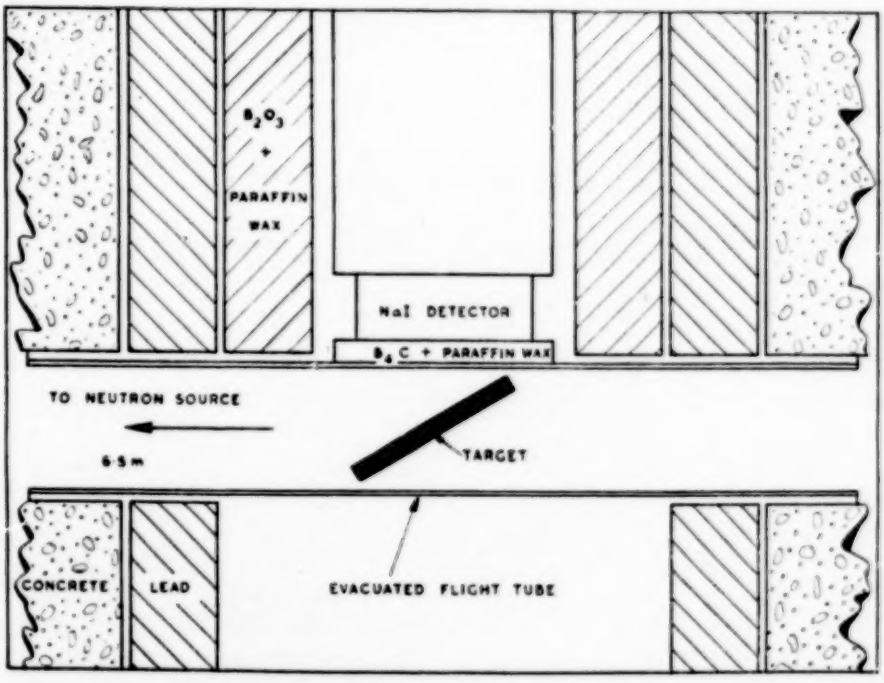

Fig. 3. Apparatus for measurement of gamma ray spectra.

oxide was placed at 45° to a pulsed neutron beam 3″ in diameter from the Harwell Linear Accelerator. A NaI(Tl) crystal 4.5″ diameter by 4″ with 10 % resolution for Cs^{137} gamma rays was used as detector. The crystal was completely surrounded by paraffin wax and boron compounds to reduce the number of

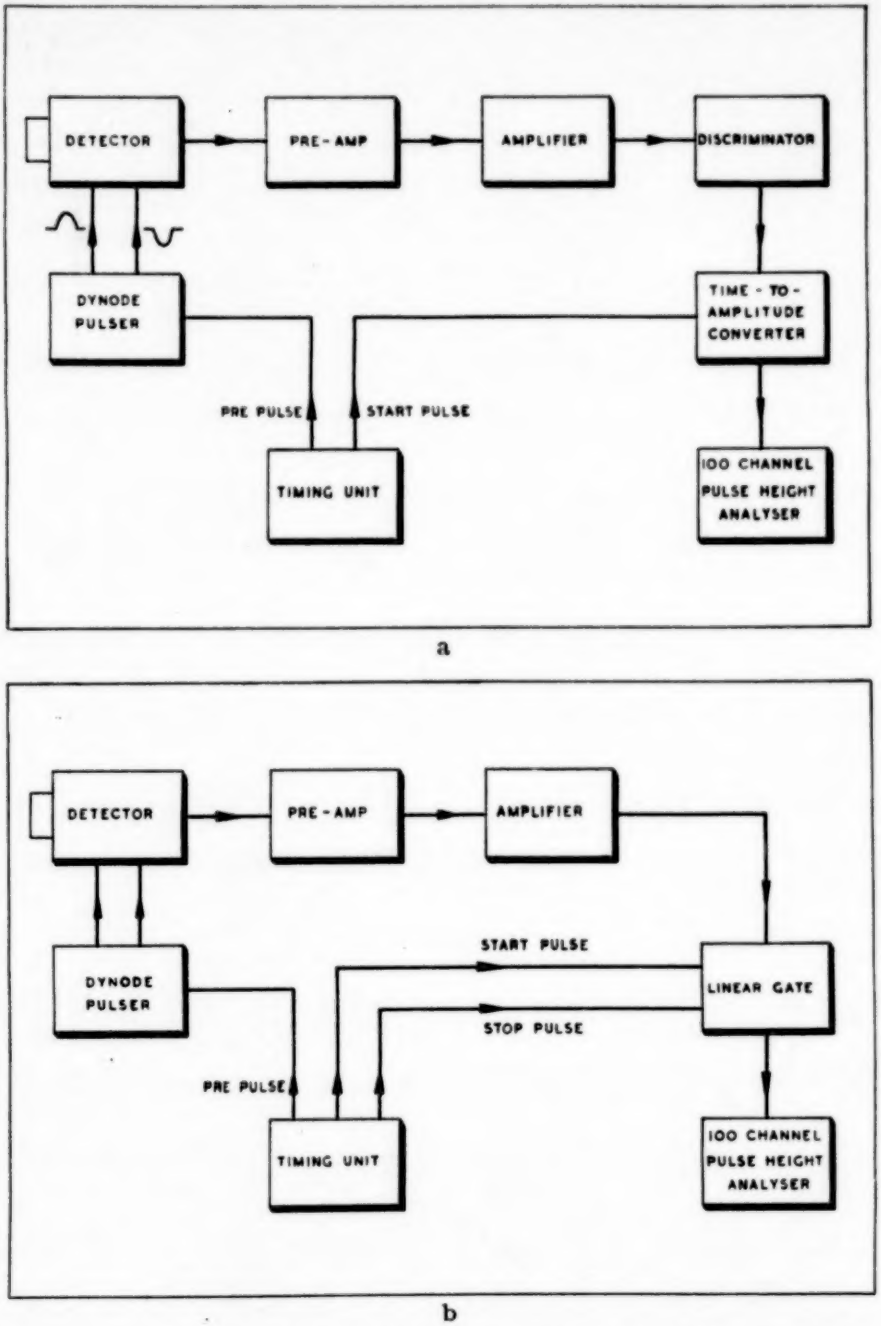

Fig. 4. (a) Block diagram of electronics for time of flight measurements.
(b) Block diagram of electronics for gamma ray spectra measurements.

scattered neutrons detected by capture in the crystal. Additional lead and concrete shielding was used to reduce the background.

Neutrons of resonance energies were obtained by timing their flight over a 6.5 metre flight path with a resolution of 0.05 microseconds per metre. The electronic equipment is shown in schematic form in fig. 4(a). The dynode pulser applies large positive and negative pulses to two successive dynodes in the photomultiplier to prevent saturation of the electronics by the very large gamma ray pulse occurring at zero time. The use of a time to amplitude converter allows the choice of timing channel widths to suit the spectrum being studied. The positions and widths of resonances are found and also their relative areas which give a measure of the total number of capture events involved in each case. The dependence of background intensity on time is also obtained from the time of flight curves.

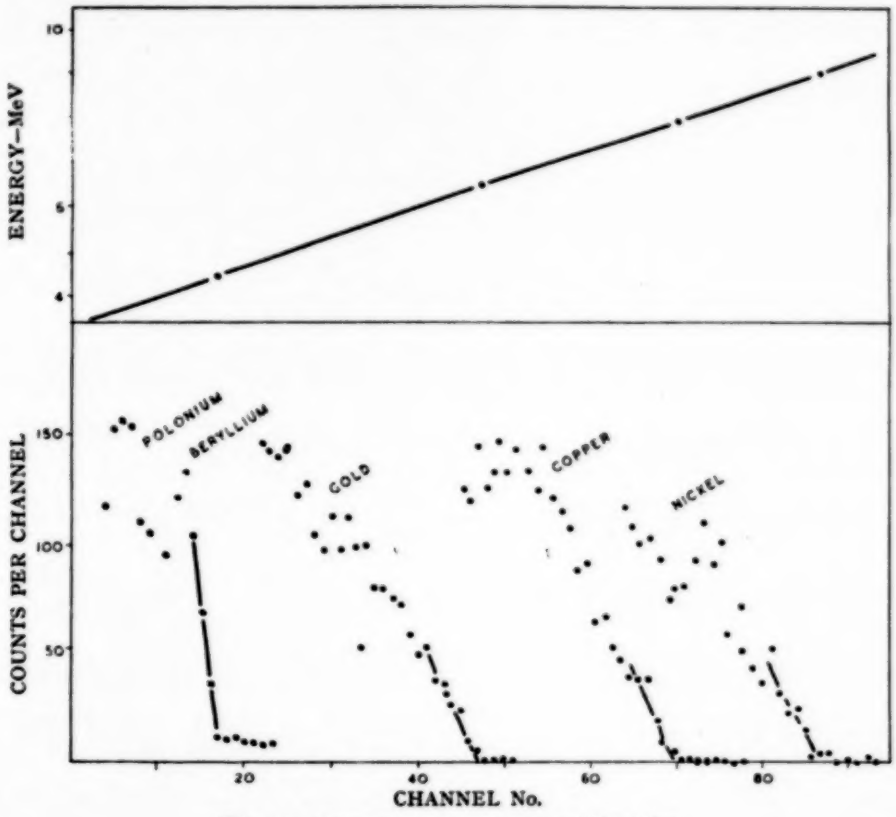

Fig. 5. Gamma ray energy calibration.

The equipment used for studying the gamma ray spectra is shown in fig. 4(b). The linear gate is opened for a time interval sufficient to span a particular resonance. The dependence of the background on gamma ray energy is obtained by making measurements between resonances. A gamma ray energy scale was obtained by measuring the gamma rays from various radioactive sources and from neutron capture in gold, copper and nickel. The latter give strong ground state gamma rays whose energies are taken from the results of thermal capture [2]). Typical spectra are shown in fig. 5. Because of the complexity of the capture spectra their most characteristic feature is the sharp rise in

count rate due to the highest energy gamma ray. The extrapolated upper edge of each spectrum was therefore used to give calibration points which are seen to lie satisfactorily on a straight line. The energy scale given on the high energy gamma ray spectra therefore indicates the place at which a gamma ray of a given energy will cause a rise in count rate. Energies determined in this way should not be in error by more than ± 0.2 MeV.

3.2. RESULTS

The gamma ray spectra will be presented for the resonances in each capturing isotope of mercury. Background has been subtracted and the results normalised to the same number of capture events for each resonance. The ordinate scales however give the actual number of counts observed and statistical errors are indicated in a few representative places.

(A) $Hg^{198}(n, \gamma)Hg^{199}$

The gamma ray spectra for the 23 and 90 eV resonances are given in fig. 6. The end point of each spectrum is at about 6.6 MeV which is in good agreement

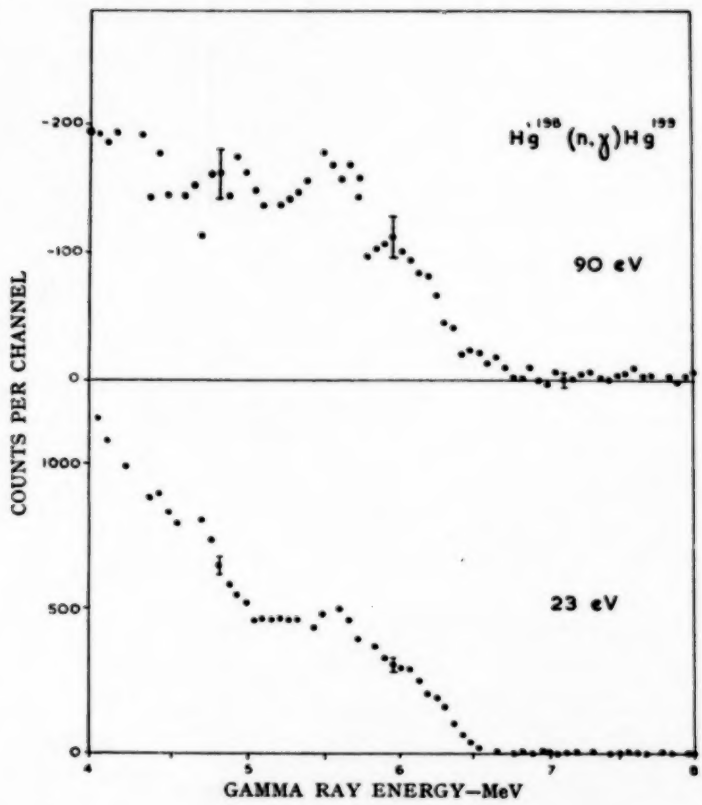

Fig. 6. Gamma ray spectra from neutron capture in Hg^{198}.

with the value of 6.68 MeV obtained for the binding energy from mass measurements (Johnson and Bhanot [12])). The ground state radiation will be electric

dipole for all resonances since the capturing state and ground state in Hg^{199} are $\frac{1}{2}^+$ and $\frac{1}{2}^-$ respectively. There are many low lying excited states in Hg^{199} which can also be reached by electric dipole radiation so that it is not surprising that the spectra show little sign of structure. The only major change in count rate occurs for the 23 eV resonance at a gamma ray energy of 5.1 MeV. However, the main feature of the two spectra is their different shape. Although there is some suggestion of the presence of a 5.1 MeV gamma ray for the 90 eV resonance, its intensity is much less than for the 23 eV resonance.

(B) $Hg^{201}(n, \gamma)Hg^{202}$

Gamma ray spectra for the resonances at 43, 73 and 209 eV are given in fig. 7. The highest energy gamma ray observed for the 209 eV resonance is at

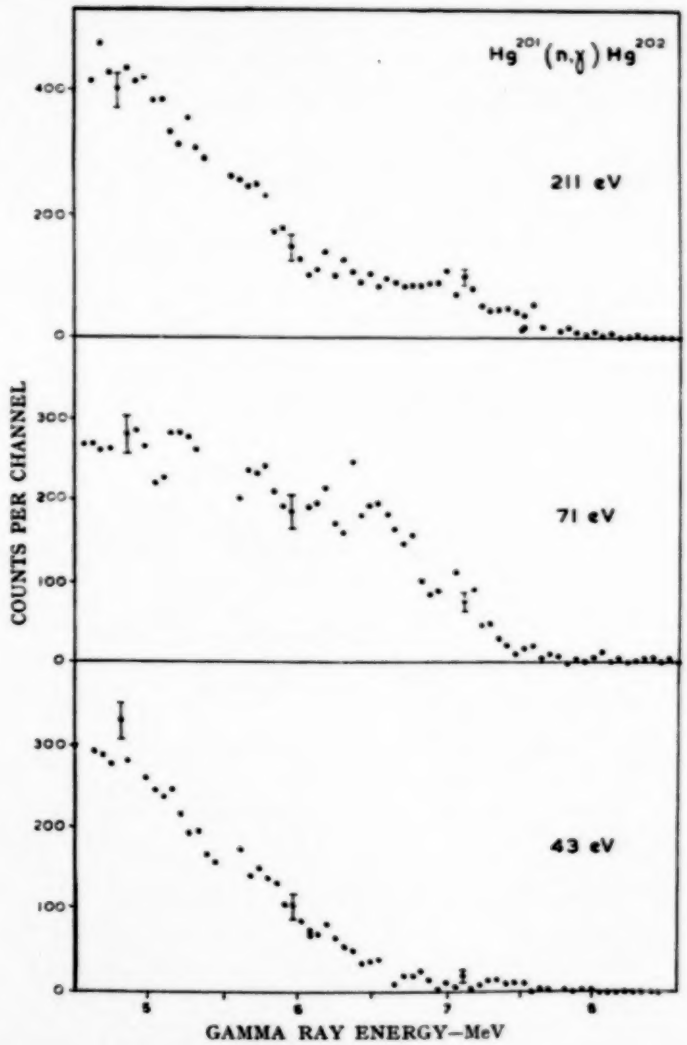

Fig. 7. Gamma ray spectra from neutron capture in Hg^{201}.

7.7 MeV which is in satisfactory agreement with the binding energy (7.78 MeV) calculated from mass measurements [12]). The other two resonances show very few counts at this energy. The first indication of a strong gamma ray for the 73 eV resonance is at 7.4 MeV and for the 43 eV resonance at 6.7 MeV. The ground state of Hg^{201} is $\frac{3}{2}^-$ so that 1^- or 2^- capturing states may be formed in Hg^{202}. In the former case electric dipole radiation is possible to the ground state (0^+), and to the first excited state ($2+$) at 439 keV. If the capturing state spin is 2, E1 radiation is possible only to the first excited state. If we assume that E1 radiation is stronger than other multipolarities the spectra for the 209 and 73 eV resonances can be explained by assuming that they are due to 1^- and 2^- capturing states respectively. However, the spectrum for the 43 eV resonance is not similar to either of the other two. If it is due to an s-wave resonance in Hg^{201}, it can only be explained by assuming the presence of strong variations in intensity of individual gamma rays from resonance to resonance. Such variations render doubtful any deductions concerning the spin of energy levels, purely from considerations of gamma ray intensities and the expected multipolarities.

(C) $Hg^{199}(n, \gamma)Hg^{200}$

The work of Kinsey and Bartholomew [13]) and Adyasevich *et al.* [14]) showed that the ground state transition is absent from thermal capture in Hg^{199}. This may be explained by assuming that thermal capture is dominated by a negative energy resonance forming a capturing state with spin 0 from which radiation to the 0^+ ground state is forbidden. Landon and Rae [5]) showed that the spectrum for the 33.5 eV resonance is of significantly higher energy than the thermal spectrum, which suggests that the 33.5 eV resonance forms a spin 1 capturing state in Hg^{200}. This is illustrated in fig. 8(a).

The observed end point for the 33.5 eV resonance is in satisfactory agreement with the values of the binding energy obtained by Adyasevich *et al.* (8.03 MeV) and Johnson and Bhanot (8.08 MeV). The thermal spectrum was obtained by making observations with and without a cadmium filter in the neutron beam and shows few counts above 6.5 MeV. Its shape agrees well with the results of previous workers (e.g. Segel [15])), bearing in mind the difference between the performance of a single sodium iodide crystal and the more elaborate detectors which they have used.

In fig. 8(b), (c), (d) the spectra for the resonances at 128, 175, 263 and 300 to 315 eV are compared with the curves of fig. 8(a). The spectrum for the 128 eV resonance is seen to be similar to the thermal spectrum and is best explained if it is assumed that a spin 0 capturing state is formed by this resonance. The other spectra are best explained by assuming that they are due to the formation of spin 1 capturing states. The ground state gamma rays make relatively small contributions to the spectra so that it is not possible to establish the spin beyond doubt in most cases. However, it will be shown in the following section that the

results of the transmission measurements give the most satisfactory set of resonance parameters when the same spin values are used.

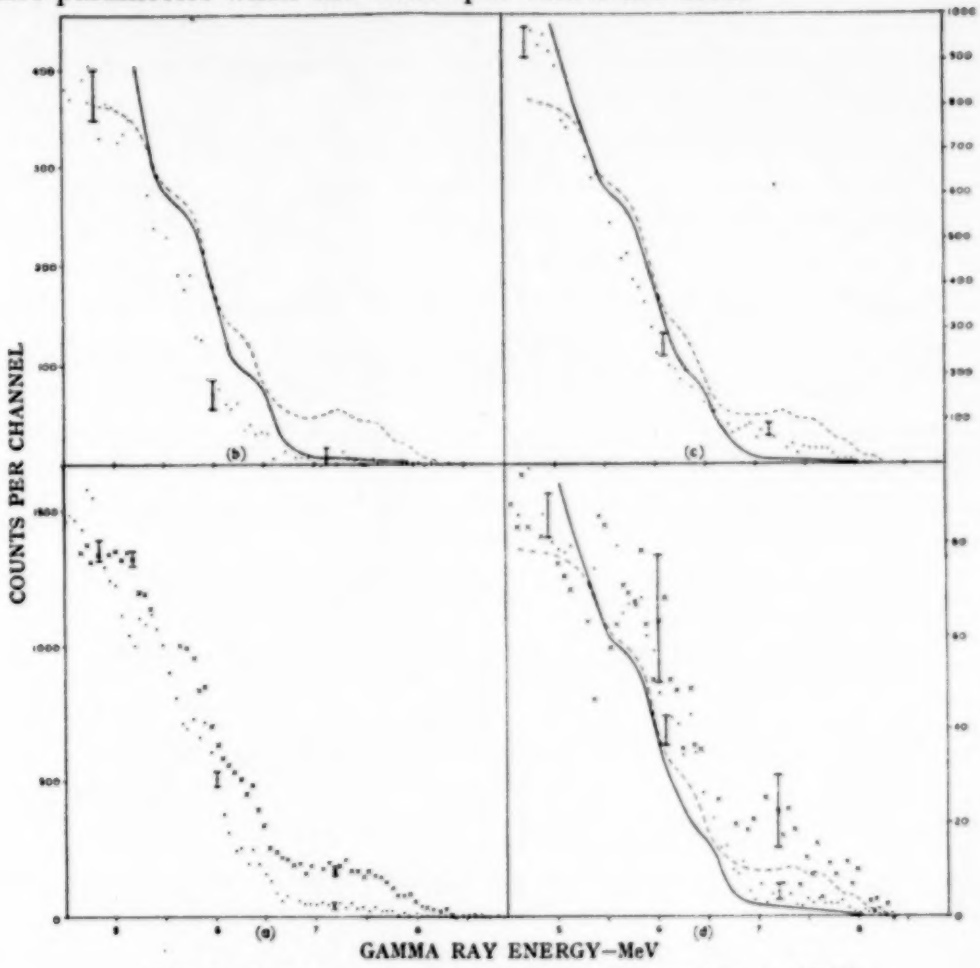

Fig. 8. Gamma ray spectra from neutron capture in Hg^{199}.

(a) . . . . Thermal
× × × × 33.5 eV

(b) ——— Thermal
– – – – 33.5 eV
. . . . 128 eV

(c) ——— Thermal
– – – – 33.5 eV
. . . . 175 eV

(d) ——— Thermal
– – – – 33.5 eV
× × × × 263 eV
. . . . 300–315 eV

TABLE 3
Intensities of high energy gamma rays

Resonance energy (eV)	Relative areas in gamma ray spectra	
	Between 7 and 8.25	Between 7.75 and 8.25
Thermal	22± 4	12±10
33.5	100	100
128	11± 3	12± 7
175	37± 4	20± 5
263	150±50	185±60
300–315	41± 6	45± 9

The areas above energies of 7 and 7.75 MeV for the various spectra are given in table 3 normalised to the results for the 33.5 eV resonance. Fluctuations in intensity are evident although these are of limited extent for the spin 1 resonances (less than a factor of 10). The possible existence of larger fluctuations means that it is only possible to suggest that the 128 eV resonance has zero spin.

It should be noted that the spectra for capturing states with the two possible spins are very similar (see e.g. fig. 8(a)). In the thermal spectrum, the absence of a ground state transition and the weakness of the transitions to the first and second excited states at 368 and 950 keV is expected from a consideration of the spins involved ($0^- \rightarrow 0^+$, $0^- \rightarrow 2^+$, $0^- \rightarrow 4^+$). However, for the spin 1 resonances the transitions to the ground and first excited states are electric dipole and their relative weakness requires explanation. The strongest transitions in both kinds of spectra occur to levels above 1.5 MeV which corresponds to the pairing energy of Hg^{200}. It is possible that these transitions are enhanced by virtue of a strong single particle configuration in the final states. The shell model interpretation of Hg^{199} indicates that the odd neutron is in a $p_{\frac{1}{2}}$ shell which gives a satisfactory explanation for the strong gamma rays to the ground and low excited states observed in the reaction $Hg^{198}(n, \gamma)Hg^{199}$. However, in Hg^{200}, the pair of neutrons go into an $i_{13/2}$ shell. The emission of ground state radiation in capture by Hg^{199} must therefore be accompanied by a considerable reshuffle of the angular momentum of the nucleus and it is not surprising that a relatively small partial width results. Partial widths approaching the single particle estimates may, however, be expected for transitions to excited states based on a nuclear multiplet involving a pair of neutrons, one of which is in a p state. Such an explanation is similar to that used by Groshev [16]), to account for the spectra of certain odd-odd nuclei.

Segel [15]) has suggested from a consideration of the gamma rays from thermal capture in Hg^{199} and the radioactive decay of Tl^{200} that all the levels observed between 1.5 and 2 MeV have negative parity. In this case electric dipole radiation would not be possible to these from either 0^- or 1^- capturing states. If the strongest gamma rays from 1^- capturing states are magnetic dipole it is even more difficult to understand their successful competition with the electric dipole high energy gamma rays. It seems most likely therefore that at least some of the excited states between 1.5 and 2 MeV have positive parity.

4. Transmission Measurements

The transmission of natural mercury samples of various thicknesses has been measured with a time of flight resolution of 0.03 microseconds per metre, using techniques which have been reported previously by Lynn *et al.* [17]). The observed total cross section is shown in fig. 1, for the energy range 30 to 2000 eV. Areas were obtained for each sample thickness for resonances between 30 and 200 eV

TABLE 4

Mercury resonance parameters

Resonance energy (eV)	Isotope	Sample thickness $\times 10^{24}$ atoms · cm^{-2}	Area (eV)	Spin J	σ_0 ($\times 10^3$ b)	Γ (eV)	Γ_n (eV)	Γ_γ (eV)
33.5±0.2	199	0.000 080 4	0.31±0.03	0	7.4 ±1.5	0.38±0.04	0.14±0.03	0.24±0.05
		0.002 19	2.71±0.05					
		0.017 8	7.79±0.11	1			0.05±0.01	0.33±0.04
		0.017 8	7.46±0.24					
43.0±0.3	201	0.001 71	0.27±0.03		0.42±0.08	0.29±0.05	0.004	0.29±0.05
		0.014 0	1.20±0.07				($g = \frac{1}{2}$)	
71.0±0.6	201	0.001 71	0.48±0.06					
		0.003 66	0.81±0.05		0.60±0.08	0.36±0.05	0.012±0.001	0.35±0.05
		0.014 0	1.87±0.13				($g = \frac{1}{2}$)	
90.0±0.8	198	0.001 30	0.90±0.08					
		0.002 77	1.24±0.07		6.0 ±0.3	0.16±0.01	0.032±0.003	0.13±0.01
		0.010 7	2.29±0.15					
128 ±1	199	0.001 24	1.26±0.11	0			0.15 ±0.03	0.33±0.06
		0.002 19	1.79±0.06		2.0 ±0.2	0.48±0.05		
		0.017 8	5.13±0.41	1			0.05 ±0.01	0.43±0.06
175 ±2	199	0.000 31	3.45±0.5	0			2.9	−1.6
		0.002 19	9.78±0.3		8.3 ±1.5	1.3 ±0.2		
		0.017 8	28.7 ±0.9	1			0.9 ±0.2	0.4 ±0.3
209 ±3	201	0.000 242	0.62±0.07	1	2.6 ±0.3	0.65±0.07	0.40 ±0.04	0.25±0.09
		0.014 0	7.11±0.20	2			0.24 ±0.02	0.41±0.08

and the values are given in table 4. These results were then corrected for the effects of sample thickness and Doppler broadening (Hughes [18])), and, in the case of the thickest samples for the effects of interference between resonant and potential scattering (Lynn [19])). The latter correction was of considerable importance for the 33.5 and 175 eV resonances. For example, for a sample such that $n\sigma_0 \approx 100$ (n is the number of nuclei per cm^2, σ_0 the peak cross section) a 10 % correction was necessary to the area of the 175 eV resonance. This represents a 20 % correction to the value of $\sigma_0\Gamma^2$ (Γ is the total width). Each area was used to define a curve of σ_0 versus Γ and an additional curve was obtained using the minimum transmission method described by Lynn and Rae [20]). The best values of σ_0 and Γ obtained from the data are included in table 4. The values of the neutron widths Γ_n and radiation widths Γ_γ corresponding to the appropriate values of the spin J of the capturing state are also given in table 4. The preferred values for the resonances in Hg^{199} are underlined.

Using the value $J = 1$ for the 33.5 eV resonance, a radiation width of 0.33 ± 0.03 eV is obtained which agrees well with the value 0.31 ± 0.04 eV given by Levin and Hughes [21]). The radiation widths for the 128 and 175 eV resonances are also in agreement with this value if they are assumed to have spins 0 and 1 respectively. The evidence for $J = 0$ for the 128 eV resonance is not conclusive but the agreement between these results and the deductions from the gamma ray spectra gives added weight to the parameters underlined in table 5.

The radiation width for the 90 eV resonance is found to be 0.13 ± 0.01 eV which is in good agreement with the value 0.145 ± 0.02 eV given by Levin and Hughes for the 23 eV resonance. The radiation width for Hg^{201} is approximately the same as for Hg^{199}. The two values for different spins for the 209 eV resonance are not sufficiently accurate to give any indication of the correct spin value. The radiation widths for the two odd isotopes are both approximately twice what would be expected on the basis of observed binding energies and level spacings using the formula given by Stolovy and Harvey [22]). Thus the peak in radiation widths observed for nuclei in this mass region does not appear to be completely explained by the effects of shell closure on binding energy and level density.

It is tempting to associate the large radiation width for Hg^{199} with the enhancement of individual transitions which has been discussed in the previous section. This implies that the presence of strong p wave single particle configurations amongst the low lying excited states dominates the capture process in this mass region. On the other hand it has been pointed out by Cameron [23]) that a peak in radiation widths around mass number 160 may be associated with the peak in neutron strength functions in this region. Hence the existence of a peak in strength functions around mass number 180 (Chase, Wilets and Edmonds [24])) may also produce a counterpart in radiation widths. In this case the capture

spectrum should be of normal shape but with unusually large partial widths for all gamma rays. In either case it is not surprising that the calculation of radiation widths by the method of Blatt and Weisskopf (see refs. [22, 23])) does not give an adequate description of the detailed variations with mass number since it does not permit the use of suitable weighting factors to allow for the nature of the initial and final states.

5. Summary

The gamma ray spectra observed for resonant neutron capture in mercury are consistent with the results obtained by previous workers for thermal capture. The identification of characteristic low energy transitions allows information to be obtained on the isotopic assignment of the resonances. The spectra obtained for each capturing isotope show high energy end points which agree with the binding energies calculated from mass measurements.

For resonances in Hg^{199} a comparison of the intensities of the high energy gamma rays leads to suggested values for the spins of the capturing states involved. These values are in agreement with the results of transmission measurements from which a complete set of resonance parameters can then be obtained. The shapes of the high energy part of the various spectra show the dependence of partial radiation widths on the nature of the initial and final states involved and also reveal the presence of considerable fluctuations from resonance to resonance even when these have the same spin.

It is a pleasure to acknowledge the co-operation of the members of the Linear Accelerator Group at the various stages of this work.

References

1) B. B. Kinsey, Neutron Capture Gamma Rays. in β and γ-Ray Spectroscopy (North-Holland Publishing Co. Amsterdam 1955) p. 195
2) L. V. Groshev, A. M. Demidov, V. N. Lubsenko and V. I. Pelekhov, Atlas of γ-ray spectra from radiative capture of thermal neutrons (Principal Commission on the Utilisation of Atomic Energy, U.S.S.R. Council of Ministers, Moscow 1958) (English Edition: Pergamon Press, London, 1959)
3) C. A. Fenstermacher *et al.*, Phys. Rev. **107** (1957) 1650
4) T. J. Kennett, L. M. Bollinger and R. T. Carpenter, Phys. Rev. Letters **1** (1958) 76
5) H. H. Landon and E. R. Rae, Phys. Rev. **107** (1957) 1333
6) E. R. Rae and F. W. K. Firk, Nucl. Instr. **1** (1957) 227
7) J. D. Fox *et al.*, Bull. Am. Phys. Soc. **3**(1958) 176; **4** (1959) 34; **4** (1959) 271
8) Vinh-Dinh Huynh, J. Julien, C. Gorge, F. Netter and J. Simic, Comptes Rendus **248** (1959) 2330
9) J. R. Bird, Proc. 2nd Int. Conf. Peaceful Uses of Atomic Energy (1958) Paper 15/P/35; J. R. Bird, M. C. Moxon and F. W. K. Firk, Bull. Am. Phys. Soc. **4** (1959) 34
10) R. R. Palmer, L. M. Bollinger, Phys. Rev. **102** (1956) 228
11) R. T. Carpenter and L. M. Bollinger, Bull. Am. Phys. Soc. **4** (1959) 271
12) W. H. Johnson Jr. and V. B. Bhanot, Phys. Rev. **107** (1957) 1669

13) B. B. Kinsey and C. A. Bartholomew, Can. J. Phys. **31** (1953) 1051
14) B. P. Adyasevich, B. D. Groshev and A. M. Demidov, Conf. Acad. Sci. U.S.S.R. on Peaceful Uses of Atomic Energy, Phys. Math. Sci., p. 195 (Consultants Bureau, N. Y. 1955)
15) R. E. Segel, Phys. Rev. **111** (1958) 1620
16) L. V. Groshev and A. M. Demidov, Atomnaya Energiya **3** (1957) 91
17) J. E. Lynn, F. W. K. Firk and M. C. Moxon, Nuclear Physics **5** (1958) 603
18) D. J. Hughes, J. Nucl. En. **1** (1955) 237
19) J. E. Lynn, Nuclear Physics **7** (1958) 599
20) J. E. Lynn and E. R. Rae, J. Nucl. En. **4** (1957) 418
21) J. S. Levin and D. J. Hughes, Phys. Rev. **101** (1956) 1328
22) A. Stolovy and J. A. Harvey, Phys. Rev. **108** (1957) 353
23) A. G. W. Cameron, Proc. Col. Conf. in Neutron Interactions with Nucleus, U.S.A.E.C. Tech. Inf. Service, TID-7547 (1957) p. 68
24) D. M. Chase, L. Wilets and A. R. Edmonds, Phys. Rev. **110** (1958) 1080

8.B *Nuclear Physics* **13** (1959) 541—548; © *North-Holland Publishing Co., Amsterdam*
Not to be reproduced by photoprint or microfilm without written permission from the publisher

THE ENERGY DEPENDENCE OF THE POLARIZATION OF ELECTRONS AND TIME PARITY

A. I. ALIKHANOV, G. P. ELISEYEV and V. A. LUIBIMOV
Institute of Theoretical and Experimental Physics of the USSR, Academy of Sciences, Moscow

Received 15 May 1959

Abstract: New measurements of the energy dependence of the polarization of the β-electrons from RaE show no significant violation of time parity.

1. Introduction

In our previous paper [1]) it was suggested that the polarization of RaE electrons may differ from v/c and this suggestion was confirmed experimentally. For the 250 keV mean energy electrons from RaE the polarization was found to equal $-(0.73\pm0.04)v/c$. Similar results have been obtained in other investigations [2–4]).

Although the β-radioactive element RaE involves first forbidden Coulomb transitions ($1^- \rightarrow 0^+$) its β-spectrum significantly differs from the Fermi spectrum which is characteristic of all other known allowed transitions and of first order forbidden Coulomb transitions.

Yamada [5]) and later others [6–8]) have satisfactorily explained this phenomenon by considering the change in the electron wave function in the field of the nucleus. They showed that for some matrix elements interference in the expression for the β-decay probability may result in mutual cancellation of the dominant terms which weakly depend on the energy; those higher order terms in the expansion which strongly depend on energy thus begin to play a more important role and this permits one to explain theoretically the experimental shape of the RaE β-spectrum.

Lewis [9]) and also Fujita *et al.*[10]) have pointed out that in this case the shape of the β-spectrum should be sensitive to any possible violation of time parity; the sensitivity in this case being so large that the experimental shape of the spectrum can be explained only by assuming that the degree of violation of time parity is very small.

Geshkenbein, Nemirovskaya and Rudik [11]) and other authors [12, 13]) have demonstrated that if the shape of the spectrum derived by Yamada is made to agree with the experimental shape, the polarization of the RaE electrons should actually differ from $-v/c$ and lie in a narrow region which contains the measured values.

Thus, the only certain case of deviation of β-electron polarization from v/c has been explained by a theory which also yields an explanation from a unified viewpoint of the anomaly in the shape of the β-spectrum. The close agreement between the experimental and theoretical values of the RaE β-electron polarization is a very strong argument in favour of the results obtained by Yamada *et al.* and hence of the conclusion made by Lewis and others that with a high degree of precision time parity is conserved.

Geshkenbein *et al.*[11]) have examined the effect of possible violation of time parity on electron polarization; to make a more reliable estimation of the degree of violation of time parity by measuring the energy dependence of the polarization. This possibility was already pointed out in ref. [1]).

The present paper is an attempt in the same direction.

2. Measurements

Electron polarization was determined by measuring the azimuthal asymmetry of transversely polarized electrons in single large angle scattering on a thin gold foil. Transformation of longitudinal into transversal polarization was performed by deflecting the electron trajectory by 90° by multiple scattering on a relatively thick scatterer.

The apparatus described in detail in the previous paper [14]) was used in the present investigation in a slightly modified form.

In order to exclude most of the systematic errors relative measurements of RaE and Tm^{170} electron polarization were carried out. According to our absolute measurements [14]) the polarization of the Tm^{170} electrons as well as those of other Coulomb transitions is to within 3 % equal to $-v/c$. On the other hand, according to our present-day knowledge there is no reason for expecting any deviation from v/c exceeding a few percent for the overwhelming majority of Coulomb transitions.

The polarization measurements were performed at various values of the mean energy of the electrons. Since the end point energies of the RaE and Tm^{170} electrons are almost equal the mean energies of the electron selected are also close to each other under identical conditions and the differences between them were taken into account by introducing small corrections to the relative values of the RaE electron polarization.

Since the RaE and Tm^{170} electron polarizations are not the same, relative measurements permit one to exclude only systematic errors which alter the value of the polarization by a certain factor; however, additive corrections cannot be eliminated in this way. A correction of the latter type is that which accounts for asymmetry of an instrumental origin. It would be convenient if these corrections were the same for RaE and Tm^{170}. Instrumental asymmetry may partly be due to a non-uniform distribution of the

active substance in the sources; it may be different for RaE and Tm^{170}. In order to eliminate this asymmetry produced by a non-uniform distribution of the activity in the sources, the latter were rotated about their axes during the measurements. Rotation through an angle about 60° was performed automatically when one source was replaced by another. Substitution and rotation of the samples was carried out without impairing the vacuum in the system. The remaining instrumental asymmetry associated with the geometry of the electron beam should not vary with change of the sources. Direct measurements of the instrumental asymmetry on an aluminium scatterer showed that it was indeed the same to within 0.5 % for RaE and Tm^{170} electrons and was about 3 %.

Each measurement run was considered complete after the sources had made a full turn. The duration of the measurement cycle was chosen so that decay of the source during the measurements was of no significance. Variation of the activity of the RaE source as a result of decay did not directly influence the measured asymmetry in as much as the measurements were carried out simultaneously with two counters in the "left" and "right" positions.

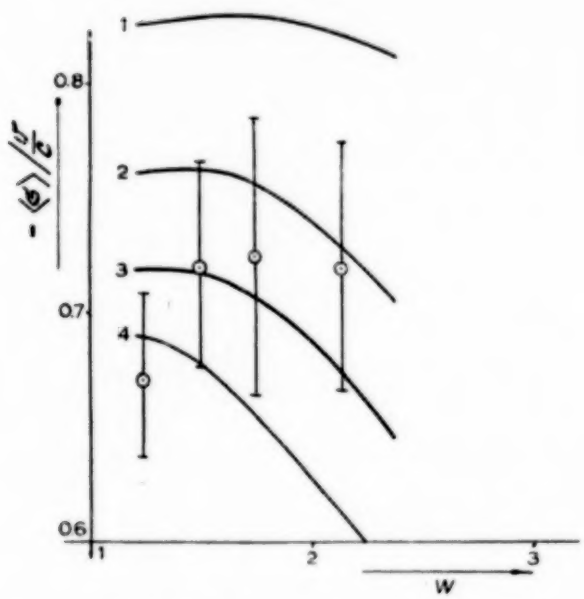

Fig. 1. Energy dependence of RaE electron polarization. Theoretical curves are calculated by the model of Geshkenbein *et al.*[11]).
Curve 1: $F = 0$, $X = 0.2$
Curve 2: $F = 0$, $X = 1.0$
Curve 3: $F = 0$, $X = 1.6$
Curve 4: $F = 0$, $X = 2.0$.

As in the preceding investigations [14, 1]) the measurements were performed at two positions of the scatterer; the second position was attained by rotating the scatterer about an axis perpendicular to the scatterer through an angle of 180°.

The background was measured by placing in the apparatus an empty frame without a scatterer. It was about $\frac{1}{5}-\frac{1}{10}$ of the intensity observed with the scatterer in position.

Depolarization of the electrons in the sources (source thicknesses: 0.8mg/cm^2 for Tm^{170} and 0.1 mg/cm^2 for RaE) was small and was taken into account as usual by means of the factor $(1-\frac{1}{2}\overline{\theta^2})$ where $\overline{\theta^2}$ is the mean square multiple scattering angle.

The activity of the Tm^{170} source was 150 mC and the initial activity of the RaE sources was 70—90 mC.

The effect due to the "covered" source on the counting rate with another source in the "working" position was small and was taken into account.

The RaE electron polarization relative to that of Tm^{170} is shown in fig. 1 for mean electron energies of 135 keV, 250 keV, 390 keV and 600 keV.

3. Discussion

As was stated above, spectrum and polarization anomalies may be accounted for by very intense interference which leads to the disappearance of the dominant terms, and a theoretical explanation of anomalies is therefore possible only if the electron wave function in the field of the nucleus is known as exactly as possible.

It has been found that in considering first forbidden Coulomb transitions all anomalous effects may be accounted for if we take into account only the highest terms $\propto r^2$ and r^3 of the expansion of the wave function (r denoting the distance from the centre of the nucleus). Exact computations involve many matrix elements which have to be considered as unknown parameters, and in this form the theory is unsuitable for comparison with experiment.

There are, however, some more or less reliable models which permit to reduce the number of parameters to three. The expressions $\propto r^2$ and $\propto r^3$ may be represented as $R_{1\mathrm{eff}}\langle r\rangle$ and $R^2_{2\mathrm{eff}}\langle r\rangle$ where $\langle r\rangle$ contains two parameters which are the matrix elements ratios $X = ig_{\mathrm{V}}\int\mathbf{r}/g_{\mathrm{A}}\int\boldsymbol{\sigma}\times\mathbf{r}$ and $Y = g_{\mathrm{V}}\int\boldsymbol{\alpha}/g_{\mathrm{A}}\int\boldsymbol{\sigma}\times\mathbf{r}$, while the third one, F, describes the violation of time parity caused by the complexity of the axial-vector coupling constant $G_{\mathrm{A}} = g_{\mathrm{A}}(1-iF)$, $G_{\mathrm{V}} = g_{\mathrm{V}}$ (g_{A}, g_{V} and F are real).

In the model of Geshkenbein *et al.* [11]), $R_{1\mathrm{eff}}$ and $R_{2\mathrm{eff}}$ were assumed to be equal to the radius of the nucleus, and expressions for the RaE spectrum and the RaE electron polarization, depending only on three parameters, were obtained, assuming A and V interaction and two-component neutrino.

Comparing the theoretical β-spectrum with the experimental one, X and Y prove to be linearly related and X must lie in the interval 0.2—2.0, while F must be in the interval

$$-0.1 < F < 0.1.$$

If we compare RaE electron polarization measured experimentally for some energy value with the calculated value, the parameters X and F now prove to be related, and thus only one parameter F remains unknown. If, finally, polarization is measured as a function of the RaE electron energy, all three parameters may in principle be determined.

The determination of parameters and, as the final result, the degree of the possible violation of time parity may be carried out in the following manner. Let us fix some value of the parameter F, characterizing violation of time parity, and compare the polarization values, measured for various electron energies, with theoretical curves computed for various values of the parameter X for which the theoretical form of the β-spectrum still agrees with the experimental one. Comparison with experiment makes it possible to find the value of the parameter X_m for which the theoretical curve describes the experimental data on polarization of electrons in the best way (in the sense of maximum probability). Thus, the most probable value of X_m may be made to correspond to each value of F. Fig. 1 shows experimental RaE electron polarization points for several energy values and curves calculated under the assumption of time parity conservation ($F = 0$) for various values of the parameter X. Curve 3 in the same figure corresponding to the value $X_m = 1.6$ gives the best agreement with experiment.

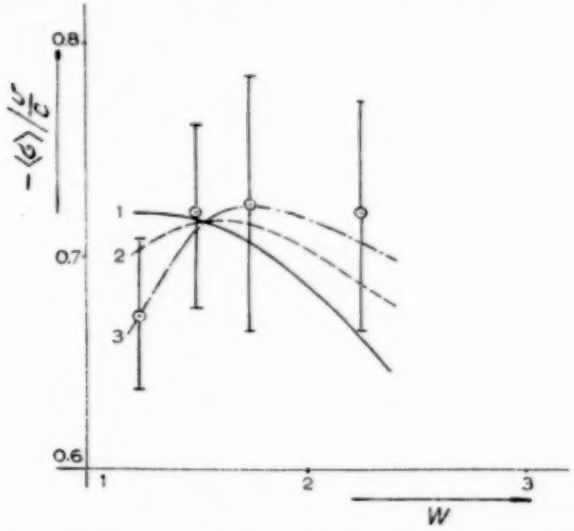

Fig. 2. Energy dependence of RaE electron polarization.
Curve 1: $F = 0$, $X_m = 1.6$
Curve 2: $F = -5.5 \times 10^{-2}$, $X_m = 0.5$
Curve 3: $F = -7.7 \times 10^{-2}$, $X_m = 0.2$.

Fig. 2 represents curves corresponding to various degrees of time parity violation for the values of X_m that yield the best agreement with the experimental points. It is clear from the figure that the curves corresponding to a certain degree of time parity violation agree with experiment better.

These data make it possible to calculate the probability of the degree of time parity violation in β-decay.

The probability density for the parameter F is represented in fig. 4.1.

Thus, comparison of experimental values of RaE electron polarization measured for various energies and the theoretical curves obtained from the model of Geshkenbein *et al.* [11]) leads to the most probable value of $F = -(7.0\pm^{1.0}_{3.5})\times 10^{-2}$ which corresponds to a phase angle between A and V interaction

$$\varphi = (176.0\pm^{2.0}_{0.5})^\circ.$$

In ref.[15]) the formulas for β-spectrum and RaE electron polarization under the assumption of some possible violation of time parity, were obtained in a different way. In ref. [13]) expressions for spectrum and polarization similarly depending on only three parameters, were obtained by neglecting certain terms and simplifying these formulas. In our notations the formulas are

$$C(W) = \frac{1}{X^2}\Big\{[Y-\xi(1+X)]^2+\xi^2F^2$$
$$+\tfrac{2}{3}(W_0-W)[Y-\xi(1+X)](1-X)-\tfrac{2}{3}\left(W-\frac{1}{W}\right)[Y-\xi(1+X)](1+X)$$
$$+\frac{W^2-1+(W_0-W)^2}{3}(X^2+\tfrac{1}{2})-\tfrac{2}{9}\left(W-\frac{1}{W}\right)(W_0-W)(1-X^2)\Big\}\ ;$$
$$\frac{\langle\sigma\rangle}{(-v/c)} = 1-\frac{\tfrac{2}{3}[Y-\xi(1+X)](1+X)+(W_0-W)(1-X^2)\tfrac{1}{3}}{X^2W\cdot C(W)}$$
$$+(\alpha Z)\tfrac{2}{3}\frac{YF}{X^2W\cdot C(W)}\frac{c}{v}\ ;$$

where $\xi \approx 15$, W is the total energy of electrons in units of mc^2, and W_0 the maximum energy of the β-spectrum, which equals 3.28.

Adjusting the theoretical shape of β-spectrum RaE to the experimental one for various values of the parameter F, Nemirovskaya obtained a relation between the parameters X and Y : $Y = f_F(X)$ † from which an expression for RaE electron polarization was obtained suitable for comparison with experimental data and depending only on two parameters X and F.

Comparison of experimental data with these formulas was carried out in the same way as the comparison with the formula of Geshkenbein *et al.* [11]). Fig. 3 shows theoretical curves in the new model corresponding to different degrees of time parity violation for different values of X_m for which fit with the experimental points is the best. Comparison between fig. 3 and

† Having taken into account the possibility of time parity non-conservation, Wegener [13]) used the relation between the parametres Y and X, obtained if time parity is conserved. Therefore, the results obtained in ref.[13]) essentially differ from those of Nemirovskaya.

fig. 2 shows that the first model [11]) and the second model [15, 13]) yield similar results. It should be noted, however, that the second model has a somewhat greater polarization sensitivity to a possible degree of time parity violation.

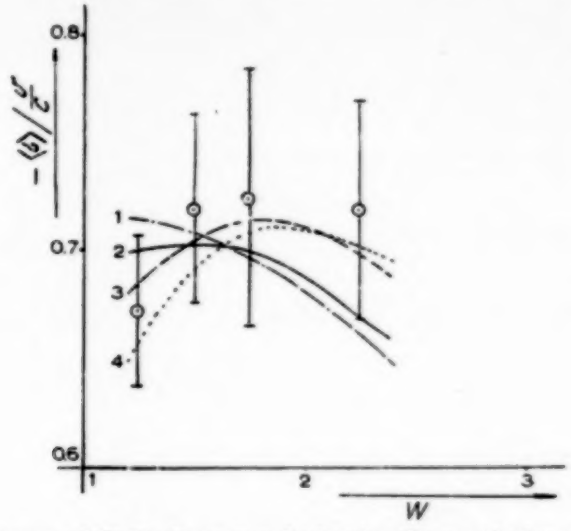

Fig. 3. Energy dependence of RaE electron polarization Theoretical curves are calculated by the model of ref.[15, 13]).

Curve 1: $F = +3.2\times10^{-2}$, $X_m = 1.4$
Curve 2: $F = 0$, $X_m = 1.0$
Curve 3: $F = -4.5\times10^{-2}$, $X_m = 0.33$
Curve 4: $F = -5.5\times10^{-2}$, $X_m = 0.2 \div 0.0$.

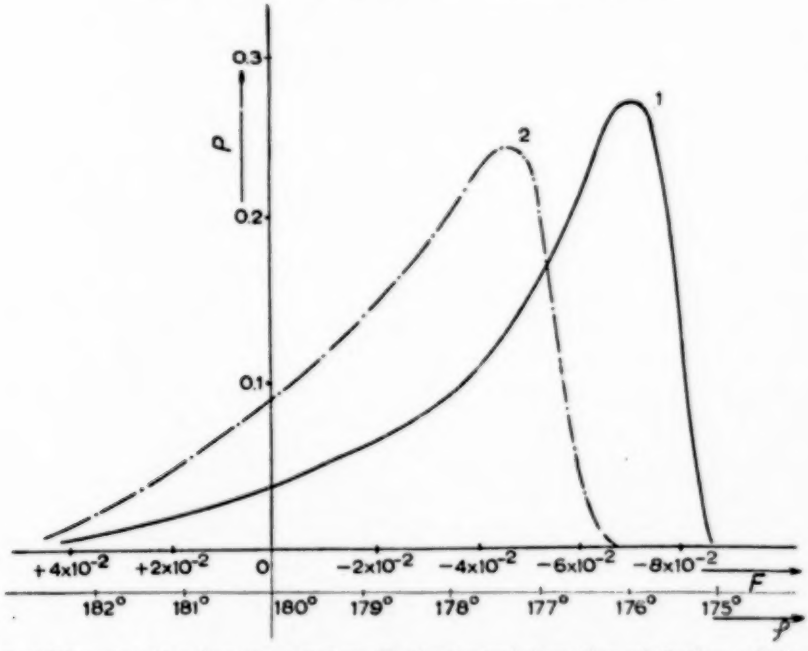

Fig. 4. Probability density for parameter F characterizing the violation of time parity in β-decay.

Curve 1 is obtained as a result of comparison of the theory of Geshkenbein *et al.*[11]) with experiment.

Curve 2 is obtained as a result of comparison of the theory of ref.[15, 13]) with experiment.

As a result of comparison of the measured values of electron polarization and those calculated according to the model [15, 13]) we obtain a probability curve for the parameter F shown in fig. 4,2 which yields the most probable value $F = -(4.5^{+1.0}_{-4.5}) \times 10^{-2}$ which corresponds to an angle between the A and V interactions $\varphi = 177.5^0 \pm^{2.5^\circ}_{0.5^\circ}$. Comparison with the theory thus shows that the result of measurement of RaE electron polarization does not contradict time parity conservation in β-decay, especially if the inaccuracy of the theory is taken into account.

The authors are indebted to M. P. Anikina for preparing the sources, A. P. Rudik and B. V. Geshkenbein for discussion of results and S. A. Nemirovskaya for some calculations carried out for this paper.

References

1) A. I. Alikhanov, G. P. Eliseyev and Luibimov, Nataf's report at the International Nuclear Physics Congress Paris (July 1958); JETP **35** (1958) 1061
2) J. S. Geiger, G. T. Ewan, A. L. Graham and D. R. Mackenzie, Bull. Amer. Phys. Soc. **113** (1958) 51
3) W. Buehring and I. Heintze, Z. Phys. **153** (1958) 237
4) H. Wegener, H. Bienlein and H. V. Issendorff, Phys. Rev. Letters **1** (1958) 460
5) M. Yamada, Prog. Theor. Phys. **10** (1953) 252
6) G. E. Lee-Whiting, Phys. Rev. **97** (1955) 463
7) E. A. Plassmann and L. M. Langer, Phys. Rev. **96** (1954) 1593
8) H. Takebe, S. Makamura and M. Taketani, Prog. Theor. Phys. **14** (1955) 317
9) R. R. Lewis, Phys. Rev. **108** (1957) 904
10) J. I. Fujeta, M. Yamada, Z. I. Matumoto and S. Makamura, Phys. Rev. **108** (1957) 1104
11) B. V. Geshkenbein, S. A. Nemirovskaya and A. P. Rudik, JETP **36** (1959) 517
12) Bincer, Church and Weneser, Phys. Rev. Letters **1** (1958) 95
13) H. Wegener, Z. Phys. **154** (1959) 553
14) A. I. Alikhanov, G. P. Eliseyev and V. A. Luibimov, JETP **34** (1958) 34
15) T. Kotani and M. Ross, Prog. Theor. Phys. **20** (1958) 643

2.L *Nuclear Physics* **13** (1959) 549—575; © *North-Holland Publishing Co., Amsterdam*
Not to be reproduced by photoprint or microfilm without written permission from the publisher

THE QUASI-ELASTIC SCATTERING OF FAST PARTICLES BY ATOMIC NUCLEI

T. K. FOWLER

Oak Ridge National Laboratory †, *Oak Ridge, Tennessee*

and

K. M. WATSON

Physics Department and Lawrence Radiation Laboratory, University of California, Berkeley, California

Received 2 July 1959

Abstract: The scattering of fast particles by atomic nuclei for large momentum transfers and small energy loss is studied. The cross sections may be expanded in inverse powers of the energy of the incident particle, using methods due to Placzek and Wick. The resulting cross sections, when applied to analysis of experiments, may be used to study short range order in nuclei. An analysis of electron, pion and proton experiments shows consistent results and also shows in a striking way the effects of the "repulsive core" in two body forces.

1. Introduction

The "direct interaction" model is frequently used to describe the interaction of a fast particle with an atomic nucleus. According to this model, the incident particle undergoes a series of binary collisions within the nucleus. Its wave function consists of a sum of wavelets scattered from the individual nucleons. For elastic scattering these wavelets add coherently. Elastic scattering is usually described by the optical model. The incident particle may collide directly with a given nucleon, causing it to recoil as if it were nearly a free particle. We should like to use the term "direct-inelastic" for this kind of scattering. A third type of scattering results when the incident particle excites only low lying levels of the nucleus. Since we have assumed the incident particle to have high energy, in this case it loses only a small part of its energy. We employ the term "quasi-elastic" for this last type of scattering.

An experimental distinction between these kinds of interaction seems possible on the basis of precise measurements of the energy of the scattered particles. When this has been done, each type of scattering will yield characteristic information concerning nuclear structure.

We propose to investigate the "quasi-elastic" scattering as a means of

† Operated by Union Carbide Corporation for the U.S. Atomic Energy Commission.

studying the structure of nuclei. Before giving a detailed, quantitative discussion, however, we shall describe this with a simple model.

Let $|n\rangle$ represent the wave function for a nucleus containing A nucleons and in the state n. $|0\rangle$ will represent the ground state. The coordinate of the α^{th} nucleon ($\alpha = 1, 2, \ldots A$) is $\mathbf{Z}_\alpha$. Now,

$$P(\mathbf{Z}_1) = \mathrm{S}\int |\langle \mathbf{Z}_1 \ldots \mathbf{Z}_A|0\rangle|^2 \mathrm{d}^3\mathbf{Z}_2 \ldots \mathrm{d}^3\mathbf{Z}_A \tag{1.1}$$

represents the probability of finding nucleon 1 at $\mathbf{Z}_1$, etc. The symbol S stands for a sum over spin and iso-spin variables.

Similarly

$$P_2(\mathbf{Z}_1, \mathbf{Z}_2) = \mathrm{S}\int |\langle \mathbf{Z}_1 \ldots \mathbf{Z}_A|0\rangle|^2 \mathrm{d}^3\mathbf{Z}_3 \ldots \mathrm{d}^3\mathbf{Z}_A \tag{1.2}$$

represents the joint probability of finding nucleon 1 at $\mathbf{Z}_1$ and nucleon 2 at $\mathbf{Z}_2$. It is convenient to rewrite P_2 as

$$P_2(\mathbf{Z}_1, \mathbf{Z}_2) = P(\mathbf{Z}_1)P(\mathbf{Z}_2)[1+G(\mathbf{Z}_1-\mathbf{Z}_2)], \tag{1.3}$$

where $G(r)$ is called the *pair correlation function*. We expect $G(r)$ to vanish for r large compared to the range of nuclear forces (which for simplicity we assume small compared to the nuclear radius R_0). Since $P(\mathbf{Z})$ and $P_2(\mathbf{Z}_1, \mathbf{Z}_2)$ are normalized to unity, it follows that

$$\int G(r)\mathrm{d}^3\mathbf{r} \approx 0. \tag{1.4}$$

If we do not sum over spin and iso-spin states for nucleons 1 and 2 in eq. (1.2), we may construct probability functions for specific states of the two nucleons.

Let us now suppose that $f(\theta)$ is the scattering amplitude for the incident particle when scattered by a neutron or proton (assumed to be the same in both cases). The scattering amplitude for A nucleons is

$$\tau = \sum_{\alpha=1}^{A} f(\theta)\mathrm{e}^{-i\boldsymbol{\kappa}\cdot\mathbf{Z}_\alpha}, \tag{1.5}$$

where

$$\boldsymbol{\kappa} = \mathbf{k}-\mathbf{k}_0 \tag{1.6}$$

is the momentum transfer and θ is the scattering angle. Here $\mathbf{k}$ is the final, $\mathbf{k}_0$ the initial momentum of the scattered particle. In writing eq. (1.5), we have neglected several phenomena such as multiple scattering, which will be considered in later sections.

The cross section for leaving the nucleus in state n is now

$$\sigma_{n0}(\theta) = |\langle n|\tau|0\rangle|^2. \tag{1.7}$$

If the nuclear excitation energy is neglected in calculating $\mathbf{k}$, then the

cross section for leaving the nucleus in any state is

$$\sigma(\theta) = \sum_n \sigma_{n0} \equiv \sigma_{\rm el} + \sigma_{\rm in}, \tag{1.8}$$

where

$$\begin{aligned} \sigma_{\rm el}(\theta) &= A^2 \sigma_{\rm f}(\theta)[c(\theta)]^2, \\ \sigma_{\rm in}(\theta) &= A\sigma_{\rm f}(\theta)[1-\{c(\theta)\}^2+\rho C(\theta)]. \end{aligned} \tag{1.9}$$

Here,

$$\sigma_{\rm f}(\theta) \equiv |f(\theta)|^2$$

and

$$c(\theta) = \int P(\mathbf{Z}) e^{-i\boldsymbol{\kappa}\cdot\mathbf{Z}} d^3\mathbf{Z} \tag{1.10}$$

$$C(\theta) = \int G(r) e^{-i\boldsymbol{\kappa}\cdot\mathbf{r}} d^3\mathbf{r}. \tag{1.11}$$

The quantity $\rho = A/\mathcal{V}$, where $\mathcal{V} = (4\pi/3)R_0^3$ is the nuclear volume.

The *elastic* scattering is given by $\sigma_{\rm el}$, which is usually described by the optical model; $\sigma_{\rm in}$ represents the inelastic scattering of which $A\sigma_{\rm f}$ includes the *direct-inelastic*. The remaining terms in $\sigma_{\rm in}$ represent the coherent contribution to the quasi-elastic scattering. Because of the normalization condition (1.4), we expect

$$C(\theta) \approx 0. \tag{1.12}$$

The ratio $(\sigma_{\rm in}/A\sigma_{\rm f})$ rises from zero for $\theta = 0$ to unity for angles characterized by the range of the pair correlations. This is illustrated in a schematic way in fig. 1.

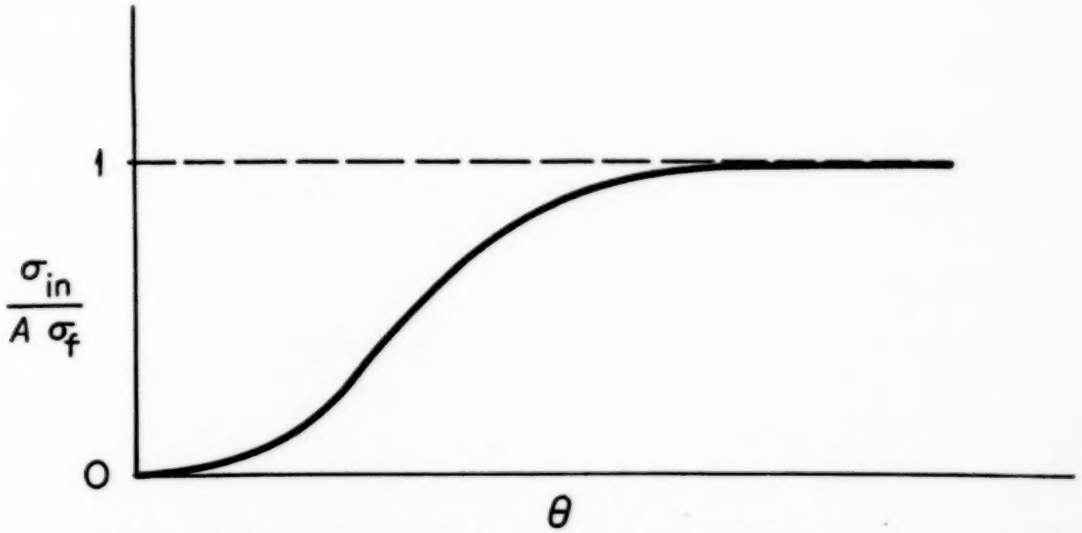

Fig. 1. The expected dependence of $\sigma_{\rm in}/A\sigma_{\rm f}$, as given by eq. (1.9), is shown schematically.

For an ideal degenerate Fermi gas of nucleons, this ratio is well-known. It is

$$1-c^2(\theta)+\rho C(\theta) = 1-\frac{A}{4\mathcal{V}}\int L^2(x) e^{i\boldsymbol{\kappa}\cdot\mathbf{r}} d^3r, \tag{1.13}$$

where

$$L(x) = \frac{3}{x^3}[\sin x - x\cos x], \quad x = P_F r. \tag{1.14}$$

Here P_F is the Fermi-momentum. When θ is small, we have

$$1 - c^2(\theta) + \rho C(\theta) \approx 0.75\frac{|\kappa|}{P_F} + \ldots \tag{1.15}$$

A number of experiments have been performed which have an application to these considerations. Fregau [1]) has studied the scattering of 187 MeV

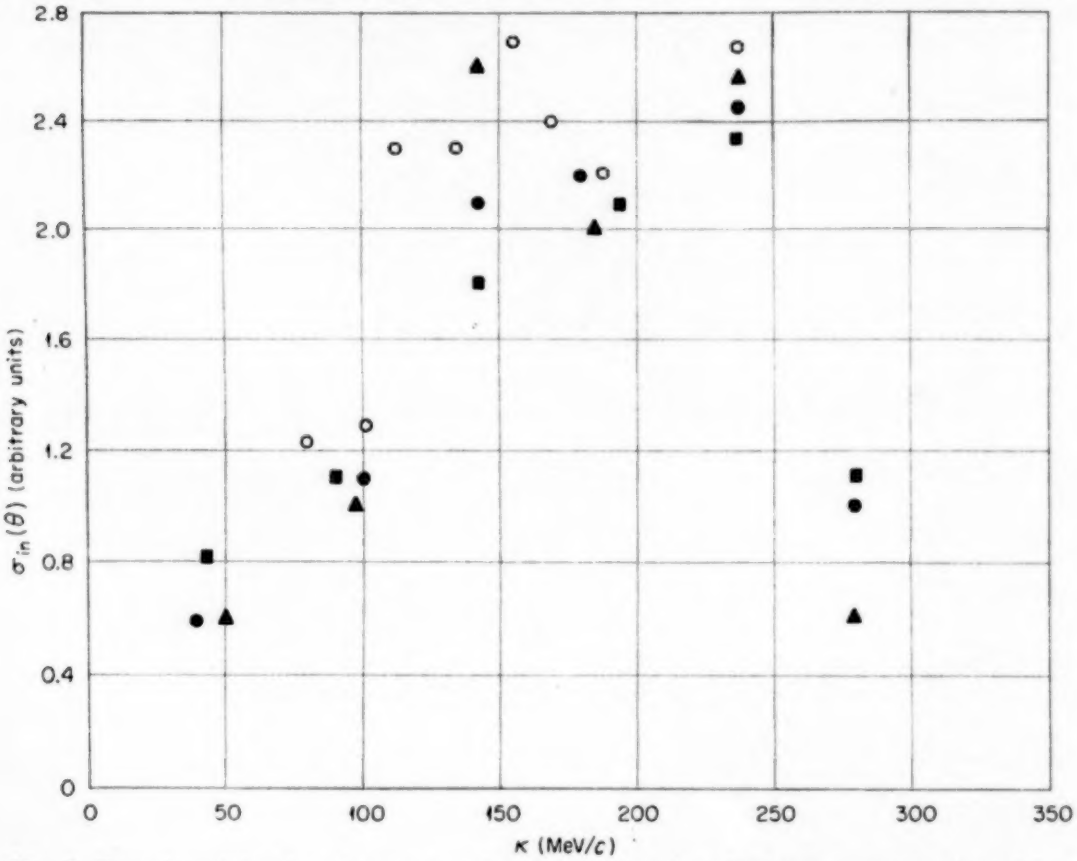

Fig. 2. Experimental values for σ_{in} are shown as a function of the momentum transfer κ. For electrons, we have divided by σ_f.
○ Electrons C^{12}(Ref.[1])) ▲ Protons Ca^{40}(Ref.[3])) ● Protons C^{12}(Ref.[3])) ■ Protons O^{16}(Ref.[3])).

electrons from carbon, observing specific energy groups of scattered electrons. Strauch and Titus [2]) have made similar measurements of the scattering of 90 MeV protons from carbon. The scattering of 185 MeV protons from C^{12}, O^{16}, and Ca^{40} has been studied by Tyrén and Maris [3]). Similarly, the scattering of 80 MeV π^--mesons from C^{12} has been investigated by Williams, Baker and Rainwater [4]). In each of the above experiments, the cross section was measured for exciting specific low-lying levels of the residual nucleus.

When these cross sections for individual excited states are added together,

one expects to obtain σ_{in}. This has been done for several experiments and the results are shown in fig. 2 (where the normalization is arbitrary). For the electron scattering we have divided by σ_t, since this varies strongly with the scattering angle.

The quantities plotted in fig. 2 correspond roughly to $[1+\rho C(\theta)]$. [$c^2(\theta)$ vanishes except for small θ.] The consistency of our results would seem to lend support for the correctness of our interpretation. Indeed, these are not in bad agreement with eq. (1.13); however, we shall postpone until section 5 a quantitative discussion of these experiments.

In the following sections we shall make a more careful study of eqs. (1.8) and (1.9). This will include influence of spin and iso-spin dependence on $f(\theta)$ and nuclear binding effects. In section 4 corrections for multiple scattering will be obtained.

2. The Parametrization of the Scattering Amplitudes

In preparation for describing the nuclear scattering, we write in suitably parametrized form the amplitudes for scattering pions, electrons and nucleons from free neutrons and protons. If the scatterer is nucleon α, the scattering matrix is

$$t_\alpha = \langle \mathbf{P}_r(\mathbf{k}, \mathbf{Q}_\alpha)|t_\alpha|\mathbf{P}_r(\mathbf{k}_0, \mathbf{P}_\alpha)\rangle \delta(\mathbf{k}+\mathbf{Q}_\alpha-\mathbf{k}_0-\mathbf{P}_\alpha). \tag{2.1}$$

Here $\mathbf{k}_0$ and $\mathbf{k}$ are the respective initial and final momenta of the scattered particle; $\mathbf{P}_\alpha$ and $\mathbf{Q}_\alpha$ are the corresponding nucleon momenta; $\mathbf{P}_r(\mathbf{k}, \mathbf{P}_\alpha)$ is the relative momentum between the projectile and α with laboratory momenta $\mathbf{k}$ and $\mathbf{P}_\alpha$.

If we do not observe charge-exchange scattering, the amplitude t_α is for pions

$$t_\alpha = a+\mathbf{b}\cdot\boldsymbol{\sigma}_\alpha+c\tau_{Z_\alpha}+\mathbf{d}\cdot\boldsymbol{\sigma}_\alpha\tau_{Z_\alpha}. \tag{2.2}$$

Here a, $\mathbf{b}$, c and $\mathbf{d}$ are functions of the particle momenta, as in eq. (2.1). τ_{Z_α} is the third component of the isobaric spin operator for the α^{th} nucleon. We let μ be the pion rest mass, M be that for the nucleon, and $\omega = (k^2+\mu^2)^{\frac{1}{2}}$. Also, we set

$$\varepsilon_k \equiv (k^2+\mu^2)^{\frac{1}{2}}-\mu, \qquad \varepsilon_0 \equiv (k_0^2+\mu^2)^{\frac{1}{2}}-\mu. \tag{2.3}$$

Now, the differential scattering cross section, averaged for neutrons and protons, is in the barycentric frame of reference

$$\bar{\sigma}_{\text{cm}}(\theta) = (2\pi)^4 \frac{\omega^2}{\left[1+\dfrac{\omega}{M}\right]^2}[|a|^2+|\mathbf{b}|^2+|c|^2+|\mathbf{d}|^2]. \tag{2.4}$$

In the laboratory coordinate system the differential cross section is

$$\bar{\sigma}_{\text{lab}} = J(\theta)\bar{\sigma}_{\text{cm}}, \tag{2.5}$$

where $J(\theta)$ is the appropriate transformation factor.

For the scattering of electrons via the electron-proton Coulomb interaction we can use the above formula if we set $\mathbf{b} = \mathbf{d} = 0$ and $a = c$. Then

$$\bar{\sigma}_{\rm cm} = (2\pi)^4 \frac{\omega^2}{\left[1+\frac{\omega}{M}\right]^2} 2|a|^2, \qquad \bar{\sigma}_{\rm lab} = J(\theta)\bar{\sigma}_{\rm cm}, \tag{2.6}$$

where ω is now the electron energy and a is the appropriate amplitude for Coulomb scattering. (Since most of our equations will be applicable for any incident particle, we shall often attempt to simplify the notation by omitting labels for specific cross sections. Thus, J, $\sigma_{\rm lab}$, etc. in eq. (2.5) are now understood to refer to electron scattering.)

For neutron or proton scattering we shall use the parametrization of Wright [5]). Let nucleon 0 be scattered by nucleon α. Then

$$\begin{aligned} t_\alpha = {} & B_0 S + B_1(\boldsymbol{\sigma}_0+\boldsymbol{\sigma}_\alpha)\cdot\hat{\mathbf{n}} + B_2\boldsymbol{\sigma}_0\cdot\hat{\mathbf{n}}\boldsymbol{\sigma}_\alpha\cdot\hat{\mathbf{n}}T \\ & + \tfrac{1}{2}(B_3+B_4)\boldsymbol{\sigma}_0\cdot\hat{\mathbf{n}}_-\boldsymbol{\sigma}_\alpha\cdot\hat{\mathbf{n}}_- T + \tfrac{1}{2}(B_3-B_4)\boldsymbol{\sigma}_0\cdot\hat{\mathbf{n}}_+\boldsymbol{\sigma}_\alpha\cdot\hat{\mathbf{n}}_+ T \\ & + \{{}^3B_0 S + {}^3B_1(\boldsymbol{\sigma}_0+\boldsymbol{\sigma}_\alpha)\cdot\hat{\mathbf{n}} + {}^3B_2\boldsymbol{\sigma}_0\cdot\hat{\mathbf{n}}\boldsymbol{\sigma}_\alpha\cdot\hat{\mathbf{n}}T \\ & + \tfrac{1}{2}({}^3B_3+{}^3B_4)\boldsymbol{\sigma}_0\cdot\hat{\mathbf{n}}_-\boldsymbol{\sigma}_\alpha\cdot\hat{\mathbf{n}}_- T + \tfrac{1}{2}({}^3B_3-{}^3B_4)\boldsymbol{\sigma}_0\cdot\hat{\mathbf{n}}_+\boldsymbol{\sigma}_\alpha\cdot\hat{\mathbf{n}}_+ T\}\tau_{z_\alpha}. \end{aligned} \tag{2.7}$$

The coefficients B depend on the relative momenta, as in eq. (2.1). Just as for eq. (2.2), we are here neither assuming nor violating charge independence, since the incident particle is assumed to be specified. Effects of the Pauli principle are supposed to be included in the definition of the B's. Finally,

$$S = \tfrac{1}{4}[1-\boldsymbol{\sigma}_0\cdot\boldsymbol{\sigma}_\alpha], \quad T = \tfrac{1}{4}[3+\boldsymbol{\sigma}_0\cdot\boldsymbol{\sigma}_\alpha]$$

and $\hat{\mathbf{n}}$, $\hat{\mathbf{n}}_-$, $\hat{\mathbf{n}}_+$ are unit vectors in the directions of $\mathbf{p}_0\times\mathbf{p}$, $(\mathbf{p}-\mathbf{p}_0)$, and $(\mathbf{p}+\mathbf{p}_0)$, respectively, where $\mathbf{p}_0$ is the initial and $\mathbf{p}$ the final momentum in the barycentric system.

We now introduce the notation

$$\begin{aligned} |a|^2 &\equiv \tfrac{1}{16}|B_0+B_2+B_3|^2+|B_1|^2, \\ |c|^2 &\equiv \tfrac{1}{16}|{}^3B_0+{}^3B_2+{}^3B_3|^2+|{}^3B_1|^2, \\ |b|^2 &\equiv 3|a|^2-\tfrac{1}{2}\,\mathrm{Re}\,\{[B_0+B_2+B_3]^*[B_2+B_3]\}+|B_2|^2+\tfrac{1}{2}|B_3|^2+\tfrac{1}{2}|B_4|^2-2|B_1|^2, \\ |d|^2 &\equiv 3|c|^2-\tfrac{1}{2}\,\mathrm{Re}\,\{[{}^3B_0+{}^3B_2+{}^3B_3]^*[{}^3B_2+{}^3B_3]\}+|{}^3B_2|^2+\tfrac{1}{2}|{}^3B_3|^2+\tfrac{1}{2}|{}^3B_4|^2-2|{}^3B_1|^2. \end{aligned} \tag{2.8}$$

The barycentric cross section, averaged over protons and neutrons (for particle α), is

$$\bar{\sigma}_{\rm cm} = (2\pi)^4\tfrac{1}{4}\omega^2[|a|^2+|b|^2+|c|^2+|d|^2] \tag{2.9}$$

and

$$\bar{\sigma}_{\rm lab} = J(\theta)\bar{\sigma}_{\rm cm}, \tag{2.10}$$

as before. Here $\omega = (k^2+M^2)^{\frac{1}{2}}$, of course.

3. Scattering from a Nucleus

In this section we consider the scattering from a nucleus, as opposed to scattering from single nucleons, as was done in section 2. † Let

$$T = \sum_{\alpha=1}^{A} (\mathbf{k}|t_\alpha|\mathbf{k}_0). \tag{3.1}$$

Now, if v_0 is the velocity of the incident particle, H_N the nuclear Hamiltonian, and W_0 the nuclear ground state energy,

$$\sigma(\theta) = \frac{(2\pi)^4}{v_0} \int k^2 \mathrm{d}k \langle 0|T^\dagger \delta(\varepsilon_k - \varepsilon_0 + H_N - W_0) T|0\rangle \tag{3.2}$$

is the differential cross section for nuclear scattering. The neglect of multiple scattering and the use of the t_α's for free nucleons are the only approximations made here. The rate of multiple scattering will be considered in section 4. The use of free-nucleon t_α's is called the *impulse approximation* [8,9]. †† The relative error incurred from this approximation is

$$E_0 \approx \frac{B_{\mathrm{av}}^2}{\varepsilon_0^2} \frac{f}{\lambda}, \tag{3.3}$$

where B_{av} is the average binding potential of a nucleon in the nucleus, f is the scattering amplitude in question, and λ is the deBroglie wave length of the incident particle.

To evaluate eq. (3.2) we consider first the expression $t_\alpha|0\rangle$. Now

$$|0\rangle = \int \mathrm{d}^3\mathbf{P}_\alpha \frac{\mathrm{e}^{i\mathbf{P}_\alpha \cdot \mathbf{Z}_\alpha}}{(2\pi)^{\frac{3}{2}}} |0, \mathbf{P}_\alpha\rangle \tag{3.4}$$

represents a Fourier expansion of $|0\rangle$ in the momentum of the α^{th} particle. Thus

$$\begin{aligned} t_\alpha|0\rangle &= \int \mathrm{d}^3\mathbf{P}_\alpha t_\alpha \frac{\mathrm{e}^{i\mathbf{P}_\alpha \cdot \mathbf{Z}_\alpha}}{(2\pi)^{\frac{3}{2}}} |0, \mathbf{P}_\alpha\rangle \\ &= \int \mathrm{d}^3\mathbf{Q}_\alpha \mathrm{d}^3\mathbf{P}_\alpha \frac{\mathrm{e}^{i\mathbf{Q}_\alpha \cdot \mathbf{Z}_\alpha}}{(2\pi)^{\frac{3}{2}}} \langle \mathbf{P}_r(\mathbf{k}, \mathbf{Q}_\alpha)|t_\alpha|\mathbf{P}_r(\mathbf{k}_0, \mathbf{P}_\alpha)\rangle \delta(\mathbf{k}+\mathbf{Q}_\alpha-\mathbf{k}_0-\mathbf{P}_\alpha)|0, \mathbf{P}_\alpha\rangle \\ &= \int \mathrm{d}^3\mathbf{P}_\alpha \mathrm{e}^{-i\boldsymbol{\kappa}\cdot\mathbf{Z}_\alpha} \langle \mathbf{P}_r(\mathbf{k}, \mathbf{P}_\alpha-\boldsymbol{\kappa})|t_\alpha|\mathbf{P}_r(\mathbf{k}_0, \mathbf{P}_\alpha)\rangle \frac{\mathrm{e}^{i\mathbf{P}_\alpha \cdot \mathbf{Z}_\alpha}}{(2\pi)^{\frac{3}{2}}} |0, \mathbf{P}_\alpha\rangle = \mathrm{e}^{-i\boldsymbol{\kappa}\cdot\mathbf{Z}_\alpha} t_\alpha|0\rangle. \end{aligned} \tag{3.5}$$

Here $\boldsymbol{\kappa}$ is the momentum transfer $(\mathbf{k}-\mathbf{k}_0)$. In the last form of this equation

† S. D. Drell and C. L. Schwartz [6]) have discussed electron-nuclear scattering in much the same spirit as is done here. T. K. Fowler [7]) has discussed the theoretical basis for much of our present considerations.

†† The estimated error in the impulse approximation given here is less than that of ref. [8,9]). The reason for this is that the leading correction term found in ref. [8,9]) can be removed by a proper definition of nucleon energies in nuclei. See ref.[10]).

we must consider t_α as operating on the state $|0\rangle$, since t_α depends upon $\mathbf{P}_\alpha = -i\boldsymbol{\nabla}_\alpha$).

With eq. (3.5), we can write eq. (3.2) in the form

$$\sigma = \sigma_{\mathrm{d}} + \sigma_{\mathrm{nd}}, \tag{3.6}$$

where

$$\sigma_{\mathrm{d}} = \frac{(2\pi)^4}{v_0} \sum_{\alpha=1}^{A} \int k^2 \mathrm{d}k \langle 0|t_\alpha^\dagger \, \mathrm{e}^{i\boldsymbol{\kappa}\cdot\mathbf{z}_\alpha} \delta(\varepsilon_k - \varepsilon_0 + H_{\mathrm{N}} - W_0) \mathrm{e}^{-i\boldsymbol{\kappa}\cdot\mathbf{z}_\alpha} t_\alpha |0\rangle, \tag{3.7}$$

$$\sigma_{\mathrm{nd}} = \frac{(2\pi)^4}{v_0} \sum_{\alpha\neq\beta=1}^{A} \int k^2 \mathrm{d}k \langle 0|t_\beta^\dagger \mathrm{e}^{i\boldsymbol{\kappa}\cdot\mathbf{z}_\beta} \delta(\varepsilon_k - \varepsilon_0 + H_{\mathrm{N}} - W_0) \mathrm{e}^{-i\boldsymbol{\kappa}\cdot\mathbf{z}_\alpha} t_\alpha |0\rangle. \tag{3.8}$$

The evaluation of σ_{d} is straightforward and is discussed in appendix A. The result is

$$\sigma_{\mathrm{d}} = A\bar{\sigma}_{\mathrm{lab}}\{1 + E_1 + E_2 + \ldots\}, \tag{3.9}$$

where E_1, E_2, etc. are correction terms due to nuclear binding. The cross section $\bar{\sigma}_{\mathrm{lab}}$ is that of eqs. (2.5), (2.6), or (2.10). From appendix A we find for the energy dependence of the E's (they also depend on θ) [11, 12])

$$E_1 = \tfrac{2}{3} \frac{\omega}{M} \frac{K_{\mathrm{av}}}{\varepsilon_0}, \qquad E_2 \approx \tfrac{1}{3} \frac{K_{\mathrm{av}} B_{\mathrm{av}}}{\varepsilon_0^2}. \tag{3.10}$$

Here K_{av} is the average kinetic energy of a bound nucleon and B_{av} is its average potential energy. (Other correction terms are described in appendix A.) Only when the terms E_0, E_1, E_2, etc. are small does one expect simple relations between the scattering from free nucleons and from nuclei.

When we have dropped the correction terms E_1, E_2, ... in eq. (3.9) and have set $\sigma_{\mathrm{d}} = A\bar{\sigma}_{\mathrm{lab}}$ it is important to recall that the final momentum of the scattered particle is evaluated as if the struck particle is free. That is, the kinematics for the collision is that for the collision of two free particles. This is shown in eq. (A.14). [In contrast to this, σ_{nd} is evaluated as if the struck nucleon were rigidly bound. See eq. (3.11) below.]

The correction terms E_0, etc. represent corrections due to nuclear structure effects. This is also true of the quantity σ_{nd}, which is non-vanishing only because of nuclear binding. For this reason, we need evaluate σ_{nd} only to lowest order when the E's are small. At the same time, we cannot make use of σ_{nd} except under conditions that it is larger than the E's.

Reference to eq. (3.8) shows that σ_{nd} may be interpreted as follows: if the first scattering is from particle α, the second from particle β must de-excite it. It is to be expected that this is an improbable sequence of events unless the nuclear excitation energy is low. A first approximation results, therefore, in setting $H_{\mathrm{N}} = W_0$ in the δ-function. Higher order terms may be obtained on expanding the δ-function in powers of $(H_{\mathrm{N}} - W_0)$ [11, 12, 7]). (It should be noted that setting $H_{\mathrm{N}} = W_0$ would not in general be a satis-

factory approximation for σ_d.) In this way we find [12, 7])

$$\sigma_{nd} = \frac{(2\pi)^4}{v_0} \sum_{\alpha \neq \beta=1}^{A} \int k^2 dk \delta(\varepsilon_k - \varepsilon_0) \langle 0 | e^{i\boldsymbol{\kappa} \cdot (\mathbf{Z}_\beta - \mathbf{Z}_\alpha)} t_\beta^\dagger t_\alpha | 0 \rangle \{1 + E_{c_1} + E_{c_2} + \ldots\}, \tag{3.11}$$

where [11, 12])

$$E_{c_1} \approx -\frac{\kappa^2}{2M} \frac{K_{av}}{\varepsilon_0^2}, \text{ etc.} \tag{3.12}$$

Here the dependence of t_α and t_β on $-i\boldsymbol{\nabla}_{Z\alpha}$ and $-i\boldsymbol{\nabla}_{Z\beta}$ is removed from the leading term (or better, we may average these over the momentum distribution of the nucleus).

We shall now discuss the leading term in σ_{nd}, following the method of Lax and Feshbach [13]). The quantity $(t_\beta^\dagger t_\alpha)$ is a matrix in spin and iso-spin space, but is no longer a coordinate space operator. For each state of given iso-spin, spin and parity of the nucleon pair (α, β), we expect a distinct pair correlation function. The evaluation of σ_{nd} involves giving the appropriate weight to each such state of a pair (α, β). Since the present experimental evidence does not warrant such detail, we shall follow Lax and Feshbach [13]) and assume only two correlation functions: one for space symmetric and one for space antisymmetric states.

Let [13])

$$|s\rangle \equiv \tfrac{1}{2}(1 + P_{\alpha\beta})|0\rangle, \qquad |a\rangle \equiv \tfrac{1}{2}(1 - P_{\alpha\beta})|0\rangle \tag{3.13}$$

be the respective projections of $|0\rangle$ which are symmetric and antisymmetric in the coordinates $\mathbf{Z}_\alpha$ and $\mathbf{Z}_\beta$. Here $P_{\alpha\beta}$ is the operator which interchanges $\mathbf{Z}_\alpha$ and $\mathbf{Z}_\beta$:

$$P_{\alpha\beta} = -\tfrac{1}{4}[1 + \boldsymbol{\sigma}_\alpha \cdot \boldsymbol{\sigma}_\beta][1 + \boldsymbol{\tau}_\alpha \cdot \boldsymbol{\tau}_\beta]. \tag{3.14}$$

In analogy to eq. (1.5) we introduce the probability densities $P_{2s}(\mathbf{Z}_1, \mathbf{Z}_2)$ and $P_{2a}(\mathbf{Z}_1, \mathbf{Z}_2)$ corresponding to the wave functions (3.13) for $\alpha = 1$, $\beta = 2$:

$$\begin{aligned} P_{2s}(\mathbf{Z}_1, \mathbf{Z}_2) &= P(\mathbf{Z}_1) P(\mathbf{Z}_2)[1 + G_s(\mathbf{Z}_1 - \mathbf{Z}_2)] \\ P_{2a}(\mathbf{Z}_1, \mathbf{Z}_2) &= P(\mathbf{Z}_1) P(\mathbf{Z}_2)[1 + G_a(\mathbf{Z}_1 - \mathbf{Z}_2)]. \end{aligned} \tag{3.15}$$

Here G_s and G_a are the respective pair correlation functions for symmetric and antisymmetric states.

In analogy to eqs. (1.10) and (1.11), we introduce

$$\begin{aligned} F_s &\equiv \int e^{i\boldsymbol{\kappa} \cdot (\mathbf{Z}_1 - \mathbf{Z}_2)} P_{2s}(\mathbf{Z}_1, \mathbf{Z}_2) d^3\mathbf{Z}_1 d^3\mathbf{Z}_2 \equiv [c(\theta)]^2 + \frac{1}{\gamma} C_s(\theta), \\ F_a &\equiv \int e^{i\boldsymbol{\kappa} \cdot (\mathbf{Z}_1 - \mathbf{Z}_2)} P_{2a}(\mathbf{Z}_1, \mathbf{Z}_2) d^3\mathbf{Z}_1 d^3\mathbf{Z}_2 \equiv [c(\theta)]^2 + \frac{1}{\gamma} C_a(\theta). \end{aligned} \tag{3.16}$$

With our assumption of only two correlation functions, we obtain the basic relations of Lax and Feshbach [13]) for the evaluation of eq. (3.11).

Let $\mathcal{O}_{\alpha\beta} = \mathcal{O}_{\beta\alpha}$ be a function of $\boldsymbol{\sigma}_\alpha$, $\boldsymbol{\sigma}_\beta$, $\boldsymbol{\tau}_\alpha$ and $\boldsymbol{\tau}_\beta$, but not of $\mathbf{Z}_\alpha$ or $\mathbf{Z}_\beta$. Then

$$\begin{aligned}\langle \mathrm{s}|e^{i\boldsymbol{\kappa}\cdot(\mathbf{Z}_\beta-\mathbf{Z}_\alpha)}\mathcal{O}_{\alpha\beta}|\mathrm{s}\rangle &= F_\mathrm{s}\langle \mathrm{s}|\mathcal{O}_{\alpha\beta}|\mathrm{s}\rangle \\ \langle \mathrm{a}|e^{i\boldsymbol{\kappa}\cdot(\mathbf{Z}_\beta-\mathbf{Z}_\alpha)}\mathcal{O}_{\alpha\beta}|\mathrm{a}\rangle &= F_\mathrm{a}\langle \mathrm{a}|\mathcal{O}_{\alpha\beta}|\mathrm{a}\rangle.\end{aligned} \tag{3.17}$$

Also,

$$\begin{aligned}\langle \mathrm{s}|\mathcal{O}_{\alpha\beta}|\mathrm{s}\rangle &= \langle 0|\mathcal{O}_{\alpha\beta}\tfrac{1}{2}(1+P_{\alpha\beta})|0\rangle \\ \langle \mathrm{a}|\mathcal{O}_{\alpha\beta}|\mathrm{a}\rangle &= \langle 0|\mathcal{O}_{\alpha\beta}\tfrac{1}{2}(1-P_{\alpha\beta})|0\rangle.\end{aligned} \tag{3.18}$$

The evaluation of these quantities is discussed in appendix B.

Now if the E_c terms are neglected, eq. (3.11) becomes

$$\sigma_\mathrm{nd} = \frac{(2\pi)^4}{v_0}(k\omega)\{\tfrac{1}{2}(F_\mathrm{s}+F_\mathrm{a})\sum_{\alpha\neq\beta=1}^{A}\langle 0|t_\beta^\dagger t_\alpha|0\rangle + \tfrac{1}{2}(F_\mathrm{s}-F_\mathrm{a})\sum_{\alpha\neq\beta=1}^{A}\langle 0|t_\beta^\dagger t_\alpha P_{\alpha\beta}|0\rangle\}. \tag{3.19}$$

Eq. (3.19) follows directly with the use of eqs. (3.17) and (3.18), where $\mathcal{O}_{\alpha\beta} = \frac{1}{2}(t_\beta^\dagger t_\alpha + t_\alpha^\dagger t_\beta)$. The evaluation of this, using the tabulation of appendix B, is straightforward. We restrict ourselves to nuclei of zero spin and iso-spin. (The corrections for non-vanishing spin and iso-spin are of relative order s/A or I/A.)

First, we introduce

$$\begin{aligned}\sigma_\mathrm{c} &\equiv (2\pi)^4\omega^2|a|^2, \\ \sigma_\mathrm{f} &\equiv (2\pi)^4\omega^2[|a|^2+|b|^2+|c|^2+|d|^2] = \frac{J(0)}{J(\theta)}\,\bar{\sigma}_\mathrm{lab}.\end{aligned} \tag{3.20}$$

These apply to any of the cases described in section 2. Then

$$\sigma_\mathrm{nd} = \tfrac{1}{2}(F_\mathrm{s}+F_\mathrm{a})[A^2\sigma_\mathrm{c}-A\sigma_\mathrm{f}]+\tfrac{1}{2}(F_\mathrm{s}-F_\mathrm{a})[-\tfrac{1}{4}A^2\sigma_\mathrm{f}+4A\sigma_\mathrm{c}], \tag{3.21}$$

again applicable for incident pions, electrons or nucleons.

To simplify this, we replace C_s and C_a in eq. (3.16) by

$$C_\mathrm{s} = C_\mathrm{p}-C_\mathrm{c}, \quad C_\mathrm{a} = -C_\mathrm{p}-C_\mathrm{c}. \tag{3.22}$$

We may think, perhaps, of C_c as arising from a "repulsive core" interaction between nucleons and C_p as being due to a "Pauli-principle" correlation.

With these definitions, we have

$$\sigma = \sigma_\mathrm{d}+\sigma_\mathrm{nd} \equiv \sigma_\mathrm{el}+\sigma_\mathrm{in},$$

where

$$\sigma_\mathrm{el} = [Ac(\theta)]^2\sigma_\mathrm{c}, \tag{3.23}$$

$$\sigma_\mathrm{in} = A\bar{\sigma}_\mathrm{lab}\left[1-c^2(\theta)\frac{J(0)}{J(\theta)}\right]-A\rho C_\mathrm{c}(\theta)\left[\sigma_\mathrm{c}-\frac{1}{A}\frac{J(0)}{J(\theta)}\bar{\sigma}_\mathrm{lab}\right]-\tfrac{1}{4}A\rho C_\mathrm{p}(\theta)\left[\frac{J(0)}{J(\theta)}\bar{\sigma}_\mathrm{lab}-\frac{16}{A}\sigma_\mathrm{c}\right]. \tag{3.24}$$

The close analogy with eqs. (1.7) and (1.8) should be noted. As in section 1, σ_el repersents elastic scattering by the nucleus, while σ_in represents the

inelastic scattering. Also,

$$C_e(0) \approx C_p(0) \approx 0,$$

so that σ_{in} is expected to vanish (or nearly vanish) for small scattering angles. (To the extent that multiple scatterings are important, this conclusion is not valid.)

The relation of C_e and C_p to the quantity C of eq. (1.11) is easily obtained. We have (see appendix B)

$$c^2(\theta)+\frac{1}{\mathscr{V}}C(\theta) = \langle 0|e^{i\boldsymbol{\kappa}\cdot(\mathbf{z}_\alpha-\mathbf{z}_\beta)}|0\rangle = F_s\langle s|s\rangle+F_a\langle a|a\rangle$$
$$= F_s\left[\tfrac{3}{8}+\frac{15}{8(A-1)}\right]+F_a\left[\tfrac{5}{8}-\frac{15}{8(A-1)}\right]. \quad (3.25)$$

For electron scattering $\sigma_e = \frac{1}{2}\sigma_t$. If the electron energy is sufficiently low for $J(\theta) \approx J(0)$, then eq. (3.24) is

$$\sigma_{in}=\tfrac{1}{2}A\sigma_{(electron\text{-}proton)}\left\{1-[c(\theta)]^2-\rho\left(\tfrac{1}{2}-\frac{1}{A}\right)C_e(\theta)-\tfrac{1}{4}\rho\left(1-\frac{8}{A}\right)C_p(\theta)\right\}. \quad (3.26)$$

Here $\sigma_{(electron\text{-}proton)}$ is the cross section for scattering electrons on free protons.

For pions and nucleons, the dependence of C_e and C_p on angle probably dominates that of σ_e and $[J(0)/J(\theta)]\bar{\sigma}_{lab}$. Thus the quantity

$$\frac{\sigma_{in}}{A\bar{\sigma}_{lab}}-1 \equiv \rho\bar{C}(\theta) \quad (3.27)$$

determines the weighted mean of C_e and C_p. (An analysis of the present experimental data will be made in section 5.)

For small angles θ the cross section σ_e may be expressed in terms of the optical model. Let the nuclear radius be written as $R_0 = A^{\frac{1}{3}}(\hbar/\mu c)\lambda$, where λ is a numerical parameter (≈ 0.8). Then for pions

$$\sigma_e(\theta=0) = \tfrac{4}{9}\left(\frac{\omega}{\mu c^2}\right)^2\lambda^6\left(\frac{\hbar}{\mu c}\right)^2\left[\frac{V_R{}^2+V_I{}^2}{(\mu c^2)^2}\right]. \quad (3.28)$$

Here V_R and V_I are the real and imaginary parts of the optical model potential, as defined by Frank, Gammel and Watson [14]).

For nucleons, we have

$$\sigma_e(\theta=0) = \tfrac{4}{9}\left(\frac{M}{\mu}\right)^2\lambda^6\left(\frac{\hbar}{\mu c}\right)^2\left[\frac{V_{cR}^2+V_{cI}^2+V_{sR}^2+V_{sI}^2}{(\mu c^2)^2}\right]. \quad (3.29)$$

Here V_{cR}, V_{cI}, V_{sR}, V_{sI} are the nucleon optical model well parameters, as defined by Riesenfeld and Watson [15]).

Equations (3.28) and (3.29) permit us to analyze σ_{in} in terms of directly measurable quantities for small angles θ. When the scattering phase shifts

are known σ_c may be directly calculated, of course. It may also be determined from measurements of polarization in pion-nucleon or nucleon-nucleon scattering.

4. The Contribution from Multiple Scattering

We shall consider only multiple scatterings each of which leads to low nuclear excitations. The justification for this rests on the assumption that a scattering with large energy loss by the incident particle can be detected experimentally. In practice one may find that invoking this assumption in an analysis based upon the total differential cross section, σ_{in}, is unduly restrictive. Since rather large momentum transfers (≈ 400 MeV/c) are necessary to probe pair separation distances of the order of the expected correlation range, it can turn out that at the larger scattering angles of interest σ_{in} includes transitions to final states suspected of being excited by multiple scattering omitted from our analysis. In that case, one would like to limit attention to a partial cross section including only small excitations rather than to consider the total differential cross section discussed in previous sections. The derivation of such a partial "quasi-elastic" cross section by the expansion method of appendix A has been discussed at length in ref. [8]) and will not be reviewed further here, except in an approximation to be applied in the data analysis of section 5. (In appendix C we give an alternate, and rather simple, partial sum which may be useful in analysis of experiments.)

Let us return to the notation of section I and suppose $f(\theta)$ to be the amplitude for scattering the given particle on a nucleon. (Again, we let f be independent of spin and iso-spin, so that it represents an "average" scattering amplitude.)

The coupled equation for multiple scattering may be written as [16])

$$\psi(\mathbf{Z}_\alpha) = X_c(\mathbf{Z}_\alpha) + \sum_{\beta \neq \alpha} P \frac{e^{ik_0 R_{\alpha\beta}}}{R_{\alpha\beta}} f(\theta)\psi(\mathbf{Z}_\beta). \tag{4.1}$$

Here $R_{\alpha\beta} = |\mathbf{Z}_\alpha - \mathbf{Z}_\beta|$ and θ is the angular deflection of the particle on being scattered from $\mathbf{Z}_\beta$ to $\mathbf{Z}_\alpha$; P is an "instruction operator" [16]) which tells us to keep only inelastic scatterings.

The wave function X_c is that for *elastic* scattering. It is, if we neglect boundary effects at the nuclear surface,

$$X_c(\mathbf{Z}_\alpha) = e^{i\mathbf{k}_0 \cdot \mathbf{Z}_\alpha}, \tag{4.2}$$

where $\mathbf{k}_0$ is the incident momentum *in* the nucleus; $\mathbf{k}_0$ is related to the momentum $\mathbf{q}$ *outside* of the nucleus by the nuclear "refractive index" n:

$$\mathbf{k}_0 = n\mathbf{q}. \tag{4.3}$$

To interpret the operator P, let us first study the perturbation expansion of eq. (4.1). This expansion for the scattering operator T of eq. (3.1) is [16])

$$T = \sum_\alpha \bar{l}_\alpha \left[1 + \frac{1}{e} P \sum_{\beta \neq \alpha} \bar{l}_\beta + \dots \right], \tag{4.4}$$

where

$$e \equiv \varepsilon_0 - \varepsilon_k + W_0 - H_N. \tag{4.5}$$

Now

$$\sigma = \frac{(2\pi)^4}{v_0} \int k^2 \mathrm{d}k \langle 0 | T^\dagger \delta(e) T | 0 \rangle \tag{4.6}$$

may be expanded in terms of the expansion (4.4). The leading term is that of section 3. The next term is

$$\sigma_{\mathrm{ms}} = \frac{(2\pi)^4}{v_0} \sum_\gamma \sum_\alpha \sum_{\beta \neq \alpha} \sum_{n' \neq n, 0} \sum_{n \neq 0} \int k^2 \mathrm{d}k \times \left\{ (0|\bar{l}_\gamma|n')\delta(\varepsilon_k - \varepsilon_0 + W_{n'} - W_0)(n'|\bar{l}_\alpha|n) \frac{1}{e(n)} (n|\bar{l}_\beta|0) + \text{c.c.} \right\}, \tag{4.7}$$

where $e(n)$ is the appropriate value of e for the state n.

If eq. (4.7) is evaluated for high energies, assuming $\gamma \neq \alpha$ or β and neglecting the angular dependence of the scattering amplitude, we find

$$\sigma_{\mathrm{ms}} = \left\{ |f|^2 f \int \Gamma(\mathbf{Z}_\alpha, \mathbf{Z}_\beta, \mathbf{Z}_\gamma) \mathrm{e}^{i(\mathbf{k}-\mathbf{k}_0)\cdot \mathbf{Z}_\gamma} \mathrm{e}^{-i\mathbf{k}\cdot \mathbf{Z}_\alpha} \mathrm{e}^{i\mathbf{k}_0 \cdot \mathbf{Z}_\beta} \frac{\mathrm{e}^{ik_0 R_{\alpha\beta}}}{R_{\alpha\beta}} \mathrm{d}^3\mathbf{Z}_\alpha \mathrm{d}^3\mathbf{Z}_\beta \mathrm{d}^3\mathbf{Z}_\gamma + \text{c.c.} \right\}, \tag{4.8}$$

where

$$\Gamma(\mathbf{Z}_\alpha, \mathbf{Z}_\beta, \mathbf{Z}_\gamma) \equiv P_3(\mathbf{Z}_\alpha, \mathbf{Z}_\beta, \mathbf{Z}_\gamma) - P_2(\mathbf{Z}_\alpha, \mathbf{Z}_\beta) P(\mathbf{Z}_\gamma) - P_2(\mathbf{Z}_\gamma, \mathbf{Z}_\alpha) P(\mathbf{Z}_\beta) - P_2(\mathbf{Z}_\beta, \mathbf{Z}_\gamma) P(\mathbf{Z}_\alpha) + 2P(\mathbf{Z}_\alpha) P(\mathbf{Z}_\beta) P(\mathbf{Z}_\gamma). \tag{4.9}$$

Here $P_3(\mathbf{Z}_\alpha, \mathbf{Z}_\beta, \mathbf{Z}_\gamma)$ is probability of finding three specific nucleons at $\mathbf{Z}_\alpha, \mathbf{Z}_\beta$, and $\mathbf{Z}_\gamma$.

We shall assume that Γ may be expressed in terms of the *pair correlation function* G:

$$\Gamma = P(\mathbf{Z}_\alpha) P(\mathbf{Z}_\beta) P(\mathbf{Z}_\gamma) [G(\mathbf{Z}_\alpha - \mathbf{Z}_\beta) G(\mathbf{Z}_\beta - \mathbf{Z}_\gamma) + G(\mathbf{Z}_\gamma - \mathbf{Z}_\alpha) G(\mathbf{Z}_\alpha - \mathbf{Z}_\beta) + G(\mathbf{Z}_\beta - \mathbf{Z}_\gamma) G(\mathbf{Z}_\gamma - \mathbf{Z}_\alpha)]. \tag{4.10}$$

Equations (4.8) and (4.10) may be interpreted as follows. For scatterings in $T^\dagger$ and T which are not *paired* from the *same* nucleon or from *neighbouring* nucleons, the net phase in eq. (4.8) is minimized by a series of scatterings on a straight line through the nucleus. Each scattering is then paired with the previous and successive scattering and for *these* we should take

$$P = G(R_{\alpha\beta}) \tag{4.11}$$

in eq. (4.1). (This choice corresponds to the second term on the right in

eq. 4.10.) In addition to the term mentioned above we may pair any scattering in a T with a scattering in $T^\dagger$ (it may be the *same* or a *neighbouring* nucleon). The inclusion of these terms leads to a transport problem [17]).

For our present elementary treatment, we shall consider these two effects separately. The choice (4.11) will first be made. Let us insert this into eq. (4.1) and seek a solution with the "ansatz"

$$\psi(\mathbf{Z}_\beta) = e^{i\mathbf{k}_0 \cdot \mathbf{Z}_\beta} Q, \tag{4.12}$$

where Q is a constant. Making this substitution, eq. (4.1) becomes

$$e^{i\mathbf{k}_0 \cdot \mathbf{Z}_\alpha} Q = e^{i\mathbf{k}_0 \cdot \mathbf{Z}_\alpha} + \sum_{\beta \neq \alpha} G(R_{\alpha\beta}) \frac{e^{i\mathbf{k}_0 R_{\alpha\beta}}}{R_{\alpha\beta}} f(\theta) e^{i\mathbf{k}_0 \cdot \mathbf{Z}_\beta} Q. \tag{4.13}$$

If we replace the sum over β by an integral,

$$\sum_\beta \to \rho \int d^3\mathbf{Z}_\beta,$$

and recall that θ is the angle between $\mathbf{k}$ and $(\mathbf{Z}_\alpha - \mathbf{Z}_\beta)$, eq. (4.13) has the solution

$$Q = \frac{1}{1-I}, \tag{4.14}$$

$$I = \rho \int d^3R \frac{e^{ik_0 R}}{R} e^{-ik_0 R \cos\theta} G(R) f(\theta) = 2\pi\rho \int R\,dR \int d(\cos\theta) e^{ik_0 R(1-\cos\theta)} G(R) f(\theta). \tag{4.15}$$

This integral must be evaluated for specific cases. At very high energies, however, the principal contribution comes from small θ, and one obtains (if $f(\theta)$ does not change appreciably for $\theta \approx 0$)

$$I \approx -\frac{2\pi\rho f(0)}{ik} R_c, \tag{4.16}$$

where

$$R_c \equiv \int_0^\infty dR\, G(R). \tag{4.17}$$

(We have used an infinite upper limit here on the assumption that the nuclear radius is large compared to R_c.) The optical model potential is

$$V_0 = -\frac{2\pi\rho f(0)}{\omega}, \tag{4.18}$$

so eq. (4.16) may be written as

$$I = -iV_0 \left(\frac{R_c \omega}{k}\right) \tag{4.19}$$

and

$$Q = \frac{1}{1 + iV_0 \left(\frac{R_c \omega}{k}\right)}. \tag{4.20}$$

Finally, the complete wave function at large distances from the nucleus is

$$\psi = X_c + \frac{e^{iqx}}{x}[P\sum_{\beta} e^{-i\kappa\cdot Z_\beta} f(\theta) e^{-k_1 D}]Q. \tag{4.21}$$

Here D is the total distance that the scattered wave has traveled through the nucleus and k_1 is the imaginary part of k. From (4.11) we obtain

$$\sigma_{in} = A\sigma_t(\theta)\{1-c^2(\theta)+\rho C(\theta)\}\Lambda|Q|^2, \tag{4.22}$$

where

$$\begin{aligned}\Lambda &\approx \frac{1}{\mathcal{V}}\int d^3Z_\beta e^{-(1/l)D} \\ &\approx \frac{6}{y^3}[1-(1+y+\tfrac{1}{2}y^2)e^{-y}].\end{aligned} \tag{4.23}$$

In this expression $y = 2R_0/l$, where R_0 is the nuclear radius and $1/l = \rho\sigma_t$.

Equation (4.15) is the corrected form of eq. (1.8). The factor Λ represents

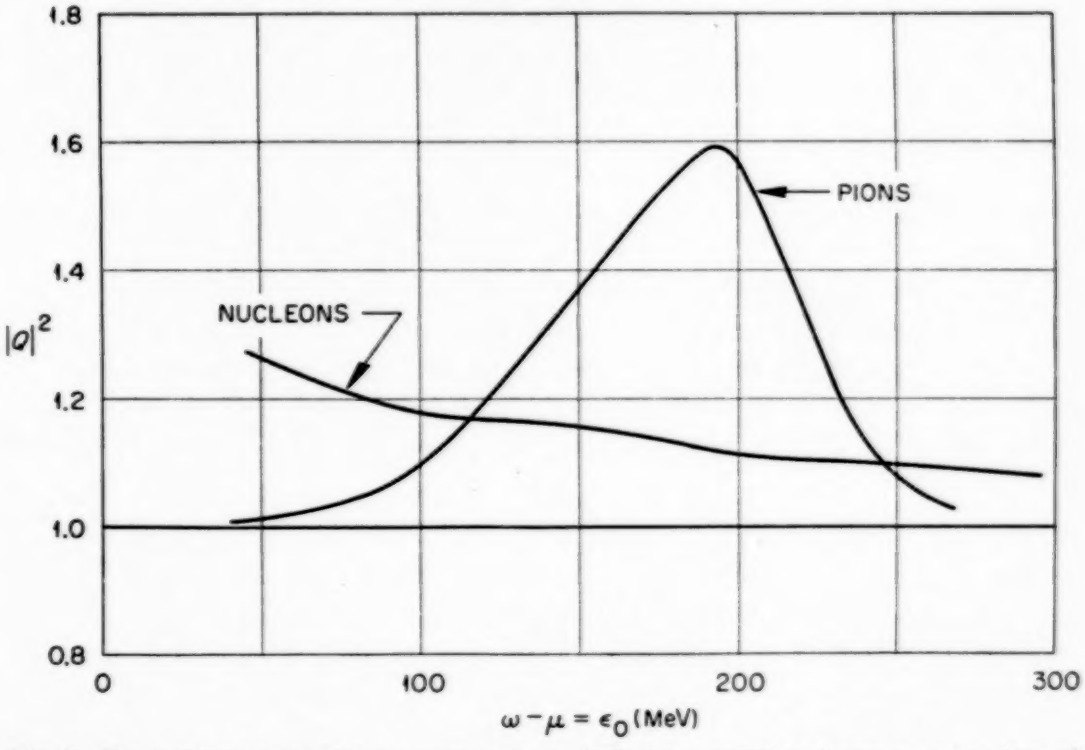

Fig. 3. The multiple scattering correction factor $|Q^2|$ of eq. (4.15) is shown as a function of energy for pion and nucleon scattering.

the correction for absorption and $|Q|^2$ that for interference of scattered wavelets.

The damping factor Λ represents the correction for the *absorption* due to the other inelastic scatterings which arise from *paired* terms in $T^\dagger$ and T, as described above. We shall not go into a more detailed discussion of these corrections here [17]).

Our approximate expressions (4.15) and (4.16) for I evidently are not valid for electron scattering, since $f(0)$ is unbounded. A more careful evaluation in this case should include the shielding of the Coulomb field for large impact parameters. The result, while finite, would seem to give a rather *large* correction for multiple interactions. A detailed study of this is of interest, but is beyond our present scope. Since this effect would seem to be of importance at only very small scattering angles, we must exclude such small angle scatterings from our analysis of the experimental electron scattering †.

The multiple scattering correction $|Q|^2$ has been evaluated for nucleons and pions. The result is shown in fig. 3.

5. Data Analysis

We now turn to a quantitative analysis of the nuclear pair correlation information contained in the quasi-elastic scattering data mentioned in the Introduction. While some information about the pair correlation function will be obtained, our purpose is more to test the self-consistency of our analysis through comparison with many experimental results. Thus we consider the scattering of electrons [1]), protons [2, 3]), and pions [4]) from several targets.

One interesting feature of the pair correlation function is the expected repulsion at *small* distances. This will show up in the data in terms of the sign of the correlation form factors C_e and C_p at *large* momentum transfers, $\kappa > 300$ MeV/c, and thus the sign of these quantities derived from the various experiments will provide a gross check on self consistency. By the convention of eq. (3.22), this sign should be *positive* for repulsion.

The analysis will be based upon the following slightly modified form of eq. (3.24):

$$\frac{\sigma_q(\theta)}{\Lambda A\bar{\sigma}_{lab}} = XB_d - B_{nd}\rho C_e\left[\frac{\sigma_e}{\bar{\sigma}_{lab}} - \frac{1}{A}\frac{J(0)}{J(\theta)}\right] - \tfrac{1}{4}B_{nd}\rho C_p\left[\frac{J(0)}{J(\theta)} - \frac{16}{A}\frac{\sigma_e}{\bar{\sigma}_{lab}}\right]. \quad (5.1)$$

A term in $c^2(\theta)$ negligible at angles of interest has been dropped. Multiple scattering effects have been included through the absorption factor, Λ, and in the fact that $\bar{\sigma}_{lab}$ is evaluated at the projectile energy *inside* the nucleus. The exclusion principle inhibition against small excitations by direct scattering is taken into account †† by the factor X. If for this purpose the nucleus is treated as a free nucleon gas confined to the nuclear volume, the

† We are indebted to Professor Henry Kendall for calling to our attention the importance of small angle electron scattering.

†† No correction comparable to $X(\kappa)$ has been applied to σ_{nd} (the second and third terms of eq. (5.1)) since coherent scattering from the correlation structure generally finds the nucleons with momenta outside the Fermi sea.

probability that a nucleon can absorb a momentum transfer κ is given by

$$X(\kappa) = \begin{cases} \frac{3}{4}\frac{\kappa}{p_F}\left[1-\frac{1}{12}\left(\frac{\kappa}{p_F}\right)^2\right], & \kappa < 2p_F \\ 1, & \kappa \geqq 2p_F \end{cases} \tag{5.2}$$

where p_F is the Fermi momentum. In relating X to the scattering angle θ, we take κ to be κ_f, the momentum transferred to a free nucleon initially at rest when the incident particle scatters at angle θ.

The principal difference between eqs. (5.1) and (3.24) is the explicit limitation to the excitation of a few nuclear levels, in keeping with the available data. Thus the total cross section σ_{in} of eq. (3.24) has been replaced by the quasi-elastic cross section, σ_q, mentioned in section 4 and discussed in ref. [7]) †. At small scattering angles, corresponding to small momentum transfers to the nucleus and hence small nuclear excitations, σ_q equals σ_{in} and eq. (3.24) is appropriate. At larger angles, however, where $\sigma_q \neq \sigma_{in}$, the highly inelastic scattering which we require to be eliminated experimentally must also be eliminated from the theoretical analysis. The limitation to quasi-elastic excitations $< \Delta$ is accomplished by the factors B_d and B_{nd}, which are respectively the fractions of σ_d (direct scattering) and σ_{nd} (coherent scattering, called "non-diagonal" by Wick [12])) contributed by scattering giving the nucleus an excitation $x < \Delta$. The B's are functions of the scattering angle. If the distribution of nuclear excitations following a direct scattering at a given angle θ is known, $B_d(\theta)$ is the fraction of the area under the distribution curve lying in the excitation range $0 < x < \Delta$; B_{nd} is determined similarly from the excitation distribution accompanying coherent scattering.

It would be advantageous to choose the experimental Δ to include the maximum pair correlation information in σ_q without introducing too much multiple scattering contamination. That is, we would choose Δ to make B_{nd} as close to unity as possible. Now, in ref. [7]) it is argued that the distribution of excitations accompanying the coherent scattering peaks at zero excitation and has a width L_b given by

$$L_b(\theta) = \left[\frac{4}{3}\frac{\kappa_b^2}{2M}K_{av}\right]^{\frac{1}{2}} \tag{5.3}$$

where $\kappa_b(\theta)$ is the momentum transfer to a rigidly bound (i.e., infinitely heavy) nucleon and K_{av} is the average kinetic energy of nucleons in the nucleus. For $K_{av} \approx 25$ MeV and κ in the interesting region ≈ 300—400 MeV/c, L_b is $\gtrsim 40$ MeV. On the other hand, the available experiments excite levels up to only ≈ 20 MeV. Then $\Delta \approx 20$ MeV and $B_{nd} \approx 0.25$, considerably

† In ref. [7]), σ_q was actually defined to include purely elastic scattering. Here, however, we mean by σ_q just the inelastic part.

less than unity. Furthermore, since for the lightest target nuclei under consideration $x < \Delta$ includes only three or four levels, the detailed shape of the distribution of excitations could become important in determining the B's. It is in fact not clear that additional data for higher levels would be helpful in the case of light nuclei. For instance, in the case of 185 MeV protons incident upon C^{12}, already at $x \approx 15$ MeV one suspects undesirable multiple scattering or other contamination in the fact that the differential cross section is peaked forward, contrary to the behaviour of a single, impulsive collision. There are, however, two possible ways out. The contamination might be less serious for other projectiles. Also, the problem of $B_{nd} < 1$ is less bothersome for heavy nuclear targets, since then the fact that many levels are included within a modest excitation range makes a smooth approximation to the excitation distribution curve more reliable. At any rate, use of the present data demands an estimate of B_{nd}, as well as B_d, and these estimates will suffer in reliability because excitation of only a few levels is involved. One might note, however, that determination of the *sign* of C_p and C_c is independent of B_{nd}, which is probably the more difficult quantity to estimate.

For definiteness, we assume the distribution of excitations accompanying coherent scattering to be half a gaussian in shape, peaked at $x = 0$, with width L_b. Then

$$B_{nd} = \frac{\int_0^\Delta dx\, g(x)}{\int_0^\infty dx\, g(x)}, \qquad g(x) = \exp\left\{-0.69\, \frac{x^2}{L_b{}^2}\right\}. \tag{5.4}$$

Since the direct scattering is analogous to scattering from a free target, the excitation distribution in that case is peaked about $x = \kappa_f{}^2/2M$, the free-nucleon recoil. Again assuming a gaussian shape, we define $B_d = 1-f$, where

$$f = \frac{\int_\Delta^\infty dx\, h(x)}{\int_{-\infty}^\infty dx\, h(x)}, \qquad h(x) = \exp\left\{-0.69 \left(x - \frac{\kappa_f{}^2}{2M}\right)^2 \Big/ L_f{}^2\right\}. \tag{5.5}$$

Here κ_f is the momentum transfer to a free nucleon and L_f has the form of L_b with κ_b replaced by κ_f. Numerical studies of scattering from harmonically bound targets indicate that eq. (5.5) is a quite good approximation, even when $\kappa_f{}^2/2M < L_f$, in which case the lower half of the true distribution is crowded into a non-gaussian shape in the region $0 < x < \kappa_f{}^2/2M$.

Returning now to eq. (5.1), we see that the right-hand-side of this equation simplifies for the cases of interest. We may expect $C_p \approx C_c$. Then, if $\sigma_c/\sigma_{lab} \approx J(0)/J(\theta)$ and $A \approx 16$, the third term tends to be small compared to the second, with the result

$$\frac{\sigma_q}{\Lambda A\bar{\sigma}_{lab}} \approx XB_d - B_{nd}\rho C_e \frac{\sigma_e}{\bar{\sigma}_{lab}}. \tag{5.6}$$

Thus only correlations due to the repulsive core appear. Equation (5.6) should apply to electron and proton scattering from C^{12}, and to proton scattering from O^{16}.

If $A \gg 16$, the terms in A^{-1} drop out, leaving

$$\frac{\sigma_q}{\Lambda A\bar{\sigma}_{lab}} = XB_d - B_{nd}\rho C_e \frac{\sigma_e}{\bar{\sigma}_{lab}} - \tfrac{1}{4}B_{nd}\rho C_p \frac{J(0)}{J(\theta)}. \tag{5.7}$$

This equation should apply to protons scattered from Ca and to π^- scattered from Cu. For protons, the J and σ factors are probably comparable so that, to the accuracy we may expect, the repulsive core correlations again dominate by a factor of ≈ 4. For 80 MeV π^- mesons, σ_e/σ_{lab} goes through a sharp minimum around 90° (cm), the interesting region, so that in this case alone the Pauli exclusion correlation dominates. For both p and π^-, then, eq. (5.7) is approximately

$$\frac{\sigma_q}{\Lambda A\bar{\sigma}_{lab}} \approx XB_d - B_{nd}\rho\gamma \frac{J(0)}{J(\theta)} \tag{5.8}$$

where $\gamma = C_e + \frac{1}{4}C_p \approx C_e$ for the (p, Ca) data, and $\gamma = \frac{1}{4}C_p$ for the (π^-, Cu) data.

In summary, as one might have guessed from the fact that only one in four nucleon pairs experience Pauli exclusion, the repulsive core correlation dominates all the available data, except that for (π^-, Cu), and we may regard our analysis as a derivation of the repulsive-core correlation function.

The results from eqs. (5.6) and (5.8) are plotted in fig. 4. Following the notation of eq. (1.11), the ordinate of fig. 4 has been labelled simply $C(\theta)$, which, as concluded above, can be regarded as $-C_e$ for all but the pion data, The data employed came from the following sources. The quasi-elastic cross sections for electron and proton scattering from various nuclei were obtained by adding cross sections for resolved levels given in ref. [1]) for electrons and refs. [2]) and [3]) for protons. For (π^-, Cu), σ_q was taken to be the difference between the results of Williams *et al.* [4]) ($\Delta \approx 20$ MeV) and Baker *et al.* [18]) ($\Delta < 5$ MeV). The two-body cross sections for scattering the various projectiles from free nucleons came from ref. [19]) for electrons, ref. [20]) for 95 MeV protons, refs. [20]) and [21]) for 185 MeV protons, and refs. [22]) and [23]) for pion phase shifts. Optical model data to compute the absorption factor Λ came from ref. [15]) for protons, ref. [24]) for pions. We took $\Lambda = 1$ for electrons. B_d and B_{nd} were calculated with $\Delta = 20$ MeV for protons and pions, $\Delta = 10$ MeV for electrons.

Though details of shape do not agree for the various cases, there is good

consistency in peak magnitudes. It should be borne in mind that these data represent a truly wide variety of inputs. The two-body cross sections for electrons, protons, and pions differ considerably in magnitude and angular and energy dependence. Also, the nuclei probed are light enough to differ in correlation structure due to the influence of the surface. In the case of C^{12},

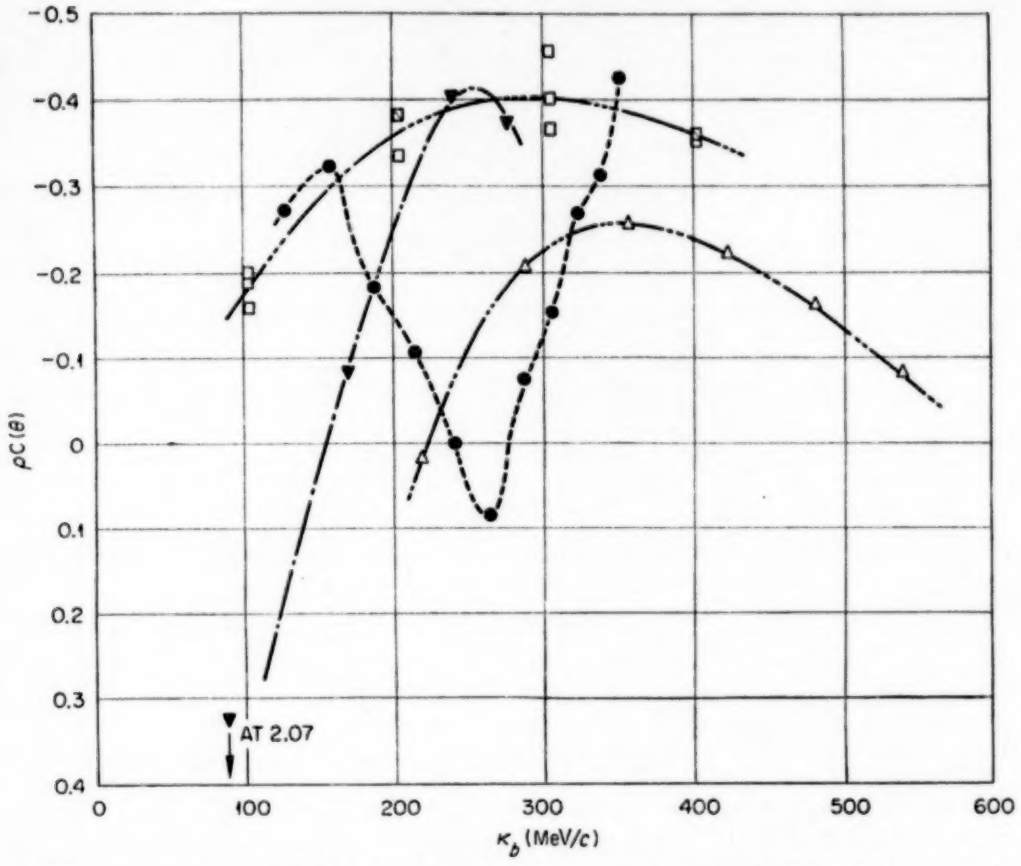

Fig. 4. The nuclear pair correlation form factor, $C(\theta)$, derived from several quasi-elastic scattering experiments is shown as a function of momentum transfer, κ. The correlation function, $G(r)$, is the Fourier transform of $C(\theta)$.

● 185-MeV e^- (C^{12} target) □ 185-MeV p (C^{12}, O^{16}, Ca^{40} Targets) △ 95-MeV p (C^{12} target)
▼ 80-MeV π^- (Cu target)

for instance, which is all surface and thus quite inhomogeneous, different projectiles, and even the same projectile at different energies, will probe different regions of the target because of the difference in their rates of absorption in passing through the nucleus. Consistency should be better for heavy, homogeneous nuclei as targets and for projectiles of such mass and energy that the nucleus is approximately transparent to them.

All in all, we would conclude that a systematic experimental search for the correlation functions in terms of an analysis along the lines presented here is justified. From the point of view of energy resolution, such experiments should be less ambitious than those already attempted in that, while

scattering giving the nucleus an excitation $\approx \Delta$ must be rejected, individual levels in the accepted range $x < \Delta$ need not be resolved.

We shall now examine briefly the results of fig. 4 to see what information about the correlation function might be gleaned from present data. Consider first the electron and proton data. The negative sign of $C(\theta)$ at large angles

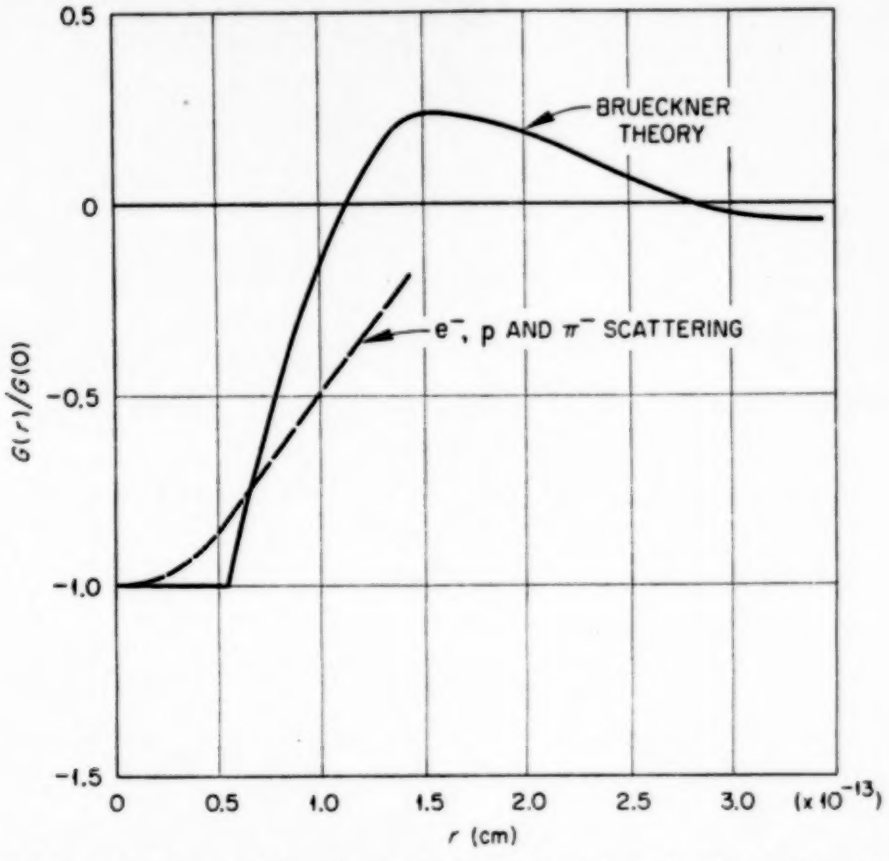

Fig. 5. The nuclear pair correlation function $G(r)$, derived from the data of fig. 4 is plotted against r, the separation distance between a pair of nucleons. A typical correlation function from Brueckner's theory of nuclear matter [25]) is shown for comparison.

(corresponding to *positive* C_c) indicates repulsion at small distances as expected. The range of this repulsion, i.e. the correlation range R_c, should be of the order κ_{max}^{-1}, where κ_{max} is the momentum transfer in the neighbourhood where $|C(\theta)|$ is a maximum. Thus, $R_c \approx 0.7 \times 10^{-13}$ cm.

If a best $C(\theta)$ fitting the points of fig. 4 could be decided upon, its Fourier transform would yield the pair correlation function

$$G(r) = \frac{1}{2\pi^2 r} \int d\kappa \, \kappa \sin \kappa r C. \tag{5.9}$$

In fig. 5 is plotted $G(r)$ derived from an average fit to fig. 4 of the form

$$\rho C(\theta) = \begin{cases} -0.4 \sin (\kappa\pi/560 \text{ MeV} \cdot c^{-1}), & \kappa < 560 \text{ MeV}/c \\ 0 \qquad\qquad\qquad\qquad\quad , & \kappa > 560 \text{ MeV}/c \end{cases} \tag{5.10}$$

Fortunately, the very uncertain region of small κ contributes little to $G(r)$ at small r, so that the result at small r is consistent with the proton scattering results at both 95 MeV and 185 MeV. No attempt was made to satisfy the constraint imposed by eq. (1.4). A typical result from Brueckner's theory of nuclear structure is included for comparison [25]).

The magnitude of G at $r = 0$ affords one final self-consistency check which is independent of what region of the nucleus is probed by a given projectile. Because of the repulsive-core interaction between nucleons, we should obtain $G(0) = -1$ for all cases. This quantity is determined primarily by the normalization of $C(\theta)$ and by the values of κ where $C(\theta)$ peaks and falls to zero. As was pointed out previously, the peak magnitude of $C(\theta)$ is about the same for each of the cases of fig. 4. Again taking C to be given by eq. (5.10) gives

$$G(0) = -1.02(R_0/a_0)^3 \tag{5.11}$$

where $R_0^3 = (\frac{4}{3}\pi\rho)^{-1}$ and $a_0 = 1.4\times 10^{-13}$ cm. Thus $G(0)$ is subject to the uncertainty in the single nucleon density. The value $R_0 = a_0$ corresponding to the expected result $G(0) = -1$ is not out of line with observed nuclear densities. Again we stress the really different nature of the experiments which independently yield this result.

Finally, we come to the pion data. What is plotted in fig. 4 is $-\rho\gamma$ from eq. (5.8). Again the sign indicates repulsion at small distances. The "average" form factor γ is comparable in magnitude to the other average form factors of fig. 4, but according to our interpretation that the electron and proton form factors are $\approx C_c$ and that, for pions, $\gamma \approx \frac{1}{4}C_p$, the peak magnitude of C_p itself would appear to be 3 or 4 times that of C_c. Though the quantitative difference seems large, qualitatively, this corresponds to an expected longer range for the exclusion principle correlation since, to preserve $G(0) = -1$, the larger form factor C_p would have to fall off faster with κ than does C_c. Unfortunately the available data does not reach the region of κ where γ falls.

A different interpretation of γ which takes into better account the strong ($\approx$ quadratic) energy dependence of $\bar{\sigma}_{lab}$ (pion-nucleon) yields C_p of smaller magnitude more consistent with C_c derived from the electron and proton data. The average of $\bar{\sigma}_{lab}(\pi, n)$ over the initial momentum of a bound nucleon is different for the direct and coherent terms of σ_q, since the one concerns the total nucleon momentum distribution, while the other concerns only the large momentum components †. Thus, in the case of pion scattering, $\bar{\sigma}_{lab}$ for coherent terms should be evaluated at E_2, a higher energy — nearer the resonance — than E_1, the energy at which $\bar{\sigma}_{lab}$ appropriate to the direct terms is evaluated. The analysis again leads to eq. (5.8) and the pion curve

† The effect is less important for electrons, because of their small mass, and for protons, because of the weak energy dependence of nucleon-nucleon scattering.

of fig. 4, but now $\gamma \approx \frac{1}{4}\beta C_p$ where $\beta = \bar{\sigma}_{lab}(E_2)/\bar{\sigma}_{lab}(E_1)$. (The energy dependence of the J-factor is weak.) Around 90°, β may be as much as 2 or 3. Then the curve in fig. 4 would be $\approx \rho C_p$, and $C_p \approx C_e$.

Appendix A

We shall now describe briefly the evaluation of eq. (3.7). The method used is essentially that of Placzek [11]) and Wick [12]), and has been applied recently to the present problem [7]). Let us expand the δ-function in eq. (3.7) as follows:

$$\delta(\varepsilon_k-\varepsilon_0+H_N-W_0) = \sum_{n=0}^{\infty} \frac{1}{n!}(H_N-\overline{W})^n \delta^n(d_0), \tag{A.1}$$

where

$$d_0 = \varepsilon_k-\varepsilon_0+(\overline{W}-W_0). \tag{A.2}$$

$\overline{W}$ will be chosen later so as to give rapid convergence of the series (A.1). Now

$$\sigma_d = \sum_{n=0}^{\infty} \frac{i}{n!} \sum_{\alpha=1}^{A} \frac{(2\pi)^4}{v_0} \int k^2 dk \delta^n(d_0) \langle 0|t_\alpha^\dagger e^{i\boldsymbol{\kappa}\cdot\mathbf{Z}_\alpha}(H_N-\overline{W})^n e^{-i\boldsymbol{\kappa}\cdot\mathbf{Z}_\alpha} t_\alpha|0\rangle. \tag{A.3}$$

To evaluate this, we must first commute $e^{-i\boldsymbol{\kappa}\cdot\mathbf{Z}_\alpha}$ past $(H_N-\overline{W})^n$. For $\boldsymbol{\kappa} = 0$ this is trivial, of course, and accordingly, for small scattering angles our correction terms will tend to be small. Now,

$$(H_N-\overline{W})^n e^{-i\boldsymbol{\kappa}\cdot\mathbf{Z}_\alpha} = e^{-i\boldsymbol{\kappa}\cdot\mathbf{Z}_\alpha}\left[\frac{\kappa^2}{2M} - \frac{\boldsymbol{\kappa}\cdot\boldsymbol{\nabla}_\alpha}{iM} + X_\alpha - \overline{W} + H_N\right]^n. \tag{A.4}$$

Here

$$X_\alpha = \sum_{\beta\neq\alpha} [e^{i\boldsymbol{\kappa}\cdot(\mathbf{Z}_\beta-\mathbf{Z}_\alpha)}-1] V_{\alpha\beta}^{ex} \tag{A.5}$$

where $V_{\alpha\beta}^{ex}$ is the space-exchange interaction between nucleons α and β. Thus,

$$\sigma_d = \sum_{n=0}^{\infty} \frac{1}{n!} \sum_{\alpha=1}^{A} \frac{(2\pi)^4}{v_0} \int k^2 dk \delta^n(d_0) \langle 0|t_\alpha^\dagger \left[\frac{\kappa^2}{2M} - \frac{\boldsymbol{\kappa}\cdot\boldsymbol{\nabla}_\alpha}{iM} + X_\alpha - \overline{W} + H_N\right]^n t_\alpha|0\rangle. \tag{A.6}$$

If H_N were to commute with t_α, and if X_α and $\boldsymbol{\kappa}\cdot\boldsymbol{\nabla}_\alpha$ were negligible, we could set $H_N = W_0$,

$$\overline{W} = W_0 + \frac{\kappa^2}{2M}, \tag{A.7}$$

and the terms with $n \neq 0$ above would vanish.

Actually, t_α depends upon $\boldsymbol{\sigma}_\alpha$, $\boldsymbol{\tau}_\alpha$, and $\mathbf{P}_\alpha = -i\boldsymbol{\nabla}_\alpha$, and so does not commute with H_N. The first order commutator of H_N with t_α contains one term due to the $\mathbf{P}_\alpha$-dependence of t_α. This leads to a correction term

$$E_3 \approx \frac{|\boldsymbol{\nabla}_{P_\alpha} t_\alpha|^2 (\boldsymbol{\nabla}_\alpha^2 B_\alpha)}{|t_\alpha|^2 \varepsilon_0} \approx \frac{\omega}{M} \frac{K_{av} B_{av} \omega}{k^2 \varepsilon_0} \tag{A.8}$$

[see eq. (3.9)]. The spin flip part of H_N and of t_α leads to a correction term of order

$$E_4 \approx \tfrac{1}{2} \frac{|t_\alpha|^2_{\text{spin flip}}}{|t_\alpha|^2} \frac{(B_{\text{av}})_{\text{spin flip}}}{\varepsilon_0}. \tag{A.9}$$

We estimate this as

$$E_4 \approx \tfrac{1}{4} \frac{B_{\text{av}}}{\varepsilon_0}. \tag{A.10}$$

Because of a tendency of the spin flip terms to cancel, E_4 might be considerably less—an unfortunate constructive interference of spin terms might make it larger, however.

The leading contribution from X_α appears to be

$$E_5 \approx \frac{\langle X_\alpha \rangle}{\varepsilon_0}.$$

Since interference terms will be important only for $\kappa|\mathbf{Z}_\alpha - \mathbf{Z}_\beta| \approx 1$, the leading term in E_5 is

$$E_5 \approx \tfrac{1}{3} \frac{B_{\text{av}}}{\varepsilon_0}. \tag{A.11}$$

The remaining correction terms in eq. (A.6) come from the commutators of $(\boldsymbol{\kappa} \cdot \boldsymbol{\nabla}_\alpha / iM)$ with H_N. These have been investigated by Wick [12]), and have E_2 (eq. (3.10)) as the leading term.

After separating out these corrections, we are left with the series

$$\sum_{n=0}^{\infty} \frac{1}{n!} \left[-\frac{\boldsymbol{\kappa} \cdot \boldsymbol{\nabla}_\alpha}{iM} \right]^n \delta^n(d_0) = \delta(d), \tag{A.12}$$

where

$$d = d_0 - \frac{\boldsymbol{\kappa} \cdot \boldsymbol{\nabla}_\alpha}{iM}. \tag{A.13}$$

Now

$$\begin{aligned} \sigma_{\text{d}} &= \frac{(2\pi)^4}{v_0} \sum_\alpha \int k^2 \mathrm{d}k \langle 0 | t_\alpha^\dagger t_\alpha \delta(d) | 0 \rangle \\ &= \frac{(2\pi)^4}{v_0} \sum_\alpha \int k^2 \mathrm{d}k \mathrm{d}^3 \mathbf{P}_\alpha \langle \mathbf{P}_r(\mathbf{k}_0, \mathbf{P}_\alpha) | t_\alpha^\dagger | \mathbf{P}_r(\mathbf{k}, \mathbf{Q}_\alpha) \rangle \langle \mathbf{P}_r(\mathbf{k}, \mathbf{Q}_\alpha) | t_\alpha | \mathbf{P}_r(\mathbf{k}_0, \mathbf{P}_\alpha) \rangle \\ &\times \delta \left(\varepsilon_k - \varepsilon_0 + \frac{Q_\alpha^2}{2M} - \frac{P_\alpha^2}{2M} \right) (P_\alpha, 0 | 0, P_\alpha). \\ &= A \, (\bar{\sigma}_{\text{lab}})_{\text{averaged over } \mathbf{P}_\alpha}. \end{aligned} \tag{A.14}$$

Here $\mathbf{Q}_\alpha = \mathbf{P}_\alpha - (\mathbf{k} - \mathbf{k}_0)$. The interpretation here is very simple. A free particle of momentum $\mathbf{P}_\alpha$ is struck. The resulting cross section is averaged over the momentum distribution of the struck particle.

The difference between this averaged cross section and the cross section for a particle at rest gives the correction E_1 of eq. (3.9). This is a simple kinematical correction, which may actually be evaluated with fair accuracy, if necessary. The model considered by Wick [12]) gave for the energy dependence of E_1 (the E's also depend on θ)

$$E_1 \approx \tfrac{2}{3}\frac{\omega}{M}\frac{K_{\mathrm{av}}}{\varepsilon_0}, \tag{A.15}$$

which is the value quoted in eq. (3.9).

We now conclude that the error incurred from dropping the E-terms in eq. (3.9) is about

$$(\tfrac{1}{2}\text{ to }\tfrac{1}{3})\frac{B_{\mathrm{av}}}{\varepsilon_0}. \tag{A.16}$$

For $\varepsilon_0 > 100$ MeV, we can expect these connections to be rather small. Experimental verification of this should be possible by studying large angle inelastic scattering from very light nuclei.

Appendix B

We wish to evaluate expectation values such as appear in eq. (3.18). Some simple examples are

$$\sum_{\alpha\neq\beta}\langle 0|\boldsymbol{\sigma}_\alpha\cdot\boldsymbol{\sigma}_\beta|0\rangle = \langle 0|(\sum_\alpha \boldsymbol{\sigma}_\alpha)^2 - 3A|0\rangle = 4S(S+1)-3A, \tag{B.1}$$

$$\sum_{\alpha\neq\beta}\langle 0|\boldsymbol{\tau}_\alpha\cdot\boldsymbol{\tau}_\beta|0\rangle = 4T(T+1)-3A, \tag{B.2}$$

$$\sum_{\alpha\neq\beta}\langle 0|\tau_{z_\alpha}\tau_{z_\beta}|0\rangle = 4T_z{}^2-A. \tag{B.3}$$

Here S and T are the respective spin and iso-spin of the nucleus, T_z is the third component of the iso-spin.

Similarly,

$$\sum_{\alpha\neq\beta}\langle 0|\boldsymbol{\sigma}_\alpha\cdot\boldsymbol{\sigma}_\beta\tau_{z_\alpha}\tau_{z_\beta}|0\rangle = 4(\mathbf{S}_{\mathrm{p}}-\mathbf{S}_{\mathrm{n}})^2-3A. \tag{B.4}$$

Here $\mathbf{S}_{\mathrm{p}}$ is the spin of the protons, $\mathbf{S}_{\mathrm{n}}$ that of the neutrons in the nucleus.

From Blatt and Weisskopf [26]), we find

$$\sum_{\alpha\neq\beta}\langle 0|P_{\alpha\beta}|0\rangle = -\tfrac{1}{4}A^2+4A+(\tfrac{5}{2}-\xi), \tag{B.5}$$

where ξ is a function of the nuclear state [26]). For a $T = S = 0$ nucleus, $\xi = \frac{5}{2}$. For example,

$$\langle \mathrm{s/s}\rangle = \tfrac{3}{8}+\frac{15}{8(A-1)}+\frac{(\frac{5}{2}-\xi)}{2A(A-1)},\quad \langle \mathrm{a/a}\rangle = \tfrac{5}{8}-\frac{15}{8(A-1)}-\frac{(\frac{5}{2}-\xi)}{2A(A-1)}. \tag{B.6}$$

Again

$$\sum_{\alpha\neq\beta}\langle 0|\boldsymbol{\sigma}_\alpha\cdot\boldsymbol{\sigma}_\beta\boldsymbol{\tau}_\alpha\cdot\boldsymbol{\tau}_\beta|0\rangle = -\{9A+4S(S+1)+4T(T+1)+4(\tfrac{5}{2}-\xi)\},$$

$$\sum_{\alpha\neq\beta}\langle 0|\boldsymbol{\tau}_\alpha\cdot\boldsymbol{\tau}_\beta P_{\alpha\beta}|0\rangle = -\tfrac{3}{4}A^2-4S(S+1)-(\tfrac{5}{2}-\xi),$$

$$\sum_{\alpha\neq\beta}\langle 0|\boldsymbol{\sigma}_\alpha\cdot\boldsymbol{\sigma}_\beta P_{\alpha\beta}|0\rangle = -\tfrac{3}{4}A^2-4T(T+1)-(\tfrac{5}{2}-\xi), \tag{B.7}$$

$$\sum_{\alpha\neq\beta}\langle 0|\boldsymbol{\tau}_\alpha\cdot\boldsymbol{\tau}_\beta\tau_{z_\beta}|0\rangle = A^2+A+4T_z{}^2-4T(T+1),$$

$$\sum_{\alpha\neq\beta}\langle 0|\tau_{z_\alpha}\tau_{z_\beta}P_{\alpha\beta}|0\rangle = -\tfrac{1}{4}A^2-2S(S+1)-2T_z{}^2-2(\mathbf{S}_\mathrm{p}-\mathbf{S}_\mathrm{n})^2-(\tfrac{5}{2}-\xi),$$

$$\sum_{\alpha\neq\beta}\langle 0|\boldsymbol{\sigma}_\alpha\cdot\boldsymbol{\sigma}_\beta\tau_{z_\alpha}\tau_{z_\beta}P_{\alpha\beta}|0\rangle = -\tfrac{3}{4}A^2+2S(S+1)+4T(T+1)$$
$$-6T_z{}^2+2(\mathbf{S}_\mathrm{p}-\mathbf{S}_\mathrm{n})^2+(\tfrac{5}{2}-\xi). \tag{B.8}$$

Appendix C

A PARTIAL CLOSURE SUM

A method described in ref. [7]) for giving a cross section summed over a restricted set of states has been employed in section 5. A different method, also discussed in ref. [7]), which may also be of use, is described below.

Let us suppose the counting equipment for the experiment considered is sensitive to the momentum of the scattered particle, giving a weight $G(k)$ to particles with momentum k. For example, it might be desirable to choose

$$\begin{aligned} G(k) &= 1 \text{ for } k < k_\mathrm{M}(\theta), \\ G(k) &= 0 \text{ for } k > k_\mathrm{M}(\theta). \end{aligned} \tag{C.1}$$

Such a counter would permit one to discriminate against scatterings with large nuclear excitation.

In this case, eq. (3.2) would be replaced by

$$\sigma(\theta) = \frac{(2\pi)^4}{v_0}\int k^2\mathrm{d}k\, G(k)\langle 0|T^\dagger\delta(\varepsilon_k-\varepsilon_0+H_\mathrm{N}-W_0)T|0\rangle. \tag{C.2}$$

Evidently, $G(k)$ affects only the integration over k and not the evaluation of the sum over nuclear states, if we simply proceed with the analysis of section 3 and appendix A. When this is done, we find that eq. (3.9) is replaced by

$$\sigma_\mathrm{d} = A\bar{\sigma}_\mathrm{lab}G(k_\mathrm{f}), \tag{C.3}$$

where k_f is defined by the vanishing of the δ-function of eq. (A.14). This is the leading term of eq. (5.2) of ref. [7]).

Similarly, eq. (3.21) is replaced by

$$\sigma_{nd} = \{\tfrac{1}{2}(F_s+F_a)[A^2\sigma_c - A\sigma_t]+\tfrac{1}{2}(F_s-F_a)[-\tfrac{1}{4}A^2\sigma_t+4A\sigma_c]\}G(k_0) \quad \text{(C.4)}$$

where k_0 is defined by the vanishing of the δ-function in eq. (3.11).

Since $k_f \geqq k_0$, this permits us to reduce or eliminate the contribution from σ_d. (It may be necessary in some cases to use the more accurate sum rules of section 5 and ref.[7]), however.)

In practice, it will usually be convenient to let $G(k)$ depend on the scattering angle.

References

1) J. H. Fregau, Phys. Rev. **104** (1956) 225
2) K. Strauch and F. Titus, Phys. Rev. **103** (1956) 200
3) Tyrén and Maris, Nuclear Physics **4** (1957) 637
4) Williams, Baker and Rainwater, Phys. Rev. **104** (1956) 1695
5) S. C. Wright, Phys. Rev. **99** (1955) 996
6) S. D. Drell and C. L. Schwartz, Phys. Rev. **112** (1958) 568
7) T. K. Fowler, Phys. Rev. **112** (1958) 1325
8) G. F. Chew, Phys. Rev. **80** (1950) 196
9) G. F. Chew and M. L. Goldberger, Phys. Rev. **85** (1952) 636
10) K. M. Watson, Revs. Mod. Phys. **30** (1958) 565
11) G. Placzek, Phys. Rev. **86** (1952) 377
12) G. C. Wick, Phys. Rev. **94** (1954) 1228
13) M. Lax and H. Feshbach, Phys. Rev. **81** (1951) 189
14) Frank, Gammel and Watson, Phys. Rev. **101** (1956) 891
15) W. Riesenfeld and K. Watson, Phys. Rev. **102** (1956) 1157
16) K. M. Watson, Phys. Rev. **105** (1957) 1388
17) See K. Watson, Phys. Rev. (to be published)
18) W. F. Baker, J. Rainwater and R. E. Williams, Phys. Rev. **112** (1958) 1763
19) R. W. McAllister and R. Hofstadter, Phys. Rev. **102** (1956) 851
20) U. E. Kruse, J. M. Teem and N. F. Ramsey, Phys. Rev. **101** (1956) 1079
21) O. Chamberlain and J. D. Garrison, Phys. Rev. **103** (1956) 1860
22) R. Gessaroli and G. Quareni, Nuovo Cimento, Ser. 10, **5** (1957) 1658
23) Jay Orear, Phys. Rev. **100** (1955) 288
24) J. O. Kessler and L. M. Lederman, Phys. Rev. **94** (1954) 689
25) K. A. Brueckner and J. L. Gammel, Phys. Rev. **109** (1958) 1023
26) J. M. Blatt and V. F. Weisskopf, Theoretical Nuclear Physics (John Wiley and Sons, New York, 1952). See eq. (3.16), p. 239

3.A *Nuclear Physics* **13** (1959) 576—582; © *North-Holland Publishing Co., Amsterdam*
Not to be reproduced by photoprint or microfilm without written premission from the publisher

GAMMARESONANZSTREUUNG AM 17.22 MeV-ZUSTAND IN C^{12}

P. PAUL und U. STIERLIN

Physikalisches Institut der Universität, Freiburg, Deutschland †

Eingegangen am 29. Juli 1959

Abstract: The absolute total cross section for elastic scattering of 17 MeV-lithium gamma rays on carbon has been measured. From this the cross section for resonant scattering on the 17.22 MeV level of C^{12} was calculated for an E1 and E2 ground state transition. The result confirms the assignment 1^-, $T = 1$ for this level. A gamma width $\Gamma_\gamma = (500 \pm 180)$ eV for the ground state transition is obtained, which is consistent with the results obtained from elastic proton scattering on this level.

1. Einleitung

Der 17.22 MeV-Zustand von C^{12} mit einer Gesamtbreite $\Gamma = 1.27$ MeV zerfällt durch γ-Emission zum 0^+-Grundzustand (γ_0) und zum 4.43-MeV-Niveau (γ_1) von C^{12}, oder unter α-Emission in den Grundzustand (α_0) und das erste angeregte Niveau (α_1) von Be^8. Neuere Experimente haben von den beiden möglichen Zuordnungen 1^- und 2^+ für das 17.22 MeV-Niveau die erste bestätigt, aber die Frage nach der Grösse der partiellen Breiten wieder aufgeworfen [1]).

Bisher waren die partiellen Breiten aus der Resonanzkurve und den Wirkungsquerschnitten der Reaktionen $B^{11}(p, \alpha)$ und $B^{11}(p, \gamma)$ in der Umgebung von $E_p = 1.4$ MeV bestimmt worden [2]). Dabei wählte man von den beiden sich ergebenden Möglichkeiten $\Gamma_p = 0.2\,\Gamma$ und $\Gamma_p = 0.8\Gamma$ aus theoretischen Überlegungen die erste, obwohl sich eine im Vergleich zur Weißkopfabschätzung verhältnismäßig kleine γ-Breite ergab. Der daraus folgende Satz an partiellen Breiten ist mit dem gemessenen Wirkungsquerschnitt der Reaktion $C^{12}(\gamma, 3\alpha)$ bei 17.6 MeV verträglich [3]).

Dagegen lieferte die direkte Messung der Protonenbreite durch elastische Protonenstreuung am 17.22 MeV-Niveau einen wesentlich kleineren Wert $\Gamma_p = 0.05\Gamma$ [4, 5]). Messungen der Wirkungsquerschnitte B^{11} (p,α) von French†† haben Ergebnisse geliefert, die mit diesem Wert für Γ_p verträglich sind.

In der vorliegenden Arbeit wurde nun eine weitere partielle Breite, nämlich die γ-Breite des Grundzustandsüberganges durch Gammaresonanzstreuung am 17.22 MeV-Niveau direkt bestimmt. Sie lässt sich aus dem

† Diese Arbeit wurde von der Deutschen Forschungsgemeinschaft und dem Ministerium für Atomkernenergie unterstützt.

†† Siehe Fußnote in Zitat [5]).

Resonanzstreuquerschnitt berechnen, da die Multipolarität des Überganges in den 0^+-Grundzustand durch die Niveauzuordnung 1^- (möglicherweise 2^+) eindeutig als E1 (bezw. E2) gegeben ist. Interferenzen mit anderen Niveaus sind beim 17.22 MeV-Zustand nicht vorhanden [6]). Infolge der starken Dämpfung der Resonanz durh die konkurrierende Partikelemission entgeht man der üblichen Schwierigkeit, mit der anregenden Strahlung in die Resonanz hineinzukommen. Der zu erwartende Wirkungsquerschnitt ist allerdings nur in der Grössenordnung von 10^{-30} cm², so daß nichtresonante kohärente Streuungen wie Rayleigh- und Thomsonstreuung nicht vernachlässigt werden können.

2. Experimente

Der experimentelle Aufbau für die Streumessungen hielt sich an die oft verwendete rotationssymmetrische Geometrie (Abb. 1), nur war die Anordnung auf möglichst große Ausbeute hin ausgelegt. Die asymmetrische Lage

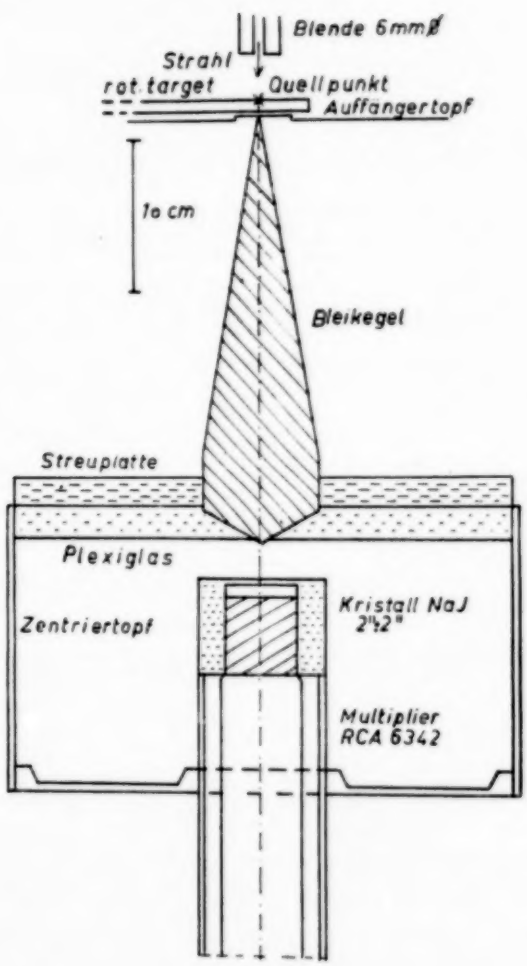

Abb. 1. Experimenteller Aufbau für die Streumessungen. Die Achse der Anordnung stand senkrecht im Raum.

des Streuringes berücksichtigt, daß die γ-Quelle punktförmig, der Nachweiskristall dagegen ausgedehnt ist. Zur Erzeugung der γ-Strahlung wurde die 441 keV-Resonanz der Reaktion $Li^7(p, \gamma)$ benutzt. Der dabei entstehende intensive Anteil an Quanten der Energie 17.6 MeV liegt oberhalb der Mitte der 17.22 MeV-Resonanz innerhalb der Resonanzbreite[7]). Da die Lithiumresonanz nur 12 keV breit und der nichtresonante Anteil vernachlässigbar ist [8]), wurde mit einem dicken Lithiumtarget gearbeitet. Den Protonenstrom von 2 mA mit einer Energie $E_p = 500$ keV liefert der 600 kV-Kaskadenbeschleuniger des Freiburger Physikalischen Institutes. Der Quellpunkt hatte 6 mm ⌀. Zum Nachweis der gestreuten Strahlung diente ein 2″ 2″-NaJ-Kristall mit der üblichen Elektronik. Ein Einkanaldiskriminator begrenzte die Energie der gezählten Quanten nach unten bei etwa 14 MeV. Gezählt wurde gegen einen zweiten 2″ 2″-NaJ-Kristall als Monitor. Der Kohlenstoffstreuer war eine Graphitplatte von 20 mm Dicke. Außer an Kohlenstoff wurde zur Kontrolle an Wasser, Aluminium und Blei in der gleichen Geometrie gestreut. Bei diesen Stoffen erfolgt Resonanzstreuung von 17 MeV-Quanten nur an der giant resonance. Alle Streukörper hatten gleiche Massen, so daß die Comptonstreuung immer gleich groß war.

Zur Bestimmung des primären γ-Flusses wurde bei gleicher Lage beider Kristalle das Spektrum der direkten Strahlung gegen den Monitor aufgenommen. Griffith gibt das Verhältnis des 17 MeV-zum 14 MeV-Anteil für die Lithiumstrahlung und die Linienformen der einzelnen Anteile für $E_p = 500$ keV und einen 2″ 1.75″ Kristall an [9]).

Damit wurde das Spektrum aufgeteilt und der primäre Fluss an 17 MeV-Quanten bestimmt. Der Fehler beträgt ± 20 % und ist gegeben durch die verschiedenen Möglichkeiten in der Auftrennung des Spektrums. Die γ-

TABELLE 1

Die gemessenen totalen Streuquerschnitte in cm^2 unter Annahme von E1- und E2-Streuung

Element	eigene Werte	Fuller und Hayward [12])	Stearns [8])
Pb	$(5.6 \pm 1) \times 10^{-27}$	$(4-8) \times 10^{-27}$	$(5-9) \times 10^{-27}$
Al	$(2 \pm 1) \times 10^{-29}$	$(2-6) \times 10^{-29}$	
O	$(1 - 5) \times 10^{-30}$		
C	$(5.8 \pm 2) \times 10^{-30}$		

Durch die Wahl der Meßgeometrie ergibt sich für eine E1- wie eine E2-Winkelverteilung innerhalb der Fehlergrenzen der numerischen Rechnung der gleiche Wert für den totalen Streuquerschnitt. Die angegebenen Fehler enthalten nur den Fehler in der Bestimmung des primären γ-Flusses und die statistischen Fehler der Streuraten. Zum Vergleich sind die entsprechenden Ergebnisse von Fuller und Hayward [12]) und Stearns [8]) gegenübergestellt. Die angegebenen Werte gehören jeweils zu den Fehlergrenzen.

Intensität, die von der Quelle über den Streuer in den Nachweiskristall gelangt, wurde sowohl für eine E1- als auch für eine E2-Winkelverteilung der Streuquanten [10]) numerisch berechnet. Die Lithiumstrahlung ist bei $E_p = 500$ keV isotrop [11]). Die Absorption durch „elektronische" Prozesse im Streukörper und der Plexiglasunterlage wurde berücksichtigt. Selbstabsorption ist vernachlässigbar. In der (aus Intensitätsgründen) verwendeten Geometrie treten kleine Abstände von den Streupunkten zum Kristall auf. Die Streustrahlung gelangt hauptsächlich über die Kante des Kristalles in denselben. Ansprechwahrscheinlichkeit und Raumwinkel des Nachweiskristalles wurden daher für alle Streupunkte experimentell unter Verwendung der Lithiumstrahlung bestimmt.

In Tab. 1 sind die so gewonnenen totalen Streuquerschnitte angegeben.

3. Diskussion

Stearns [8]) hat für Blei mit 17 MeV-Lithiumstrahlung und einer Energiediskrimination bei 14 MeV den Streuquerschnitt für elastische γ-Streuung gemessen. Weitere Vergleichswerte für die elastische Streuung an Blei und Aluminium lassen sich den mit Bremsstrahlung gemessenen Kurven von Fuller und Hayward [12]) für eine Energie von 17.6 MeV entnehmen. Tab. 1. zeigt, daß die in der vorliegenden Arbeit erhaltenen Wirkungsquerschnitte mit den früheren Resultaten für beide Elemente gut übereinstimmen. Alle nichtresonanten Streueffekte, besonders die mit Bremsstrahlung zusammenhängenden, werden von Stearns bei Blei ausführlich diskutiert und als vernachlässigbar gefunden [8]).

Aus der Zunahme der elastischen giant resonance-Streuung mit etwa Z^3 folgt dann, daß alle nichtresonanten Streuungen, deren Wirkungsquerschnitt mit einer höheren Potenz von Z wächst, auch für die Messungen an Kohlenstoff und Wasser vernachlässigbar sind. Photoneutronen fallen unter die Diskriminationsschwelle. Es bleiben also für die Ergebnisse bei Kohlenstoff und Sauerstoff neben Comptonstreuung und Resonanzstreuung nur Rayleigh- und Thomsonstreuung zu berücksichtigen. Alle drei elastischen Streuanteile können miteinander interferieren. Die Wirkungsquerschnitte für Raleigh- und Thomsonstreuung wurden nach den klassischen Formeln berechnet. Diese gelten auch bei hohen γ-Energien bis auf 25 % Abweichung im Falle der Rayleighstreuung [13]). In der verwendeten Geometrie ergab sich Rayleighstreuung als vernachlässigbar.

Für den totalen Streuquerschnitt bei Sauerstoff ergeben die Experimente als wahrscheinlichsten Wert 1×10^{-30} cm². Unter Berücksichtigung der Maximalfehler lässt sich jedoch ein Wert von 5×10^{-30} cm² nicht ausschliessen. Der Streuquerschnitt für Thomsonstreuung errechnet sich zu 3.2×10^{-30} cm². Der giant resonance-Streuquerschnitt liegt in der Größenordnung von

10^{-30} cm² †. Das Messergebnis deutet also darauf hin, daß Comptonstreuung für die Messungen an Sauerstoff und Kohlenstoff vernachlässigbar ist.

Für Kohlenstoff liefert das Experiment einen totalen Streuquerschnitt von $(5.8 \pm 2) \times 10^{-30}$ cm² für Dipol- und Quadrupolverteilung. Der Thomsonstreuquerschnitt beträgt 1.8×10^{-30} cm². Der Resonanzstreuanteil muss daher unter Berücksichtigung der Interferenz zwischen Thomson- und Resonanzstreuung ausgerechnet werden. Dies wurde für Dipol-Dipol- und Dipol-Quadrupolinterferenz durchgeführt. Die Energie der Lithiumstrahlung beträgt unter Berücksichtigung von Rückstossverlusten und Dopplerverteilung 17.69 MeV ±10 keV mit einer Breite von 25 keV. Sie ist also „scharf" im Vergleich zur Resonanzbreite $\Gamma = 1.27$ MeV des 17.22 MeV-Zustandes in C^{12}. Somit ist die relative Phase von Resonanz- und Thomsonstreuanteil eindeutig bestimmt. Da die eingestrahlte γ-Energie oberhalb des Resonanzmaximums liegt [7]), ist die Interferenz konstruktiv. Der relative Phasenwinkel beträgt $|\delta| = 52°$. Dabei wurden Resonanzform und Gesamtbreite des 17.22 MeV-Zustandes der Resonanzkurve der Reaktion $B^{11}(p, \gamma)$ in der Umgebung von $E_p = 1.4$ MeV entnommen [7]). Es ergibt sich ein Resonanzstreuquerschnitt von 1.8×10^{-30} cm² für E1- und 1.9×10^{-30} cm² für E2-Streuung. Der Fehler beträgt in beiden Fällen ±70 %, wobei nur die in Tab. 1 angegebenen Meßfehler berücksichtigt sind.

4. Ergebnis

Mit diesen Werten für den Resonanzstreuquerschnitt wurden aus der Breit-Wigner-Formel für (γ, γ)-Prozesse [14]) für die beiden Niveauzuordnungen 1^- und 2^+ die γ-Breiten des Grundzustandsüberganges berechnet. Es ergibt sich für 1^-, d.h. einen E1-Übergang, $\Gamma_{\gamma 0} = 500$ eV ±35 %, und für 2^+, also einen E2-Übergang, $\Gamma_{\gamma 0} = 400$ eV ±35 %. Aus den Breiten ergeben sich die Matrixelemente der Übergänge $|M|^2 = 0.16$ für E1 und $|M|^2 = 76$ für E2 in Weißkopfeinheiten. Da ein derart hoher Wert von $|M|^2$ für einen E2-Übergang sehr unwahrscheinlich ist, ist der Übergang in den Grundzustand mit größter Wahrscheinlichkeit E1. Die Zuordnung 1^- für das 17.22 MeV-Niveau in C^{12} wird dadurch bestätigt. Wie ein Vergleich verschiedener E1-Übergänge in leichten Kernen zeigt [15]), liegt der Wert $|M(E1)|^2 = 0.16$ Weißkopfeinheiten innerhalb der Streubreite und ist um einen Faktor 4 größer als der Mittelwert. Die Isobarenspinzuordnung $T = 1$ für das 17.22 MeV-Niveau wird dadurch unterstützt. Unter Verwendung des mehrfach gemessenen Wirkungsquerschnittes der Reaktion $B^{11}(p, \gamma)$ bei $E_p = 1.4$ MeV [7]) ergibt sich aus der in der vorliegenden Arbeit gemessenen γ_0-Breite $\Gamma_{\gamma 0} = 500$ eV eine Protonenbreite $\Gamma_p = 80$ keV. Diese stimmt innerhalb der Fehlergrenzen mit dem Ergebnis der Protonenstreumessungen von Dearnalay *et al.* [5]) überein.

† Abgeschätzt aus den (γ, n)-Querschnitten. Ein direkter Vergleichswert liegt nicht vor.

TABELLE 2

Die partiellen Breiten des 17.22 MeV-Zustandes in C^{12}

	aus $\sigma(p,\alpha)$ [a]) $\sigma(p,\gamma)$ [b]) $\sigma(g,3\alpha)$ [c])		aus $\sigma(p,\alpha)$ [a]) $\sigma(p,\gamma)$ [b])		aus $\sigma(p,\alpha)$ [d]) $\sigma(p,0)$ [d]) $\sigma(\gamma,\gamma)$ [e])	
Γ [b])	1.27	MeV	1.27	MeV	1.27	MeV
Γ_p	1	MeV	200	keV	60	keV
Γ_{α_1}	200	keV	1	MeV	1	MeV
Γ_{α_0}	7	keV	35	keV	35	keV
Γ_{γ_0}	40	eV	160	eV	500	eV
Γ_{γ_1}	20	eV	80	eV	250	eV

[a]) Beckman, Huus and Zupančić [2]); [b]) Huus und Day [7]); [c]) Mann und Titterton [3]); [d]) Dearnalay, Dissanaike, French und Jones [5]); [e]) vorliegende Arbeit.

Aus diesen beiden direkt gemessenen partiellen Breiten lassen sich mit Hilfe der (p, α)- und (p, γ)-Wirkungsquerschnitte alle übrigen berechnen. In Tab. 2 sind die neuen Werte den bisher in der Literatur angegebenen [1]) gegenübergestellt. Besonders stark sollten sich die neuen Größen der partiellen Breiten in einem (γ, α)-Wirkungsquerschnitt auswirken, der sich mit den neuen Werten um einen Faktor 60 größer ergibt als mit den bisher angegebenen. Der von Mann und Titterton [3]) mit Lithiumstrahlung gemessene Wirkungsquerschnitt der Reaktion $C^{12}(\gamma, 3\alpha)$ ist allerdings mit den bisher verwendeten Breiten verträglicher als mit dem neuen Satz, wenn man das bisher allgemein verwendete Verzweigungsverhältnis [1]) $\sigma(p,\alpha_0)/\sigma(p,\alpha_1)$ zu Grunde legt. Dies könnte darauf hindeuten, daß dieser Wert für das Verzweigungsverhältnis zu klein ist; Γ_{α_0} und Γ_{α_1} müßten dann noch modifiziert werden.

An der Idee zur vorliegenden Arbeit ist Herr Dr. V. Soergel mitbeteiligt. Ihm haben die Autoren f[illegible]nregungen, Herrn Dr. H. J. Rose für ausführliche Diskussion[illegible]anken.

Literatur

1) F. Ajzenberg-Selove und T. Lauritsen, Nuclear Physics **11** (1959) 1
2) O. Beckmann, T. Huus und C. Zupančić, Phys. Rev. **91** (1953) 606
3) A. K. Mann und E. Titterton, Proc. Phys. Soc. **69** (1956) 817
4) G. W. Trautfest und S. Rubin, Phys. Rev. **103** (1956) 196
5) G. Dearnalay, G. A. Dissanaike, A. P. French und G. L. Jones, Phys. Rev. **108** (1957) 743
6) H. E. Gove und E. B. Paul, Phys. Rev. **97** (1955) 184

7) T. Huus und R. B. Day, Phys. Rev. **91** (1953) 599
8) M. B. Stearns, Phys. Rev. **87** (1952) 706
9) G. M. Griffith, Canad. Journ. Phys. **33** (1955) 209
10) D. R. Hamilton, Phys. Rev. **58** (1940) 122
11) M. B. Stearns und B. D. McDaniel, Phys. Rev. **82** (1951) 450
12) E. G. Fuller und E. Hayward, Phys. Rev. **101** (1956) 691
13) J. S. Levinger, Phys. Rev. **87** (1952) 656
14) K. G. Malmfors, in Siegbahn, Beta- and Gamma-ray Spectroscopy, (North Holland, 1955) Kap. 18,2 S. 521
15) D. H. Wilkinson, Phil. Mag. **1** (1956) 127

7.C *Nuclear Physics* **13** (1959) 583—593; © *North-Holland Publishing Co., Amsterdam*
Not to be reproduced by photoprint or microfilm without written permission from the publisher

CENTRAL AND PERIPHERAL COLLISIONS BETWEEN FAST NUCLEONS (I)

V. S. BARASHENKOV, V. M. MALTSEV and E. K. MIHUL
Joint Institute for Nuclear Research, Dubna

Received 22 May 1959

Abstract: About 83 percent of all inelastic collisions occurring at energies of 9 GeV in the examined model are collisions involving the central regions of the nucleons. For calculation of these "central collisions" methods of the statistical theory of multiple production of particles can be employed. With the exception of small angles and events in which a small number of particles participate, the data thus obtained are in good agreement with the experiments.

About 17 per cent of nucleon-nucleon collisions are peripheral collisions. Data on collisions between peripheral π-mesons and a nucleon can be obtained by using the statistical theory and experimental data on (πN) collisions at $E \geqq 1$ GeV. The mean energy loss of the nucleon and the mean multiplicity of the particles produced in (NN) collisions are in good agreement with the experimental data. The ratio of the number of charged particles moving forward to that of the charged particles moving backward in the c.m.s. of the colliding nucleons is close to the experimental value.

Account of peripheral collisions also improves the agreement between the theoretical and experimental angular distributions of the charged particles produced in (NN) collisions.

1. Introduction

Depending on the magnitude of the impact parameter one may distinguish in inelastic (pp) and (pn) collisions those which occur between the central parts of the nucleons and those collisions in which the periphery of one nucleon and the central region of the other are involved [1–3]).

The diagrams in figs. 1—3 show these two possible types of (NN) collisions †. In order to describe "central collisions" (see fig. 1) the statistical theory of multiple production should be sufficient ††, whereas for peripheral collisions (see figs. 2 and 3) a more detailed quantal approach appears to be necessary.

† The possibility of a third type of (NN) collisions for larger impact parameters, when the peripheries of both nucleons collide, has been mentioned in ref.[1]). The method of calculation of the cross section for peripheral collisions used below takes automatically into account this contribution. Collisions of pion shells will not be considered by us in detail here.

†† Collisions which we provisionally call "central" can furthermore be distinguished with respect to the value of the impact parameter b which may take any value between zero and $2r_0$, r_0 being the radius of the central part of a nucleon (see below). "Head-on collisions" for which the impact parameter b is zero are part of the central collisions.

Important information about the two types of collisions can be obtained by investigating the angular distributions of the charged particles produced in (NN) collisions and the relative numbers of stars with small and large number of prongs.

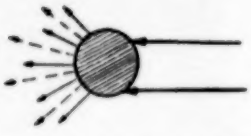

Fig. 1. Central inelastic collisions of nucleons. The solid lines refer to nucleons, the dotted curves to π mesons. The shaded junction is calculated by the statistical theory.

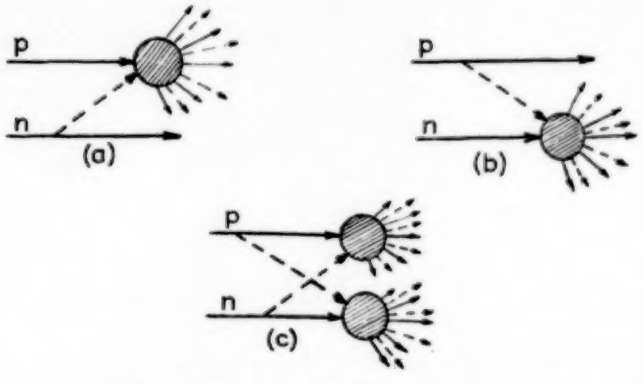

Fig. 2. Peripheral inelastic collision. The solid lines represent nucleons; the dotted lines π mesons.

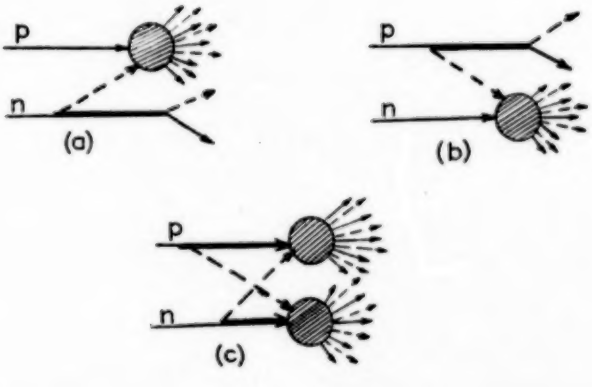

Fig. 3. Peripheral inelastic collision of nucleons. After emission of a π meson the nucleon passes into an isobar state. The thin solid lines are nucleons; the thick solid lines are isobars; the dotted lines are π mesons.

However, at present no complete analysis can be proposed. Our purpose is to ascertain in which respects the theory and experiments are inconsistent at present and to use this as a starting point for possible development of the theory and also to draw attention to those experiments which require increased accuracy.

2. Analysis of the Experimental Data

2.1. CENTRAL COLLISIONS

The angular distribution of fast charge particles † produced in the collisions between nucleons with an energy of about 9 GeV †† was calculated by means of the statistical theory of multiple production. The results were compared with the experimental data of ref. [4]). With the exception of small angles satisfactory agreement between experimental and theoretical curves was obtained within the limits of the experimental errors. Now we can compare the more accurately calculated theoretical curve to the more complete experimental data †††.

An experimental histogram for (NN)-collisions based on the data in ref.[6]) (average values for (pp) and (pn) collisions) is given in fig. 4. This

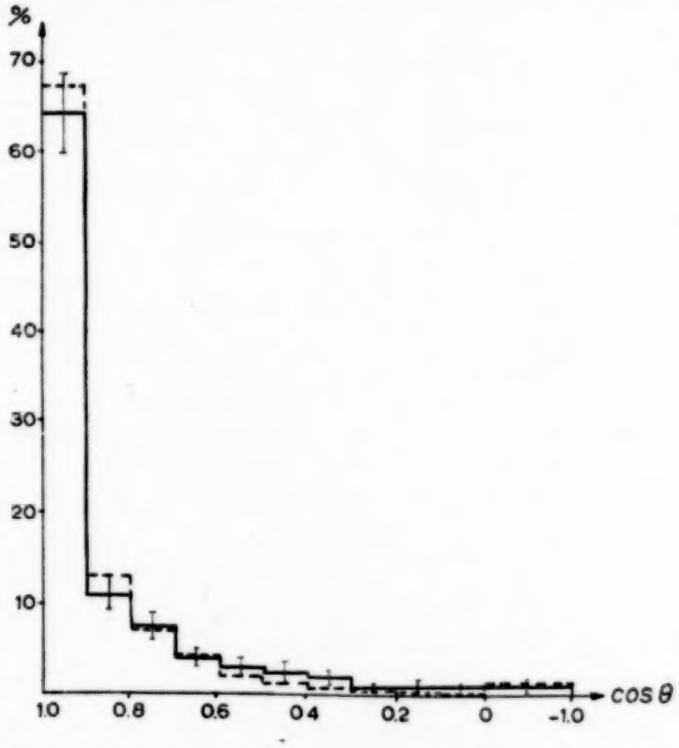

Fig. 4. Angular distribution of charged particles emitted in (NN) collisions in a solid angle $\Delta\Omega = \Omega(\theta_2) - \Omega(\theta_1)$ (in percent). The solid curve is the experimental histogram. Mean statistical errors are indicated. The dotted curve is the theoretical histogram. Laboratory system of coordinates.

† That is, of π^+-mesons with an energy $E_\pi \geqq 0.08$ GeV and of protons with an energy $E_p \geqq 0.5$ GeV.

†† Theoretical values for an energy $E = 9$ GeV were obtained by interpolation of the corresponding quantities evaluated in ref. [5]) for $E = 5$; 7; 10 GeV.

††† 115 cases of (pp) and 63 cases of (pn) collisions compared to 39 (pp) and 11 (pn) collision events analysed in ref.[4]). Besides, it should be noted that in ref.[6]) selection of (NN) interactions was more stringent. In contrast to ref.[4]) in our theoretical computations we also took into account the contribution of $\pi^\pm$-mesons and protons produced in reactions with strange particles (cf. ref.[5])).

histogram satisfactorily agrees, within experimental errors, with the theoretical histogram given in the same figure. However, the experimental values (from ref. [7])) for small angles, $\theta \leqq 10°$, are considerably greater than the theoretical ones. The ratio of the experimental values to the theoretical ones is only 15—20 per cent smaller than that obtained earlier [4]). There are experimental indications that the deviations are mainly due to protons [4]). If the momentum spectrum of charged particles computed within the framework of the statistical theory (comp.[4])) is used to transform the experimental angular distribution obtained in ref. [6]) from the laboratory system of coordinates into the centre-of-mass system of the colliding nucleons it will be found that in the c.m.s. the angular distribution is anisotropic. (The same was found to apply to the angular distribution obtained in ref. [4]).)

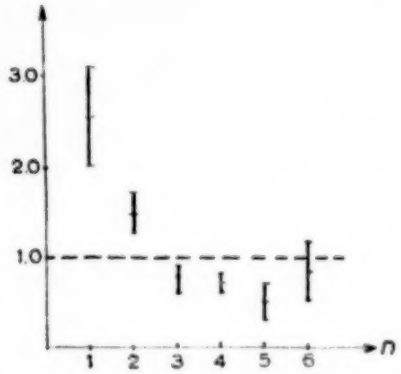

Fig. 5. Ratio of the experimental number of stars possessing various numbers of prongs to the number calculated by the statistical theory. The number of prongs in the star is plotted along the abscissa axis. An even number of prongs is produced in (pp) collisions and an odd number in (pn) collisions. Mean statistical errors are indicated.

The ratio of the experimental number of nucleon-nucleon stars with various number of prongs to that of stars calculated by means of the statistical theory [5]) †, is given in fig. 5. Some disagreement with the statistical theory is observed only for stars involving a small number of prongs.

Besides the above mentioned discrepancies there is one other very important discrepancy between the experimental data and statistical theory: the experimental ratio of the number of charged particles emitted into the forward hemisphere in the c.m.s. of the colliding proton and neutron (i.e. in the direction of motion of the primary proton) to the number of particles emitted into the backward hemisphere is $(\rightarrow/\leftarrow) = 1.6 \pm 0.2$ (in accordance with the data of refs. [7,8]); the error is the mean statistical) while calculations based on the statistical theory yield for this ratio the value $(\rightarrow/\leftarrow) = 1.0$.

We note that charge asymmetry $(\rightarrow/\leftarrow) > 1$ was also observed in inelastic (pn) collisions at $E \approx 1.5$ GeV [9]).

† For sake of simplicity, the contribution from charged strange particles and antiprotons, which is approximately 10 %, is not taken into account.

Thus, comparison of the experimental results with predictions of the statistical theory of multiple production reveal some important differences in the case of small angles and events in which a small number of particles are produced. Since the angular distributions averaged over large angular intervals (see fig. 4), as well as the average number of created particles (see refs.[3, 4])) and also the mean energy loss of the incident nucleon in an (NN) collision process (see ref.[12])) all turn out to be close to the values obtained from the statistical theory [5]), it may be concluded that most (NN)-collisions are collisions between the central parts of the nucleons.

2.2. PERIPHERAL COLLISIONS

In order to estimate roughly the contribution from peripheral collisions we restrict ourselves to investigation of "one-meson graphs", a and b (figs. 2 and 3). More complicated processes with the exchange of two mesons, such as those, corresponding to the graphs c in figs. 2 and 3 are not considered for the moment.

The cross section for peripheral (NN)-collisions is

$$\sigma_p = 2\int_{\mu}^{\varepsilon^*} \sigma(\varepsilon)Q(\varepsilon)\mathrm{d}\varepsilon, \qquad (1)$$

where μ is the π-meson mass, $\varepsilon^* = E - \sqrt{\frac{1}{2}M(E+M)}$, $E = \gamma M$, $\gamma^2 = (1-\beta^2)^{-1}$; E is the total energy of the nucleon, M is its mass, $\sigma(\varepsilon)$ is the total cross section for (πN) interaction at an energy ε; $Q(\varepsilon)$ is the energy spectrum of peripheral mesons moving together with the nucleon.

The values of $q(\varepsilon) = \gamma\beta^3 Q(\varepsilon)/f^2$ are presented in fig. 6 for a 9 GeV nucleon; $f^2 = 0.08$. The computations were performed by the method suggested by

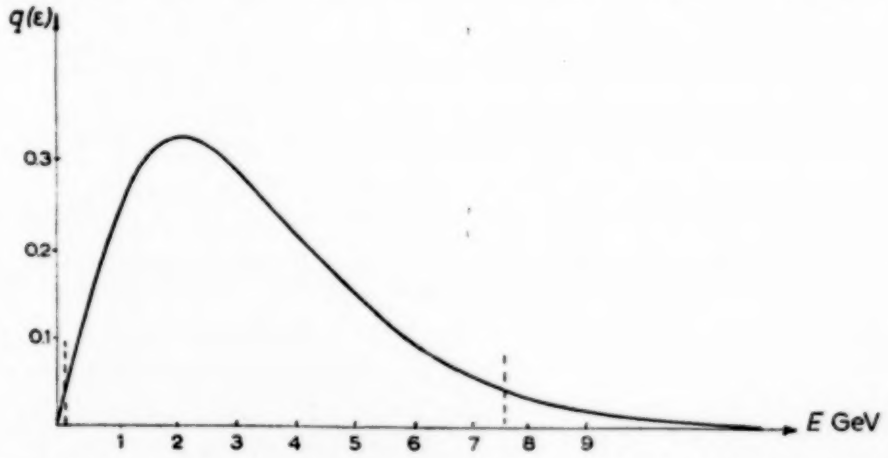

Fig. 6. Energy spectrum of the peripheral mesons of a nucleon moving in the laboratory system of coordinates with a kinetic energy of 9 GeV. The energy of the meson in GeV is plotted along the abscissa axis. The dotted lines denote the limits of integration, $\varepsilon = \mu$ and $\varepsilon = \varepsilon^*$.

Heitler and Peng [10]). The value $r_0 = 0.6\times 10^{-13}$ cm has been chosen by us for the minimum impact parameter, i.e. for the radius of the central region

of the nucleon. This value follows from a comparison of various experimental data on the interaction of nucleons and pions with nucleons at energies $E > 1$ GeV [11, 12]). Nucleon collisions with impact parameters $r > r_0$ will be considered to be peripheral.

In order to calculate $Q(\varepsilon)$ it is necessary to know the distribution of the meson cloud in a nucleon for all the values of $r > r_0$. It has been shown [2, 3]) that for meson clouds of nucleons at distances $r \gtrsim 10^{-13}$ cm from the centre of the nucleon appreciable errors may be introduced if the contribution from two-meson states is not taken into account. The asymptotic expressions for the meson field in a nucleon used in ref. [10]) are valid, strictly speaking, only for $r \gg 10^{-13}$ cm. However, in estimating the mean energy of the peripheral mesons $\bar{\varepsilon}$ one may also use these expressions as a rough approximation of the exact expressions for distances $r \approx (0.6 \text{ to } 1.0) \times 10^{-13}$ cm. In this case, as can be seen from fig. 6, $\bar{\varepsilon} \approx 3$ GeV (see also sec. 5). Since the cross section $\sigma(\varepsilon)$ for (πN) interactions at energies $\geqq 1$ GeV, which represents the main part of σ_p remains almost constant ($\sigma \approx 30$ mb) we have

$$\sigma_p \approx 2\sigma \int_{\mu}^{\varepsilon^*} Q(\varepsilon) d\varepsilon \simeq \frac{1}{\beta^2} 5 \text{ mb}, \tag{2}$$

which is $\approx 17\,\%$ of the cross section for inelastic (NN) interactions and agrees with the results of optical analysis of (NN) interactions at $E > 1$ GeV [12]). The quantity σ_p almost does not change with variation of the primary proton energy, since $\beta \approx 1$. We made use of the experimental value of the cross section for (πN) collisions which takes into account collisions between the incident π-meson and nucleon core and also collisions between the π meson and the peripheral π-meson shell of the nucleon. As a result the calculated cross section for peripheral collisions (2) automatically takes into account collisions between the π-meson shell and core as well as collisions between the π meson shells of the colliding nucleons ($(\pi\pi)$ collisions).

3. Charge Asymmetry in Inelastic (pn) Collisions

In order to estimate the average number of charged particles produced in the collision of the peripheral meson of the incident nucleon with the nucleon at rest we made use of the statistical theory of multiple production, this being quite justified since the computed data on (πN) collisions in the region $E = (1 \text{ to } 5)$ GeV are in good agreement with the experimental data [15, 17]). All the statistical calculations were carried out under the same assumptions and by means of the same methods as in ref.[15]).

The average numbers of protons and $\pi^{\pm}$-mesons produced in (πN) collisions calculated in this way are presented in table 1 ($E_\pi = \bar{\varepsilon} = 3$ GeV).

TABLE 1

Colliding particles	Mean number of particles	Mean number of $\pi^{\mp}$-mesons
π^- p	0.41	1.69
π^+ p	0.75	1.87
π^0 p	0.59	1.69
π^- n	0.25	1.87
π^+ n	0.59	1.69
π^0 n	0.41	1.69

Taking into account the relative probabilities for various channels one can write the reaction corresponding to the sum of the graphs a and b (fig. 2) in the form

$$\begin{aligned}\vec{p}+\overleftarrow{n} \to \tfrac{1}{3}\{\vec{p}+(\vec{\pi}^0+\overleftarrow{n})\}+\tfrac{2}{3}\{\vec{n}+(\vec{\pi}^+ +\overleftarrow{n})\} \\ +\tfrac{1}{3}\{(\vec{p}+\overleftarrow{\pi}^0)+\overleftarrow{n})\}+\tfrac{2}{3}\{(\vec{p}+\overleftarrow{\pi}^-)+\overleftarrow{p}\}.\end{aligned} \tag{3}$$

The arrows denote the directions of the particle velocities in the c.m.s. of the colliding nucleons. Particles, the collisions of which lead to multiple production of secondary particles and diffractional scattering, are singled out by the parentheses. Charge asymmetry per inelastic (NN) collision event is

$$(\rightarrow/\leftarrow) = \vec{n}/\overleftarrow{n}, \tag{4}$$

where

$$\vec{n} = (\vec{n}_d\sigma_d+\vec{n}_{1n}\sigma_{1n})/(\sigma_d+\sigma_{1n}), \tag{5}$$

$$\overleftarrow{n} = (\overleftarrow{n}_d\sigma_d+\overleftarrow{n}_{1n}\sigma_{1n})/(\sigma_d+\sigma_{1n}), \tag{6}$$

Here, $\vec{n}_d$ and $\overleftarrow{n}_d$ are the numbers of charged particles produced in diffractional scattering of a peripheral meson by a nucleon and emitted in the c.m.s. of the colliding nucleons in the forward and backward hemispheres; $\vec{n}_{1n}$ and $\overleftarrow{n}_{1n}$ are similar quantities referring to inelastic collision between the peripheral meson and nucleon; σ_d is the cross section for the diffractional (πN) scattering; σ_{1n} is the cross section for inelastic (πN) scattering.

Using the data in table 1 we obtain $(\rightarrow/\leftarrow) \approx 1$ ($(\rightarrow/\leftarrow) \approx 0.8$ and $(\rightarrow/\leftarrow) \approx 1.0$ for protons and $\pi^{\mp}$-mesons separately †.) Thus, in the case considered it has not been possible to obtain any appreciable charge asymmetry in the forward direction. This conclusion remains true even when the mean energy of the peripheral meson $\bar{\varepsilon}$ or, what is equivalent, the value of r_0 changes in wide limits.

Account of the graph 2c also cannot alter this conclusion since a similar number of charged particles is produced in both (πN) collisions.

† Here account has been taken of the fact that in the energy region of interest $\sigma_d/\sigma_{1n} = \frac{1}{2}$ to $\frac{1}{3}$. If diffractional (πN) scattering is not considered, $(\rightarrow/\leftarrow) \approx 0.9$.

However, if we take into account the fact that the mean energy of virtual mesons in the nucleon cloud for $r > 0.6 \times 10^{-13}$ cm is close to the resonance energy in the coordinate system related to the nucleon, the nucleon-meson interaction will mainly occur in the $T = P = \frac{3}{2}$ "isobar state". After interaction between the peripheral meson and nucleon the isobar decays into a nucleon and a π-meson †:

$$\begin{aligned} N^{++} &\to (p\pi^+) \\ N^{+} &\to \tfrac{2}{3}(p\pi^0)+\tfrac{1}{3}(n\pi^+) \\ N^{0} &\to \tfrac{1}{3}(p\pi^-)+\tfrac{2}{3}(n\pi^0) \\ N^{-} &\to (n\pi^-) \end{aligned} \tag{7}$$

with a lifetime in the laboratory coordinate system

$$\tau \sim \tau_1/\sqrt{1-\beta^2} = \tau_1(E-\bar{\varepsilon})/m' \approx 15\tau_0 \gg \tau_0. \tag{8}$$

Here, $\tau_1 \approx 3\tau_0$ is the lifetime of the isobar state as derived from experiments with mesons of a few hundred MeV energy; τ_0 is the mean interaction time between the colliding particles; β is the isobar velocity; $m' = 1.32\,M$ is the isobar mass.

Graphs a and b in fig. 3 correspond to this case. Taking into account the relative probabilities for various channels of the reaction we obtain

$$\begin{aligned} \vec{p}+\overleftarrow{n} \to \tfrac{1}{2}\{\vec{N}^{++}+(\vec{\pi}^-+\overleftarrow{n})\}+\tfrac{1}{3}\{\vec{N}^{+}+(\vec{\pi}^0+\overleftarrow{n})\}+\tfrac{1}{6}\{\vec{N}^{0}+(\vec{\pi}^+ +\overleftarrow{n})\} \\ +\tfrac{1}{2}\{(\vec{p}+\overleftarrow{\pi}^+)+\overleftarrow{N}^-\}+\tfrac{1}{3}\{(\vec{p}+\overleftarrow{\pi}^0)+\overleftarrow{N}^0\}+\tfrac{1}{6}\{(\vec{p}+\overleftarrow{\pi}^-)+\overleftarrow{N}^+\}. \end{aligned} \tag{9}$$

By using the results of the statistical calculation presented in table 1 †† and relations (4)—(7) we obtain $(\to/\leftarrow) = 1.4$, ($(\to/\leftarrow) \approx 3.3$ and $(\to/\leftarrow) \approx 1$ for protons and π mesons separately †††). It is clear that because of symmetry properties in the case of (pp) collisions, $(\to/\leftarrow) = 1$.

The charge asymmetry $(\to/\leftarrow) > 1$ is mainly due to protons created in the decay of the isobar (in particular N^{++}). This special property of protons is in agreement with the experimental indications *.

Just as in the case of processes corresponding to the graphs a and b in fig. 2, variation of the mean energy $\bar{\varepsilon}$ of the peripheral mesons in a wide

† The superscripts denote the charge of the isobar.

†† The resonance interaction of π-mesons and nucleons produced in (πN) collisions was automatically taken into account in the statistical calculation of the results presented in table 1 (see ref.[14,15]).

††† Here we again assume $\sigma_d/\sigma_{in} = \frac{1}{2}$ to $\frac{1}{3}$. If diffractional (πN) scattering is neglected, $(\to/\leftarrow) = 1.3$.

* It is not difficult to show in a general form, that the ratio $(\to/\leftarrow)$ due only to π-mesons is equal to unity. It is quite sufficient for this purpose to take into account the fact that after the substitution $p \leftrightarrow n$ a greater number of charged particles will move backwards. But since we have to perform simultaneously the substitutions $\pi^0 \leftrightarrow \pi^0$ and $\pi^{\pm} \leftrightarrow \pi^{\mp}$, the numbers of charged mesons moving forward and backward do not change. (It was M. I. Podgoretsky who drew our attention to this.)

interval (or, what is equivalent, variation of r_0) does not change the conclusion regarding the forward charge asymmetry. This asymmetry decreases appreciably only for small r_0 when a great number of charged particles are created in (πN) collisions.

Protons produced in isobar decay as well as those from processes involving diffractional scattering of the peripheral meson are emitted in the c.m.s. of the colliding nucleons at small angles †. As follows from fig. 4 charged particles produced in central collisions are distributed in this coordinate system approximately isotropically. Thus, in spite of the fact that peripheral collisions comprise only ≈ 17 % of the central collisions the charge asymmetry in the small angle region may completely be due to peripheral collisions. If account is taken of the fact that multiply produced charged particles produced in peripheral (πN) collisions are also distributed in a broader angular interval than protons produced in decay of isobars or in diffractional (πN) scattering processes, then the charge asymmetry will be found to be somewhat larger.

For large angles θ the theoretical value of the ratio $(\rightarrow/\leftarrow)$ tends to unity. Experimentally, this ratio considerably exceeds unity (1.6 ± 0.2) even for $\theta = \frac{1}{2}\pi$. However, the conclusions about the charge asymmetry (ref.[7,8]) are based on a recalculation of the experimental angular distribution of the particles from the laboratory system to the centre of mass system of the colliding nucleons. Since the experimental energy spectrum of the particles produced in (NN) collisions at present is almost unknown, the transition to the c.m.s. carried out in ref.[7,8]) contains errors. These errors are apparently smaller in the small angle region; however, it would be premature to attempt a quantitative treatment ††. An experimental investigation of the quantity $(\rightarrow/\leftarrow)$ as a function of the scattering angle θ is a problem of fundamental importance.

4. Mean Number of Particles Produced in the Inelastic Collisions of Nucleons

In our rough model of peripheral collisions in which we made use of a mean energy of the peripheral mesons $\bar{\varepsilon}$, one can hope to estimate with a small error only those effects which depend on the average number of particles created in the collisions. For peripheral collisions involving a small number of particles the mean energy ε is lower than that used by us ($\varepsilon \approx \bar{\varepsilon}$) since the statistical weights of the processes yielding a small number of

† Since the mean momentum of protons produced in isobar decay is approximately 0.23 GeV/c in the isobar coordinate system it is not difficult to see that in the centre of mass system of the colliding nucleons most of these protons will be emitted at angles $\theta < 15°$ to $20°$.

†† For example, the statistical error is of the same magnitude as the effect itself in the most interesting region, that of small angles. Thus, $(\rightarrow/\leftarrow) = 1.3\pm0.3$ for equivalent angular intervals $\theta = 0°$ to $26°$ and $\theta = 154°$ to $180°$. However, there are experimental indications that the charge asymmetry is mainly observed at angles $\theta < 60°$ and $\theta > 120°$.

particles in (πN) collisions decrease with increasing energy. On the contrary, for (πN) collisions in which large numbers of particles are produced, the mean energy ε is higher because the statistical weights of such processes increase with increasing energy.

The average number of charged particles produced in a peripheral (pn) collision is $n_p = \overrightarrow{n} + \overleftarrow{n} = 3.1$ which is close to the number of charged particles $n_c = 3.2$ produced in central collisions.

The theoretical values of the numbers of charged particles produced per inelastic (pp) or (pn) collisions are $n_{(pp)} = 3.5$, $n_{(pn)} = 3.2$ and slightly exceed the corresponding experimental values $n_{(pp)} = 3.22 \pm 0.12$ and $n_{(pn)} = 2.62 \pm 0.13$ [7]). However, at present no great importance should be attached to this difference. It is quite possible that it is due to the fact that the particles produced in a collision between the primary proton and a quasi-free nucleon in the peripheral region of the atomic nucleus can be absorbed by the nucleus and cause its decay. The criteria of selection for (NN)-collisions used in refs. [4,6,7]) exclude automatically such events. For (NN) stars with a great number of prongs the angular distribution of the produced particles is broader and the absorption of particles in the nucleus is consequently more probable. Therefore it may be expected that the number of multi-prong stars cited in refs. [4,6,7]) is slightly too high. This effect is more probable for (pn) collisions since most of (pp) collisions are collisions with hydrogen nuclei whereas in all (pn) collisions the neutron is quasi-free. These arguments are also borne out by the fact that the ratio $[n_{(pn)\ theor} - n_{(pn)\ exper}]/n_{(pn)\ exper}$ for (pn) collisions turns to be larger than the corresponding ratio for (pp) collisions.

The model under consideration also allows us to calculate the average number of charged particles emitted in the laboratory system within a given solid angle interval. As the calculations show, the theoretical number of particles emitted in the small angle range $\theta < 10°$ turns to be close to the experimental number, if peripheral collisions are taken into account (cf. sec. 2 and ref. [4])). However, this question requires more careful investigation since the model used by us is too crude. Account of the law of conservation of momentum may turn out to be important for the angular distributions of particles of stars possessing a small number of prongs.

5. Conclusion

As can be seen we have been able to explain all the fundamental experimental results on inelastic (pp) and (pn) scattering by considering both central and peripheral collisions †. In the second part of this paper we shall consider in detail the mean energy losses suffered in central and peripheral collisions (preliminary results are given in ref.[12])).

In conclusion the authors wish to express their deep gratitude to D. I. Blokhintsev for interesting discussions and valuable advice and to V. I. Veksler for stimulating discussions and valuable critical remarks. We are also grateful to N. P. Bogachov and I. M. Gramenitsky for discussions of the results of experimental investigations [6, 7]).

Note added in proof: V. I. Veksler informed us that I. E. Tamm also considered a model with a residual isobar to account for the angular asymmetry in nucleon collision.

† It should be noted that division of inelastic collisions into central and peripheral, also holds for (πN) collisions. Peripheral collisions in this case are due to ($\pi\pi$) interactions. Optical analysis of (πN) collisions at energies $E = 1$ to 5 GeV indicate that such collisions appreciably contribute to the total scattering cross section [17]).

References

1) D. I. Blokhintsev, CERN Symposium **2** (1956) 155
2) D. I. Blokhintsev, V. S. Barashenkov and B. M. Barbashev, Uspekhi Fiz. Nauk **68** (1959) 417
3) V. S. Barashenkov, Multiple production of particles in the experiments with 9 GeV protons, Materials of the All-Union Conference on Quantum Field Theory and Theory of Elementary Particles (Uzhgorod, October 2–6, 1958)
4) V. S. Barashenkov, V. A. Belyakov, E. G. Bubelev, Wang Shou Feng, V. M. Maltsev, Ten Gyn and K. D. Tolstov, Nuclear Physics **9** (1958) 74;
V. S. Bareshenkov, Wang Shou Feng and K. D. Tolstov, Atomnaya Energia **5** (1958) 453
5) V. S. Barashenkov, B. M. Barbashov and E. G. Bubelev, Nuovo Cimento **7**, Suppl. (1958) 117;
V. S. Barashenkov, B. N. Barbashov, E. G. Bubelev and B. M. Maksimenko, Nuclear Physics **5** (1957) 17
6) N. P. Bogachev, S. A. Bunyatov, U. P. Merekov and V. M. Sidorov, Dokl. Akad. Nauk **121** (1958) 617
7) N. P. Bogachev, S. A. Bunyatov, I. M. Gramenitsky, V. B. Lyubimov, Yu. P. Merekov, M. I. Podgoretsky, V. M. Sidorov and D. Tuvdendorg (in print); JINR p—356;
I. M. Gramenitsky, Report at Seminar on Inelastic (NN) Interactions (Dubna, March 1959)
8) V. I. Veksler, Report at the Second International Conference on Peaceful Use of Atomic Energy (Geneva, 1958)
9) W. B. Fowler, R. P. Shutt, A. M. Thorndike and W. I. Whittermore, Phys. Rev. **95** (1956) 1026
10) W. Heitler and H. W. Peng, Proc. RIA **40** (1943) 101
11) V. S. Barashenkov, Optical analysis of the interaction of fast nucleons and pions with nucleons and nuclei, Materials of the All-Union Conference on Quantum Field Theory and Theory of Elementary Particles (Uzhgorod, October 2–6, 1958)
12) V. S. Barashenkov, V. A. Belyakov, Wang Shou Feng, V. V. Glagolev, I. Dolkhazhav, I. F. Kirillova, R. M. Lebedev, V. M. Maltsev, P. K. Markov, K. D. Tolstov, E. N. Tsyganov, M. G. Shafranova and Yao Tsing-se, Nuclear Physics (in print)
13) D. I. Blokhintsev, V. S. Barashenkov and B. M. Barbashov, Nuovo Cimento **12** (1959) 602
14) S. Z. Belenky, V. M. Maksimenko, A. I. Nikishov and I. L. Rosental, Uspekhi Fiz. Nauk **62** (1957) I;
V. M. Maksimenko, JETP **35** (1958) 1302
15) V. S. Barashenkov and V. M. Maltsev, Acta Phys. Polonica **17** (1958) 177
16) R. C. Whitten and M. M. Blogh, Phys. Rev. **111** (1958) 1676; further references for $E = 1$ to 5 GeV are given there
17) D. I. Blokhintsev, V. S. Barashenkov and V. G. Grishin, Nuovo Cimento **9** (1958) 249; JETP **35** (1958) 311

1.C:2.D *Nuclear Physics* **13** (1959) 594—620; © *North-Holland Publishing Co., Amsterdam*
Not to be reproduced by photoprint or microfilm without written permission from the publisher

DENSITÉ DE NIVEAUX D'UN SYSTÈME DE NUCLÉONS EN INTERACTION DANS UNE COUCHE

ROGER BALIAN

Centre d'Études Nucléaires de Saclay, Gif-sur-Yvette (S. et O.)

Reçu le 29 juin 1959

Abstract: Using perturbation theory, the grand partition function is calculated for the completely degenerate system of interacting nucleons inside a shell. The level density is then derived by the Darwin-Fowler method. The purpose is to compare these results to exact levels known for a p-shell. The method gives fairly good results, even for a small number of particles, provided that the self-consistent field is taken into account, and the calculation is carried out in a coherent way; there is no advantage in performing the saddle point method after integration of the level density.

1. Introduction

La densité de niveaux d'un système composé d'un grand nombre de particules peut se déduire de la grande fonction de partition par des méthodes statistiques [1]). Ce problème se traite en toute généralité pour des nucléons (ou des „excitations élémentaires") indépendants [2]), ou interagissant dans l'approximation de longue portée [3]). L'emploi de la méthode des perturbations pour le calcul de la grande fonction de partition [4]) permet de tirer, par la méthode du col, la densité de niveaux d'un système de nucléons en interaction. On se propose ici de tester la validité des approximations faites, en comparant, dans un modèle particulier, les résultats de cette théorie approchée aux niveaux exacts.

Dans le modèle utilisé, les nucléons sont dans un puits moyen à symétrie sphérique; toutes les couches sont complètes, à l'exception de l'une d'entre elles, de moment angulaire l, comprenant N particules et $\mathcal{N} = 4\,(2l+1)$ états individuels; on néglige la partie de l'interaction entre les particules qui induit des transitions entre ces états et ceux des autres couches; à l'intérieur de la couche, l'interaction est indépendante du spin et du spin isobarique, et est invariante par rotation. Dans ces conditions, on est ramené au problème de N particules dont l'hamiltonien est l'interaction V à l'intérieur de la couche, l'hamiltonien non perturbé étant nul. On est à l'opposé du modèle à particules indépendantes: le système non perturbé est complètement dégénéré; c'est l'interaction qui sépare les niveaux.

Dans la section 2, nous rappellerons la solution exacte du problème pour une couche p. Dans la section 3, nous calculerons la grande fonction de partition $Z(\alpha, \beta)$ et nous en déduirons la densité de niveaux par la méthode

de Darwin-Fowler. Pour obtenir cette densité de niveaux à une grande énergie d'excitation, nous serons amenés à introduire des valeurs de β négatives. En effet, le nombre de niveaux est fini, contrairement à ce qui se passe usuellement en thermodynamique, où l'énergie des niveaux excités n'est pas bornée supérieurement; le système, de matrice densité $\rho = e^{-\beta H}/\operatorname{tr} e^{-\beta H}$, est dans un état pur non seulement lorsque $\beta \to +\infty$ (l'état fondamental), mais aussi lorsque $\beta \to -\infty$ (l'état d'énergie maximum). Les valeurs positives et négatives de β jouent donc des rôles symétriques. La section 4 sera consacrée aux résultats.

2. Diagonalisation Exacte de l'Hamiltonien dans une Couche p [5,6])

L'interaction est caractérisée par ses valeurs moyennes V_L dans des états à deux particules de moment orbital total L ($L = 0, 1, 2$ dans la couche p).

Les états à N particules qui diagonalisent V sont ceux pour lesquels le moment angulaire orbital total L, et le type de symétrie de la fonction d'onde d'espace sont bien définis. La valeur de V dans ces états est

$$V = \tfrac{1}{2}(V_1+V_2)\tfrac{1}{2}N(N-1)+\tfrac{1}{3}(V_0-V_2)[N-\tfrac{1}{2}L(L+1)]-\tfrac{1}{6}(2V_0-3V_1+V_2)\Xi; \tag{1}$$

$\Xi = n_A - n_S$ ne dépend que du type de symétrie de la fonction d'onde d'espace. C'est la différence entre le nombre de liaisons antisymétriques et le nombre de liaisons symétriques du diagramme d'Young de la fonction d'espace.

Lorsque la force est du type Wigner, les fonctions d'onde individuelles dans la couche p sont des combinaisons linéaires de $xR(r)$, $yR(r)$ et $zR(r)$; tous les éléments de matrice de V s'expriment en fonction des deux paramètres

$$\mathscr{L} = \int x_1^2 x_2^2 |R(r_1)|^2 |R(r_2)|^2 V(r_{12}) \mathrm{d}\mathbf{r}_1 \mathrm{d}\mathbf{r}_2,$$

$$\mathscr{K} = \int x_1 x_2 y_1 y_2 |R(r_1)|^2 |R(r_2)|^2 V(r_{12}) \mathrm{d}\mathbf{r}_1 \mathrm{d}\mathbf{r}_2,$$

et l'interaction s'écrit

$$V = (\mathscr{L}-2\mathscr{K})\tfrac{1}{2}N(N-1)+\mathscr{K}[N-\tfrac{1}{2}L(L+1)-2\Xi].$$

Une variation de $\mathscr{L}$ introduit simplement une translation d'ensemble des niveaux; une variation de $\mathscr{K}$ une homothétie. Cette propriété permet de rapporter les courbes de densités de niveaux approchées correspondant à diverses valeurs de $\mathscr{L}$ et de $\mathscr{K}$ à la même courbe exacte.

Pour un mélange Wigner-Majorana, en introduisant de même les paramètres $\mathscr{L}'$ et $\mathscr{K}'$, on a

$$V_0 = (\mathscr{L}+2\mathscr{K})+(\mathscr{L}'+2\mathscr{K}')$$
$$V_1 = (\mathscr{L}-3\mathscr{K})-(\mathscr{L}'-3\mathscr{K}'),$$
$$V_2 = (\mathscr{L}-\mathscr{K})+(\mathscr{L}'-\mathscr{K}'),$$

et les deux termes dépendant de L et Ξ ne sont plus proportionnels.

Les positions exactes des niveaux se déduisent immédiatement de la classification des fonctions d'onde à N particules suivant le type de symétrie Ξ, L, le spin total S, et le spin isobarique T, que nous rappelons dans le tableau 1.

TABLEAU 1

Classification des fonctions d'onde de N particules dans une couche p

N	Type de symétrie d'espace	Ξ	L	(S, T)	Dégénérescence pour chaque valeur de L
2	(2)	−1	0, 2	(0, 1) (1, 0)	6,30
	(1, 1)	+1	1	(0, 0) (1, 1)	30
3	(3)	−3	1, 3	$(\frac{1}{2}, \frac{1}{2})$	12, 28
	(2, 1)	0	1, 2	$(\frac{1}{2}, \frac{1}{2})$ $(\frac{1}{2}, \frac{3}{2})$ $(\frac{3}{2}, \frac{1}{2})$	60, 100
	(1, 1, 1)	3	0	$(\frac{1}{2}, \frac{1}{2})$ $(\frac{3}{2}, \frac{3}{2})$	20
4	(4)	−6	0, 2, 4	(0, 0)	1, 5, 9
	(3, 1)	−2	1, 2, 3	(0, 1) (1, 0) (1, 1)	45, 75, 105
	(2, 2)	0	0, 2	(0, 0) (1, 1) (0, 2) (2, 0)	20, 100
	(2, 1, 1)	2	1	(0, 1) (1, 0) (1, 1) (1, 2) (2, 1)	135
5	(4, 1)	−5	1, 2, 3, 4	$(\frac{1}{2}, \frac{1}{2})$	12, 20, 28, 36
	(3, 2)	−2	1, 2, 3	$(\frac{1}{2}, \frac{1}{2})$ $(\frac{1}{2}, \frac{3}{2})$ $(\frac{3}{2}, \frac{1}{2})$	60, 100,140
	(3, 1, 1)	0	0, 2	$(\frac{1}{2}, \frac{1}{2})$ $(\frac{1}{2}, \frac{3}{2})$ $(\frac{3}{2}, \frac{1}{2})$ $(\frac{3}{2}, \frac{3}{2})$	36, 180
	(2, 2, 1)	2	1	$(\frac{1}{2}, \frac{1}{2})$ $(\frac{1}{2}, \frac{3}{2})$ $(\frac{3}{2}, \frac{1}{2})$ $(\frac{3}{2}, \frac{3}{2})$ $(\frac{1}{2}, \frac{5}{2})$ $(\frac{5}{2}, \frac{1}{2})$	180
6	(4, 2)	−5	0, 2, 2, 3, 4	(0, 1) (1, 0)	6, 30, 30, 42, 54
	(4, 1, 1)	−3	1, 3	(0, 0) (1, 1)	30, 70
	(3, 3)	−3	1, 3	(0, 0) (1, 1)	30, 70
	(3, 2, 1)	0	1, 2	(0, 1) (1, 0) (1, 1) (1, 1) (0, 2) (2, 0) (1, 2) (2, 1)	192, 320
	(2, 2, 2)	3	0	(0, 1) (1, 0) (1, 2) (2, 1) (0, 3) (3, 0)	50

Lorsque le nombre N est supérieur à $\frac{1}{2}\mathscr{N}$ (pour une couche quelconque), on peut former la fonction d'onde à $\mathscr{N}-N$ particules,

$$\psi(\mathscr{N}-N) = \int \mathrm{d}(N)\psi^*(N)\psi(\mathscr{N}),$$

$\psi(\mathscr{N})$ étant la fonction d'onde de la couche complète. Soit, dans le formalisme de la seconde quantification,

$$|\psi(N)\rangle = \sum_{i>j>\ldots} C_{ij\ldots}\xi_i^+\xi_{j\ldots}^+|0\rangle,$$
$$|\psi(\mathscr{N}-N)\rangle = \sum_{i>j>\ldots} C^*_{ij\ldots}\ldots\xi_j\xi_i|\psi(\mathscr{N})\rangle.$$

Le potentiel s'écrit, avec les notations de la troisième partie,

$$V = \tfrac{1}{4}\sum_{klmn} \langle kl|V|mn\rangle \xi_k^+ \xi_l^+ \xi_m \xi_n, \tag{2}$$

ou encore

$$V = \tfrac{1}{4}\sum_{klmn} \langle kl|V|mn\rangle \xi_m \xi_n \xi_k^+ \xi_l^+ + \tfrac{1}{2}\sum_{kn}\sum_{l} \langle kl|V|ln\rangle [\xi_k^+ \xi_n - \xi_n \xi_k^+]. \tag{3}$$

Si $|\psi(N)\rangle$ est fonction propre de V (écrit sous la forme (2)) on voit immédiatement que $\langle\psi(\mathcal{N}-N)|$ est aussi fonction propre du premier terme de V (écrit sous la forme (3)) avec la même valeur propre; le second terme ne dépend que du nombre de particules, puisque (équation (20))

$$\sum_l \langle kl|V|ln\rangle = e_1 \delta_{kn}.$$

Il donne la contribution supplémentaire $e_1(\frac{1}{2}\mathcal{N}-N)$ à l'énergie. Par suite, les états à N particules et ceux à $\mathcal{N}-N$ particules se correspondent un à un, et leurs énergies sont liées par

$$E_{\mathcal{N}-N} = E_N + e_1(\tfrac{1}{2}\mathcal{N}-N). \tag{4}$$

3. Calcul de la Grande Fonction de Partition et de la Densité de Niveaux

3.1. MÉTHODE DE DARWIN-FOWLER [1])

La densité de niveaux à N particules et d'énergie E étant $\rho(E, N)$, la grande fonction de partition s'écrit

$$Z(\alpha, \beta) = e^{\phi(\alpha,\beta)} = \int dE dN \rho(E, N) e^{-\beta E + \alpha N} \tag{5}$$

et la densité des niveaux s'obtient par la transformée de Laplace inverse

$$\rho(E, N) = \frac{1}{(2\pi i)^2} \int d\beta d\alpha e^{\phi + \beta E - \alpha N}, \tag{6}$$

l'intégrale sur α et β étant prise sur des parallèles à l'axe des imaginaires, d'abscisses α_0 et β_0.

Le calcul de cette intégrale par la méthode du col permet de déduire de ϕ la densité des niveaux. Les valeurs de α et β au col sont déterminées par les équations

$$\frac{\partial \phi}{\partial \alpha} = N, \tag{7a}$$

$$\frac{\partial \phi}{\partial \beta} = -E. \tag{7b}$$

Une expression approchée pour ρ s'en déduit en prenant α_0 et β_0 au col, et en développant au voisinage de α_0 et β_0:

$$\rho(E,N) \approx \frac{1}{2\pi}\frac{e^S}{\sqrt{D}}, \qquad S \equiv [\phi+\beta E-\alpha N]_{col},$$
$$D \equiv \begin{vmatrix} \phi''_{\alpha^2} & \phi''_{\alpha\beta} \\ \phi''_{\beta\alpha} & \phi''_{\beta^2} \end{vmatrix}_{col}, \tag{8}$$

les quantités S et D étant prises pour les valeurs de α et β tirées des équations (7).

Nombre de niveaux

De la même façon, on peut tirer de ϕ l'intégrale de ρ, c'est-à-dire le nombre $\nu(E,N)$ ou $\nu'(E,N)$ de niveaux d'énergie inférieure à E, ou supérieure à E:

$$\nu'(E,N) = \nu(+\infty,N)-\nu(E,N);$$

comme

$$\frac{\partial \nu}{\partial E}(E,N) = \rho(E,N),$$

on a

$$\nu(E,N) = \frac{1}{(2\pi i)^2}\int d\beta d\alpha \frac{e^{\phi+\beta E-\alpha N}}{\beta} \quad \text{pour} \quad \beta_0 > 0,$$
$$\nu'(E,N) = \frac{1}{(2\pi i)^2}\int d\beta d\alpha \frac{e^{\phi+\beta E-\alpha N}}{-\beta} \quad \text{pour} \quad \beta_0 < 0. \tag{9}$$

L'application de la méthode du col pour ν ou ν' conduit aux nouvelles équations

$$\frac{\partial \phi}{\partial \alpha} = N, \tag{10a}$$

$$\frac{\partial \phi}{\partial \beta} - \frac{1}{\beta} = -E. \tag{10b}$$

Pour une racine β_0 positive de ces équations, on peut calculer

$$\nu(E,N) \approx \frac{1}{2\pi}\frac{e^S}{|\beta_0|\sqrt{D_1}},$$
$$D_1 \equiv \begin{vmatrix} \phi''_{\alpha^2} & \phi''_{\alpha\beta} \\ \phi''_{\beta\alpha} & \phi''_{\beta^2}+\dfrac{1}{\beta^2} \end{vmatrix}_{col}. \tag{11}$$

Pour une racine β_0 négative, on obtient $\nu'(E,N)$ par la même formule.

Résolution des équations du col

Si on considère β et N comme variables indépendantes, l'équation (7a) ou (10a), $N = \partial\phi/\partial\alpha$, détermine α au col comme fonction de β et de N; les équations (7b) ou (10b) donnent, après remplacement de α par l'expression obtenue, l'énergie E en fonction de β et de N; de même les équations (8) et

(11) donnent ρ ou ν en fonction de β et de N. Les diverses fonctions de β et de N. qui s'introduisent ainsi ne sont pas indépendantes; elles sont liées par les relations remarquables suivantes (analogues à celles qui s'introduisent en thermodynamique):

$$\frac{\partial S}{\partial \beta} = \beta \frac{\partial E}{\partial \beta} \qquad \text{(calcul de } \rho\text{)}, \qquad (12a)$$

$$\frac{\partial S}{\partial \beta} = \beta \frac{\partial E}{\partial \beta} + \frac{1}{\beta} \qquad \text{(calcul de } \nu\text{)}; \qquad (12b)$$

$$\frac{\partial S}{\partial N} = \beta \frac{\partial E}{\partial N} - \alpha, \qquad (13)$$

$$\frac{\partial \alpha}{\partial \beta} = \frac{\partial E}{\partial N}; \qquad (14)$$

$$D = -\frac{\partial E}{\partial \beta} \Big/ \frac{\partial \alpha}{\partial N} \qquad \text{(calcul de } \rho\text{)}, \qquad (15a)$$

$$D_1 = -\frac{\partial E}{\partial \beta} \Big/ \frac{\partial \alpha}{\partial N} \qquad \text{(calcul de } \nu\text{)}. \qquad (15b)$$

Ces relations facilitent la résolution des équations du col. En effet, au lieu de tirer des équations du col (7) ou (10) α et β en fonction de E et N, puis de reporter dans les expressions (8) ou (11) pour avoir la densité des niveaux en fonction de E pour N fixé, il est plus commode d'éliminer seulement α. Les courbes de densités de niveaux en fonction de l'énergie, pour N fixé, sont alors données par leur représentation paramétrique de paramètre β, et on peut s'aider des relations (12) à (15) pour éliminer α.

3.2. CALCUL DE LA GRANDE FONCTION DE PARTITION PAR LA MÉTHODE DES PERTURBATIONS [4])

Dans le formalisme de la seconde quantification, la grande fonction de partition s'écrit, en introduisant un champ self-consistant H_0,

$$Z(\alpha, \beta) = \mathrm{tr}\, \mathrm{e}^{-\beta H_0 - \beta(V - H_0) + \alpha N}, \qquad (16)$$

où

$$N = \sum_i \xi_i^+ \xi_i,$$
$$V = \tfrac{1}{4} \sum_{ijkl} \langle ij|V|kl\rangle \xi_i^+ \xi_j^+ \xi_k \xi_l; \qquad (17a)$$

ξ_i^+ est l'opérateur de création dans l'état $|i\rangle$ à une particule, caractérisé par les projections m_i, s_i, t_i du moment orbital, du spin et du spin isobarique; $|ij\rangle$ désigne l'état antisymétrisé à deux particules dans les états i et j, de bra conjugué $\langle ji|$. L'élément de matrice vaut

$$\langle ij|V|kl\rangle = \sum \langle llm_j m_i|LM\rangle\langle llm_k m_l|LM\rangle V_L[\delta_{s_j s_k}\delta_{s_i s_l}\delta_{t_j t_k}\delta_{t_i t_l} - (-)^L \delta_{s_i s_k}\delta_{s_j s_l}\delta_{t_i t_k}\delta_{t_j t_l}] \quad (17b)$$

$$= \sum_{\substack{LM \\ SM^S \\ TM^T}} \langle llm_j m_i|LM\rangle\langle llm_k m_l|LM\rangle\langle \tfrac{1}{2}\tfrac{1}{2} s_j s_i|SM^S\rangle\langle \tfrac{1}{2}\tfrac{1}{2} s_k s_l|SM^S\rangle$$

$$\langle \tfrac{1}{2}\tfrac{1}{2} t_j t_i|TM^T\rangle\langle \tfrac{1}{2}\tfrac{1}{2} t_k t_l|TM^T\rangle[1-(-)^{L+S+T}]V_L. \quad (17c)$$

Etant donné la symétrie du problème, le champ self-consistant H_0 est simplement proportionnel à N:

$$H_0 = N\mathscr{E}.$$

La méthode des perturbations conduit au développement

$$\phi = \log Z = \sum_i \log\,(1+e^{\alpha-\beta\mathscr{E}}) + \sum_{p=1}^{\infty} (-)^p \frac{\beta^p}{p!}\langle (V-H_0)^p\rangle_c, \quad (18)$$

le dernier terme étant à prendre sur tous les diagrammes connexes d'ordre p. On tracera les diagrammes à la Hugenholtz; chaque interaction est alors représentée soit par $\langle ij|V|kl\rangle$, soit par $-\mathscr{E}$, et il faut attribuer le poids $\frac{1}{2}$ à chaque double ligne. Aux lignes descendantes et montantes sont attachés les facteurs

$$f_- = \frac{1}{1+e^{-\alpha+\beta\mathscr{E}}}, \qquad f_+ = \frac{1}{1+e^{\alpha-\beta\mathscr{E}}}. \quad (19)$$

Ces facteurs étant indépendants de l'indice de ligne, car tous les états non perturbés ont même énergie $\mathscr{E}$, les sommations sur les états ne portent que sur les éléments de matrice et se font indépendamment de l'ordre des vertex dans le temps.

En raison des propriétés de conservation de V, l'état correspondant à la ligne entrante est le même que celui de la ligne sortante pour une partie irréductible de diagramme. On peut effectuer les sommations d'éléments de matrice correspondant à certaines de ces parties diagonales.

Pour une sous-échelle d'ordre n (fig. 1a), compte non tenu du signe et des facteurs $\frac{1}{2}$ des doubles lignes, on pose

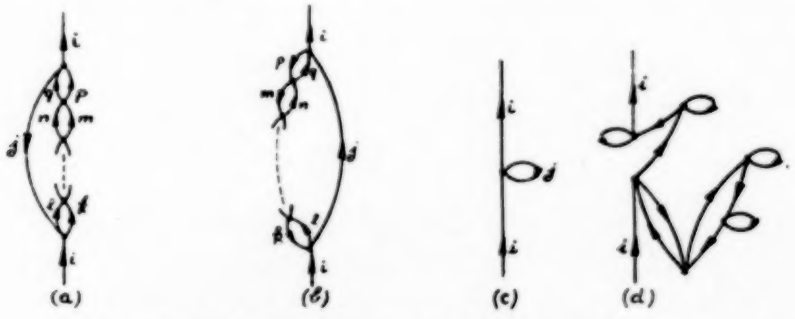

Fig. 1. Exemples de parties diagonales:

a) Sous-échelle
b) Polarisation
c) Une boucle passive
d) Plusieurs boucles passives.

$$2^{n-1}e_n = \sum_{\substack{j\\ kl\\ \vdots\\ mn\\ pq}} \langle ji|V|pq\rangle\langle qp|V|mn\rangle \ldots \langle lk|V|ij\rangle$$
$$= 2^{n-1}\sum_j \langle ji|V^n|ij\rangle = \frac{2^{n+1}}{\mathcal{N}} \sum_L [4-(-)^L](2L+1)V_L{}^n. \tag{20}$$

Pour une partie diagonale de type polarisation d'ordre n (fig. 1b), on pose

$$p_n = \sum_{\substack{j\\ kl\\ \vdots\\ mn\\ pq}} \langle pi|V|jq\rangle\langle mq|V|pn\rangle \ldots \langle jl|V|ki\rangle$$
$$= \sum_\lambda \left(\frac{2\lambda+1}{\mathcal{N}}\right)\left\{\left[\sum_L [4-(-)^L](2L+1)\begin{Bmatrix} l & l & \lambda \\ l & l & L\end{Bmatrix} V_L\right]^n + 15\left[-\sum_L (2L+1)\begin{Bmatrix} l & l & \lambda \\ l & l & L\end{Bmatrix} V_L\right]^n\right\}.$$

Dans ce calcul, on a transformé chaque élément de matrice écrit sous la forme (17c) à l'aide de la relation

$$\sum_M \langle jjm_1m_2|JM\rangle\langle jjm_3m_4|JM\rangle$$
$$= (-)^J(2J+1)\sum_{\lambda\mu}(-)^{m_3+m_3}\begin{Bmatrix} j & j & \lambda \\ j & j & L\end{Bmatrix}\langle jj-m_3m_1|\lambda\mu\rangle\langle jj-m_2m_4|\lambda\mu\rangle.$$

On a utilisé les relations d'orthogonalité des coefficients de Clebsch-Gordan, et on a effectué les sommations sur les variables de spin grâce aux formules de sommation sur les coefficients de Racah.

En particulier, une boucle passive (fig. 1c) donne la contribution $e_1 = -p_1$, et une partie diagonale formée de n boucles passives (fig. 1d) donne $e_1{}^n$, quelle que soit la disposition de ces boucles.

Si on prend un champ self-consistant au premier ordre, les boucles passives et les interactions $-\mathscr{E}$ s'éliminent, à condition de prendre

$$\langle i'|H_0|i\rangle = \sum_j \langle i'j|V|ji\rangle f_-,$$

soit

$$H_0 = e_1 f_- N, \qquad \mathscr{E} = e_1 f_-. \tag{22}$$

Le facteur f_- est donc donné par l'équation

$$f_- = \frac{1}{1+e^{-\alpha+\beta e_1 f_-}}, \tag{23}$$

qui admet une solution unique pour $\beta e_1 > -4$.

On doit alors prendre pour ϕ tous les diagrammes connexes sans boucle passive ni interaction H_0, sauf en ce qui concerne les diagrammes d'ordre 1, qui ne s'éliminent pas, à cause du facteur $\frac{1}{2}$ de la double ligne.

Le calcul a été poussé jusqu'à l'ordre 4; on décompose chaque diagramme en parties diagonales du type précédent; la sommation sur l'indice de la

ligne traversant les parties diagonales donne un facteur $\mathcal{N}$. Il reste ensuite à dénombrer les diagrammes différant entre eux par l'ordre des vertex, en associant à chacun d'eux le poids dû aux doubles lignes, le signe et le produit des facteurs f_+ ou f_-.

On trouve ainsi les contributions suivantes à $\phi/\mathcal{N}$ (fig. 2):

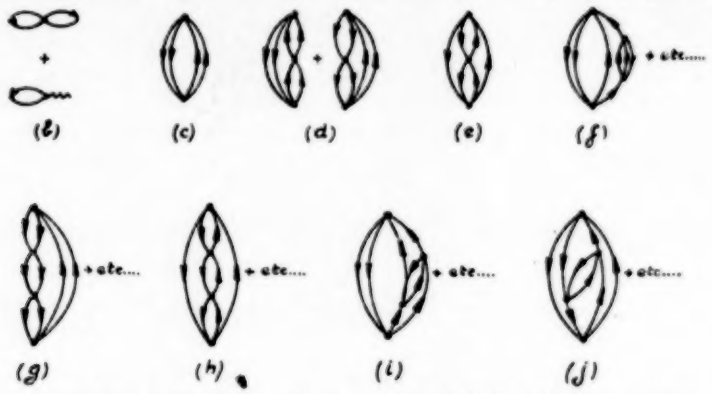

Fig. 2. Les diagrammes contribuant à l'expression (24) de ϕ (avec champ self-consistant)
(b) ordre 1
(c) ordre 2
(d) et (g) échelles d'ordre 3 et 4
(e) et (h) polarisation d'ordre 3 et 4
(f) ordre 4: deux sous-échelles d'ordre 2
(i) et (j) les autres diagrammes d'ordre 4.

$$\textit{ordre } 0: \quad -\log f_+, \tag{24a}$$

$$\textit{ordre } 1: \quad -\tfrac{1}{2}\beta e_1 f_-^{\,2}+\beta e_1 f_-^{\,2}, \tag{24b}$$

$$\textit{ordre } 2: \quad \tfrac{1}{4}\beta^2 e_2 f_-^{\,2} f_+^{\,2}, \tag{24c}$$

$$\textit{ordre } 3: \quad -\tfrac{1}{12}\beta^3 e_3 f_-^{\,2} f_+^{\,2}(f_-^{\,2}+f_+^{\,2}) \tag{24d}$$

$$-\tfrac{1}{6}\beta^3 p_3 f_-^{\,3} f_+^{\,3}, \tag{24e}$$

$$\textit{ordre } 4: \quad \tfrac{1}{12}\beta^4 e_2^{\,2} f_-^{\,3} f_+^{\,3}[f_-^{\,2}-4f_- f_+ + f_+^{\,2}] \tag{24f}$$

$$+\tfrac{1}{48}\beta^4 e_4 f_-^{\,2} f_+^{\,2}[f_-^{\,4}+4f_-^{\,2} f_+^{\,2}+f_+^{\,4}] \tag{24g}$$

$$+\tfrac{1}{8}\beta^4 p_4 f_-^{\,4} f_+^{\,4} \tag{24h}$$

$$+\tfrac{1}{6}\beta^4 q f_-^{\,3} f_+^{\,3}[f_-^{\,2}-f_- f_+ + f_+^{\,2}] \tag{24i}$$

$$+\tfrac{1}{24}\beta^4 r f_-^{\,3} f_+^{\,3}[f_-^{\,2}-4f_- f_+ + f_+^{\,2}]. \tag{24j}$$

Dans les deux derniers types de diagrammes la sommation sur les éléments de matrice de V introduit deux coefficients nouveaux q et r, qui se calculent exactement comme les coefficients e_n et p_n. On trouve

$$q = \frac{1}{2l+1}\sum_{L_1 L_2 L_3} (2L_1+1)(2L_2+1)(2L_3+1)[4-(-)^{L_1+L_2+L_3}][4-(-)^{L_1}-(-)^{L_2}-(-)^{L_3}]$$
$$\times \begin{Bmatrix} L_1 l & l \\ l & L_2 l \\ l & l & L_3 \end{Bmatrix} V_{L_1} V_{L_2} V_{L_3}^2, \tag{25}$$

expression qui ne diffère de p_3 que par le remplacement de V_{L_3} par $V_{L_3}^2$, et

$$r = \frac{1}{2l+1} \sum_{LL'L''L'''\lambda} (2L+1)(2L'+1)(2L''+1)(2L'''+1)(2\lambda+1) \begin{Bmatrix} ll\lambda \\ ll \end{Bmatrix} \begin{Bmatrix} ll\lambda \\ ll'' \end{Bmatrix} \begin{Bmatrix} L'L''\lambda \\ l\ l\ l \end{Bmatrix}$$
$$\{(4-(-)^L)(4-(-)^{L'})(1+(-)^{L+L'''})(1+(-)^{L'+L''})-15(-)^{L'+L''}\} V_L V_{L'} V_{L''} V_{L'''}. \quad (26)$$

Si on n'introduit pas de champ self-consistant on a simplement

$$f_- = \frac{1}{1+e^{-\alpha}}, \qquad f_+ = \frac{1}{1+e^{\alpha}}. \quad (27)$$

Mais il faut prendre pour ϕ tous les diagrammes connexes, qui s'obtiennent en ajoutant de toutes les manières possibles des boucles passives aux diagrammes précédemment introduits.

Le résultat peut s'écrire immédiatement en remarquant que, dans ce cas particulier, le développement en puissances de la perturbation est un développement en puissances de β. On aura donc les contributions de tous les diagrammes jusqu'à l'ordre 4 en développant en série l'expression (24) jusqu'à l'ordre 4 en β. Les deux premiers termes de cette expression fournissent les contributions des diagrammes constitués uniquement de boucles passives. On trouve (à l'ordre 3) l'expression suivante:

$$\begin{aligned} \frac{\phi}{\mathcal{N}} = &- \log f_+ - \tfrac{1}{2}\beta e_1 f_-^2 + \tfrac{1}{4}\beta^2 e_2 f_-^2 f_+^2 + \tfrac{1}{2}\beta^2 e_1^2 f_-^3 f_+ \\ &- \tfrac{1}{12}\beta^3 e_3 f_-^2 f_+^2 (f_+^2 + f_-^2) - \tfrac{1}{6}\beta^3 p_3 f_-^3 f_+^3 \\ &+ \tfrac{1}{6}\beta^3 e_1^3 (f_-^5 f_+ - 4 f_-^4 f_+^2) + \tfrac{1}{2}\beta^3 e_1 e_2 (f_-^4 f_+^2 - f_-^3 f_+^3) + \dots \end{aligned} \quad (28)$$

3.3. CALCUL DE LA DENSITÉ DE NIVEAUX

Dans la résolution des équations du col, en partant de l'expression de ϕ avec champ self-consistant, on utilise les relations

$$\begin{aligned} \frac{\partial f_-}{\partial \alpha} = -\frac{\partial f_+}{\partial \alpha} = \frac{f_+ f_-}{1+\beta e_1 f_+ f_-}, \\ \frac{\partial f_-}{\partial \beta} = -\frac{\partial f_+}{\partial \beta} = -e_1 f_- \frac{\partial f_-}{\partial \alpha}. \end{aligned} \quad (29)$$

On désigne par $A = N/\mathcal{N}$ le nombre relatif de particules dans la couche, et par $T = (\mathcal{N}-N)/\mathcal{N} = 1-A$ nombre relatif de trous dans la couche. Les expressions E, S et D sont calculées par des développements en puissances des βV_L, limités au même ordre que celui qui provient de la méthode des perturbations pour ϕ. On obtient ainsi les mêmes résultats que si on avait utilisé l'expression (28) poussée jusqu'à l'ordre 4, mais avec moins de calculs, l'introduction du champ self-consistant à l'ordre 1 étant bien adaptée à la symétrie trous-particules du problème.

Les équations du col s'écrivent

$$A = f_- + \frac{(f_+ - f_-)}{1+\beta e_1 f_+ f_-}\left[\tfrac{1}{2}\beta^2 e_2 f_+^2 f_-^2 - \tfrac{1}{6}\beta^3 e_3 f_+^2 f_-^2 (f_+^2 - f_+ f_- + f_-^2) - \tfrac{1}{2}\beta^3 p_3 f_+^3 f_-^3 + \ldots\right],$$
$$\frac{E}{\mathcal{N}} = \frac{e_1 f_-}{\mathcal{N}}\frac{\partial \phi}{\partial \alpha} - \tfrac{1}{2} e_1 f_-^2 - \tfrac{1}{2}\beta e_2 f_+^2 f_-^2 + \tfrac{1}{4}\beta^2 e_3 f_+^2 f_-^2 (f_+^2 + f_-^2) + \tfrac{1}{2}\beta^2 p_3 f_+^3 f_-^3 + \ldots \quad (30)$$

La résolution donne (ces résultats sont encore valables si l'on ne suppose pas $\beta e_1 AT$ petit devant l'unité)

$$\alpha = \log\frac{A}{T} + \beta e_1 A - \tfrac{1}{2}\beta^2 e_2 AT(T-A) + \beta^3\left[\tfrac{1}{6} e_3 AT(T-A)(A^2 - AT_+ T^2) + \tfrac{1}{2} p_3 A^2 T^2 (T-A)\right] + \ldots; \quad (31a)$$

$$E = \tfrac{1}{2}\mathcal{N} e_1 A^2 - \beta\mathcal{P} + \tfrac{1}{2}\beta^2 \mathcal{Q} - \tfrac{1}{3}\beta^3(\mathcal{R} - \tfrac{1}{2}\mathcal{N} e_2^2 A^3 T^3) + \ldots \quad \text{(calcul de } \rho\text{)}, \quad (31b)$$

$$E = \frac{1}{\beta} + \tfrac{1}{2}\mathcal{N} e_1 A^2 - \beta\mathcal{P} + \tfrac{1}{2}\beta^2 \mathcal{Q} - \tfrac{1}{3}\beta^3(\mathcal{R} - \tfrac{1}{2}\mathcal{N} e_2^2 A^3 T^3) + \ldots \quad \text{(calcul de } \nu \text{ ou } \nu'\text{)}; \quad (31c)$$

où on a posé

$$\begin{aligned}
\mathcal{P} &= \tfrac{1}{2}\mathcal{N} e_2 A^2 T^2, \\
\mathcal{Q} &= \mathcal{N} A^2 T^2\left[\tfrac{1}{2} e^3 (A^2 + T^2) + p_3 AT\right], \\
\mathcal{R} &= \mathcal{N} A^2 T^2\left[\tfrac{1}{4} e_4 (A^4 + 4A^2 T^2 + T^4) + \tfrac{3}{2} p_4 A^2 T^2 + 2qAT(A^2 - AT + T^2) + \tfrac{1}{2} r AT(A^2 - 4AT + T^2)\right].
\end{aligned} \quad (31d)$$

On tire de ces expressions ρ et ν par

$$S \equiv \phi + \beta E - \alpha N = \log\frac{\mathcal{N}^{\mathcal{N}}}{N^N (\mathcal{N}-N)^{\mathcal{N}-N}} - \tfrac{1}{2}\beta^2 \mathcal{P} + \tfrac{1}{3}\beta^3 \mathcal{Q} - \tfrac{1}{4}\beta^4(\mathcal{R} - \tfrac{1}{2}\mathcal{N} e_2^2 A^3 T^3) + \ldots \quad (32)$$

$$D = -\frac{\partial E}{\partial \beta} \Big/ \frac{\partial \alpha}{\partial N}, \quad (33a)$$

$$\frac{\partial \alpha}{\partial N} = \frac{1}{\mathcal{N} AT}\left[1 + \beta e_1 AT - \tfrac{1}{2}\beta^2 e_2 AT(A^2 - 4AT + T^2) + \ldots\right]; \quad (33b)$$

$$-\frac{\partial E}{\partial \beta} = \mathcal{P} - \beta\mathcal{Q} + \beta^2(\mathcal{R} - \tfrac{1}{2}\mathcal{N} e_2^2 A^3 T^3) + \ldots \quad \text{(calcul de } \rho\text{)}, \quad (33c)$$

$$-\frac{\partial E}{\partial \beta} = \frac{1}{\beta^2} + \mathcal{P} - \beta\mathcal{Q} + \beta^2(\mathcal{R} - \tfrac{1}{2}\mathcal{N} e_2^2 A^3 T^3) + \ldots \quad \text{(calcul de } \nu\text{)}. \quad (33d)$$

Dans le calcul de ρ, l'énergie E (donnée par la formule (31b)) est une fonction monotone de β pour β assez petit. Dans le calcul de ν ou ν', l'énergie est donnée par la formule (31c); à chaque valeur de E correspondent deux

valeurs de β de signes contraires (fig. 3) dont l'une fournit $\nu(E,N)$ et l'autre $\nu'(E,N)$.

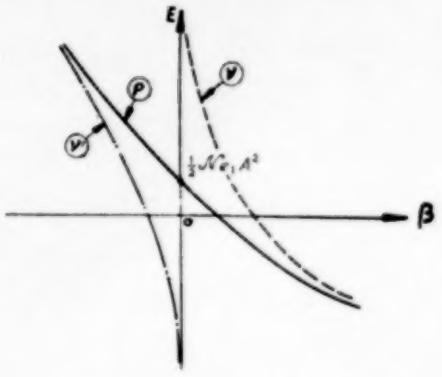

Fig. 3. Variation de E en fonction de β, dans le calcul (par la méthode du col) de ρ, de ν et de ν'.

3.4. DENSITÉ DE NIVEAUX AYANT UN MOMENT ANGULAIRE DONNÉ

D'une manière analogue, on introduit

$$\mathscr{Z}(\alpha,\beta,\mu) = \operatorname{tr} e^{-\beta H+\alpha N+\mu M}, \tag{34}$$

où M est le moment angulaire orbital total du niveau.

La méthode des perturbations donne (sans introduction d'un potentiel self-consistant)

$$\Phi = \log \mathscr{Z}(\alpha,\beta,\mu) = \sum_i \log(1+e^{\alpha+\mu m_i}) + \sum_{p=1}^{\infty} (-)^p \frac{\beta^p}{p!} \langle V^p \rangle_c \tag{35}$$

et les facteurs attachés aux lignes dépendent maintenant de l'indice de la ligne. En conservant les notations (27), on a

$$\begin{aligned} f_-^{\,i} &= \frac{1}{1+e^{-\alpha-\mu m_i}} = f_- + f_+ f_- \mu m_i - f_+ f_- (f_- - f_+) \tfrac{1}{2}\mu^2 m_i^{\,2} + \ldots, \\ f_+^{\,i} &= \frac{1}{1+e^{\alpha+\mu m_i}} = f_+ - f_+ f_- \mu m_i + f_+ f_- (f_- - f_+) \tfrac{1}{2}\mu^2 m_i^{\,2} + \ldots. \end{aligned} \tag{36}$$

En se limitant aux termes en μ^2, on trouve pour Φ le développement

$$\begin{aligned} \frac{\Phi}{\mathscr{N}} &= -\log f_+ + \tfrac{1}{2}\mu^2 \tfrac{1}{3} l(l+1) f_+ f_- \\ &- \tfrac{1}{2}\beta e_1 f_-^{\,2} + \tfrac{1}{2}\mu^2 \tfrac{1}{3} l(l+1) \tfrac{1}{2}\beta f_-^{\,2} f_+ (2e_1 f_- - g_1 f_+) \\ &+ \tfrac{1}{4}\beta^2 e_2 f_+^{\,2} f_-^{\,2} + \tfrac{1}{2}\mu^2 \tfrac{1}{3} l(l+1) \tfrac{1}{4}\beta^2 f_+^{\,2} f_-^{\,2} [(f_+ - f_-)^2 g_2 - 4 f_+ f_- e_2] \\ &+ \tfrac{1}{2}\beta^2 e_1^{\,2} f_-^{\,3} f_+ + \tfrac{1}{2}\mu^2 \tfrac{1}{3} l(l+1) \tfrac{1}{2}\beta^2 f_-^{\,3} f_+ [(f_+ - f_-)^2 e_1^{\,2} - 2 f_+ f_- e_1 g_1 + \tfrac{1}{2} f_+^{\,2} g_1^{\,2}] + \ldots. \end{aligned} \tag{37}$$

On a posé

$$\sum_{ij} \langle ij|V|ji\rangle (m_i+m_j)^2 = \mathscr{N} \tfrac{1}{3} l(l+1) g_1 = \tfrac{4}{3} \sum_L [4-(-)^L](2L+1)L(L+1)V_L, \tag{38a}$$

$$\sum_{ijkl} \langle ij|V|lk\rangle\langle kl|V|ji\rangle(m_i+m_j)^2 = 2\mathcal{N}\tfrac{1}{3}l(l+1)g_2 = \tfrac{8}{3}\sum_L [4-(-)^L](2L+1)L(L+1)V_L{}^2. \quad (38b)$$

Les équations du col sont maintenant

$$N = \frac{\partial\Phi}{\partial\alpha}, \quad (39a)$$

$$M = \frac{\partial\Phi}{\partial\mu}, \quad (39b)$$

$$E = -\frac{\partial\Phi}{\partial\beta}, \quad (39c)$$

que l'on résoud en fonction de β, N et M, par des développements limités:

$$\mu = \frac{3M}{l(l+1)\mathcal{N}AT}(1-\beta(e_1-\tfrac{1}{2}g_1)AT+\ldots), \quad (40a)$$

$$\frac{1}{1+e^{-\alpha}} = A(1+\beta e_1 AT+\tfrac{1}{2}\beta^2A^2T(T-A)e_1{}^2-\tfrac{1}{2}\beta^2\tfrac{1}{2}AT^2(T-A)e_2+\ldots) - \frac{3M^2}{2l(l+1)}\frac{(T-A)}{\mathcal{N}^2AT}[1+\beta e_1A(T-A)+\ldots]+\ldots, \quad (40b)$$

$$E = \mathcal{N}\tfrac{1}{2}e_1A^2-\beta\mathcal{P}+\ldots - \frac{3M^2}{2l(l+1)\mathcal{N}}[(e_1-\tfrac{1}{2}g_1)+\beta(T-A)^2\tfrac{1}{2}g_2-\beta(A^2+T^2)e_2\ldots]. \quad (40c)$$

La densité de niveaux ayant une valeur de M fixée, est donnée par la formule du col:

$$\rho \approx \frac{1}{(2\pi)^{\frac{3}{2}}} e^{\phi+\beta E-\alpha N-\mu M} \begin{vmatrix} \Phi''_{\mu^2} & \Phi''_{\mu\alpha} & \Phi''_{\mu\beta} \\ \Phi''_{\alpha\mu} & \Phi''_{\alpha^2} & \Phi''_{\alpha\beta} \\ \Phi''_{\beta\mu} & \Phi''_{\beta\alpha} & \Phi''_{\beta^2} \end{vmatrix}_{\text{col}}^{-\frac{1}{2}} \quad (41a)$$

qui fournit, à l'ordre le plus bas en β et en M,

$$\rho(E,N,M) \approx \frac{\mathcal{N}^{\mathcal{N}+\frac{1}{2}}\exp\left\{-\frac{3M^2}{2l(l+1)\mathcal{N}AT}-\frac{1}{2\mathcal{P}}\left[E-\tfrac{1}{2}\mathcal{N}e_1A^2+\frac{3M^2}{2l(l+1)\mathcal{N}}(e_1-\tfrac{1}{2}g_1)\right]^2\right\}}{N^{N+\frac{1}{2}}(\mathcal{N}-N)^{\mathcal{N}-N+\frac{1}{2}}(2\pi)^{\frac{3}{2}}\sqrt{\tfrac{1}{3}\mathcal{P}\mathcal{N}l(l+1)AT}}. \quad (41b)$$

La densité de niveaux ayant un L donné est alors

$$\rho(E,N,L) \approx -\frac{\partial}{\partial M}\rho(E,N,M=L+\tfrac{1}{2}) \approx (L+\tfrac{1}{2})\frac{\mathcal{N}^{\mathcal{N}+\frac{1}{2}}\exp\left\{-\frac{3L(L+1)}{2l(l+1)\mathcal{N}AT}-\frac{1}{2\mathcal{P}}\left[E-\tfrac{1}{2}\mathcal{N}e_1A^2+\frac{3L(L+1)}{2l(l+1)\mathcal{N}}(e_1-\tfrac{1}{2}g_1)\right]^2\right\}}{N^{N+\frac{1}{2}}(\mathcal{N}-N)^{\mathcal{N}-N+\frac{1}{2}}(2\pi)^{\frac{3}{2}}\sqrt{\mathcal{P}}(\tfrac{1}{3}\mathcal{N}l(l+1)AT)^{\frac{3}{2}}}. \quad (41c)$$

4. Comparaison des Résultats et Discussion

La méthode approchée introduit trois types d'erreurs: celles qui proviennent de la méthode du col, de la méthode des perturbations et de la résolution des équations par des développements limités à l'ordre correspondant.

4.1. SYMÉTRIE TROUS-PARTICULES

Les expressions de $\rho(N, \beta)$ ou de $\nu(N, \beta)$ sont symétriques dans l'échange de A et T; le seul terme dissymétrique est le terme $\frac{1}{2}\mathcal{N} e_1 A^2$ dans l'expression (31) de l'énergie. Ce résultat est d'ailleurs valable à tous les ordres, le seul diagramme dissymétrique en f_+ et f_- étant celui d'ordre 1.

La densité de niveaux approchée pour $\mathcal{N}-N$ particules se déduit donc simplement de celle pour N particules par la translation

$$\frac{e_1}{2\mathcal{N}}[(\mathcal{N}-N)^2-N^2] = e_1(\tfrac{1}{2}\mathcal{N}-N).$$

Ce résultat étant le même que celui de la théorie exacte (formule (4)). il suffit donc d'effectuer la comparaison des résultats pour $N \leqq 6$.

4.2. INFLUENCE DU NOMBRE DE PARTICULES

Les comparaisons ont été effectuées pour un nombre N de particules compris entre 2 et 6, pour ρ ou ν, pour diverses valeurs des paramètres V_0, V_1, V_2 et à divers ordres de la méthode des perturbations. Dans tous les cas la précision de la méthode statistique et la convergence des développements est indépendante de N, même si ce nombre est petit (fig. 4). D'ailleurs le succès de la méthode du col est lié à la grandeur de $\mathcal{N}$ et non de N, et d'autre part $N/\mathcal{N}$ n'est jamais assez petit pour que la contribution des échelles soit prépondérante dans la méthode des perturbations. On peut donc appliquer les méthodes statistiques même pour un nombre de particules faible.

4.3. DENSITÉS À L'ORDRE 2: RÉSULTATS GLOBAUX

Si on se limite dans S et D à l'ordre le plus bas correspondant à ϕ arrêté à l'ordre 2, on a pour ρ la gaussienne

$$\rho(E, N) = \frac{\mathcal{N}^{\mathcal{N}+\frac{1}{2}}}{\sqrt{2\pi}\, N^{N+\frac{1}{2}}(\mathcal{N}-N)^{\mathcal{N}-N+\frac{1}{2}}} \frac{e^{-(E-\frac{1}{2}\mathcal{N}e_1A^2)^2}}{\sqrt{2\pi\mathcal{P}}} \tag{42}$$

Nombre total de niveaux

L'intégration de ρ sur toutes les valeurs de E donne

$$\frac{\mathcal{N}^{\mathcal{N}+\frac{1}{2}}}{\sqrt{2\pi}\, N^{N+\frac{1}{2}}(\mathcal{N}-N)^{\mathcal{N}-N+\frac{1}{2}}},$$

qui n'est autre que l'approximation de Stirling pour le nombre exact de

niveaux à N particules $\mathcal{N}!/N!(\mathcal{N}-N)!$. Ceci est dû au fait que la méthode du col s'applique indépendamment sur α et sur β, que celle qui porte sur β n'introduit pas d'erreur (ϕ est du second degré en β) et que celle sur α ne dépend que du terme d'ordre zéro de ϕ, et se réduit à l'approximation de

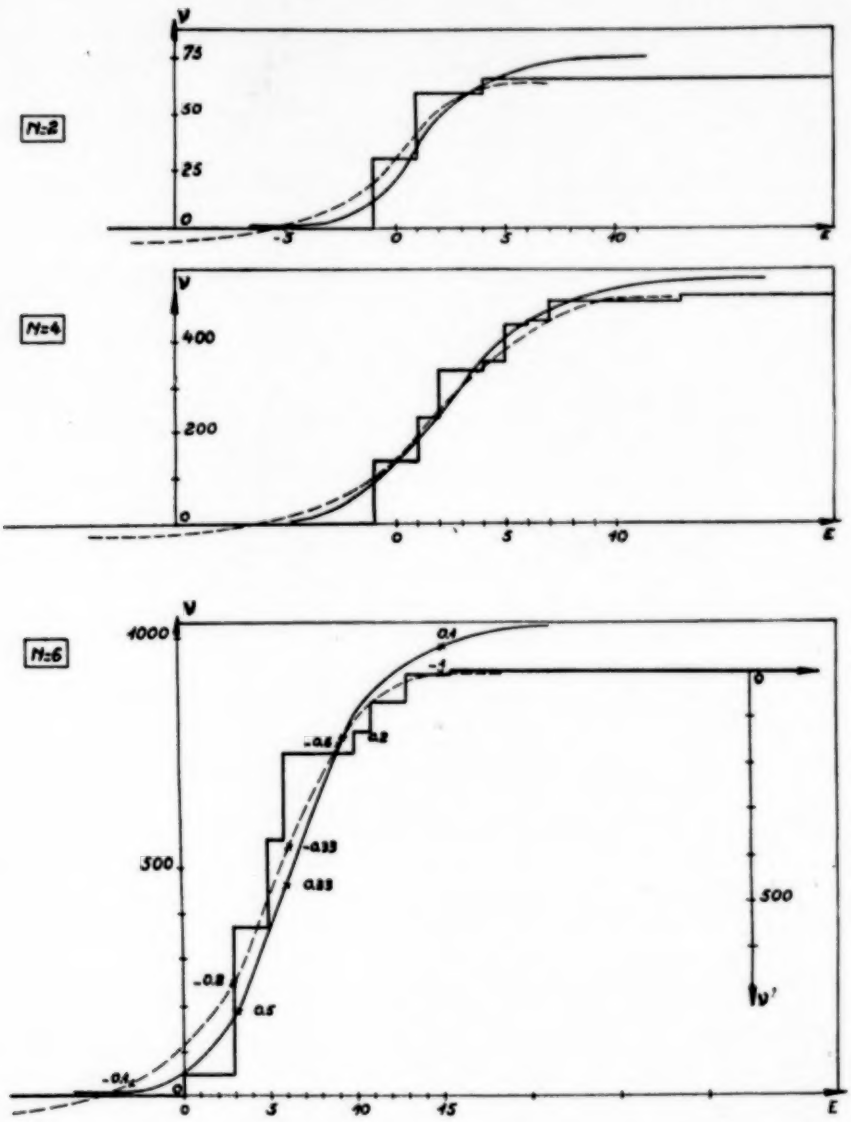

Fig. 4. Courbes de ν et ν' pour diverses valeurs de N (force de Wigner $\mathcal{K} = 1$, $\mathcal{L} = 2$; ϕ arrêté à l'ordre 2 avec champ self-consistant). La courbe en escalier représente l'intégrale exacte de la densité de niveaux, la courbe en trait plein $\nu(E)$; en ce qui concerne $\nu'(E)$, on a facilité la comparaison en portant (en pointillé) en ordonnées la différence entre le nombre total exact de niveaux et $\nu'(E)$. On a inscrit en quelques points les valeurs de β correspondantes.

Stirling. Des erreurs supplémentaires s'introduisent si l'on prend à la place du premier terme de D le développement de $\partial\alpha/\partial N$, ou si l'on pousse à un ordre plus élevé dans la perturbation, car ϕ n'est alors plus quadratique en β.

Centre de la distribution

Le centre de la gaussienne est le point

$$E = \tfrac{1}{2}\mathcal{N}e_1A^2 = \tfrac{1}{24}(V_0+5V_1+5V_2)N^2$$

alors que le centre de la distribution exacte des niveaux est

$$E = \tfrac{1}{24}(6V_1+6V_2)N(N-1).$$

Ces valeurs sont voisines à condition que le nombre de particules ne soit pas trop faible ($N \ll N^2$), et que V_0, V_1 et V_2 ne soient pas trop différents.

De la même façon, la position exacte des niveaux ayant un L donné est, dans le cas où $V_1 = \frac{1}{3}[2V_0+V_2]$,

$$E = \tfrac{1}{2}(V_1+V_2)\,\tfrac{1}{2}N(N-1)+\tfrac{1}{3}(V_0-V_2)[N-\tfrac{1}{2}L(L+1)],$$

alors que le centre de la gaussienne $\rho(E, N, L)$ (formule 41c) est le point

$$E = \tfrac{1}{2}\mathcal{N}e_1A^2 - \frac{3L(L+1)}{2l(l+1)\mathcal{N}}(e_1-\tfrac{1}{2}g_1) = \tfrac{1}{2}\mathcal{N}e_1A^2-\tfrac{1}{16}(2V_0+5V_1-5V_2)\tfrac{1}{2}L(\,L+1)$$
$$= \tfrac{1}{2}\mathcal{N}e_1A^2-\tfrac{1}{3}(V_0-\tfrac{5}{8}V_2)\,\tfrac{1}{2}L(L+1).$$

L'accord est grossièrement bon dans les mêmes conditions que pour $\rho(E, N)$. Il était évident, étant donné que l'on s'était limité aux termes en μ^2 dans ϕ, que l'on trouverait une dépendance en $\frac{1}{2}L(L+1)$, mais il est remarquable que le coefficient de ce terme soit indépendant de N.

Nombre de niveaux ayant un L donné

En intégrant $\rho(E, N, L)$ sur l'énergie, on trouve que le nombre total des niveaux ayant un L donné est égal, pour un N fixé, à

$$\frac{\mathcal{N}^{\mathcal{N}+\frac{1}{2}}}{\sqrt{2\pi}\,N^{N+\frac{1}{2}}(\mathcal{N}-N)^{\mathcal{N}-N+\frac{1}{2}}}(L+\tfrac{1}{2})\,\frac{\exp\left\{-\dfrac{3L(L+1)}{2l(l+1)\mathcal{N}AT}\right\}}{\sqrt{2\pi}\,[\frac{1}{3}l(l+1)\mathcal{N}AT]^{\frac{1}{2}}}.$$

On a porté (fig. 5) les valeurs exactes et les valeurs approchées du nombre total de niveaux ayant un L donné. L'accord est qualitativement bon: le facteur $(L+\frac{1}{2})$ correspond à la croissance de la dégénérescence pour L faible, le facteur exponentiel à la décroissance du nombre de niveaux de L élevé. La statistique donne donc de bons résultats, compte tenu de la faible valeur de L.

Étalement de la distribution

Pour les densités de niveaux $\rho(E, N)$ et $\rho(E, N, L)$, la largeur de la gaussienne est $\sqrt{\mathcal{P}}$. Ce résultat correspond assez mal au véritable étalement des niveaux. Par exemple, cette largeur $\sqrt{\mathcal{P}}$ n'est nulle que si $V_0 = V_1 = V_2 = 0$, alors que tous les niveaux sont confondus si $V_0 = V_1 = V_2$, et tous les niveaux ayant un L donné sont confondus si $V_1 = \frac{1}{3}[2V_0+V_2]$. Pour une force

de Wigner avec $\mathscr{K} = 1$ et $\mathscr{L}$ variable, $\sqrt{\mathscr{P}}$ varie alors que les niveaux ne subissent qu'une translation (dernière ligne du tableau 2); mais cette variation n'est pas considérable.

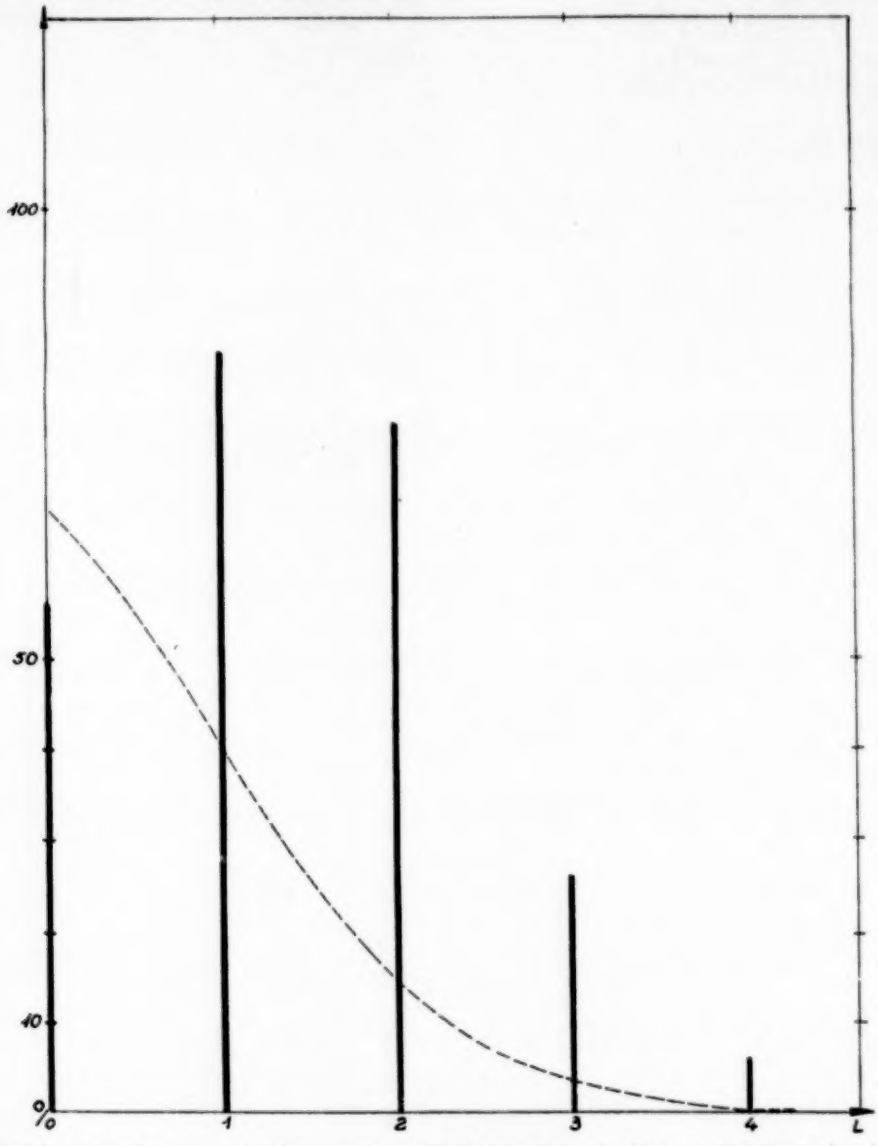

Fig. 5. Nombre de niveaux ayant une valeur de L donnée, pour $N = 6$. Les lignes représentent le nombre exact de niveaux (après division par le facteur $2L+1$), et la courbe en pointillé la valeur approchée.

Le fait de se limiter à une gaussienne donne donc un accord assez satisfaisant en ce qui concerne le centre de la distribution et le nombre total de niveaux; mais on n'obtient ni la dissymétrie de la véritable distribution ni l'étalement exact.

4.4. MÉTHODE DU COL SUR LE NOMBRE DE NIVEAUX

Il semble naturel que l'application de la méthode du col sur le nombre de niveaux ν, dont la courbe exacte est en escalier, donne de meilleurs

résultats que sur la densité de niveaux ρ, dont la courbe exacte est plus singulière. Pour faciliter la comparaison, on a intégré ρ calculé par la méthode du col. En partant de ϕ arrêté à l'ordre 2, et en prenant pour D le développe-

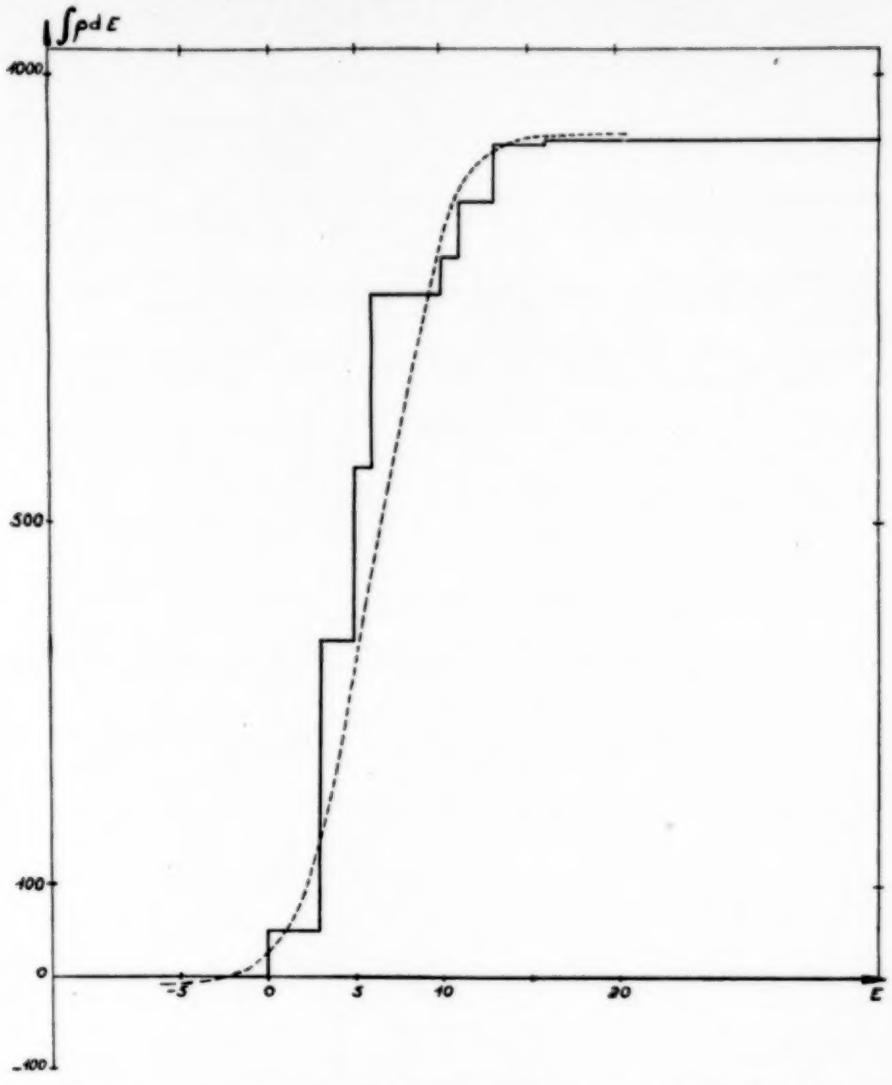

Fig. 6. Intégrale de ρ pour $N = 6$ (force de Wigner $\mathscr{X} = 1$, $\mathscr{L} = 2$; ϕ arrêté à l'ordre 2 avec champ self-consistant). La constante d'intégration a été choisie de manière que la courbe (en pointillé), ait le même écart avec la courbe exacte (en escalier) pour $E = +\infty$ et pour $E = -\infty$.

ment limité correspondant, on voit (fig. 4 et 6) que les résultats sont bien meilleurs en calculant directement ν ou ν'. Il en est de même à l'ordre 4 pour lequel, dans le calcul de ρ (33),

$$D = \mathscr{N} AT \mathscr{P} \left\{ 1 - \beta \left(e_1 AT + \frac{2}{\mathscr{P}} \right) \right.$$

$$\left. + \beta^2 \left[e_1^2 A^2 T^2 + e_1 AT \frac{2}{\mathscr{P}} + \frac{\mathscr{R}}{\mathscr{P}} - \tfrac{1}{2} e_2 AT (A^2 + 8AT + T^2) \right] + \ldots \right\} \quad (43a)$$

peut devenir négatif, alors que dans le calcul de ν ou ν' la quantité

$$D_1 = \mathcal{N}AT\mathcal{P}[1-\ldots] + \frac{\mathcal{N}AT}{\beta^2}[1-\beta e_1 AT+\beta^2 e_1^2 A^2T^2+\tfrac{1}{2}\beta^2 e^2 AT(A^2-4AT+T^2)+\ldots] \quad (43b)$$

est partout positive (fig. 7).

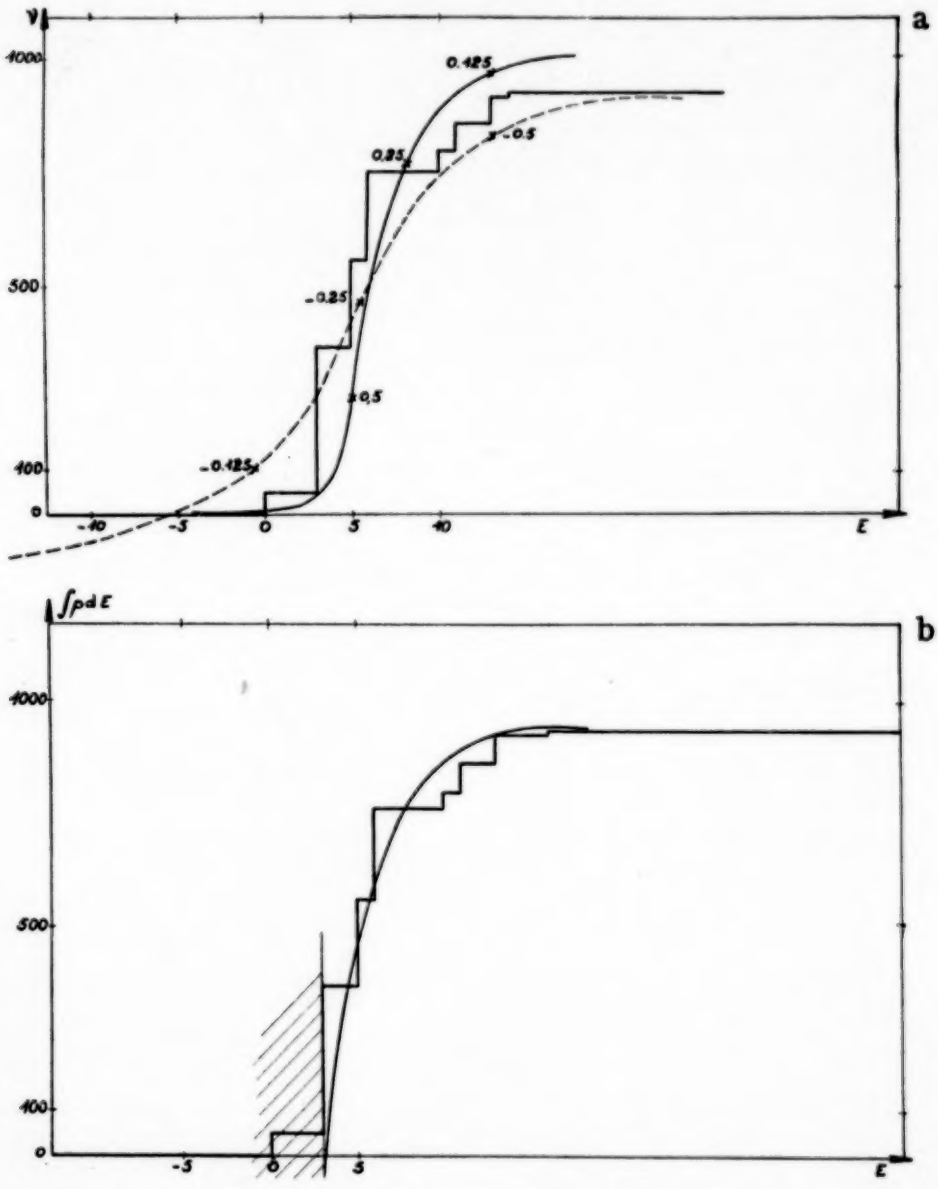

Fig. 7. Comparaison au 4e ordre en ϕ de ν, ν'(courbes a) et de l'intégrale de ρ (courbe b), pour $N = 6$, avec une force de Wigner $\mathcal{H} = 1$, $\mathcal{L} = 2$.

Cependant, la méthode du col sur ν ou ν' introduit des erreurs systématiques supplémentaires. Par exemple, le nombre total de niveaux devrait être égal à $\nu(E = +\infty, N)$, ou à $\nu'(E = -\infty, N)$ ou à $\nu(E, N)+\nu'(E, N)$.

Or

$$\nu(E=+\infty,N)=\nu'(E=-\infty,N)=\frac{\mathcal{N}^{\mathcal{N}+\frac{1}{2}}}{\sqrt{2\pi}\,N^{N+\frac{1}{2}}(\mathcal{N}-N)^{\mathcal{N}-N+\frac{1}{2}}}\frac{e}{\sqrt{2\pi}},$$

$$\nu(E=\tfrac{1}{2}\mathcal{N}e_1A^2,N)+\nu'(E=\tfrac{1}{2}\mathcal{N}e_1A^2,N)\approx\frac{\mathcal{N}^{\mathcal{N}+\frac{1}{2}}}{\sqrt{2\pi}\,N^{N+\frac{1}{2}}(\mathcal{N}-N)^{\mathcal{N}-N+\frac{1}{2}}}\sqrt{\frac{e}{\pi}}.$$

L'erreur introduite, $e/\sqrt{2\pi}=1.085$ ou $\sqrt{e/\pi}=0.930$, est faible; elle n'est

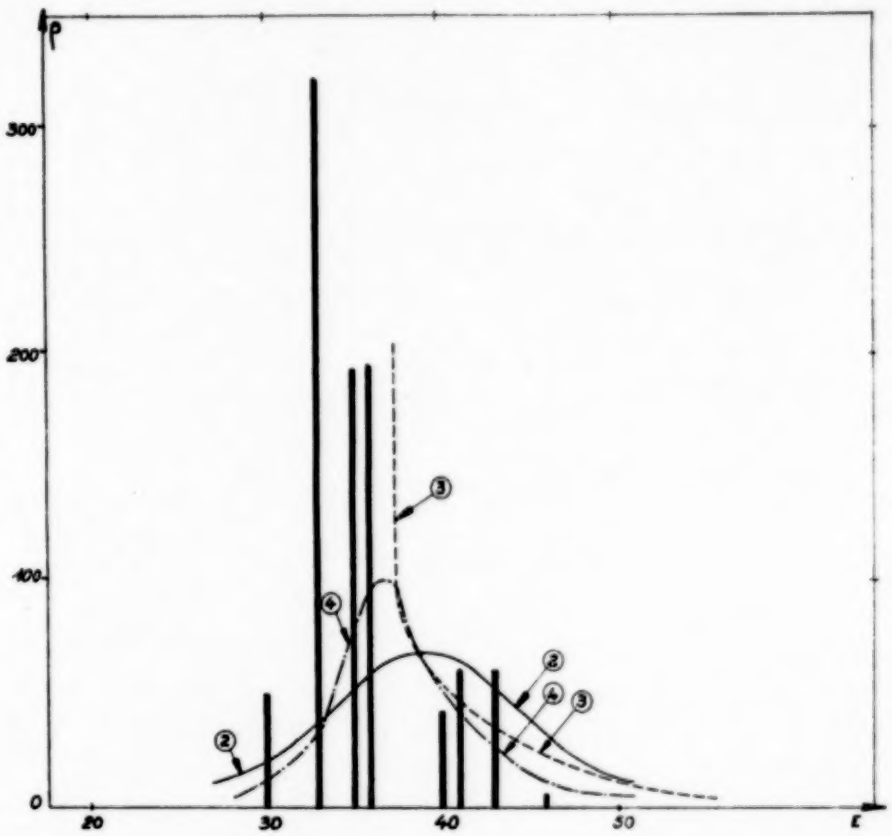

Fig. 8. Courbes de ρ aux ordres 2, 3 et 4 pour $N=6$ (force de Wigner $\mathcal{K}=1$, $\mathcal{L}=4$. On a indiqué la position des niveaux exacts, ainsi que leur dégénérescence.

due qu'à l'emploi de la méthode du col, le résultat ne dépendant que du terme d'ordre zéro dans ϕ. D'autre part, si l'on calcule le terme suivant de la méthode du col, soit par un développement en série de l'intégrant au voisinage du col, soit en suivant la ligne de plus grande pente, on trouve que son rapport au terme principal est

$$\frac{3}{4}\frac{1}{(1+\mathcal{P}\beta^2)^2}.$$

Ce terme correctif n'est donc négligeable que lorsqu'il en est de même du terme complémentaire de D_1, de sorte que la difficulté du signe de D_1 n'est pas résolue. D'ailleurs, le domaine d'énergie dans lequel il est négligeable

($-E$ grand pour ν, $+E$ grand pour ν') ne couvre pas entièrement la région où se trouvent les niveaux exacts (fig. 9). Malgré ces résultats meilleurs à l'ordre 2 et 4, l'application de la méthode du col sur ν est donc suspecte.

4.5. CONVERGENCE

Le développement (28) étant le développement en puissances de β de la fonction analytique $\log \sum_{E,N} e^{-\beta E+\alpha N}$, converge à l'intérieur d'un cercle de

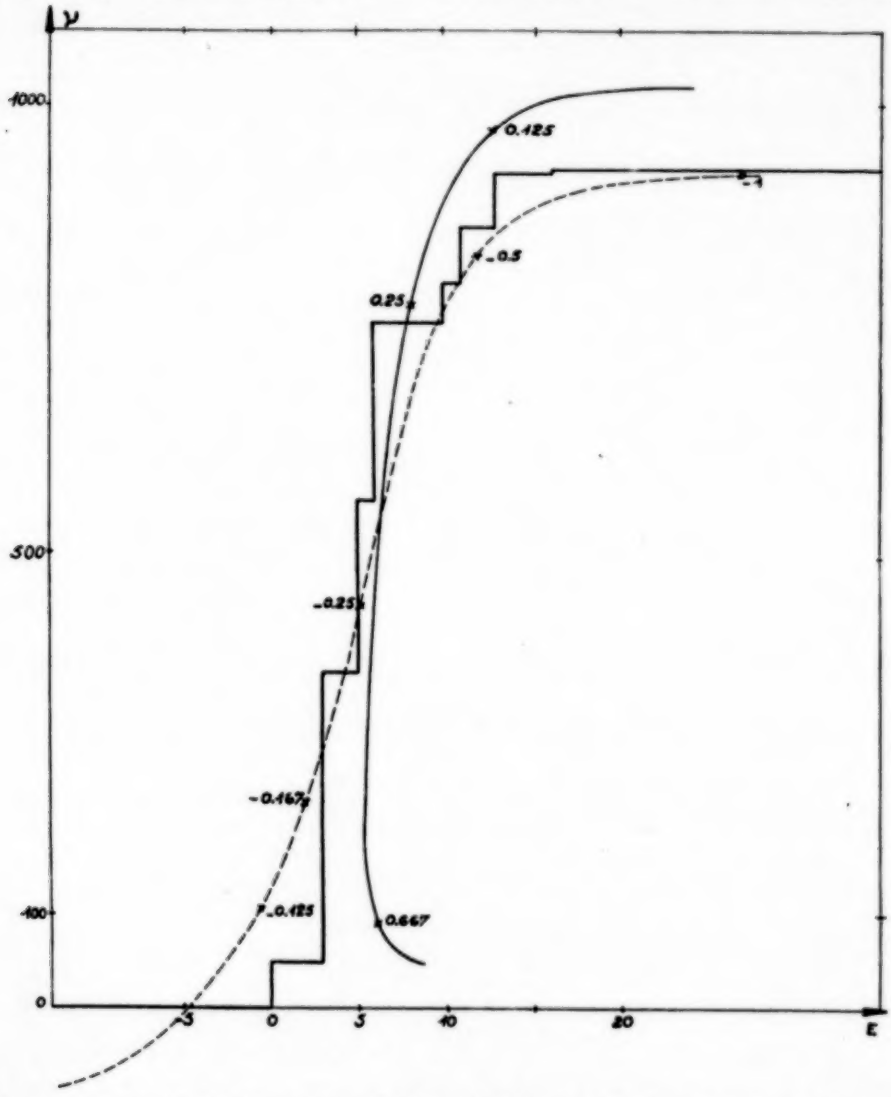

Fig. 9. Courbes de ν et ν' à l'ordre 3 pour $N = 6$ (force de Wigner $\mathscr{K} = 1$, $\mathscr{L} = 2$). La convergence est mauvaise pour $|\beta|$ grand, alors que le 1er terme correctif à la méthode du col est supérieur à $\frac{1}{3}$ du terme principal lorsque $|\beta| < 0.22$.

rayon non nul. La convergence est donc rigoureuse dans une petite région autour du point $E = \frac{1}{2}\mathscr{N} e_1 A^2$. D'ailleurs, les résultats pour ρ dans cette région s'améliorent lorsqu'on prend des termes supplémentaires (fig. 8).

Mais cette convergence n'est pas bonne. Le tableau 2 montre par exemple pour $N = 6$ pour diverses forces de Wigner ou de Majorana, les

coefficients des développements en puissances de β. On voit donc qu'on peut espérer de bons résultats seulement au centre de la distribution des niveaux.

Le fait que la convergence ne soit pas bonne entraîne en particulier que, si l'on s'arrête à l'ordre 3, la fonction $E(\beta)$ (fig. 3), au lieu d'être décroissante partout, ne l'est que dans une région limitée autour du centre de la distribution, par le point $E = \frac{1}{2}\mathcal{N}e_1A^2 - (\mathcal{P}^2/2\mathcal{Q})$. C'est pourquoi, même qualitativement, l'ordre 3 donne de très mauvais résultats loin du centre de la distribution (fig. 8) surtout pour le nombre ν ou ν' de niveaux dans la branche correspondant au signe de $\mathcal{Q}$ (fig. 9).

TABLEAU 2

Valeurs numériques des coefficients des développements en puissances de β introduits dans la représentation paramétrique $\rho(N,\beta)$, $E(N,\beta)$ pour diverses valeurs de l'interaction

	$\mathcal{K}=1$ $\mathcal{Q}=0$	$\mathcal{K}=1$ $\mathcal{Q}=2$	$\mathcal{K}=1$ $\mathcal{Q}=4$	$\mathcal{K}'=1$ $\mathcal{Q}'=0$	$\mathcal{K}'=0.1$ $\mathcal{Q}'=1.2$	$\mathcal{K}'=1$ $\mathcal{Q}'=1$
(1) $\mathcal{Q}/\mathcal{P}$	−1.9	2.5	8.3	−1.9	0.8	1.2
(2) $\dfrac{\mathcal{R}-\frac{1}{2}\mathcal{N}e_2^2A^3T^3}{\mathcal{P}}$	22	2.5	56	4.4	−1.4	11
(3) e_1AT	−4.5	1	6.5	3	0	3.2
(4) $\frac{1}{2}e_2AT(A^2+4AT+T^2)$	−3.4	−1.6	−5.4	−3.4	−1.3	−1.8
(5) β_{max}	0.4	0.7	0.25	0.45	0.73	0.45
(6) $\dfrac{\Delta E}{2\sqrt{\mathcal{P}}}$	1.8	2.5	1.4	2	2	1.5

Le terme indépendant de β étant ramené à l'unité par mise en facteur, (1) et (3) sont les coefficients des termes en β, (2) et (4) ceux des termes en β^2. ΔE étant la distance entre le niveau fondamental et le niveau excité le plus haut, la ligne (5) donne une idée de la valeur maximum $\beta_{max} = \Delta E/2\mathcal{P}$ prise par β aux limites de la région des niveaux. La ligne (6) compare la largeur de cette région a l'écart quadratique $\sqrt{\mathcal{P}}$ donné par la théorie statistique à l'ordre 2.

Le fait que les courbes de ν ou ν' donnent des résultats meilleurs à l'ordre 2 qu'à l'ordre 4 (fig. 4, 7, 9) ne peut être qu'une coincïdence. La convergence limite $|\beta|$ supérieurement, alors que la méthode du col sur ν le limite inférieurement ($\mathcal{P}\beta^2 \gg 1$) (fig. 9). Il est donc établi que la méthode du col sur ν ne présente aucun avantage.

4.6. COHÉRENCE DES DÉVELOPPEMENTS LIMITÉS

Il existe deux manières, après avoir résolu les équations du col, de calculer D par des développements en puissances de l'interaction (c'est-à-dire de β) arrêtés au même degré que celui de la méthode des perturbations. Celle que

nous avons employée jusqu'à présent consistait à prendre dans le développement de D autant de termes que l'ordre de ϕ le permettait. On avait ainsi à l'ordre 2

$$D = \mathscr{N}AT\mathscr{P}$$

ce qui donnait une gaussienne, et à l'ordre 4 l'expression (43a).

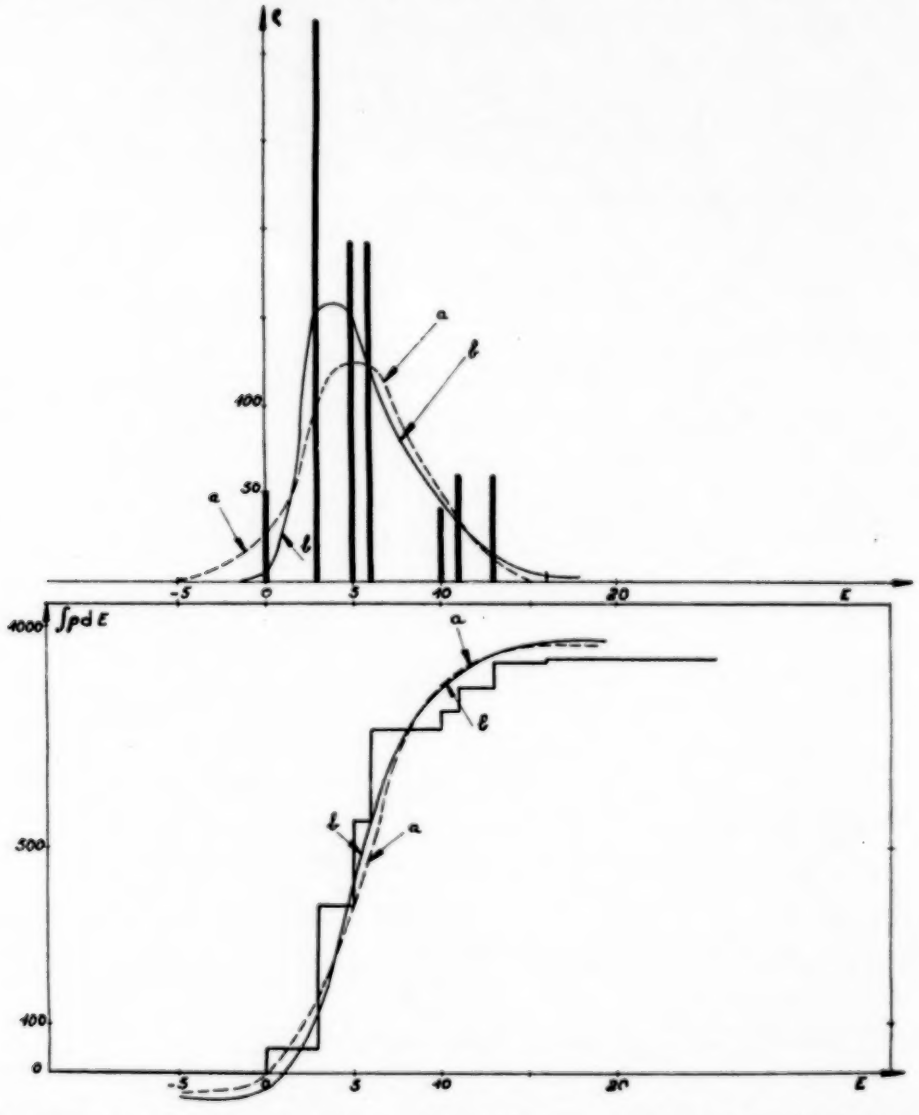

Fig. 10. Courbes de ρ pour $N = 6$, $\mathscr{K} = 1$, $\mathscr{L} = 2$, en conservant dans D les développements en puissances de l'interaction de $-\partial E/\partial\beta$ et de $\partial\alpha/\partial N$. La courbe a) correspond à l'ordre 2 et la courbe b) à l'ordre 4. Les résultats sont encore meilleurs après intégration.

On peut procéder autrement en utilisant la relation exacte

$$D = -\frac{\partial E}{\partial \beta} \Big/ \frac{\partial \alpha}{\partial N}$$

et en prenant dans les développements de $\partial E/\partial\beta$ et $\partial\alpha/\partial N$, séparément,

autant de termes que la méthode des perturbations le permet. A l'ordre 2, on a alors

$$D = \frac{\mathscr{N} AT \mathscr{P}}{[1+\beta e_1 AT - \frac{1}{2}\beta^2 e_2 AT(A^2-4AT+T^2)]}$$

et à l'ordre 4

$$D = \frac{\mathscr{N} AT \mathscr{P}\left[1-\dfrac{\beta \mathscr{Q}}{\mathscr{P}}+\beta^2\left(\dfrac{\mathscr{R}}{\mathscr{P}}-\frac{1}{2}e_1 AT\right)\right]}{[1+\beta e_1 AT - \frac{1}{2}\beta^2 e_2 AT(A^2-4AT+T^2) + \text{termes en } \beta^3 \text{ et } \beta^4]}.$$

Cette méthode est bien meilleure que la première. A l'ordre 2 on trouve en effet une courbe ayant la dissymétrie cherchée (fig. 10a). A l'ordre 4, le déterminant est positif dans toute la région des niveaux; la difficulté essentielle dans le calcul de ρ, le changement de signe de D (fig. 7b), disparaît ainsi. De plus la forme de la courbe est améliorée dans la région où D était positif (fig. 10b).

Les résultats des deux méthodes sont très différents parce que $-\partial E/\partial\beta$ et $\partial\alpha/\partial N$ n'ont pas le même nombre de termes et que les développements convergent mal; leur rapport est donc différent de ce qu'on obtient en effectuant une division de développements limités. Par exemple, $(1-\beta)/(1+\beta)$ est positif pour $-1 < \beta < 1$, alors que la première méthode conduirait à $1-2\beta$ qui est positif pour $\beta < 0.5$ seulement.

Le succès de la deuxième méthode tient à ce qu'elle introduit le minimum d'erreurs dans le maniement des développements limités. En effet, on a déduit de l'expression $E(N, \beta)$ la densité de niveaux par les formules exactes (14), (15a) et (12a):

$$\alpha = \int \frac{\partial E}{\partial N} \mathrm{d}\beta, \qquad D = -\frac{\partial E}{\partial \beta} \Big/ \frac{\partial \alpha}{\partial N}, \qquad S = \int \beta \frac{\partial E}{\partial \beta} \mathrm{d}\beta.$$

La seule approximation est (en dehors de la méthode du col) l'utilisation d'un développement limité de $E(N, \beta)$. Au contraire, dans la première méthode, on ajoute à cette erreur celle de prendre D sous forme d'un développement limité.

Le calcul direct de D est d'ailleurs plus long que celui qui est basé sur l'emploi de la formule (15a).

4.7. RÔLE DU CHAMP SELF-CONSISTANT

Jusqu'à présent, nous avons introduit seulement des développements en puissances de l'interaction; l'introduction du champ self-consistant ne nous a servi qu'à simplifier les calculs. Pour en tenir compte exactement, il faut résoudre les équations du col en supposant βe_1 de l'ordre de grandeur de l'unité, et en développant en puissances de l'interaction en ce qui concerne les autres paramètres. L'expression que l'on obtient ainsi à l'ordre 4 pour $E(N, \beta)$ est alors précisément l'expression (31b), au terme en e_2^2 près qui

dépend maintenant de βe_1 (mais on peut négliger cette petite correction).

Nous trouvons ainsi la raison principale du succès de la deuxième méthode pour le calcul de D: elle tient exactement compte du champ self-consistant, puisqu'elle n'introduit pas d'autre erreur que celle sur $E(N, \beta)$. Au contraire le développement de D en puissances de β n'en tient pas compte.

L'examen du tableau 2 montre d'ailleurs que lorsque le champ self-consistant, donné dans la ligne (3), est faible (2ème et 5ème colonnes), les coefficients des termes en β^2 (lignes (2) et (4)) sont petits. La convergence du développement $E(N, \beta)$ est donc meilleure lorsque le champ self-consistant est faible.

Le rôle fondamental du champ self-consistant est confirmé par l'étude de la convergence des développements (24) et (28) de $\phi(\alpha, \beta)$ (fig. 11). Le développement (28) en puissances de la perturbation, bien qu'il converge rigou-

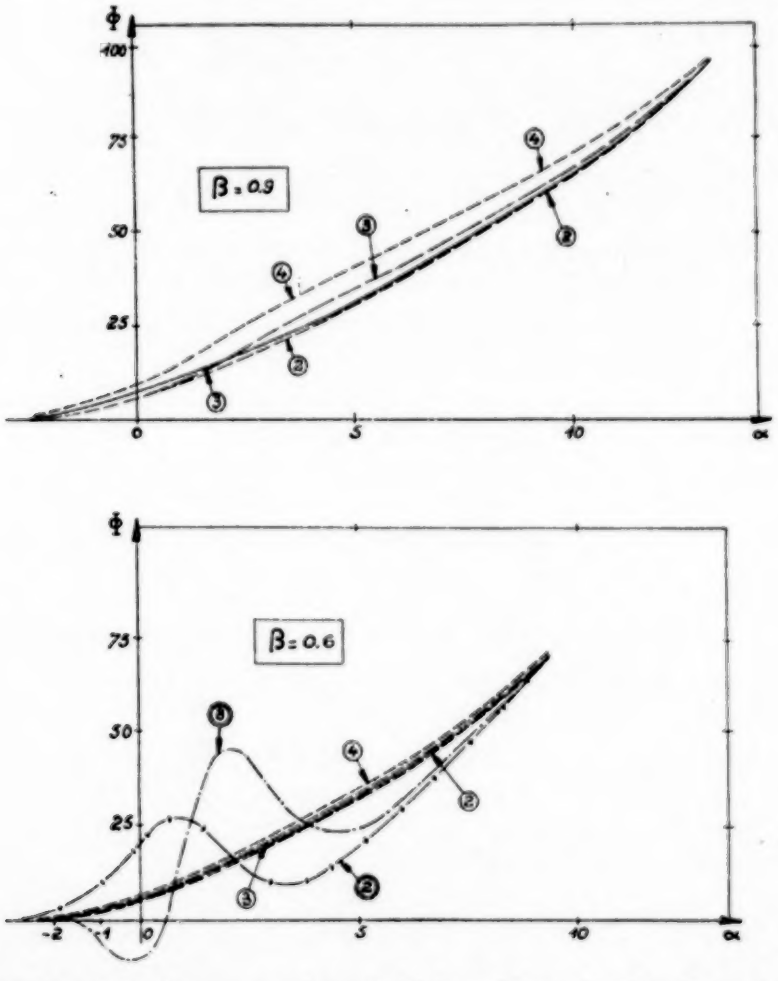

Fig. 11. La surface ϕ (α, β) pour une force de Majorana $\mathscr{K}' = 1$, $\mathscr{L}' = 0$, représentée par des coupes à β constant, dans la région utile pour les calculs de densités de niveaux. La courbe en trait plein représente la valeur exacte de ϕ, les courbes en pointillés correspondent à l'expression (24) tenant compte du champ self-consistant, et les courbes en pointillés mixtes au développement (28) en puissance de l'interaction. Les nombres 2, 3 et 4 se réfèrent à l'ordre auquel ces développements sont arrêtés.

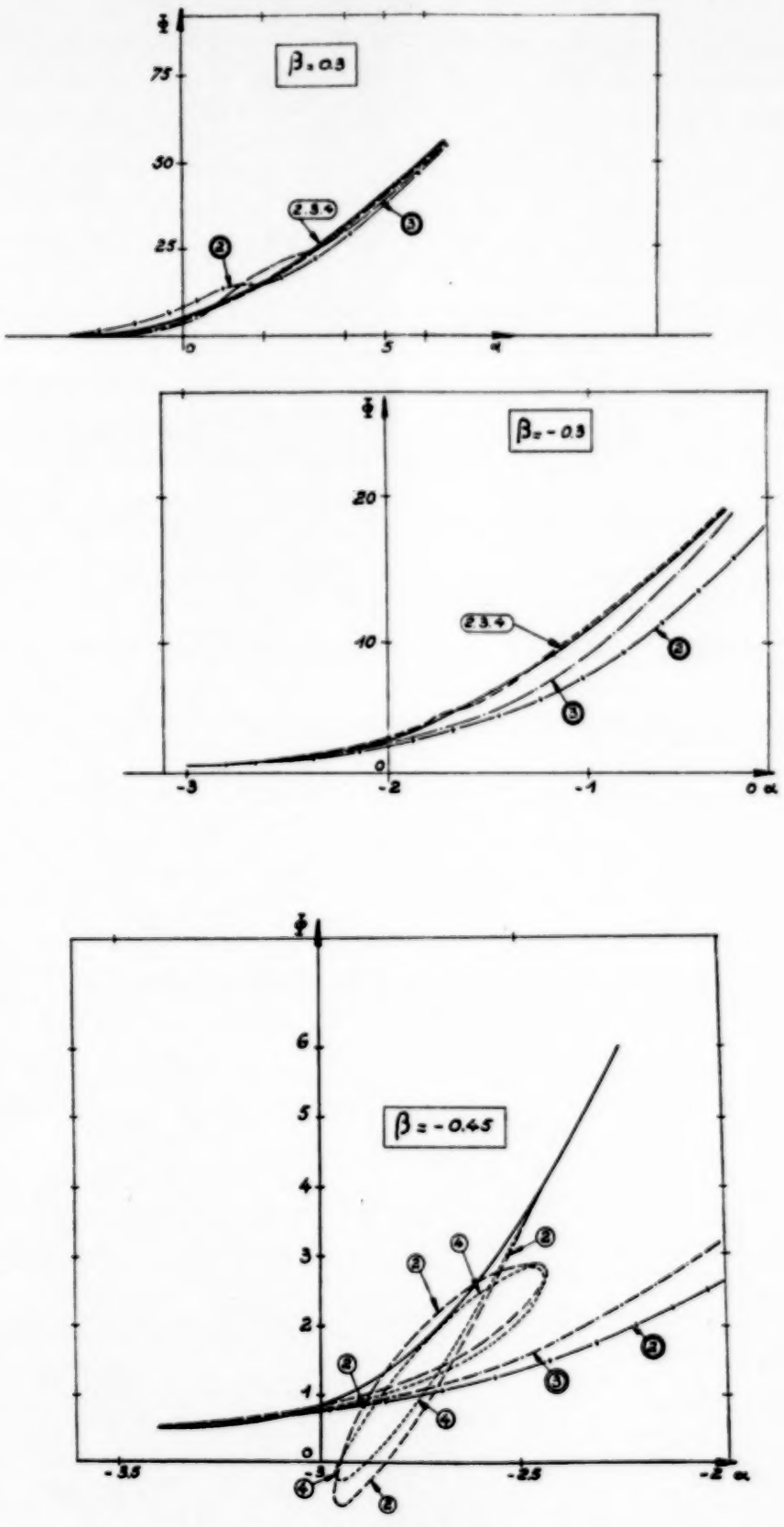

Fig. 11 (suite)

reusement pour α et β assez petits, donne de très mauvais résultats, soit que le rayon de convergence soit très faible, soit que la convergence soit trop lente. Au contraire, le développement (24) (tenant compte du champ self-consistant à l'ordre 1) donne déjà au second ordre une courbe voisine de la courbe exacte, et les courbes des ordres suivants montrent qu'il converge rapidement.

Cette conclusion est infirmée dans la région où $1+\beta e_1 f_+ f_- < 0$, car le champ self-consistant, et par suite ϕ, y ont trois déterminations. Aucune de celles-ci ne donne le résultat exact avec une bonne approximation.

En conclusion, la méthode statistique donne de bons résultats, même pour un nombre très faible de particules, si on applique la méthode du col pour la densité de niveaux. L'emploi de la méthode du col pour l'intégrale de la densité de niveaux introduit des erreurs supplémentaires, et ne présente aucun avantage. L'emploi, dans la résolution des équations du col, de formules exactes reliant les expressions en fonction de N et de β, de l'énergie, de α, de „l'entropie" S, et du déterminant des dérivées secondes, permet de réduire l'erreur au minimum en ramenant tout à une seule expression approchée. Enfin, la convergence est bien meilleure si l'on tient compte exactement du champ self-consistant, tout au moins lorsque celui-ci a une seule détermination. Il est vraisemblable que les résultats seraient encore meilleurs si on prenait un champ self-consistant à un ordre plus élevé que le premier. Plutôt que de pousser aux ordres supérieurs de la méthode des perturbations, il vaut donc mieux utiliser la méthode avec champ self-consistant.

L'auteur tient à remercier tout particulièrement le Professeur C. Bloch qui l'a constamment guidé durant ce travail, et Monsieur V. Gillet qui a collaboré à la 2ème et à la 3ème partie.

Bibliographie

1) R. H. Fowler, Statistical Mechanics (Macmillan, New-York, 1936)
2) T. Ericson, Nuclear Physics **6** (1958) 62; **8** (1958) 265
3) C. Bloch, Phys. Rev. **93** (1954) 1094
4) C. Bloch et C. De Dominicis, Nuclear Physics **7** (1958) 459
5) E. P. Wigner, Phys. Rev. **51** (1939) 947
6) Eliott et Lane, Handbuch der Physik, vol. **39**, p. 323

NORTH-HOLLAND BOOKS

ASYMPTOTIC METHODS in ANALYSIS

by **N. G. DE BRUIJN** *Professor of Mathematics at the University of Amsterdam*

Asymptotics is that part of analysis which considers problems of the type dealt with in this book

Contents

Ch. I. Introduction
Ch. II. Implicit Functions
Ch. III. Summation
Ch. IV. The Laplace Method for Integrals
Ch. V. The Saddle Point Method
Ch. VI. Applications of the Saddle Point Method
Ch. VII. Indirect Asymptotics
Ch. VIII. Iterated Functions
Ch. IX. Differential Equations

6×9″ XII+200 pages Guilders 20.00 (40s.)

NORTH-HOLLAND BOOKS

ANALYTICAL and CANONICAL FORMALISM in PHYSICS

by ANDRÉ MERCIER

Head of the Department of Theoretical Physics University of Berne

6×9″ VIII + 222 pp. Guilders 20.00 (40s.)

CONTENTS

i. Lagrangian Formalism
ii. Lagrangian Density
iii. Canonical Formalism
iv. Canonical Form of Electrodynamics
v. Hamiltonian Densities
vi. Transformations
vii. Canonical Formalism with Vanishing Jacobian Determinant

Those who are not highly specialized in these matters but do want to get a fairly broad knowledge of the subject are not aware of the fact that the greater parts of this formalism, including many specific conclusions of physical concern, do not involve in the least quantum theory, i.e. "quantization" of the fields. To show this and to provide the reader with a fairly complete presentation of the ***classical*** (i.e. not yet quantized) theory of fields is one of the main aims of the book.

This formalism is presented with great generality. Some special topics have also been included when they are found to be of importance in connection with the problems raised; however, they are not elaborated with the same generality, but just formulated as far as is found necessary for the understanding of these connections; for instance we can name: tensorial formalism and spinorial formalism.

A special chapter has been devoted to transformations of several kinds including canonical transformations, reversibility and the like as well as their interrelations, so that the ground is prepared for an understanding of the CPT-Theorems.

A short chapter on Dirac's dynamics with vanishing Jacobian closes the book.

The work builds upon the well-known ***Principles of Analytical Dynamics*** by the same author (in French), where particular weight is laid upon the homogeneous formalism, but it can easily be read with profit without knowledge of the latter by any advanced students in physics, astronomy or mathematics as well as by research workers who want to get a thorough practice in the use of these methods.

Many examples and as many as 124 problems illustrate the formalism exposed.

Sole Agency for U.S.A.: Interscience Publishers Inc.-New York

NORTH-HOLLAND PUBLISHING COMPANY - AMSTERDAM